PERFORMANCE-BASED BLAST RESISTANT DESIGN OF REINFORCED CONCRETE FRAME STRUCTURES UNDER DISTANT EXPLOSIONS

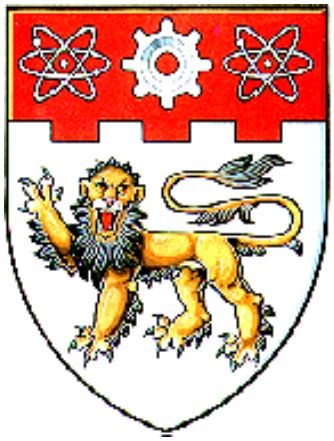

RONG HAICHENG

SCHOOL OF CIVIL AND ENVIRONMENTAL ENGINEERING

NANYANG TECHNOLOGICAL UNIVERSITY

2005

PERFORMANCE-BASED BLAST RESISTANT DESIGN OF REINFORCED CONCRETE FRAME STRUCTURES UNDER DISTANT EXPLOSIONS

Rong Haicheng

School of Civil and Environmental Engineering

A thesis submitted to the Nanyang Technological University in fulfillment of the requirements for the Degree of Doctor of Philosophy

2005

To my family

ACKNOWLEDGMENTS

It is difficult to use a single page to express my appreciation to all those who have contributed to the success of my research over the last three and half years. Herein, I would like to take this opportunity to thank those whose contributions to the research were indispensable.

First and foremost, I would like to express my sincere gratitude to my supervisor, Associate Professor Li Bing for his warm encouragement, patient guidance and stimulus throughout this research. His unwavering enthusiasm and interest in scientific research is much appreciated and unforgettable. It is a great benefit and honour to work with him. I would also like to thank Professor Pan Tso-Chien for his active role, helpful discussions and useful comments on my research, and to Professor Sam Kiger from University of Missouri-Columbia and Professor John Mander from the University of Canterbury, New Zealand who served as the outside readers.

The scholarship provided by the School of Civil and Environmental Engineering, Nanyang Technological University throughout this study is gratefully acknowledged.

Special thanks are given to my family for their fundamental support and encouragement during my stay in Singapore.

Finally, I would like to dedicate this work to Mr. Huang Zhiwei, for his great and consistent encouragement, patience and love during the course of this work.

Funding for this work was provided through the Protective Technology Research Centre, NTU Contract No: PTRC-CSE/LEO/99.05 under DSTA/NTU funding. The support is gratefully acknowledged.

TABLE OF CONTENTS

ABSTRACT

Numerical finite element analyses to evaluate the structural dynamic responses are performed on a six-storey reinforced concrete frame structure under distant explosion conditions. The finite element models involved are discussed and experimentally verified. Results show that the whole dynamic response process of the frame structure can be approximately divided into two stages. Localized responses of the blast-loaded members are critical at response stage I while the global responses of the structural system dominate at response stage II.

To keep the localized responses of the blast-loaded members under control in meeting the expected performance level, a performance-based blast resistant design approach for reinforced concrete structural members is developed with the energy spectra. Given the objective performance level defined by the combination of target displacement and target displacement ductility factor, a design procedure to uniquely determine the effective depth and longitudinal reinforcement ratio of the member is addressed and implemented into the practical design examples. The accuracy of the approach in terms of controlling the responses of maximum displacement and displacement ductility factor for the designed member under the given blast loading is numerically evaluated by comparing them with their respective design targets. Two error indices quantifying the errors between the responses of designed member and the design targets are defined and their simplified formulae are derived with extensive numerical studies and statistical analyses. The applications of the error indices formulae into the modification of the developed design approach as well as the probabilistic performance assessment of the designed member under blast loadings are exhibited.

To ensure the global responses in terms of maximum inter-storey drift ratio (MIDR) at the expected global performance level, a new design method is presented for a multi-storey reinforced concrete frame structural system based on the equivalent static force (ESF). The calculation model of the ESF that produces the same MIDR effect as that under the distant blast condition is discussed. Several design examples

are employed to demonstrate the method implementation while verifications of the MIDR responses of the designed frame structures are carried out with numerical dynamic analyses

LIST OF TABLES

LIST OF FIGURES

Figure Page

LIST OF SYMBOLS

A_s	cross sectional area of the tension reinforcement
$a,\ b$	parameter
a_1, a_2, a_3	parameters
b_w	width of the web of the element
C	non-dimensional energy factor
COV	coefficient of variation
c	depth of the equivalent rectangular stress block
DIF	dynamic increase factor
d	effective depth of the element measured from the extreme compression fiber to the centroid tensile reinforcement
d'	distance from the extreme compression fiber to the centroid of compression reinforcement
d_c	distance between the centroid of compression and tension reinforcement
E_c	Young's modulus of elasticity for concrete
E_{el}	ultimate elastic energy
$E_{\max}$	maximum strain energy
E_s	Young's modulus of elasticity for steel
E_{e_y}, E_{e_μ}	mean values of e_y and e_μ
e_y , e_μ	nominal random variables
$e_{y,n}$	n percentages of non-exceedance probabilities for e_y
$e_{\mu,m}$	m percentages of non-exceedance probabilities for e_μ
F_1	peak value of the force
$f(t, t_d)$	a non-dimensional time function
F_s , F_a	the force produced respectively by original and additional springs

F_{ser}	uniformly distributed service loads
f_c , f_{dc}	strength of concrete in compression in static and dynamic conditions
f_{dv}	dynamic stirrup yield strength
f_s , f_{ds}	strength of flexural steel in static and dynamic conditions
f_t , f_{dt}	tensile strength of concrete in static and dynamic conditions
I	average moment of inertia of the cross section
I_c	moment of inertia of the cracked concrete cross section
I_g	moment of inertia of the gross concrete cross section (neglecting all reinforcing steel),
i	impulse
K_{LE} , K_{ME}	transformation load and mass factor
K_{LME}	transformation load-mass factor
K_s	initial stiffness for an elastic-perfectly-plastic SDOF system
K_a	elastic stiffness for an additional spring
k_a	equivalent elastic stiffness for the reinforced concrete elements
k_e	initial stiffness of the equivalent elastic-perfectly-plastic SDOF system of the designed member
l	length of the element
M_{add}	additional mass on the beam contributed by adjacent floors
M_N	moment capacity at the support of one-way elements
M_P	moment capacity at the mid-span of one-way elements
M_u	ultimate moment
m	equivalent mass of the equivalent SDOF system
m_a	mass of the reinforced concrete member
P	external static force
P_i	probability of performance at the *i*th level
P_r	pressure
P_{st}	equivalent static force

p	the effective pressure stress
q	Mises equivalent deviatoric stress
q_u	ultimate uniformly distributed force of the reinforced concrete member
R	standoff distance
RF	reaction force
R_m	ultimate strength of the equivalent SDOF system
SC	support condition
T	period
T_c	total depth
t	time
t_d	load duration
V_c	shear capacity of the unreinforced concrete
V_d	ultimate support reactions
V_u	ultimate shear force
W	explosive weight, the constant total energy
W_a	strain energy in the additional spring
W_k	kinetic energy
W_s	strain energy
y	displacement
y_e	elastic (recoverable) displacement
y_e^{eq}	elastic displacement response of the equivalent SDOF system of the designed reinforced concrete member under the blast force
y_e^{rc}	elastic displacement response of designed reinforced concrete member at the significant point under the blast force
y_m^{eq}	maximum displacement response of the equivalent SDOF system of the designed reinforced concrete member under the blast force
y_m^{rc}	maximum displacement response of the designed reinforced concrete member at the significant point under the blast force
y_t	target displacement

y_{te},	parametric design target of displacement
y_{td}	displacement at the end of the blast loading duration t_d
y_m	maximum displacement
$\dot{y}$	velocity
$\dot{y}_{td}$	velocity at time t_d
$\ddot{y}$	acceleration
α, β	coefficient
$\varepsilon, \varepsilon_1, \varepsilon_2$	arbitrary small value
$\dot{\varepsilon}$	strain rate
$\dot{\varepsilon}_s$	static strain rate
φ	capacity reduction factor
ζ_y^{rc}	displacement error index
ζ_μ^{rc}	displacement ductility error index
γ	reduction coefficient
η	non-dimensional displacement
λ	equivalent static force factor
λ_{samp}	sample points of λ
λ_{upp}	upper-envelop line of λ
λ_{low}	lower-envelop line of λ
μ^{eq}	displacement ductility response of the equivalent SDOF system of the designed reinforced concrete member under the blast force
μ^{rc}	displacement ductility response of the designed reinforced concrete member at the significant point under the blast force
μ_t	target displacement ductility ratio
μ_{te}	parametric design target of displacement ductility factor
ρ	longitudinal tension reinforcement ratio
ρ'	longitudinal compression reinforcement ratio
$\rho_{\min}$	minimum longitudinal tension reinforcement

ρ_v	shear reinforcement ratio
σ_{e_y} , σ_{e_μ}	standard deviations
$\sigma_c(\varepsilon_{uniaxial}^{pl})$	the hardening (and softening) parameter
ξ	time parameter
Δ_m	maximum inter-storey drift ratio (MIDR)
Δ_m^P	MIDR under the external static force P
$\Delta_m^{P_{st}}$	MIDR under the equivalent static force P_{st}
$\Delta_{td,m}$	maximum inter-storey drift ratio at the end of the blast force
Δ_t	target maximum inter-storey drift ratio

CHAPTER ONE

INTRODUCTION

1.1 Problem Statements

Blast loading is a type of extraordinary dynamic load, which is characterized by its great intensity and short duration [B1, B2, B5, B7, F1, T1, O1]. Due to the devastating effects of blast loading, the dynamic responses and potential damage mechanisms of the structure that has to withstand such a blast are one of the major concerns of current research works [B6, B7, D2, E2, G1, K6, L2, L3, L5, M16]. Many explosion tests and numerical studies have been carried out in this field to date however they are predominantly concentrated upon the structural responses under the blast loadings produced by close-in detonations. Considering that the possibility of the accidental or incidental explosions of the petroleum refineries, the chemical plants, the ammunition storage areas, or nuclear devices of substantial yields, the surrounding distant civilian structures are likely to be loaded by an intense blast wave that is produced in these bomb events and spreads from the explosion source. The structural dynamic responses and corresponding damage distributions in these distant blast incidents may be quite distinct from those in the close-in explosion environments, however little research has been done on this field. The related literatures available to date have been very limited and are mainly oriented towards a single-storey and multi-bay military structure, which is common to the ammunition manufacturing and storage facilities [B1, B4, T2, N4]. Considering that most of civilian reinforced concrete frame structures have multi-storey levels, the identification of the dynamic behaviours and damage distributions of multi-storey reinforced concrete frame structures under the distant intense surface explosion conditions becomes increasingly important.

The reinforced concrete members within the frame structures that are directly loaded by the blast loadings from distant intense surface explosions may sustain severe damages or collapse entirely, but if additional reinforcements in the appropriate positions have been used for these members, the structure might have enough strength and ductility to withstand the blast more effectively, resulting in a reduction of the damages. Thus designing and detailing the reinforced concrete members to improve their dynamic behaviours in response to the blast loadings is deemed necessary. Considering the large magnitude of the blast loadings induced by intense surface explosions and the relatively low probability of their occurrence, the requirement for structural members to remain elastic under the blast loading conditions is not economically justifiable. Thus it is deemed to be more reasonable to design the members with some levels of inelastic deformation allowed. Many performance-based blast resistant design guidelines have been presented in the ASCE Manual 42 [A2], TM5-855-1 [T1], TM5-1300 [T2], Allgood [A3], Biggs [B1], Mays and Smith [M3] with the explicit consideration of inelastic deformation. The concept of the performance basis is that the design should be able to ensure that the damage of the structure will not exceed a certain limit. The permissible level of damage is termed a performance level, which can be specified by any structural dynamic response parameter such as the displacement, the displacement ductility factor, or the drift ratio [B12, F2, G8, H7, K16, K17, P4, P5, X1]. By establishing different objective performance levels for the structural member with either the target displacements or the target displacement ductility factors in these design guidelines [A2, A3, B1, M3, T1, T2], the blast resistant design is carried out so that the predicted response of the designed member under the blast loading does not exceed its corresponding target. However an important question remains as to whether a single target of the displacement or the displacement ductility factor involved in the design could provide an adequate control of the member's responses to satisfy the expected performance under the given blast condition. Moreover these design methods are performed basically by transforming the continuous members into equivalent single-degree-of-freedom (SDOF) systems and taking the responses of the SDOF systems as those of the designed members without considerations of their differences.

As for the structural system, the blast resistant design is predominantly focused on the prevention of the progressive collapse triggered by the failure of some critical members. Many design guidelines [A4, D3, F3, F4, G3, I1] have been issued for providing the approach of evaluating and preventing the failure of structural systems in such a way. However, under distant intense blast conditions, numerical studies indicate that the global response of the structural system in terms of side-sway become more critical [L4]. As a result, it is necessary to keep the side-sway response under control within the required performance level (damage limit) during the design of reinforced concrete frame structures against the distant blast loadings. Currently, the design manual "Blast Resistant Structures" [N4] and the ASCE special publication "Design of Blast Resistant Buildings in Petrochemical Facilities" [B4] have suggested different side-sway limits corresponding to various damage levels and a trial design method based on some approximations was recommended for simple single-storey and multi-bay military structures. However, there are still no well-developed design methods available to date against distant blast loadings for the multi-storey reinforced concrete frame structures. The need for research and development will no doubt remains.

1.2 Research Objectives and Scopes

The main objective of this thesis is to analyse the dynamic responses for multi-storey reinforced concrete frame structures under distant intense surface explosion conditions and to develop performance-based blast resistant design methods for reinforced concrete frame structural members as well as structural systems to keep their responses under control thus to meet the target performance level. The research is conducted with the following focuses:

- to trace the dynamic responses and the corresponding damage distributions for a multi-storey reinforced concrete frame structure with/without exterior cladding panels under distant explosion conditions through the numerical finite element analysis.
- to develop a performance-based blast resistant design approach for a one-

way reinforced concrete member depending on energy spectra for the purpose of the adequate control of the designed member's responses to meet the expected performance level under the given blast conditions.

- to study the differences between the responses of the reinforced concrete member designed with the developed approach and those of the corresponding SDOF system under the given blast force and incorporate these differences into the design.
- to present a method of performance-based blast resistant design for a multi-storey reinforced concrete frame structural system in keeping its global response in terms of maximum inter-storey drift ratio (MIDR) under proper control thus to satisfy the performance requirement, by transforming the blast forces from distant explosions into the equivalent static forces (ESF).

1.3 Thesis Organization, Originality and Main Contributions

The introduction of the problems, the objectives and the scopes of this study are defined in this chapter.

Chapter 2 presents the nonlinear dynamic analysis of multi-storey reinforced concrete frame structures to evaluate their dynamic responses as well as damage distributions against the blast loadings from distant explosions. This is accomplished using the program ABAQUS. The effects of the exterior cladding panels on the structural responses are identified.

Chapter 3 is concerned with the development of a new performance-based blast resistant design approach for one-way reinforced concrete structural members by using energy spectra, which are constructed from the elastic-perfectly-plastic SDOF system. The expected performance level is defined by both the target displacement and target displacement ductility factor of the member at the significant point (e.g. the mid-span of a member with two ends constrained or the free-end of a cantilever member). By controlling the responses of maximum displacement and displacement ductility factor for the equivalent SDOF system of the designed member to exactly

reach the corresponding targets, the design process is discussed to uniquely determine the effective depth and longitudinal reinforcement ratio of the member. The effectiveness of the developed blast design approach is evaluated in Chapter 4. The actual responses of maximum displacement and displacement ductility factor for designed member at the significant point under the given blast condition are investigated with numerical finite element analysis and compared with their corresponding design targets.

The developed design approach using energy spectra is accomplished by the assumption that the maximum displacement and displacement ductility responses of the designed reinforced concrete member can be represented by the corresponding responses of its equivalent SDOF system under the blast loading. In fact, due to the complexities of the nonlinear dynamic behaviours of reinforced concrete members under blast conditions, some differences between them do appear which further induce the errors of the maximum displacement and displacement ductility responses for the designed member under the given force with the respective design targets. A study of these errors is carried out in Chapter 5 where two error indices are defined and their simplified formulae are derived through extensive numerical studies and statistical analyses.

Chapter 6 applies the formulae of the error indices into the modification of the blast resistant design approach developed in Chapter 3 for the purpose of establishing more effective control of the maximum displacement and displacement ductility responses of the designed reinforced concrete member rather than those of the corresponding equivalent SDOF system in achieving the respective design targets. Several design examples of the members are exhibited with the modified design approach followed by a comparison with those obtained from the original design process. In addition, a simpler procedure of implementing these two error indices to estimate the distribution of the maximum displacement and displacement ductility responses for designed members under blast loadings is presented and applied into the probabilistic performance assessment of the members accounting for different types of uncertainties.

A new method of blast resistant design for a multi-storey reinforced concrete frame structural system based on the transformation of the distant blast loading into the equivalent static force (ESF) is discussed in Chapters 7 and 8, where the maximum inter-storey drift ratio (MIDR) response parameter is taken as the global performance indicator. The ESF is calculated in such a way that the same MIDR effect will be produced as that under the distant blast condition. Chapter 7 focuses on the model for the calculation of ESF as well as the corresponding design method based on ESF for a SDOF system with the requirement of controlling its maximum displacement response. The extension of the calculation model for ESF and the design method with ESF for a SDOF system to a performance-based design for multi-storey reinforced concrete frame structures in controlling their MIDRs under distant blast conditions is discussed in Chapter 8. The implementation of the developed design method into practical design examples is demonstrated followed by the nonlinear dynamic evaluation of the design results.

Chapters 2 to 8 are organized in the form of technical papers. Chapter 9 concludes the work of the present study and recommend some future work.

The originality and main contribution of present work are:

- evaluating and comparing the dynamic responses and corresponding damage distributions for the multi-storey reinforced concrete frame structures with/without the exterior cladding panels under the blast loadings from distant explosions.
- developing a new approach for the blast resistant design of reinforced concrete members by using energy spectra, which could overcome the disadvantages in the existing design guidance .
- assessing the accuracy of the developed design approach in controlling the maximum displacement and displacement ductility responses for the designed member by comparing them with the corresponding design target.
- deriving the simplified formulae of the two error indices which quantify the differences of the maximum displacement and displacement ductility

responses for the designed member under the given blast force with their respective design targets.

- applying the formulae of the error indices into the modification of the developed design method so as to effectively control the actual responses of the designed members rather than those of the corresponding equivalent SDOF systems.
- implementing the error indices formulae into the probabilistic performance assessment of designed members against blast loadings without numerical finite element analysis.
- presenting a new design method for a multi-storey reinforced concrete frame structure against a blast loading from distant intense explosion in controlling its MIDR response based on the ESF, which is computed to produce the same MIDR effect as that under the blast action.
- evaluating the effectiveness of the presented ESF-based blast resistant design method in terms of controlling the MIDR response of multi-storey reinforced concrete frame structures as compared to the design target.

CHAPTER TWO

RESPONSES OF MULTI-STOREY REINFORCED CONCRETE FRAME STRUCTURES TO DISTANT EXPLOSIONS

Synopsis

Limited research has been carried out upon the dynamic responses for multi-storey reinforced concrete frame structures subjected to blast loadings from distant intense surface explosions. This chapter presents numerical analysis with the program ABAQUS on a six-storey reinforced concrete frame structure under two blast conditions occurring at a standoff distance of 100 m produced by the explosives respectively equivalent to a 50 ton TNT and 250 ton TNT. To incorporate the effects of exterior cladding panels, two cases are involved in the analysis for the six-storey frame structure with/without exterior cladding panels. The finite element models involved are verified by comparing the numerical results of a reinforced concrete beam and slab for blast loadings with the experimental data. The results indicate that the whole dynamic response process of the frame structure with/without exterior cladding panels can be approximately divided into two stages. The localized responses of the blast-loaded members are critical at response stage I while with the increase in time, the structural global response becomes dominant at response stage II. Flexural responses are more important in the plastic deformation of the structural members as compared to the corresponding shear responses. Due to the variation of the blast forces received, the dynamic responses are much more severe for the frame structure with exterior cladding panels than the one without exterior wall panels under the same blast condition.

Keywords: Reinforced concrete frame structure, Distant explosions, Blast loadings, Local and global responses, Damage distribution, Response stages

2.1 Introduction and Background

The behaviours of civilian reinforced concrete structures under blast conditions have become a major concern to structural engineers due to the recent surge in explosive events worldwide. After the trigger of a blast, a blast wave including a high-pressure shock front is formed and expands outward from the centre of detonation [B9, G2, H5, K7, K8, K15, N1, N2, T1]. As the blast wave strikes a building, the overpressure and drag force of the blast wave load on the structure, the interaction between which is significantly complicated [A2, B1, N1, T1]. However, considering the relative distance of the detonation centre with the target structure as well as the size of the structure itself, two classes of blast wave-structure interaction can be generally identified as shown in Figure 2.1 [S1]. The first class is the interaction of a blast wave produced by the detonation of a smaller charge loading a target structure at a short standoff distance, which is typical for most terrorist attacks such as car bombings [C1, C5, H2, L1, L3]. The second class is the interaction of a blast wave on a relatively distant structure as might be present due to an accidental severe surface explosion of petroleum refineries, chemical plants and ammunition storage areas, fuel train explosions, or nuclear devices of substantial yields, and so on [C6, G2, K1, M7].

The profiles of blast loadings on the structure are different within these two classes of blast wave-structure interaction. In the first class, the blast pressures are produced locally to individual structural members and the members are likely to be loaded sequentially [S1, L1, L2]. By comparison, in the second class of blast wave-structure interaction, the target structure is engulfed due to the diffraction of the blast wave and a normal squashing force will be applied to every exposed surface. There is also a translational drag force, which tends to move the structure bodily laterally [A2, S1, T3].

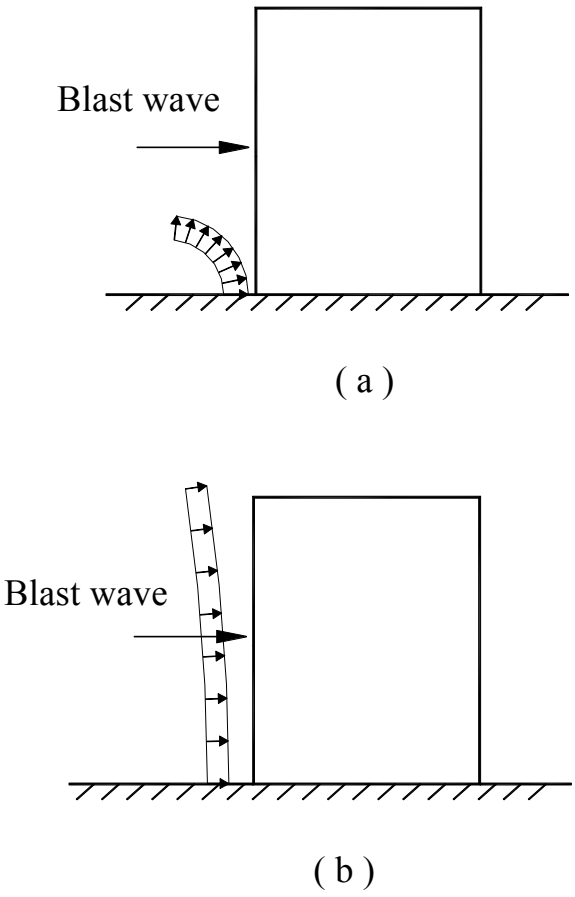

Figure 2.1 Two classes of blast wave-structure interaction [S1]

Many explosion tests and numerical analyses have been carried out on the behaviours of structures in the first class of blast wave-structure interaction where the blast pressures are applied locally to individual structural members resulting in the possibility of an excessive local failure of several critical structural members and further the progressive collapse present in a non-redundant structure [C1, E2, L2, L3, M6]. Therefore the study is focused dominantly on two aspects: the local responses of structural members under blast loadings and the progressive collapse of the structure under gravity loads with some members destroyed or severely damaged. The first aspect has been widely covered to date in many articles where the potential and observed failure mechanisms [C2, E3, K2, K4, M12, M15, P3, R1, S6, Z1] of structural members, the constitutive models to characterize the inelastic material behaviour [B6, B10, C7, K6, K9, M8, M9, M17], and the blast resistant

design procedures of structural members in controlling their responses [A2, A3, B1, B4, M3, T1, T2] are studied. As concerning the second aspects, General Services Administration (GSA) [G3], Interagency Security Committee (ISC) security criteria [I1], and ASCE 7-98 [A4], Federal Emergency Management Agency (FEMA-273 and FEMA-274) [F3, F4], and Department of Defence (DoD) [D3] have issued the guidelines for evaluating the progressive collapse hazard which provide general information about the approach and method of evaluating the progressive collapse potential. Moreover, various analytical methods used to evaluate the possibility of progressive collapse are developed which cover greatly from simple linear elastic static procedure [H3, M10] to complex nonlinear time history analysis [K10, K11, L2, L3, V1].

However little research has been devoted to behaviours of civilian structures and their possible failure mechanisms in the second class of blast wave-structure interaction and the available literature about it is very limited. By simplifying the members and the structural system into equivalent single-degree-of-freedom (SDOF) systems, Biggs [B1] provided a blast resistant design procedure for one-storey structures, which was demonstrated with a design example of a one-storey windowless aboveground frame structure in resisting the blast loading produced by a 0.5 MT weapon at about 1.7 km. Baker [B2] examined the responses for one and two-storey planar steel frames loaded by the blast forces through numerical simulations with the method for including plasticity in the frames by Majid [M11] and Yamada [Y1]. The method was based on the formation of plastic hinges at the ends of the members and computed the rotations of these hinges during plastic deformation.

Although the blast incidents producing the second class of blast wave-structure interaction are very rare, when they do occur the consequence can be extremely severe, particularly upon the structures not specifically designed to withstand the blast effects. There have been cases of the severe damage or even collapse of the surrounding buildings within such incidents [C9, K1]. To minimize the blast consequences to the buildings, an effective blast resistant design is needed. For this

purpose, knowledge of structural dynamic behaviours and the corresponding potential damage distributions under such blast situations is imperative, however it is limited to date in contemporary released publications. Further study of the structural behaviours in the second class of blast wave-structure interaction should be employed especially for multi-storey reinforced concrete frame structures which are mostly common to the civilian buildings, accounting for the complicated interaction between the blast wave and structure as well as the nonlinear material properties of concrete and reinforcement.

This chapter aims to study the dynamic responses and damage distributions of a multi-storey reinforced concrete frame structure loaded by blast waves from distant intense surface explosions employing nonlinear dynamic finite element analysis with the program ABAQUS [A1]. The finite element models involved are verified by comparing the numerical results of a reinforced concrete beam and slab with the corresponding experimental data by Seabold [S3] and Keennan [K3]. Since the exterior cladding panels might have noticeable effects on the structural behaviours under blast conditions, two types of the multi-storey frame structure with/without exterior cladding panels are analysed. The corresponding structural dynamic responses and damage distributions are identified and compared. The findings from this study are used to reach conclusions and recommendations in the blast resistant design concerning explosive safety for civilian reinforced concrete frame structures.

2.2 Blast Loadings

In this investigation, the main concern is upon the dynamic responses of frame structure when subjected to blast loadings produced by distant intense surface explosions, where compared with the size of the target, the hemispherical wave front can be reasonably idealized to be planar blast wave front and essentially parallel to the front faces of the target shown in Figure 2.1 [A2, B11, S1, T1]. As the blast wave strikes on the front face of a closed target, a reflected pressure is instantly developed. The blast wave diffracts around the target, subjecting first the sides and roof and finally the rear face to pressures equal to incident overpressure

(air-blast pressure occurring in the free-field). At the same time, these faces are as well loaded by drag pressures that are a function of a drag coefficient and the dynamic pressure associated with the air-flow behind the shock causing drag or wind type loads. This drag pressure causes a push on the front face of the target followed by a suction force on the back and sides as the blast dynamic pressure passes over and round the target [A2, B11, N3, S1].

Determination of the exact blast loadings of a distant explosion on the front, top and the sides, and the rear faces of the closed target is almost unrealistic considering the complicated process of the interaction of the blast wave with the concerned target. In order to reduce the complex problem of blast loadings to reasonable terms, a computational procedure is recommended in the US manual TM5-855-1 [T1] based on two assumptions that (a) the target is generally rectangular in shape, and (b) the object being loaded is in the region of the Mach reflection [B1, B9, G2, K12, H1, N1]. These two assumptions are rational for the derivation of the blast loadings on rectangular targets in a relatively large standoff blast environment. The simplified loading configurations on various faces are shown in Figure 2.2 whose parameter can be calculated with the equations listed in Appendix 1 for a closed rectangular aboveground target, i.e. a column, a beam, or a closed structure.

The computation of the blast loadings on a frame structure is relatively more complicated than that plotted in Figure 2.2 since the whole structure could not be arbitrarily taken as a closed rectangular target. The loading profiles applied to the frame structure are dependent on the out-of-plane strength and stiffness of exterior cladding panels due to the direct action of blast loadings on them, as well as their connection with the frame members of beams and columns. In this study, two extreme cases are considered that:

- the exterior cladding panels are constructed with the material of reinforced concrete with significant strength and stiffness.
- there is no exterior cladding panels for the frame structure (bare frame structure);

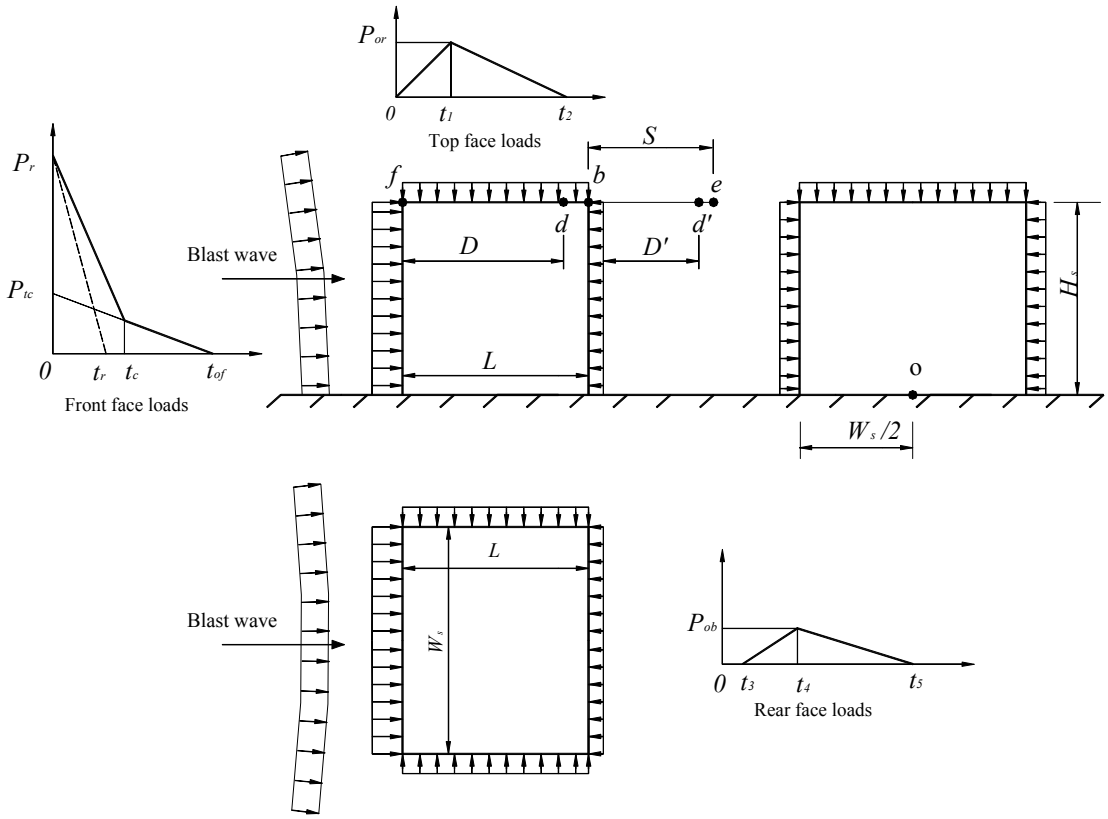

Figure 2.2 Blast loadings on a simply closed rectangular target [T1, F1]

In the case of frame structure with exterior cladding panels made of reinforced concrete, the cladding panels possess the significant out-of-plane strength, stiffness and strong connection with other frame members. As the blast wave hits the outer surfaces of the structure (outer surfaces of exterior cladding panels, exterior beams and columns), the blast wave could not go into the building and the blast loadings on the cladding panels would be transferred to the primary frames in terms of reaction forces. These transferred reaction forces together with the blast loadings acting directly on the outer surfaces of the exterior beams and columns will produce dynamic responses of the structure, which is different from those of the bare frame structure. For this case, it is reasonable to treat the whole structure as a closed target, based on which the blast forces upon the front, roof and rear faces are computed according to the equations in Appendix 1.

As for the second case, the blast wave front would enter the building producing a high pressure on the rear faces of the columns. Appendix 1 could not be directly used for computing the blast loadings on a bare frame structure since the whole structure could not be taken as a closed rectangular target. However, the shock wave front in the distant surface explosion condition is essentially parallel to the front faces of blast loaded columns. By taking each column as a closed rectangular target, the blast forces on the front and rear faces of the columns could be evaluated according to Appendix 1 where the parameters (L, W_s and H_s) are equal to those of each column. The blast loadings on both side faces of each column are identical as well as on the top and bottom surfaces of each slab leading to a zero consultant force due to the blast wave approximates to a planar wave, and therefore they are not taken into account in the following analysis.

In addition to blast overpressure effects, intense surface explosions produce ground shocks as results of the directly induced ground motion propagating through the soil or rock, which might affect structural responses. However considering the fact that the target to be studied is located at a large standoff distance relative to the source of the explosion, the magnitude of the ground shock has been greatly diminished and the arrival time of the shocks to the structures is different from that of blast wave. Therefore the direct ground shocks are ignored in this analysis.

2.3 Design of the Target Frame Structure

For the study of the dynamic behaviours of frame structures under the distant blast conditions, a three-dimensional six-storey reinforced concrete frame structure is designed according to BS8110 code [B3]. The loads involved in the design include the dead loads (5.0 kPa), the super imposed dead loads (1.0 kPa), the live loads (4.0 kPa), and the wind loads calculated in accordance with the BS 6399 code by taking the wind speed to be 30 m/sec. The layout of the structure and the reinforcement details of structural members are shown in Figure 2.3.

Two blast waves produced by the detonations equivalent to a 50 ton TNT (blast condition I) and 250 ton TNT (blast condition II) at the ground level with a standoff distance of 100 m are considered in the study. In these blast conditions where the standoff distance is significantly larger than the size of the target structure, the blast waves can be reasonably modelled with a planar wave as displayed in Figure 2.3. The waves engulf the whole structure producing blast pressures on exposed surfaces of the structure uniformly distributed not only along the width of the structure but also along the height. Due to the symmetry of both the configuration of the target structure and the blast pressure distributions on it, a three-dimensional sub-frame including a planar frame and half of adjacent components is modelled to simulate the whole structural dynamic responses.

In order to incorporate the effects of exterior cladding panels on the structural blast responses, two extreme cases are considered for the six-storey frame structure in this study. In the first case, the exterior cladding panels are assumed made of reinforced concrete with sufficiently out-of-plane strength and stiffness to prevent the blast waves from entering the building, therefore the modelling of the structural responses have to include the exterior cladding panels (whose reinforcement arrangements are found in Figure 2.3c), together with the floor slabs, beams and columns. In the second case, the structure is formed without exterior cladding panels. As discussed previously, the frame structure in such a situation is a bare frame against the blast loadings, accordingly only the beams, columns and floor slabs are modelled for the following numerical simulations. The appearances of these two different sub-frame structures are demonstrated in Figure 2.4.

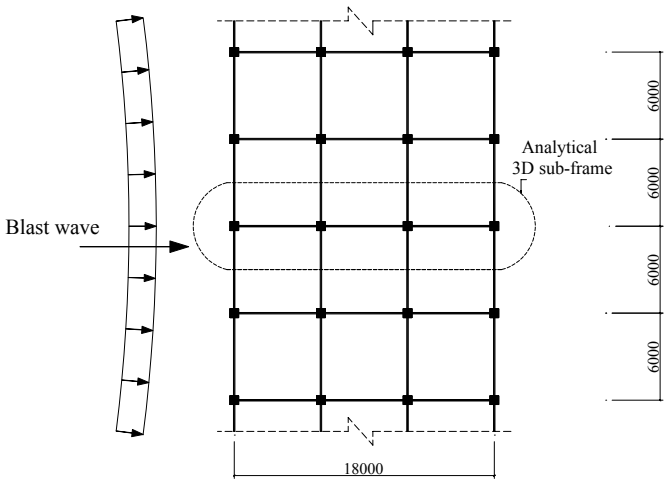

(a). Structural layout

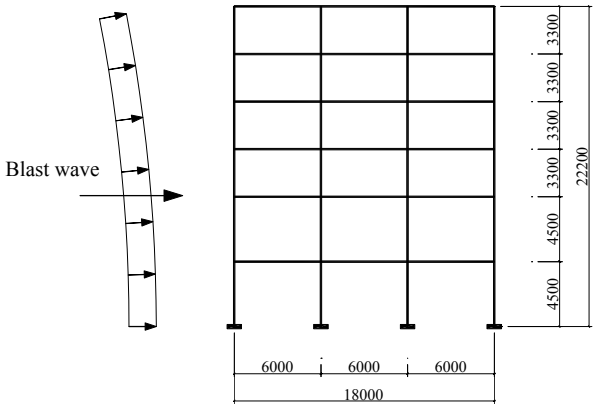

(b). Elevation view

Beam section (1st-6th storey)			Column section	
End	Mid-span	Interior support	1st-2nd storey	3th-6th storey
2T25+2T20 600 3T20 300 (Link R10@200)	2T20 600 4T20 300 (Link R10@200)	2T25+2T20 600 3T20 300 (Link R10@200)	12T20 600 600 (Link R10@200)	4T25+8T20 500 500 (Link R10@200)
Floor slab depth = 150mm; R10@ 200mm in two directions with a concret cover of 25 mm for top and bottem reinforcement Cladding panel depth = 150mm; R10@ 200mm in two directions with a concret cover of 25 mm for top and bottem reinforcement				

(c). Reinforcement details of structural members

Figure 2.3 Details of the target six-storey frame structure

2.4 Finite Element Models

The three-dimensional six-storey sub-frame structures are modelled to perform the numerical simulations of the structural dynamic responses under blast conditions I and II by utilizing the program ABAQUS [A1]. The finite element models consist of the structural modelling, material modelling of concrete and reinforcement, the analysis steps and loads, plus the integration methods.

2.4.1 Structural modelling

Two types of structural members are included in the sub-frames, which are the frame members composed of beams and columns and the planar members including exterior cladding panels and floor slabs. In order to obtain more accurate simulations of the structural responses in blast conditions, three-dimensional continuum solid elements should be employed in modelling these structural members. However it will include considerably heavy computational efforts due to the complicated nonlinear behaviours of the concrete and reinforcement as well as the extremely large size of the finite element model for a multi-storey frame structural system built with the three-dimensional solid elements. For simplicity, beam elements for modelling frame beams and columns, together with shell elements for exterior cladding panels and floor slabs are adopted. The accuracy of the numerical simulation results of the responses for different structural member modelled with the beam or shear elements will be examined with available testing data in the latter part.

Two types of beam elements: Euler-Bernoulli beam element and Timoshenko beam element are generally involved in the finite element analysis. Since the Euler-Bernoulli beam element does not allow for transverse shear deformation, it is only applicable for modelling the behaviours of beams and columns in the situation where their flexural responses dominate. However as pointed out by many researchers [C2, K2, R1], the shear responses of frame members could be important in blast conditions. Accordingly, Timoshenko beam element, which allows for the

transverse shear deformation, has been employed in the analyses. The verification of this type of beam element in simulating the responses of reinforced concrete members under severe short duration dynamic loads has been proven in a lot of research [K2, K18, K19, R1].

Shell elements are generally used to model structural members in which one dimension, the thickness, is significantly smaller than the other dimensions such as the cladding panels and floor slabs. Considering the important shear deformation of cladding panels and slabs when loaded by blast forces as well as their large inelastic deformation [C8, H4, K3, K4, K13], the shell element that allows the transverse shear deformation and accounts for finite membrane strains and arbitrarily large rotations is employed in the simulation. This shell element is quite effective in the numerically predicted responses of cladding panels or slabs with the experimental verification in the latter section of this chapter.

Reinforcement in the concrete structures is modelled by means of rebars, which are one-dimensional strain theory elements (rods) defined singly or embedded in oriented surfaces. In this analysis, each rebar is placed at its corresponding location for the beam elements while the layers of rebar are defined for the shell elements with the needed data-input of reinforcing bar's area and location, and the space length.

The structural modelling for the six-storey frame structure with/without exterior cladding panels is shown in Figure 2.4. The bottom ends of structural columns are perfectly fixed to the solid ground and symmetry boundary conditions are applied to the edges of the slabs and cladding panels.

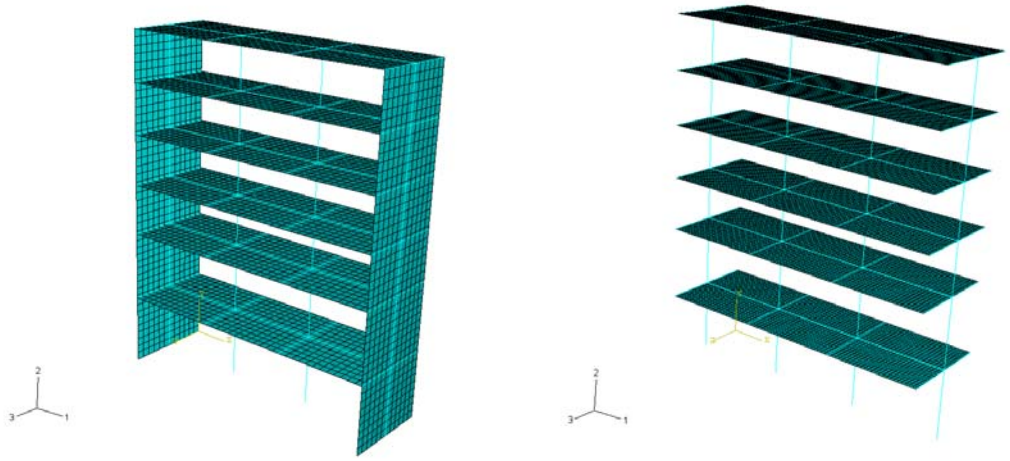

(a). Frame structure with reinforced concrete exterior cladding panels

(b). Frame structure without exterior cladding panels (bare frame structure)

Figure 2.4 Modelling of the three-dimensional six-storey sub-frame structure

2.4.2 Material modelling

The dynamic responses of reinforced concrete structures under blast conditions are dependent on the material properties of the concrete and reinforcement. To obtain valid numerical simulations of the dynamic responses of the structures, the accurate modelling of the material properties becomes essential. In the finite element analysis, three types of material behaviours including that of the concrete, reinforcing bars and the bondages between them should be taken into account. It is presumed that the bars are perfectly bonded with concrete herein. Although it will impose some errors, it is the only practical solution for the numerical simulations of the responses of reinforced concrete structural systems, considering the unmanageable size of the computational works and the lack of reliable data on this topic in blast environments.

The smeared cracking model is utilized to represent the tensile behaviour of concrete. In this model, concrete cracking appears as the maximum principal tensile stresses reach a failure surface and will affect the stress and material stiffness associated with each material point in related elements. To simulate the softening

effect of the concrete in tension after its cracking, a bilinear tension stress-strain curve is used and shown in Figure 2.5, where ε_u^{cr} is taken as 10^{-3}. The selection of this value is based on the assumption that the strain softening after failure reduces the stress linearly to zero at a total strain of about 10 times the strain at failure of concrete in tension, which is typically 10^{-4} in standard concretes [A5, H6]. The concrete tensile strength f_t used in the analysis is determined from the compressive strength f_c [C3]

$$f_t = 0.30 f_c^{2/3} \tag{2.1}$$

In compression, concrete is simulated with an elastic-plastic model where the elastic stress state is limited by a yield surface. Once yielding has occurred, an associated flow rule with isotropic hardening is used. This yield surface can be written in terms of the first two stress invariants

$$f = q - \sqrt{3} a_0 p - \sqrt{3}\sigma_c(\varepsilon_{uniaxial}^{pl}) \tag{2.2}$$

where p is the effective pressure stress, q is Mises equivalent deviatoric stress, and a_0 is a constant, which is chosen from the ratio of the ultimate stress reached in biaxial compression to the ultimate stress reached in uniaxial compression. $\sigma_c(\varepsilon_{uniaxial}^{pl})$ is the hardening (and softening) parameter, which is defined from the uniaxial compression data of the concrete as a function of the plastic strain. Poisson's ratio is approximate to be 0.20.

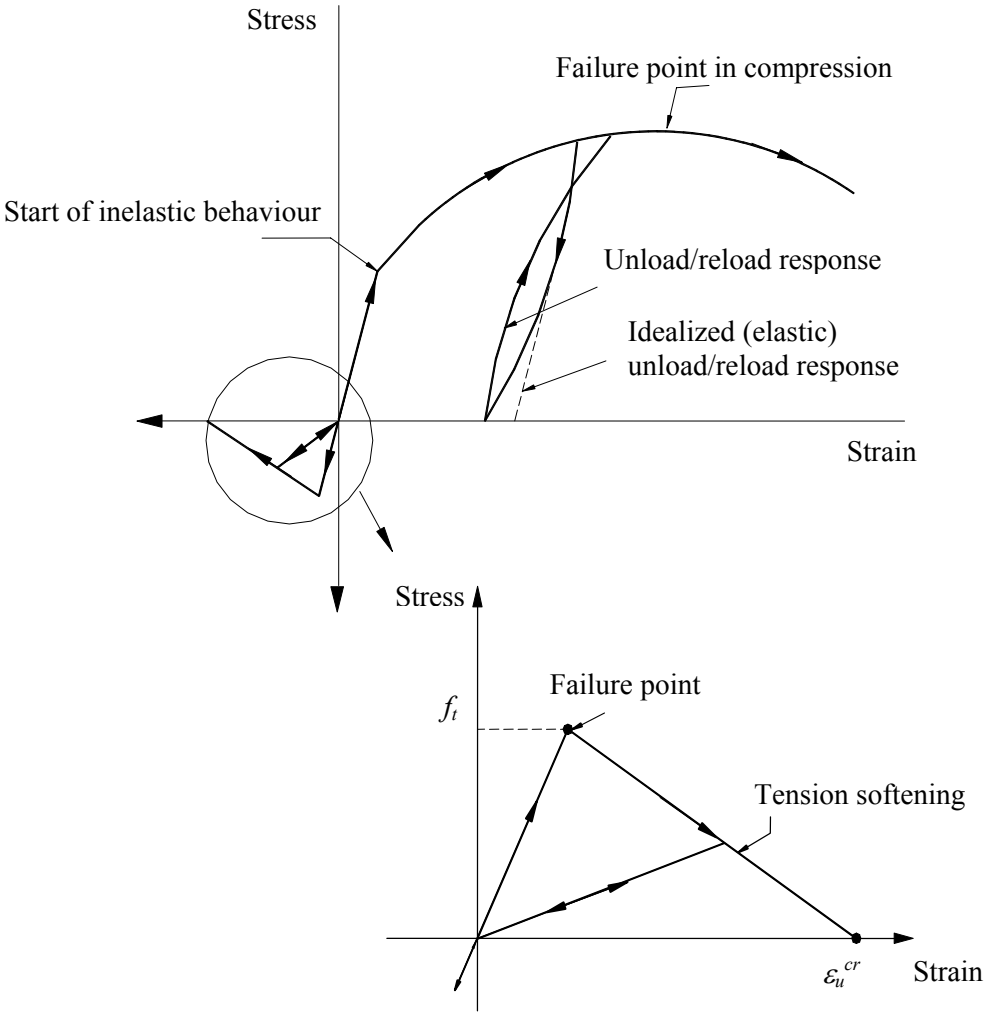

(a). Concrete in compression and tension

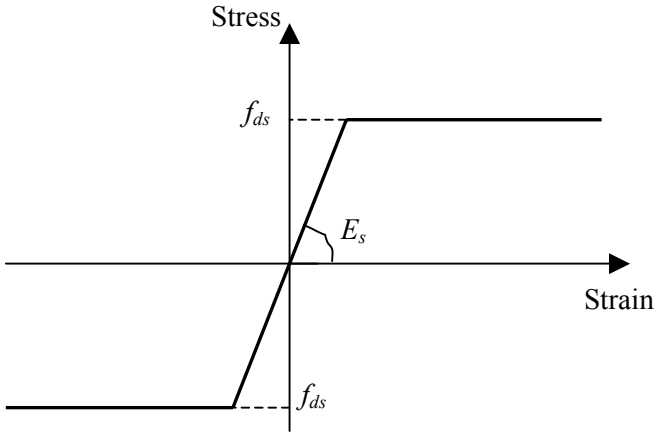

(b). Reinforcement

Figure 2.5 Material modelling

The stiffness used in the analysis for unloaded concrete in tension and compression is given in Figure 2.5. When the cracked concrete is unloaded, the secant unloading modulus is utilized as stiffness so that the strain across the crack is reduced linearly to zero as the stress approaches zero. If the load is removed at some point after inelastic straining has occurred for the concrete in compression, the unloading response is softer than the initial elastic response, but this effect is ignored in this model. Thus initial elastic stiffness is used when the concrete in compression is unloaded.

The Von-Mises yield criterion is used to describe the constitutive behaviour of the reinforcement. The stress and strain relationship of reinforcement is also shown in Figure 2.5, where the reinforcement is modelled with an elasto-plastic curve. The strain hardening of reinforcement is not considered in this analysis since it is hard to define under the blast conditions in the case of lacking enough experimental data. The ultimate strain value is often not reported in current literatures due to the difficulty of determining exactly when the peak stress occurs as well as the confusion between ultimate strain and rupture strain

In order to consider the fact that under higher loading rates both concrete and reinforcement exhibit increased strengths [D4, D5, F5, F6, G4, G5, G6, G7, M14, R2, T4], a dynamic increase factor (DIF), the ratio of the dynamic to static strength, is employed in this analysis. The expressions by Malvar and Crawford [M1, M2] are utilized which are derived from a literature review of the extensive test data about the effects of strain rate on the strength of concrete and reinforcement. For the concrete compressive strength, DIF is given as

$$DIF = \begin{cases} \left(\dot{\varepsilon}/\dot{\varepsilon}_s\right)^{1.026\alpha_s} & \dot{\varepsilon} \le 30s^{-1} \\ \gamma_s\left(\dot{\varepsilon}/\dot{\varepsilon}_s\right)^{1/3} & \dot{\varepsilon} > 30s^{-1} \end{cases} \tag{2.3}$$

where $\dot{\varepsilon}$ is the strain rate in the range of 30×10^{-6} to $300\ s^{-1}$; $\dot{\varepsilon}_s = 30\times10^{-6}\ s^{-1}$ (static strain rate); $\log\gamma_s = 6.156\,\alpha_s - 2$; $\alpha_s = 1/(5+9\,f_c/f_{co})$; $f_{co} = 10$ MPa; f_c

is the static compressive strength of concrete. For the concrete in tension, the formula is

$$DIF = \begin{cases} \left(\dot{\varepsilon}/\dot{\varepsilon}_s\right)^{\delta} & \dot{\varepsilon} \le 1.0 s^{-1} \\ \beta\left(\dot{\varepsilon}/\dot{\varepsilon}_s\right)^{1/3} & \dot{\varepsilon} > 1.0 s^{-1} \end{cases} \tag{2.4}$$

where $\dot{\varepsilon}$ is the strain rate in the range of 10^{-6} to 160 s^{-1}; $\dot{\varepsilon}_s = 10^{-6}\ s^{-1}$; $\log\beta = 6\delta - 2$; $\delta = 1/(1+8 f_c/f_{co})$; f_{co} = 10 MPa. A plot of the proposed formulae for the DIF of concrete in tension and compression is shown in Figure 2.6, which indicates that the strength enhancement is different for tension and compression.

The DIF formula for the yield stress of reinforcement [M1, M2] is

$$DIF = \left(\dot{\varepsilon}/10^{-4}\right)^{\alpha} \tag{2.5}$$

where $\alpha = \alpha_{fs}$ and $\alpha_{fs} = 0.074 - 0.04 f_s/414$; f_s is the reinforcement static yield strength in MPa. This formula is valid for reinforcement with yield stresses between 290 and 710 MPa and for strain rates between 10^{-4} and 225 s^{-1}. The plot of DIF is also shown in Figure 2.6.

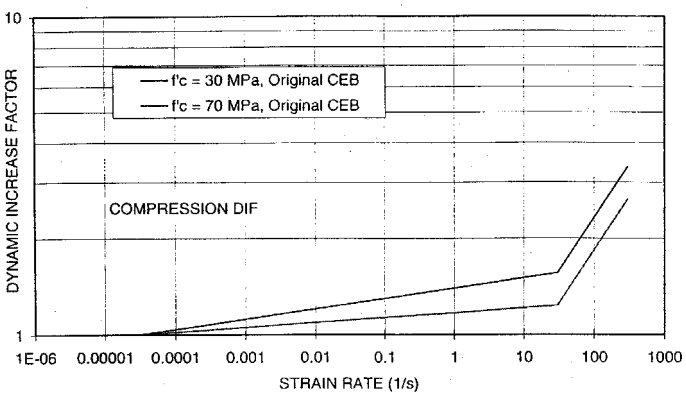

Concrete in compression

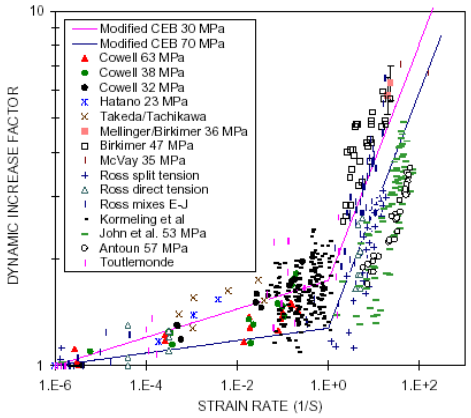

Concrete in tension

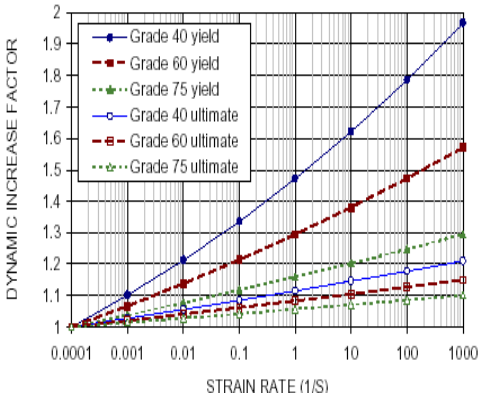

Reinforcement

Figure 2.6. DIFs for concrete and reinforcement [M1, M2]

To integrate Equations (2.3) ~ (2.5) into the analysis, the user subroutine USDFLD is used which allows the user to define the field variable at a material point as a function of any of available material point quantities. Thus by taking the strain rate as a field variable, the strain rate-dependent material properties can be introduced in the analysis since such properties can be easily defined as functions of the strain rate with Equations (2.3) ~ (2.5).

2.4.3 Analysis steps and loadings

In the simulation of the structural blast responses, two steps of analyses are carried out according to different loading stages. Before the occurrence of an explosion, the service loads have been already imposed on the structure. The intensity and distribution of the stresses and strains induced by the service loads will influence the structural behaviours under blast conditions. Thus nonlinear static analysis is performed priorly for the three-dimensional sub-frame structure under service loads. The loads involved in this step include the live loads, the dead loads and the super imposed dead loads. The second step is the dynamic response simulation of frame structures loaded by blast pressures where the nonlinear dynamic analysis is performed. The functions of blast pressures on the structures are necessary in this step, which are discussed respectively as follows for the bare frame structure and the frame with exterior cladding panels.

For the frame structure with reinforced concrete exterior cladding panels, by taking the whole structure as a closed rectangular target, the blast force functions on the front, top and rear surfaces are evaluated with Appendix 1 as demonstrated in Figure 2.7. In this case, the reflected pressure dominates in the blast loadings on the front cladding panels while the blast pressures on the top and rear surfaces are composed of the incident overpressure and dynamic pressure. As for the bare frame structure, the planar wave enters the structure loading each exposed columns, thus by taking each column as a closed rectangular target, the functions of blast forces on its front and rear faces are obtained according to Appendix 1 and the results within blast conditions I and II mentioned above are shown in Figure 2.8 where the shadow area stands for the net blast pressure on each column. It is demonstrated that due to the relatively small dimension of the column width, the reflected pressure decays rapidly and the drag force correlated with dynamic pressure plays a much important role in the net blast loadings on the columns. With the columns becoming further away from the explosive source, the peak pressure lessens while the lag time rises up. The increase of the explosive weight at the same standoff distance leads to the rise of the peak pressure while some decline in the duration.

Comparison of Figure 2.8a with Figure 2.7 indicates that there are obvious differences in the spatial distribution as well as the time history for blast loadings acting on the structures with/without exterior cladding panels.

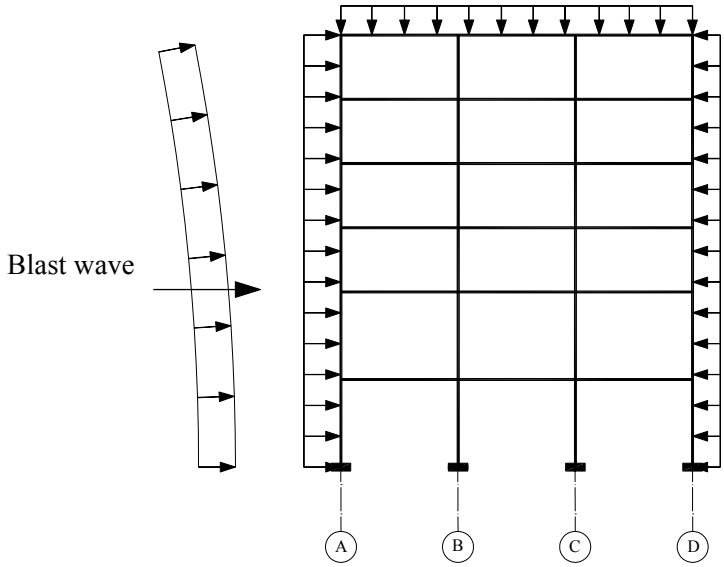

(a). Blast wave on the frame structure with exterior cladding panels

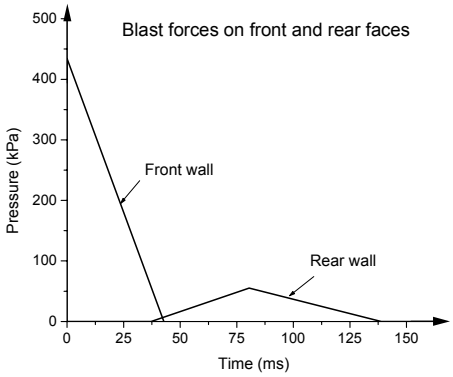

(b). Loads on the front and rear faces

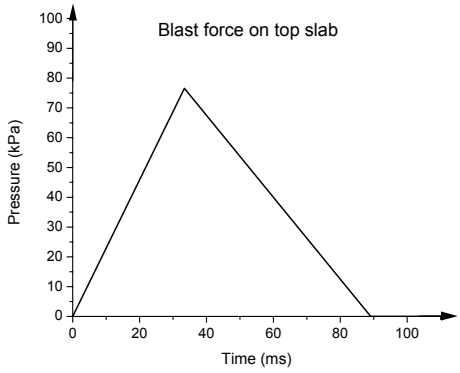

(c). Loads on the roof slabs

Figure 2.7 Blast loadings on the frame structure with exterior cladding panels under condition I

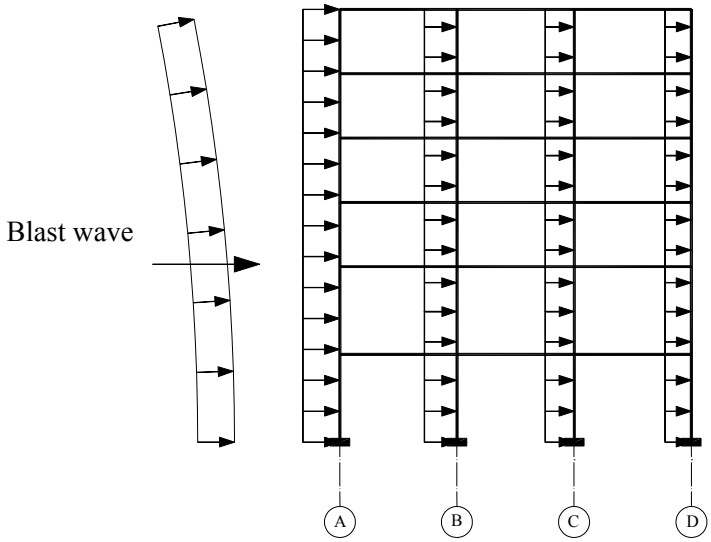

Blast wave on the bare frame structure

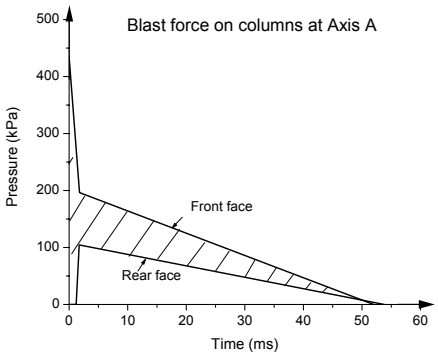

Loading on columns at Axis A

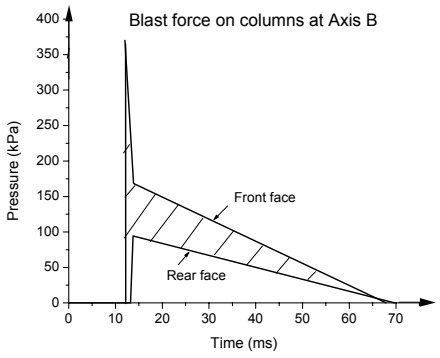

Loading on columns at Axis B

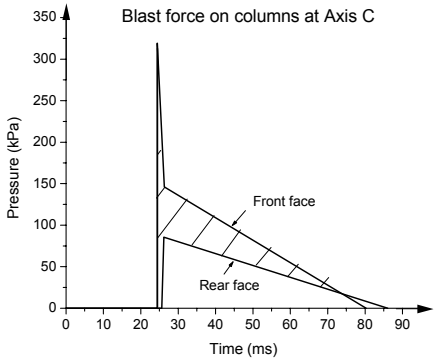

Loading on columns at Axis C

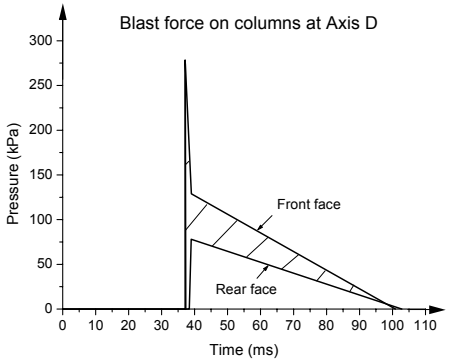

Loading on columns at Axis D

(a): Under blast condition I

Figure 2.8 Blast loadings on the bare frame structure under conditions I and II

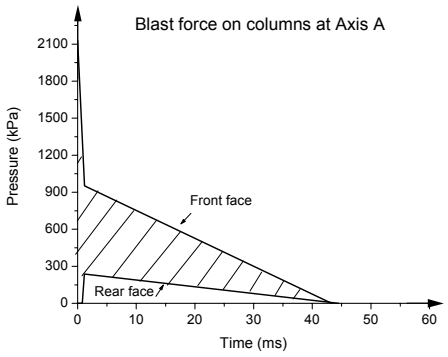

Loading on columns at Axis A

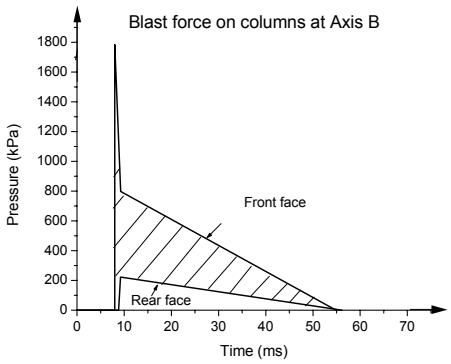

Loading on columns at Axis B

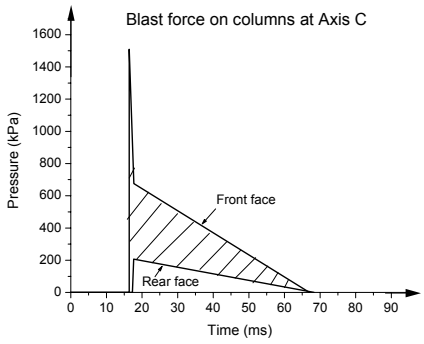

Loading on columns at Axis C

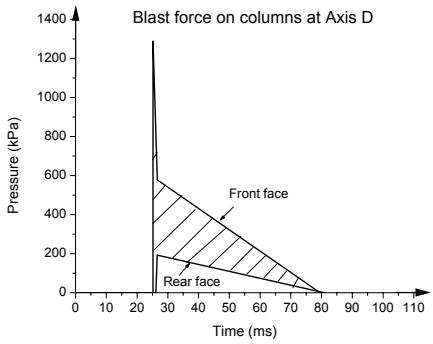

Loading on columns at Axis D

(b): Under blast condition II

Figure 2.8 (Continued)

2.4.4 Integration method

A general implicit dynamic integration method is employed to solve the nonlinear dynamic problems. In order to ensure the accuracy of the numerical solutions with this method, an automatic incrementation scheme is adopted to calculate the length of each time increment through a half-step residual control, where the half-step residual is the equilibrium residual error (out-of-balance forces) halfway through a time increment. The acceptable half-step residual tolerance is specified by the HAFTOL option in ABAQUS [A1], which has dimensions of force and is usually chosen by comparison with typical actual force values such as applied forces; in this investigation it is taken to be nearly approximate to the maximum blast pressure

applied to the structure. Such an action will lead to a highly accurate solution for a problem including plasticity. This automatic incrementation scheme is especially effective for the case where a sudden blast event initiates a dynamic problem and the structural response involves large amounts of energy being dissipated by plasticity effects. In such a case small time increments will be required immediately after the sudden blast event, while at later time the response can be modelled accurately with large time increments. Moreover in order to limit the range of each time step in the numerical simulations, a minimum and a maximum allowable time increment are taken as 1×10^{-7} s and 0.01 s, respectively.

2.5 Verification of Finite Element Models

The verification of the finite element models as mentioned above is carried out by implementing it into the analysis of a simply supported beam subjected to blast loadings tested by Seabold [S3] and a square slab, clamped and longitudinally restrained along all edges exposed to uniform lateral pressure tested by Keennan [K3]. The computed and experimental displacement-time histories at the mid-span for the beam and the centre of the slab are compared in Figure 2.9.

It can be observed from Figure 2.9 that for the simply supported beam the peak experimental response of 28.5 mm was recorded at 19.5 ms, which agrees well with the analytical results for which the computed peak displacement of 28.8 mm is reached at 19.2 ms. The recorded permanent deformation of this beam was 20.8 mm and it also compared well with the predicted deflection of 21.7 mm. As for the reinforced concrete slab, the maximum deflection at the centre recorded in the experiment was 12.0mm appearing at time 7.4 ms, which is fairly close to the numerically predicted one of 11.9 mm at 7.2 ms. In addition, the analytical and experimental results of top compressive strain history of concrete, strain history of main reinforcement, support reaction history, and mid-span velocity history of RC structural member are also compared in Figure 2.9. It is demonstrated that the numerical analysis reasonably agrees with the observed experimental behaviours. Therefore the numerical model has the ability to simulate the failure process of

concrete and reinforcement, which are thus applied into the nonlinear analysis of the blast-loaded six-storey frame structures in Figures 2.7 and 2.8.

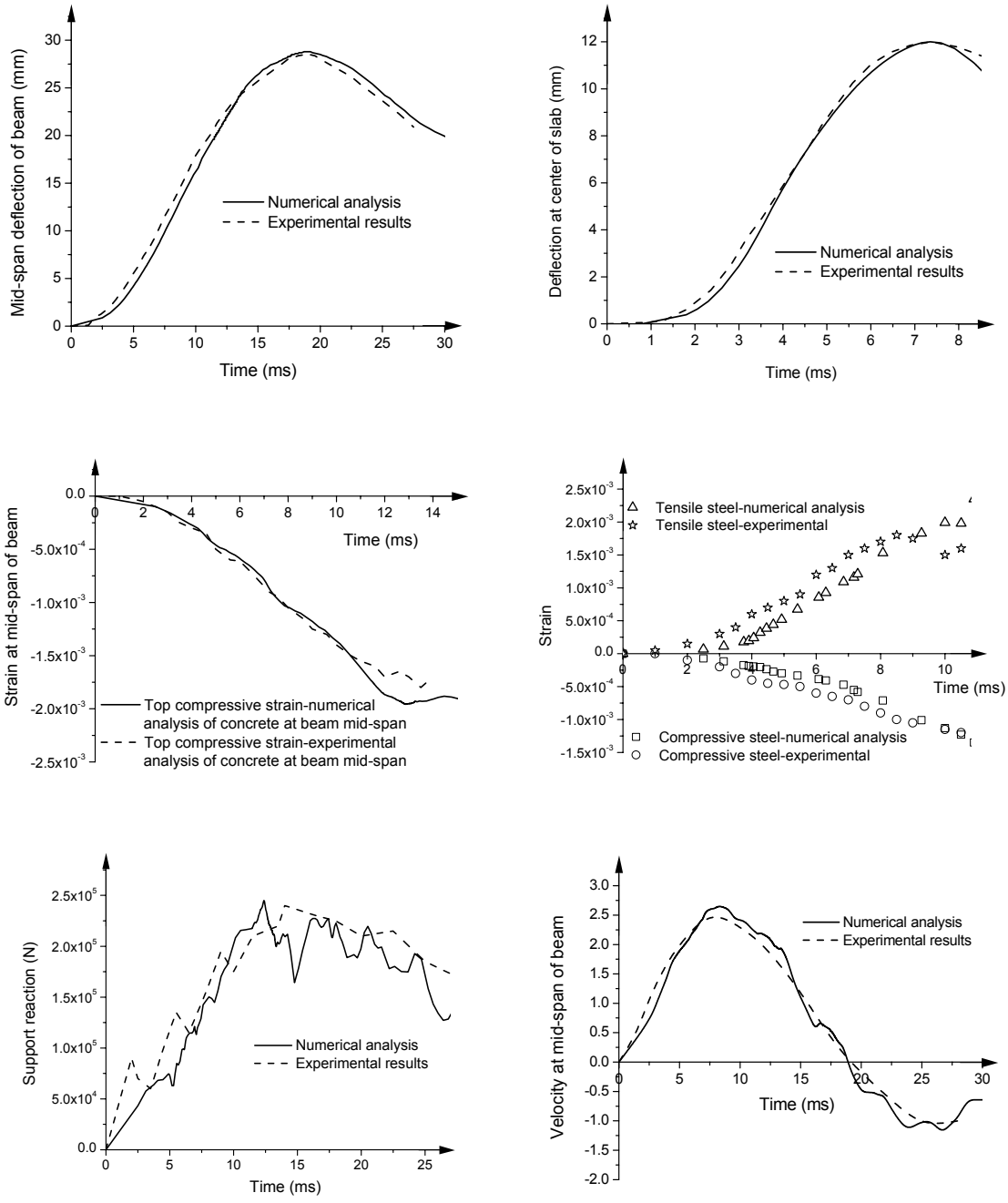

Figure 2.9 Verifications of finite element models by comparison of the numerical results with the experimental ones

2.6 Numerical Results and Discussion

With the finite element models described above, three numerical case studies are carried out to evaluate the dynamic responses and damage distributions of the designed six-storey reinforced concrete frame structure with/without exterior cladding panels under blast conditions I and II with the results respectively discussed in the following.

2.6.1 First case study: frame structure with exterior cladding panels under blast condition I

2.6.1.1 A general view of structural responses

In order to obtain a general view of the dynamic responses of the six-storey frame structure with reinforced concrete exterior cladding panels under the considered blast condition I, its energy responses including the kinetic energy and the plastic strain energy are plotted in Figures 2.10 and 2.11. In these figures, the symbols of KE_{ws} and PE_{ws} are respectively the kinetic energy and plastic strain energy within the whole structure; KE_{bm} and PE_{bm} represent these two kinds of energy within the critical blast-loaded members (including the front exterior cladding panels and columns, the top-storey beams and roof slabs) while KE_{om} and PE_{om} stand for the kinetic energy and plastic strain energy within other structural members.

From Figure 2.10, it can be observed that from 0 ms to 30 ms, KE_{bm} composes the most significant part of KE_{ws} covering averagely about 85% of it, which reflects the predominant role of the localized responses of the critical blast-loaded members in the structural responses during this time. Later, the ratio of KE_{bm} / KE_{ws} decreases rapidly to a value of near 23% at about 50 ms while further it keeps almost constant. This constancy after 50 ms demonstrates that the dynamic response of the structure is in a mode where the global response of the structural system as a whole dominates. As a consequence, the whole dynamic responses of the structure can be divided into two stages at an approximate time of 40 ms as shown in Figure 2.10b.

Within response stage I, the dynamic responses are concentrated on several critical blast-loaded members while as the time goes by, more structural members are motivated and the structural global responses become much more obvious at response stage II.

The plastic strain energy response of the structure shows the same stage division as that demonstrated in Figure 2.11b where the ratio of PE_{bm} / PE_{ws} versus time is plotted. PE_{bm} accounts for almost all of PE_{ws} during the time of 40 ms, however with the global response of the structure motivated later, more plastic deformation occurs on the members other than the critical blast-loaded ones and thus the ratio of PE_{bm} / PE_{ws} declines. A more detailed description of the structure responses and its damage propagation with time will be made in the following sections according to the divided two response stages.

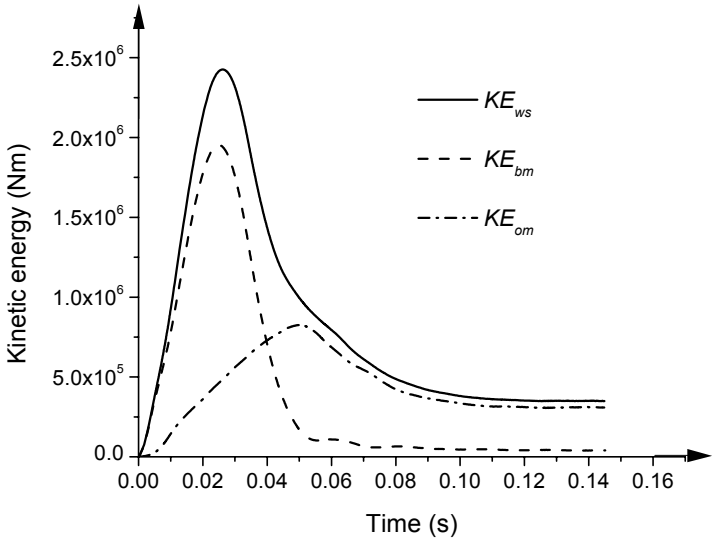

(a). Kinetic energy versus time for various structural members

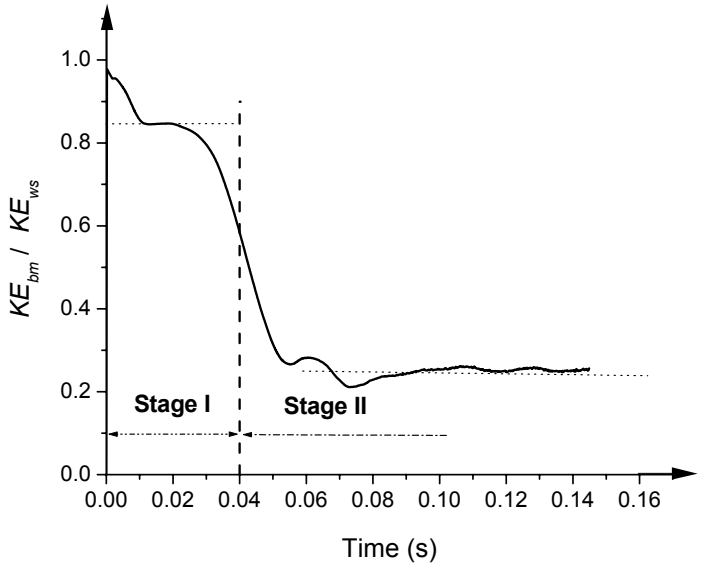

(b). Ratio of KE_{bm} / KE_{ws} versus time

Figure 2.10 Response of the kinetic energy (First case study)

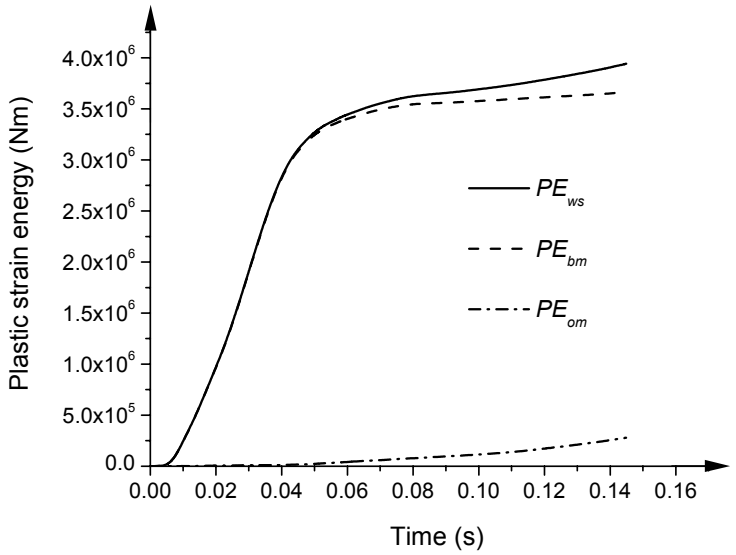

(a). Plastic strain energy versus time for various structural members

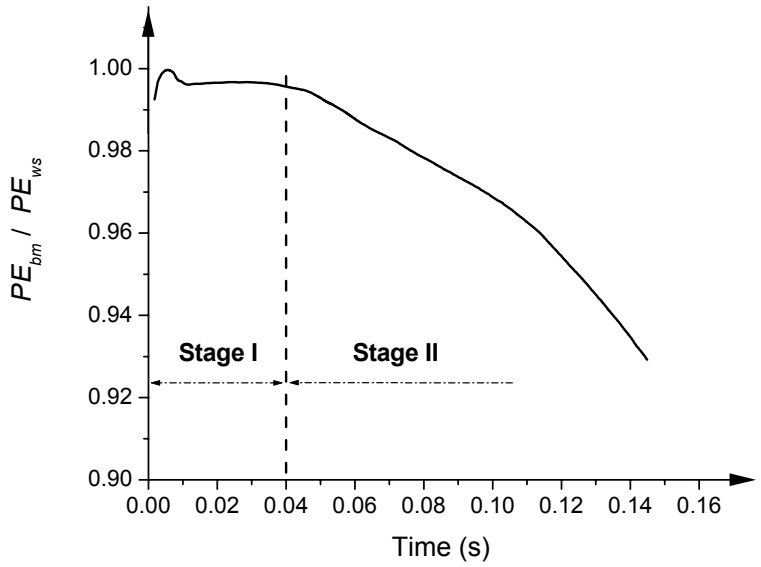

(b). Ratio of PE_{bm} / PE_{ws} versus time

Figure 2.11 Response of the plastic strain energy (First case study)

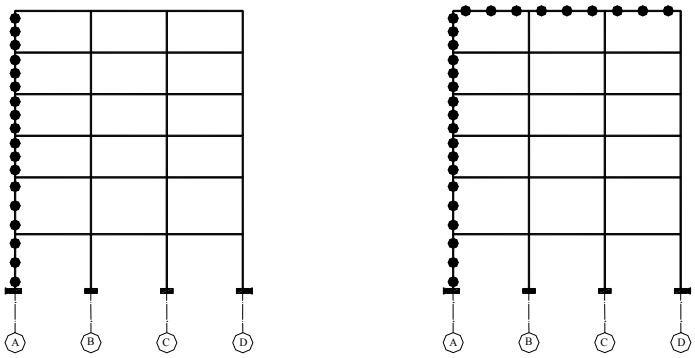

MIDR= 0.12% MIDR= 0.67%

t = 15 ms t = 40 ms

Response stage I

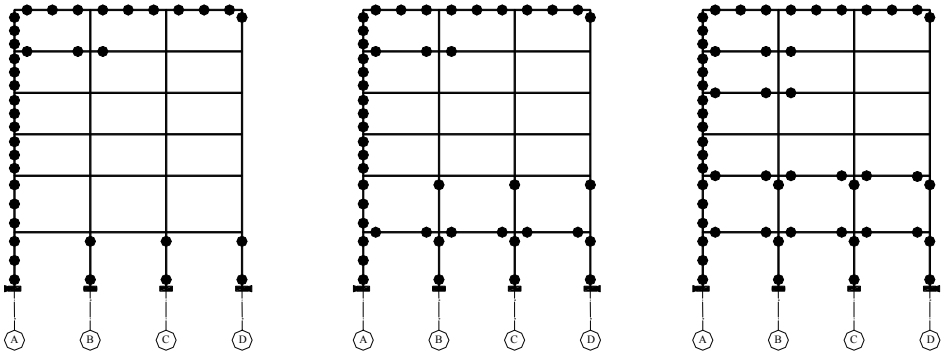

MIDR= 1.20% MIDR= 2.13% MIDR= 2.88%

t = 60 ms t = 100 ms t = 180 ms

Response stage II

Figure 2.12 Damage propagation with time (First case study)

2.6.1.2 Response stage I

Since at response stage I, both kinetic energy and plastic strain energy responses are concentrated on the critical blast-loaded members, special attention is laid on their dynamic responses and corresponding damage with the plastic hinges distributions

plotted in Figure 2.12. A flexural plastic hinge is assumed to initiate when the longitudinal tensile reinforcement first yields at a point along the beam element and the hinge will continue to spread over a continuous portion of the beam. Thus the occurrence time of the hinge corresponds with the first appearance of plastic strain of reinforcement whose variation with time can be found from the numerical analysis in ABAQUS [A1].

It is observed that due to the intensive localized responses on these members induced by the blast loadings during this stage, three plastic hinges have been formed on the bottom, mid-height and top sections for the front columns at 15 ms as well as the left end, mid-span and right end sections for the top-storey beams at 40 ms; this results in a typical damage mechanism similar to that on the flexural structural members. The difference between the time of forming this damage mechanism on the front columns and top-storey beams is caused by the difference of the time when the peak blast pressures acting on them is reached. As for the other frame members (beams and columns), almost no plastic deformation is present.

The flexural deformation plays a relatively important role on the dynamic responses of structural members under this distant blast condition as indicated in Figure 2.13, where typical moment-curvature and shear force-shear strain curves for different cross sections of the first-storey, fourth-storey and top-storey columns at Axis A as well as the top-storey beam between Axis B and Axis C are plotted. It can be seen that there exist linear relationships between the shear forces and the shear strains for these cross sections while all the irrecoverable deformation is induced by their curvature responses. These phenomena are reflected on the cross sectional responses of other structural members as well.

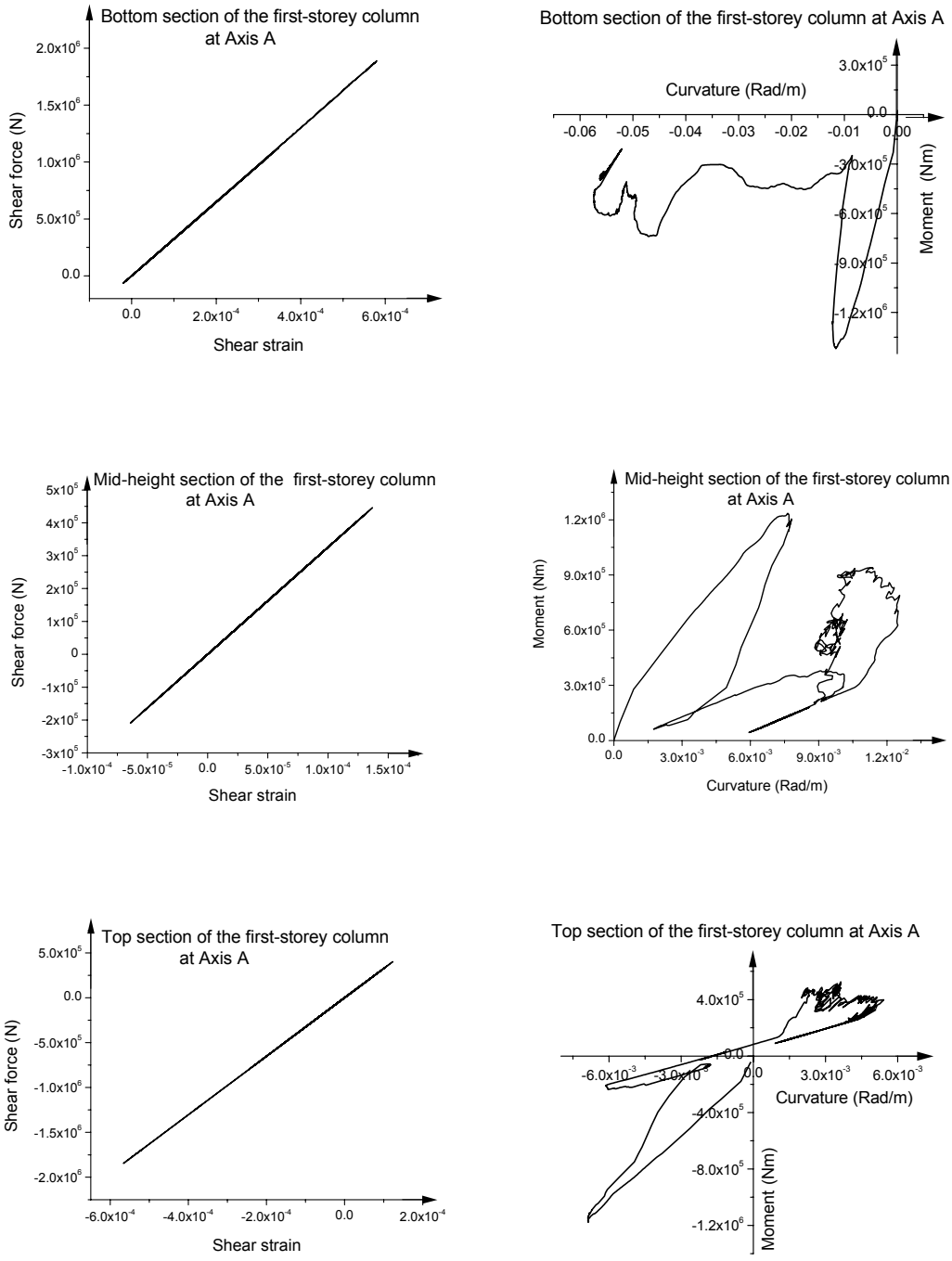

(a). Flexural and shear responses of the first-storey column at Axis A

Figure 2.13 Responses of some critical blast-loaded members (First case study)

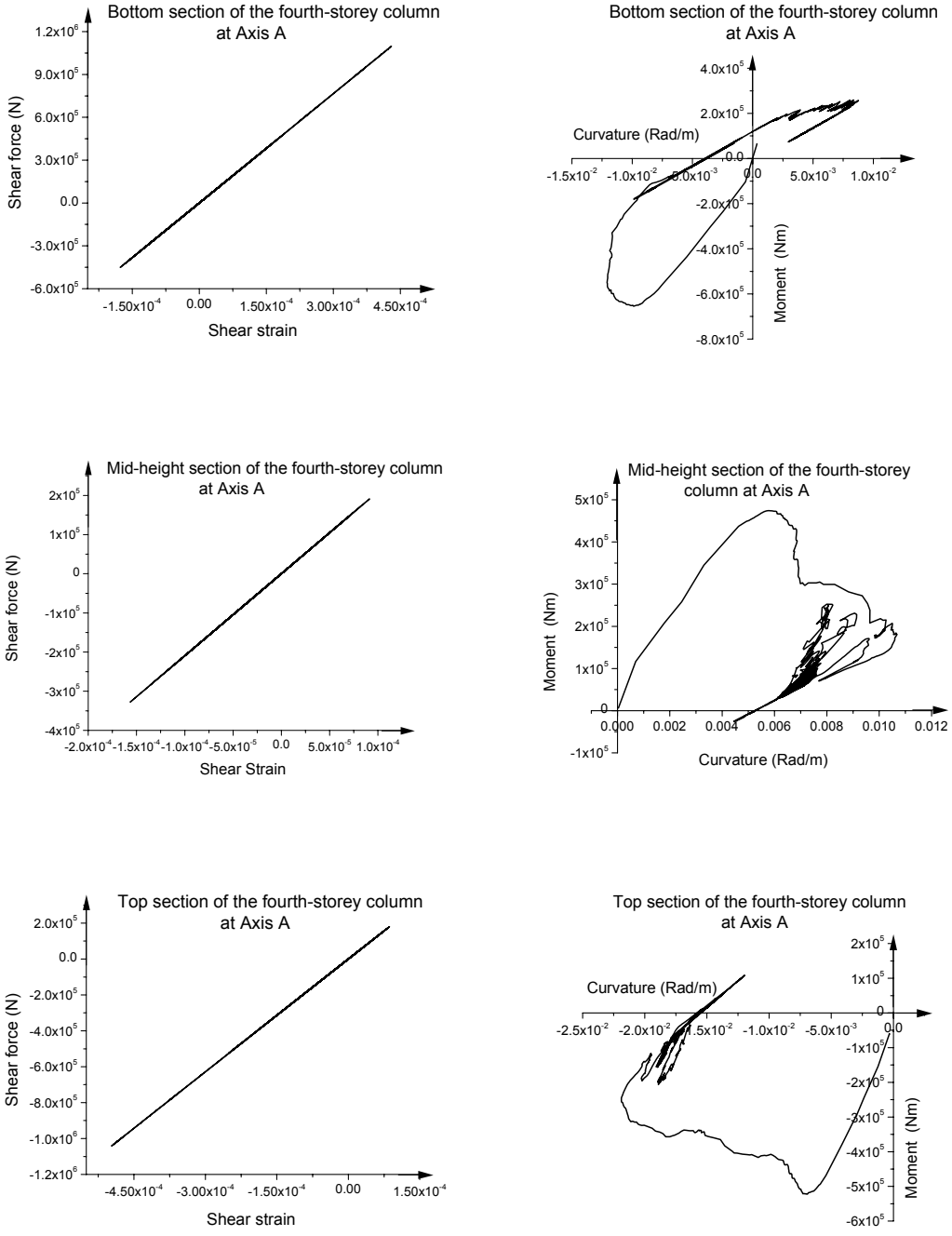

(b). Flexural and shear responses of the fourth-storey column at Axis A

Figure 2.13 (Continued)

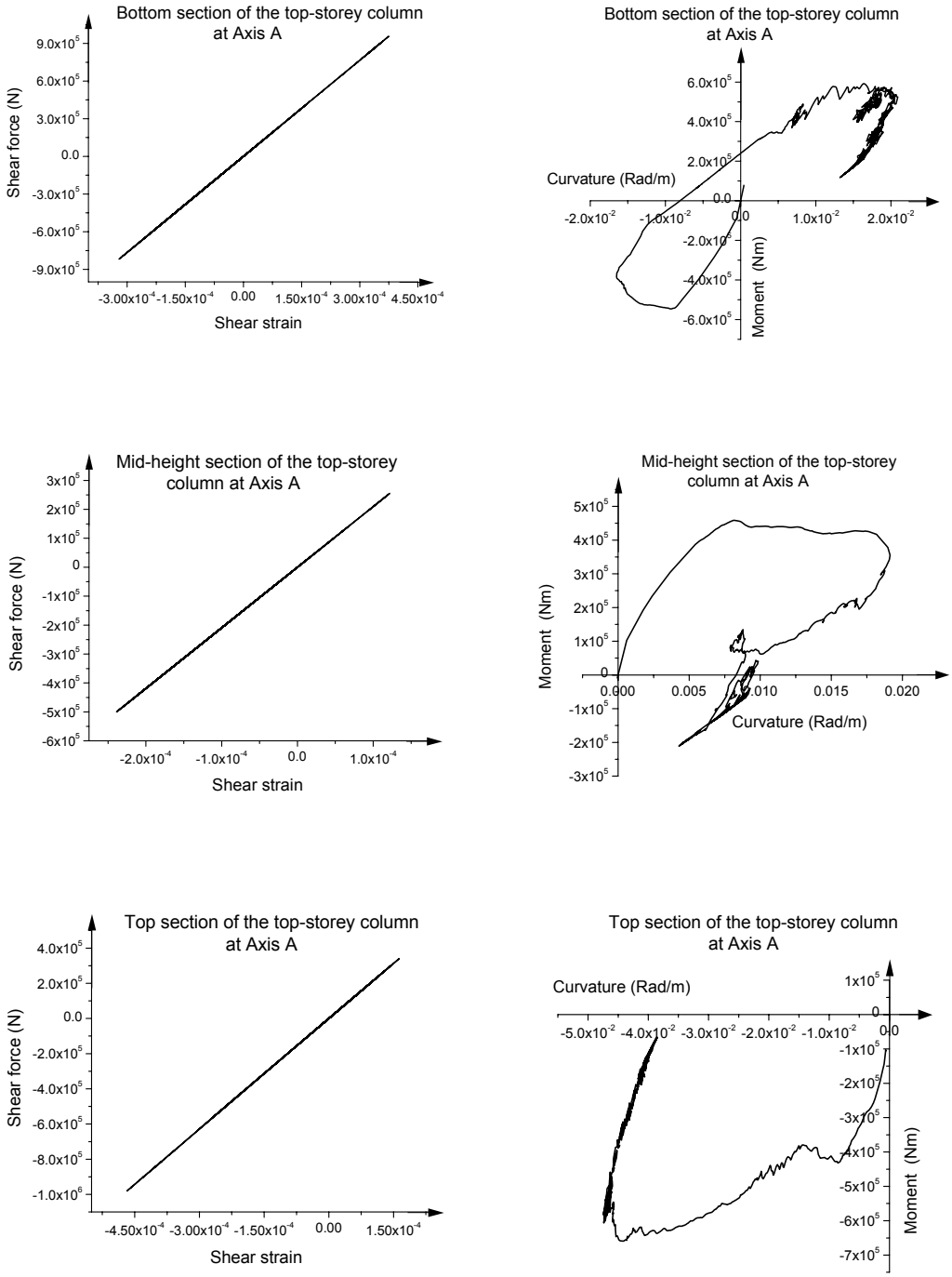

(c). Flexural and shear responses of the top-storey column at Axis A

Figure 2.13 (Continued)

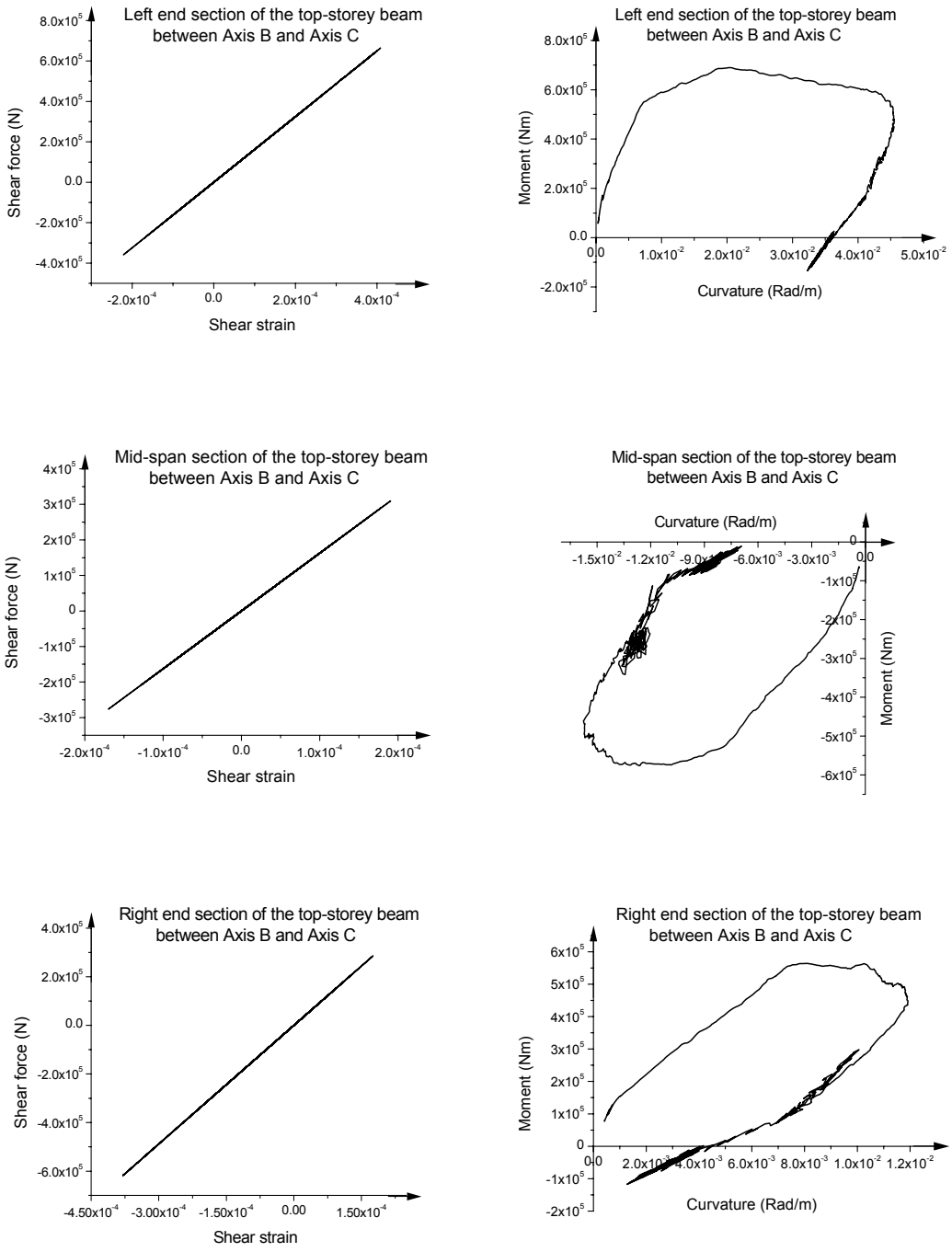

(d). Flexural and shear responses of the top- storey beam between Axis B and Axis C

Figure 2.13 (Continued)

Due to the direct action of the blast loadings on them as well as their large area to receive the blast loadings during response stage I, the responses of the front exterior cladding panels are significantly severe as illustrated in Figure 2.14. The lateral deformation at the centre of the first-storey exterior cladding panel has reached 653 mm at the end of response stage I, which is approximately equivalent to a support rotation of 16.5^{o}. According to the actual resistance deflection function presented in TM5-1300 [T2], the resistance due to the tensile membrane action produced under the continuous reinforcement conditions well as adequate lateral constraint, increases with increasing deflection up to incipient failure at approximately 12^{o} support rotation. Based on this, the cladding panel is almost in a failure state at the end of response stage I.

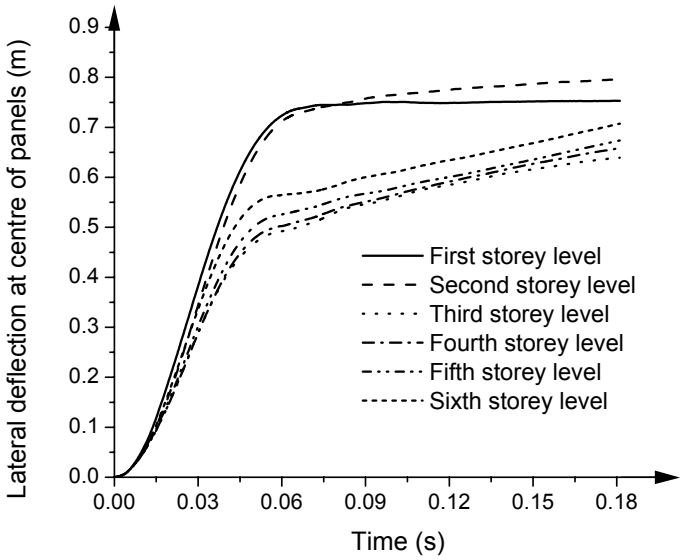

Figure 2.14 Lateral deflection of the front cladding panels (First case study)

As for the global responses of the structural system, the storey lateral displacement (storey drift) responses are plotted in Figure 2.15a. It is indicated that all floor levels have the similar drifts (about 30 mm) at the time of 40 ms, except for the roof whose drift is somewhat smaller, therefore a concentrated maximum inter-storey drift ratio (MIDR), the ratio of maximum inter-storey drift (the drift difference between adjacent storeys) to the inter-storey height, is 0.67% occurring at the first

storey. The contour of the storey drifts for the structure at this time location can be found in Figure 2.15b.

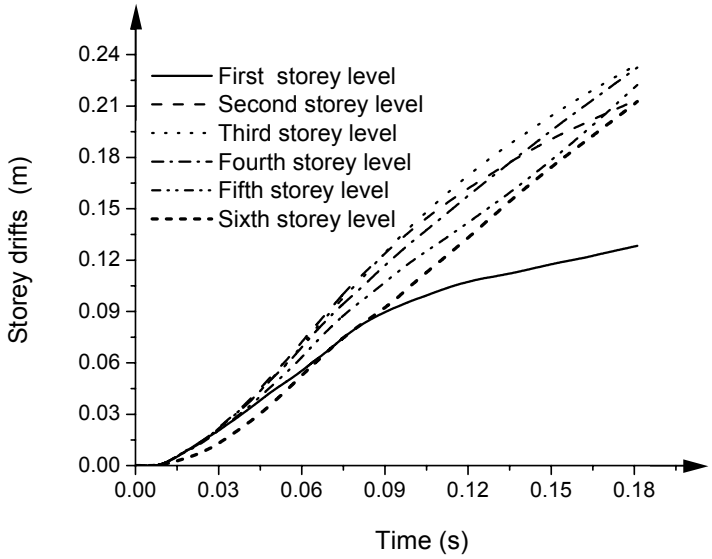

(a). Storey drift responses

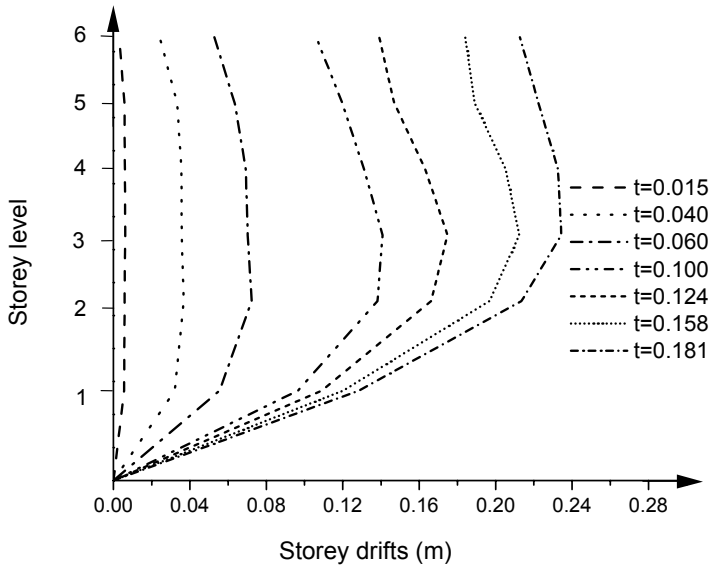

(b). Contour of the storey drifts at different time stations

Figure 2.15 Storey drifts for the structure (First case study)

2.6.1.3 Response stage II

At response stage II, the structural dynamic response is in a mode where the global response of the structural system as a whole dominates, hence the distribution of damage as well as its propagation with time is in a different manner with those at response stage I. As shown in Figure 2.12, during response stage II, plastic hinges are formed firstly on both end sections of the first-storey columns at a time of about 60 ms as the inter-storey drift within this storey increases. Later, damage spreads upward with more plastic hinges successively formed on those connected cross sections around the joints located in the first and second floor levels. Since the plastic hinges formed at this stage are caused by large global sideway responses, they appear only at the end sections of structural members.

To gain a better understanding of structural global responses, the storey drift distributions with time for this frame structure under blast condition I are demonstrated in Figures 2.15. It can be seen that during the time up to 80 ms the structural global responses are obviously concentrated within the first storey while the inter-storey drifts within other storey levels are trivial. As the time lengthens, the increase gradient for the first-storey drift drops to a relatively small value and the structural global response begins to focus on the second-storey level. The structural maximum inter-storey drifts within the two critical storey levels (the first and the second storeys) have reached 129 mm and 85 mm, which are equivalent to a MIDR of 2.88 % and 1.90 % respectively at the time of 180 ms. Referring to Table 2.1 where a global damage criteria based on the inter-storey drift ratio for a frame structure under blast conditions have been suggested in the reference [B4], the frame structure at time 180 ms is damaged to a high level.

Table 2.1 Three response levels [B4]

Response level	Inter-storey drift ratio	Damage description
low	1/50	localized building/component damage
medium	1/35	widespread building/component damage
high	1/25	building/component losing structural integrity and having possibility of collapse due to environment condition

From the structural global responses significantly concentrated in the first and second-storey levels at the time of 180 ms, it can be deduced that plastic rotations of the joints distributed in the first and second floor levels are focused on those cross sections at the ends of the connected columns and beams as shown in Figure 2.12. Typical moment-curvature and shear force-shear strain curves for these cross sections where plastic hinges are formed at response stage II are plotted in Figure 2.16. It is clear that plastic deformation is induced by their flexural responses where irrecoverable curvatures appear at the end sections of the members.

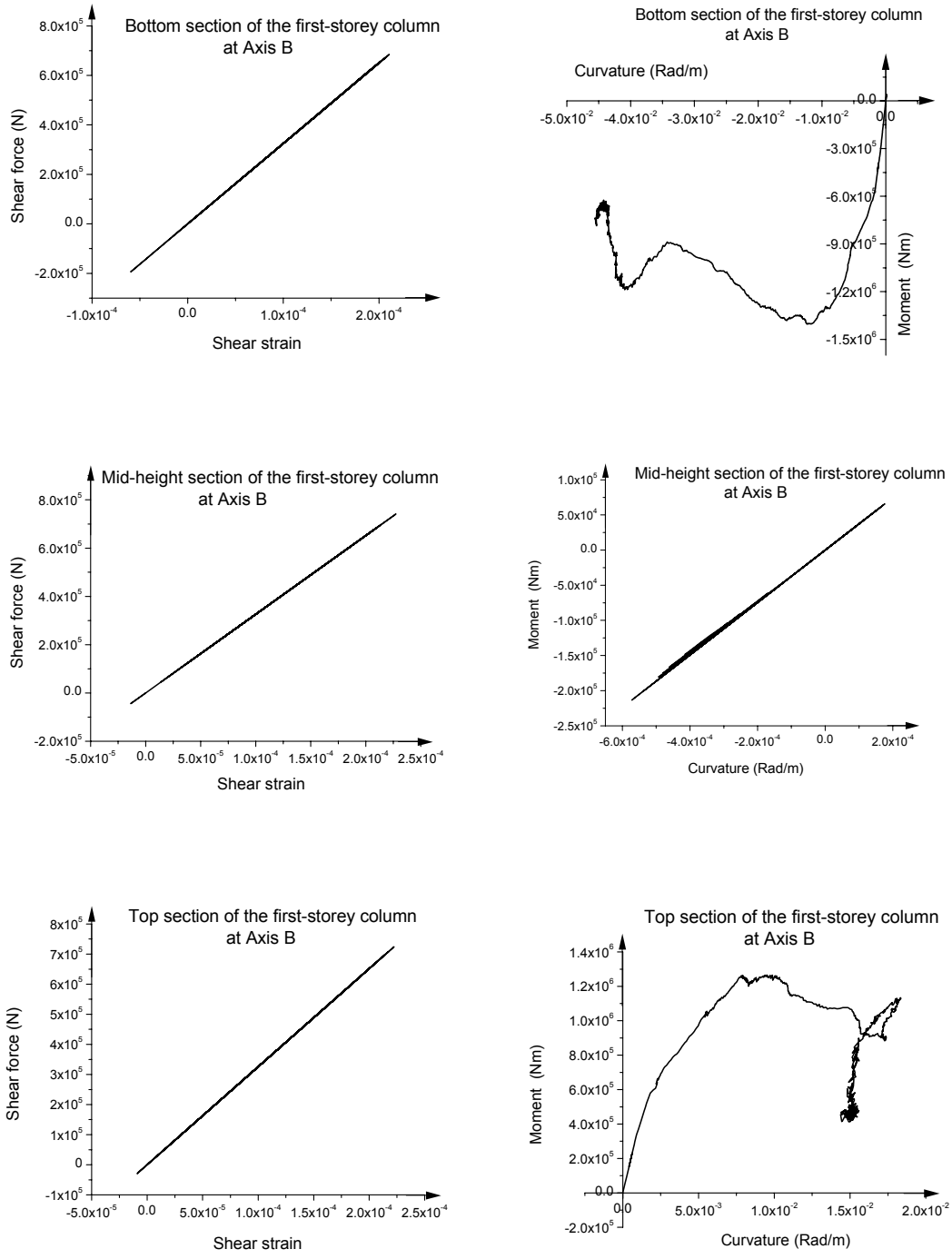

(a). Flexural and shear responses of the first-storey column at Axis B

Figure 2.16 Responses of some structural members other than blast-loaded ones (First case study)

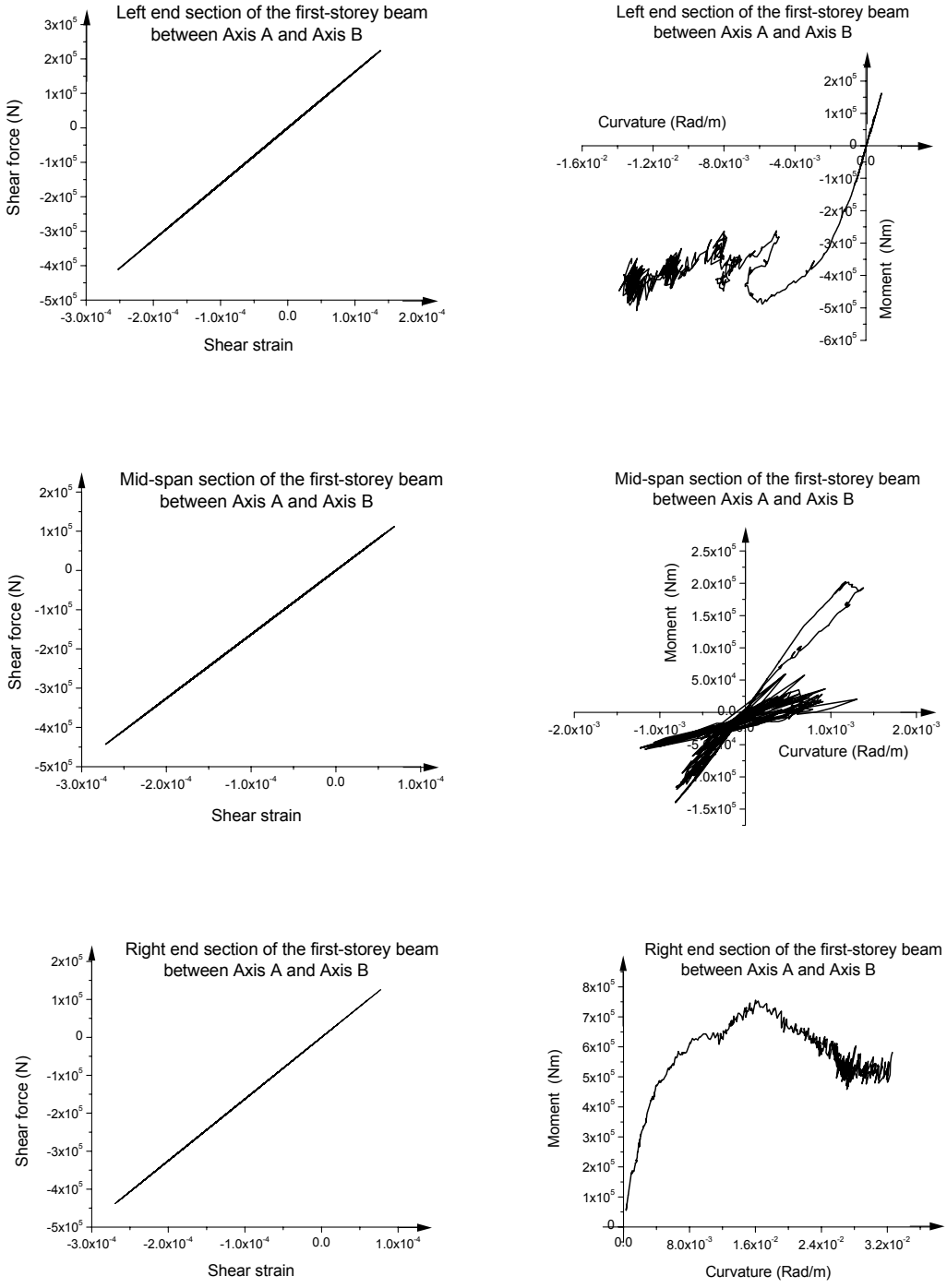

(b). Flexural and shear responses of the first-storey beam between Axis A and Axis B

Figure 2.16 (Continued)

2.6.2 Second case study: bare frame structure under blast condition I

The numerical simulation results of the energy responses for the six-storey bare frame structure under blast condition I are presented in Figure 2.17. It can be seen that due to the absence of the exterior cladding panels, this bare frame will experience much slighter dynamic responses when compared with the first case study. Therefore much less damage is induced as shown in Figure 2.17b where only a small magnitude of 1.0 kNm of plastic energy appears on the floor slabs. As for the frame members (columns and beams), there is no plastic deformation on them.

The responses of structural storey drift plotted in Figure 2.18a demonstrate that the maximum inter-storey drift, which happens to the second-storey level, is only about 9.5 mm, equivalent to a MIDR of 0.21%. The MIDRs within other storey levels are smaller than this value and thus there is no global damage to the structure under this blast condition [S4]. In addition, from the storey drift contours at different time stations shown in Figure 2.18b, it is obvious that the maximum storey drift occurs firstly at the first storey whereas with the lengthening of time, it will move upwardly to the second storey and third storey until it is present on the top storey in sequence. Thus a transverse wave is formed in the frame structure.

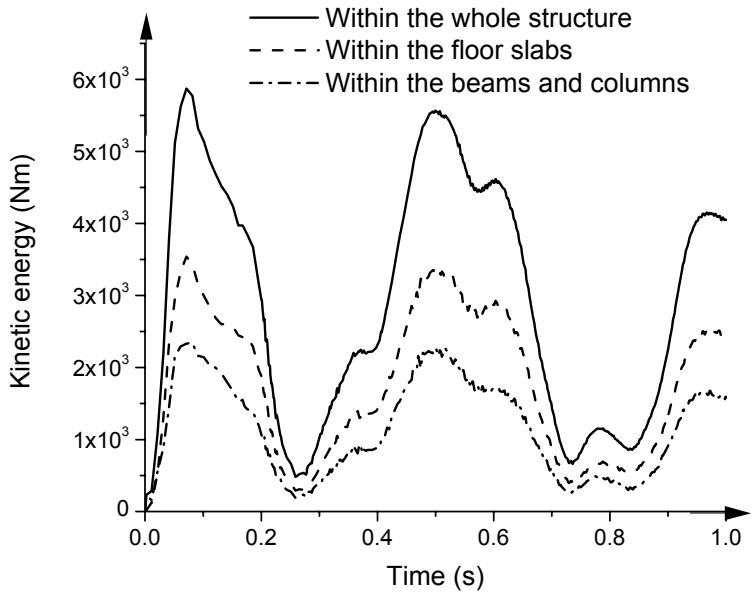

(a). Kinetic energy versus time for various structural members

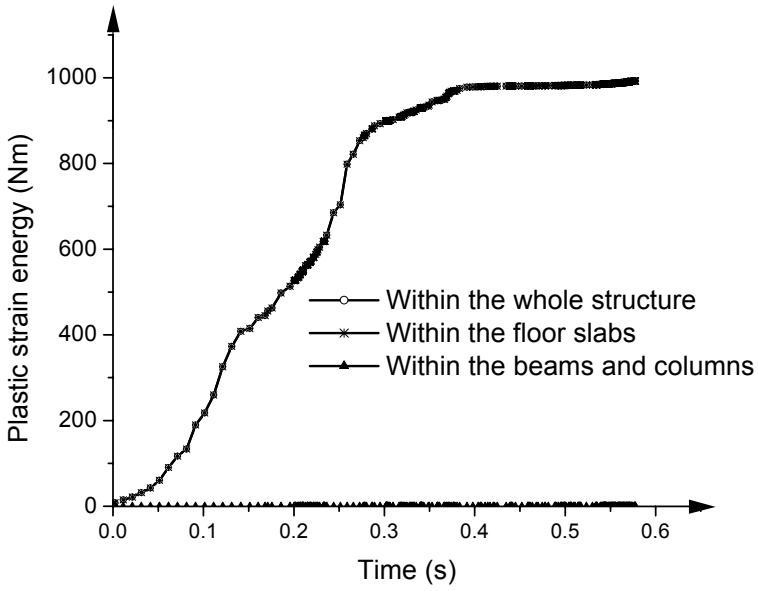

(b). Plastic strain energy versus time for various structural members

Figure 2.17 Responses of the kinetic energy and plastic strain energy (Second case study)

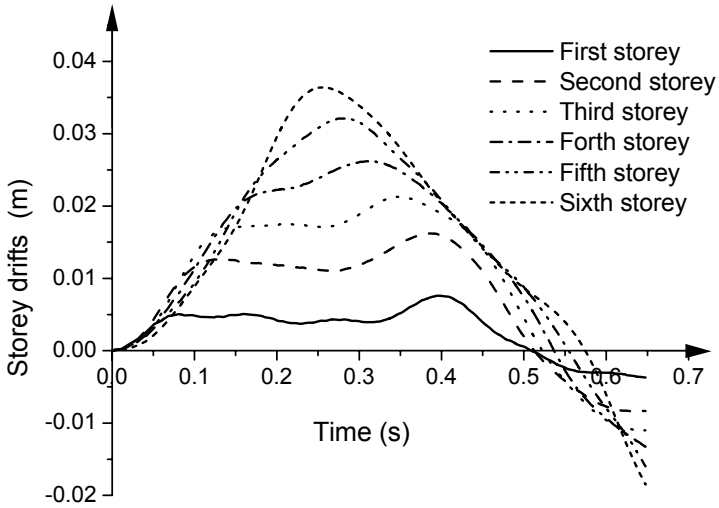

(a) Storey drift responses

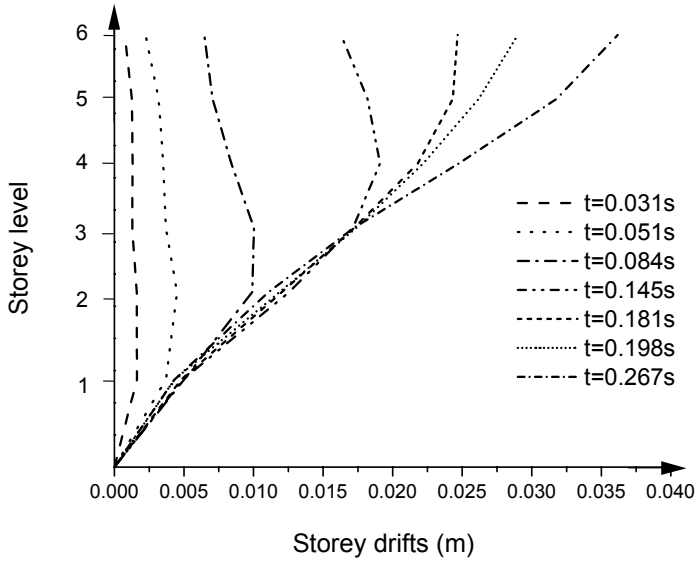

(b) Contour of the storey drifts at different time stations

Figure 2.18 Storey drifts for the structure (Second case study)

2.6.3 Third case study: bare frame structure under blast condition II

2.6.3.1 A general view of structural responses

In order to further study the behaviours of the bare frame structure without exterior cladding panels under a more severe distant blast condition as well as the corresponding damage distributions, the numerical analysis of the bare six-storey frame structure under blast condition II with a 250 ton equivalent TNT at a 100 m distance is performed as well. The energy responses are plotted in Figures 2.19 and 2.20 where three sets of symbols of KE_{ws} and PE_{ws}, KE_{bm} and PE_{bm}, KE_{om} and PE_{om} represent the kinetic energy and plastic strain energy within the whole structure, the critical blast-loaded members including all columns, and the other structural members respectively.

From the kinetic energy responses in Figure 2.19, it is indicated that KE_{bm} composes the most part of KE_{ws} at the start of the response stage. The ratio of KE_{bm} / KE_{ws} then decreases dramatically up to a later time of about 20ms, after which it keeps almost constant with a slight high frequency vibration. Therefore, similar to the first case study, the whole dynamic response process of the bare frame structure in this blast condition can be approximately divided into two stages at about 10 ms. At response stage I, the dynamic responses are greatly localized on the blast loaded frame columns while the global responses of the structure become dominant at response stage II. However none of the plastic strain energy is developed during response stage I, as indicated from the plastic strain energy responses within various structural members in Figure 2.20. At response stage II, the plastic strain energy occurs initially on some structural columns (PE_{bm} / PE_{ws} nearly unit) but later they spread over other members with PE_{bm} occupying only about 23% of PE_{ws} after 600 ms, The detailed dynamic responses of the bare frame structure and damage distributions at each stage are described in the following.

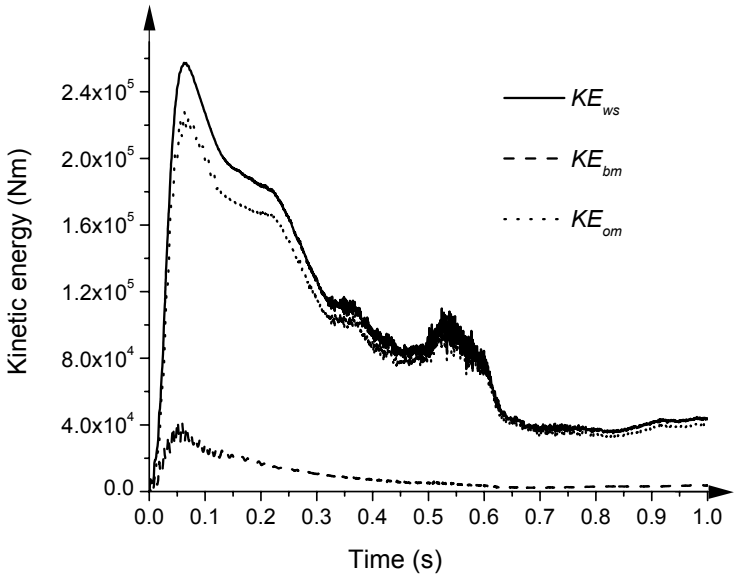

(a). Kinetic energy versus time for various structural members

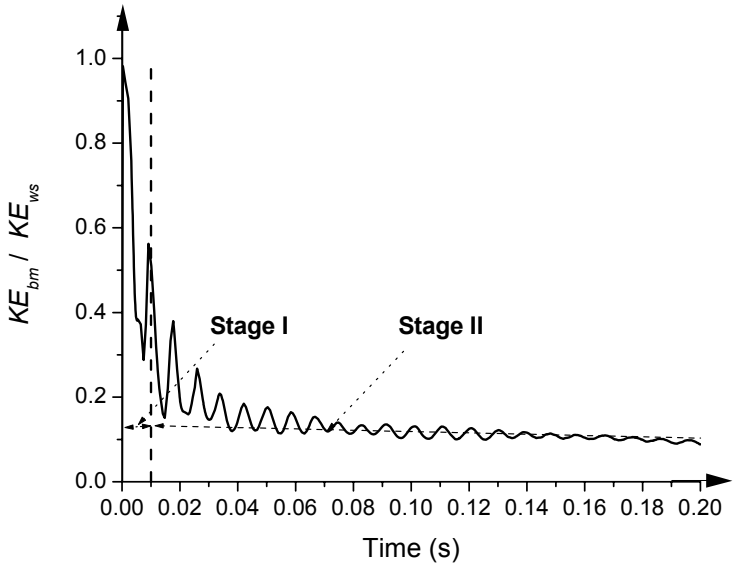

(b). Ratio of KE_{bm} / KE_{ws} versus time

Figure 2.19 Response of the kinetic energy (Third case study)

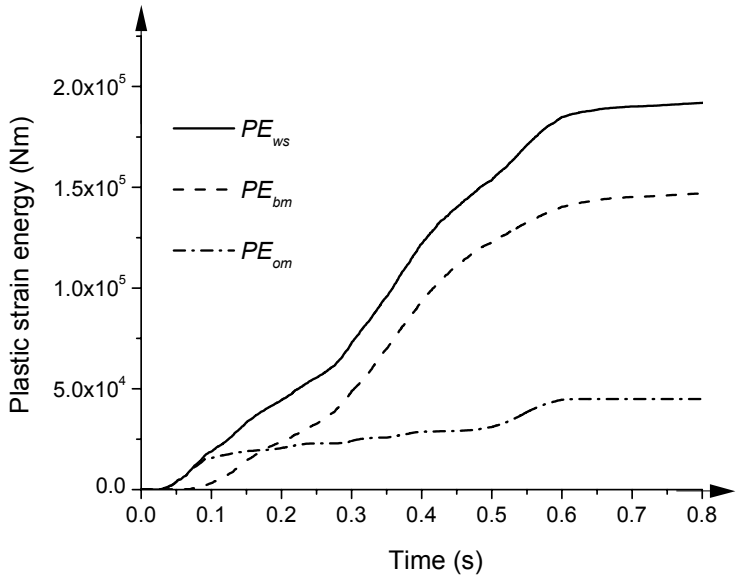

(a). Plastic strain energy versus time for various structural members

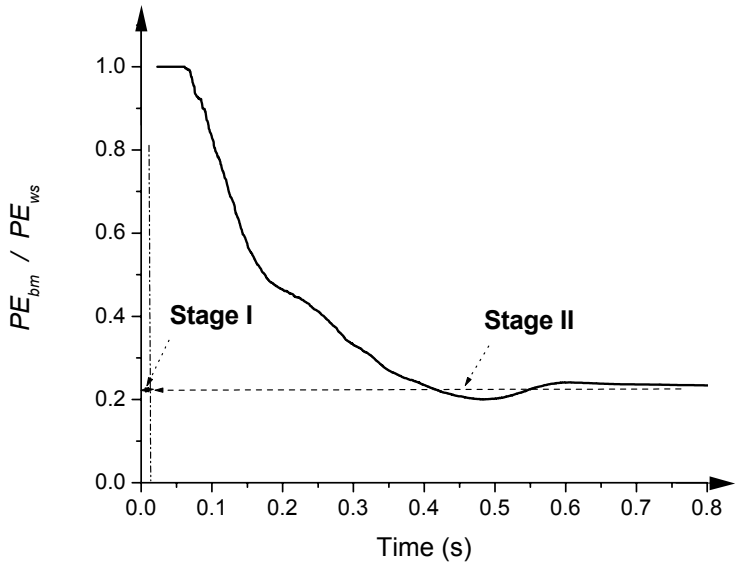

(b). Ratio of PE_{bm} / PE_{ws} versus time

Figure 2.20 Response of the plastic strain energy (Third case study)

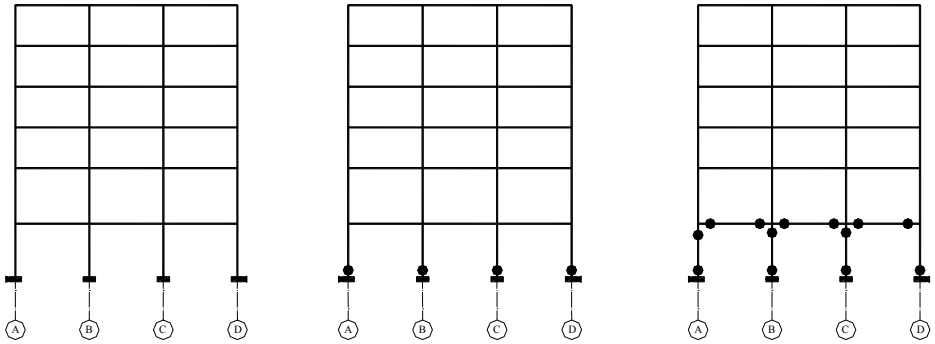

MIDR= 0.12% MIDR= 0.66% MIDR= 1.25%

t = 20 ms t = 50 ms t = 100 ms

Response stage I **Response stage II**

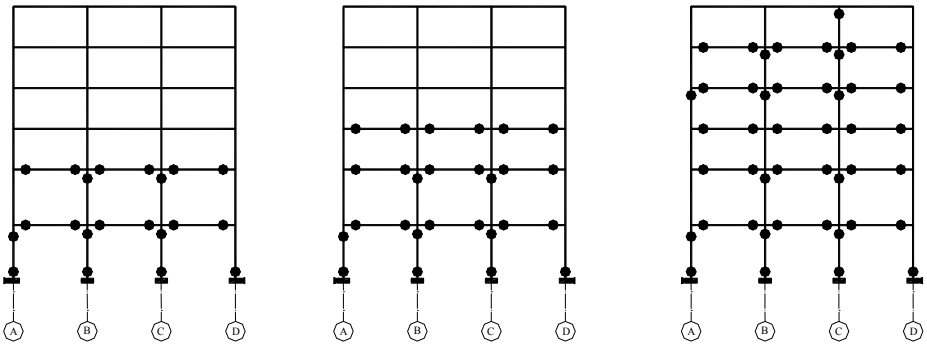

MIDR= 1.73% MIDR= 2.05% MIDR= 2.21%

t = 200 ms t = 300 ms t = 400 ms

Response stage II

Figure 2.21 Damage propagation with time (Third case study)

2.6.3.2 Response stage I

At response stage I, although the dynamic response is concentrated on the blast loaded structural columns, no any plastic strain energy is present in them.

Accordingly, no localized damage appears to the columns within this stage as shown in the Figure 2.21.

2.6.3.3 Response stage II

As the kinetic energy converts into the global responses of the bare frame structure as a whole at response stage II, plastic hinges appear firstly to the bottom sections of the first-storey columns and then as time passes, the plastic hinges tend to spread gradually upward to the cross sections of other frame members around the joints located in the upper floor levers. The process of this type of structural damage in this numerical case study is displayed in Figure 2.21.

Further studies of the dynamic responses of different cross sections are performed, where the typical shear force-shear strain and moment-curvature responses for some columns and beams are plotted in Figures 2.22. It shows the linear shear responses of these cross sections while the change of the moments with curvatures nonlinearly. Certain irrecoverable flexural responses can be observed to the end sections when unloading, which accounts for the inelastic storey drift of the whole structure.

The developments of the plastic hinges at response stage II also indicate that the global damage of the bare frame structure has a tendency to disperse from the bottom storey levels to the upper storey levels. In accordance with this, significant storey drift responses will be activated. This can be further observed in Figure 2.23 where the storey drift responses and the corresponding contours at a variety of time stations are plotted. Similar to the second case study, a transverse wave is present with the maximum storey drift travelling from the bottom to the top. The maximum inter-storey drift occurs in the second-storey that is 0.123m equivalent to 2.77% of MIDR. According to Table 2.1, the bare frame structure is damaged globally to a high level.

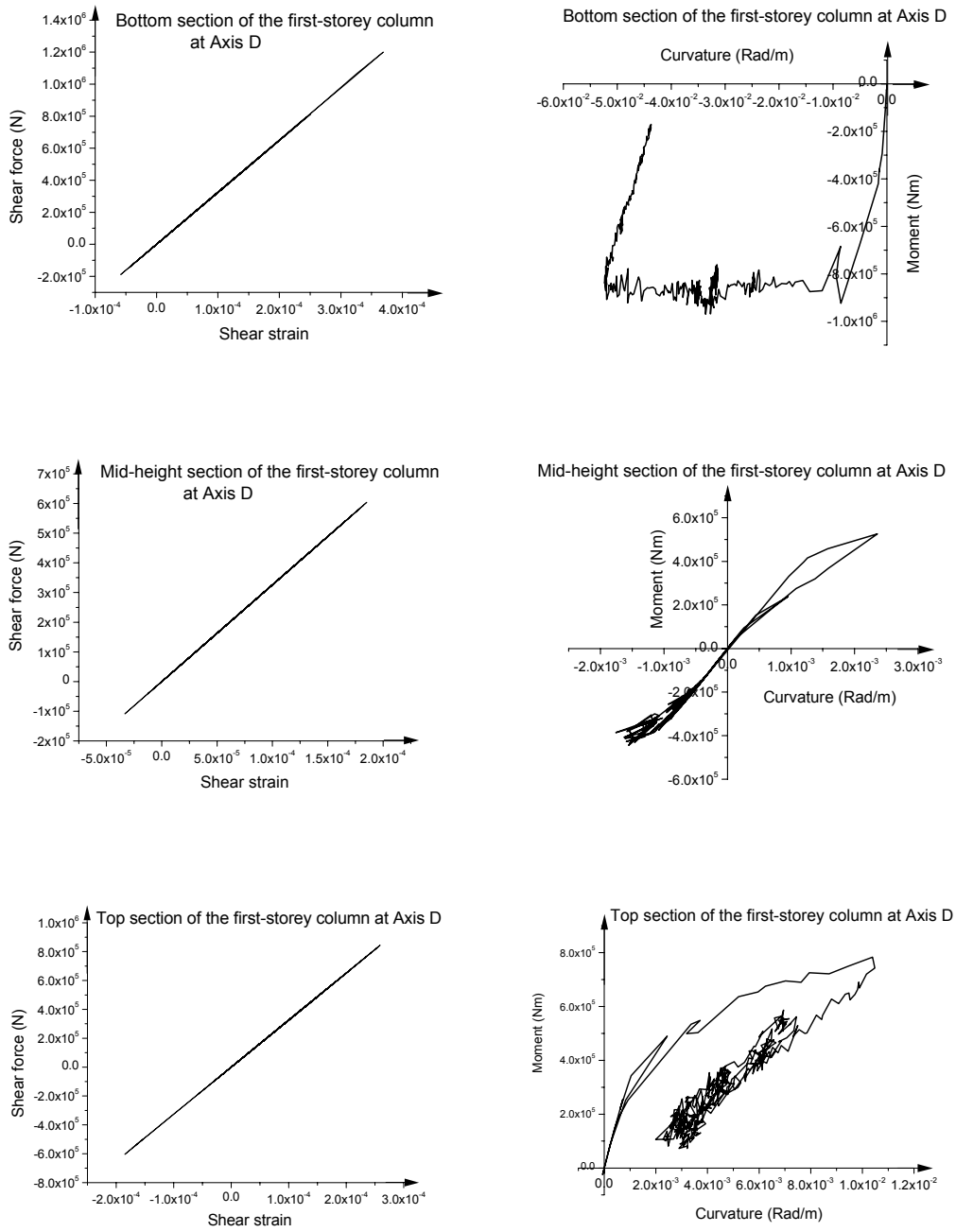

(a). Flexural and shear responses of the first-storey column at Axis D

Figure 2.22 Responses of some critical column and beam (Third case study)

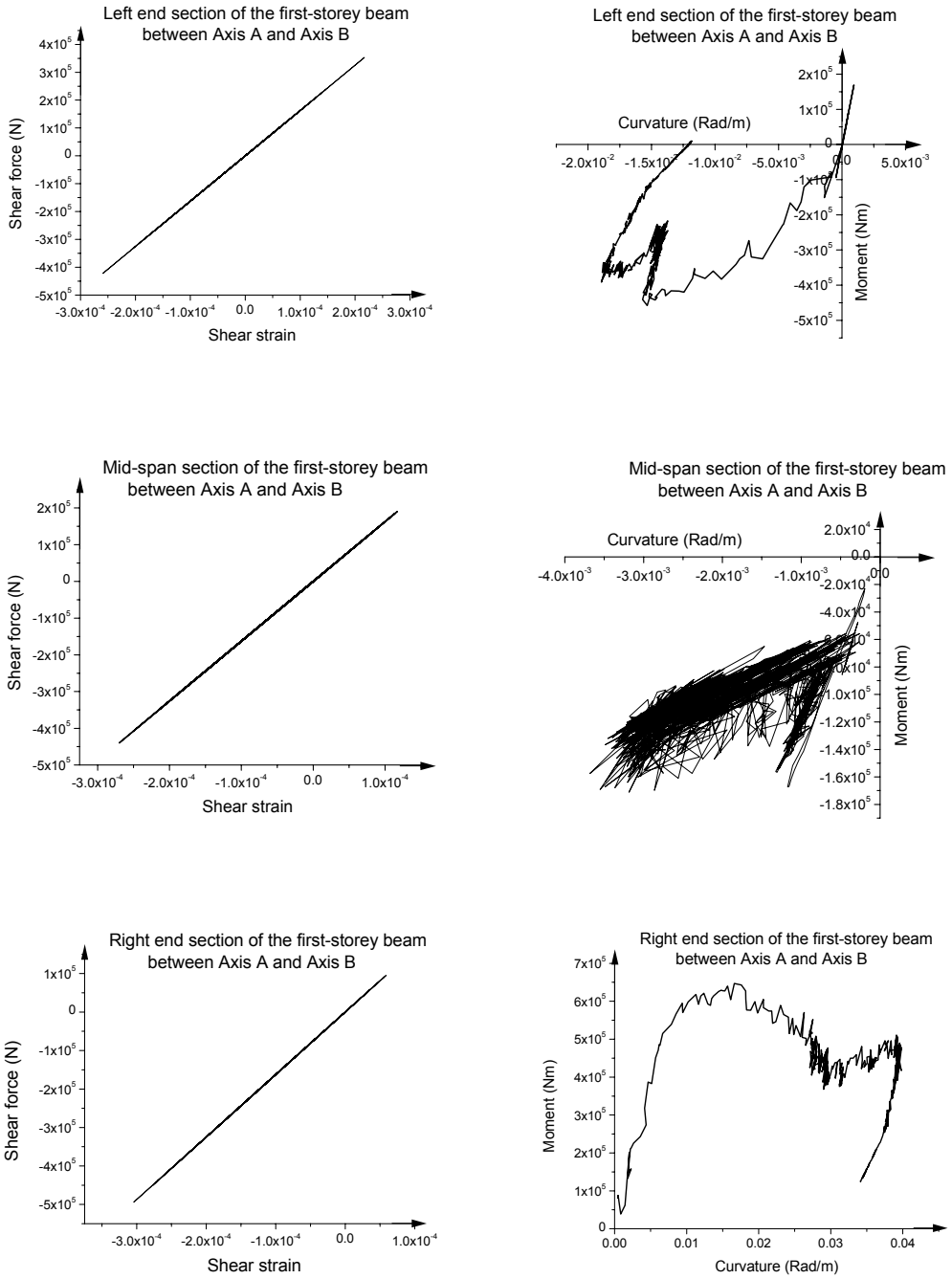

(b). Flexural and shear responses of the first-storey beam between Axis A and Axis B

Figure 2.22 (Continued)

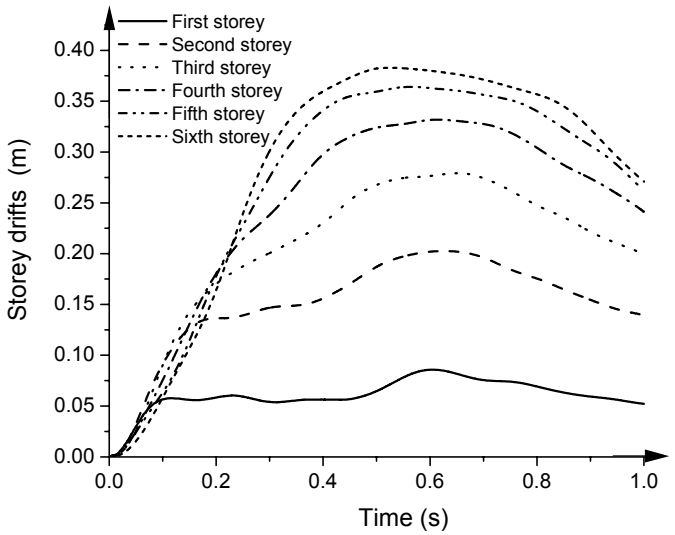

(a) Storey drift responses

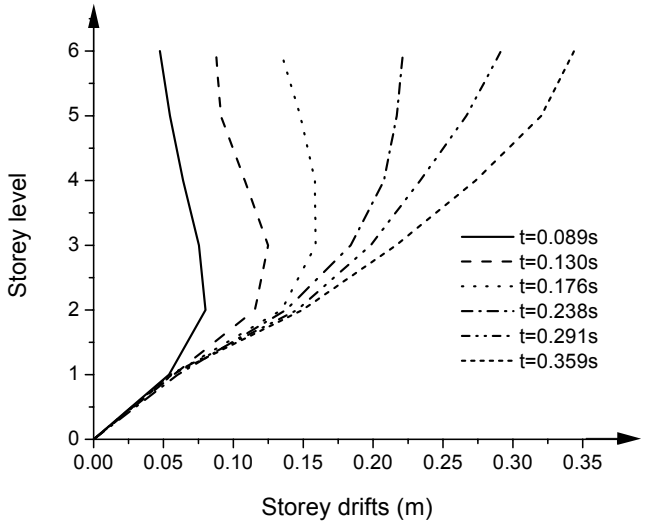

(b). Contour of the storey drifts at different time stations

Figure 2.23 Storey drifts for the structure (Third case study)

2.6.4 Comparisons of three case studies

Comparisons of above three numerical case studies indicate some similarities and dissimilarities, which will be discussed respectively as follows.

Similarities — The whole process of the structural dynamic responses can be approximately divided into two stages. Localized responses of the blast-loaded members are critical at response stage I while the global responses of the structural system dominate at response stage II. In addition, the flexural responses play a more important role in the plastic deformation of the frame beams and columns in comparison to their respective shear responses.

Dissimilarities — The first dissimilarity existing in the first and second case studies is that the damage is much more severe for the frame structure with reinforced concrete exterior cladding panels than those for the bare frame structure under the same blast condition. Due to the diffraction of the blast waves around the columns, reflected pressure will quickly reduce to zero for the bare frame structure and only the drag forces associated with the dynamic pressure are critical in the net blast loadings on the structure. However the exterior cladding panels cause the structure to be loaded with reflected blast pressure, overpressure, and dynamic pressure, thus the blast forces received by the frame structure with cladding panels are much greater. To dissipate the work produced by such a large blast force, some plastic deformation would appear to the structure producing damage to some extent as expected in the first case study.

Comparing the first case study with the third one indicates that within response stage I, local damage on the critical blast loaded members including the front exterior cladding panels and columns, and the top-storey beams occurs for the frame structure with exterior cladding panels under blast condition I. However no local damage is present to the blast loaded members (all columns) at this stage for the bare frame structure under blast condition II. This difference is induced by the fact that the blast loadings acting on these two kinds of frame structure differ

greatly as discussed above. Due to the significantly blast force received by the front exterior cladding panels and the roof slabs in blast condition I, a large amount of plastic deformation have been developed on them within response stage I, which further produces considerably distributed reaction forces in the opposite direction to the connected frame columns and beams. This force plus the direct action of the blast loadings creates a lot of localized damage on these columns and beams.

The third dissimilarity exists in the trend of the global responses developments at response stage II. The responses of the bare frame structure have the tendency to spread from the bottom to upper storey levels due to a transverse wave formed for the structural storey drift responses as indicated in the second and third case study. However this trend is not obvious in the first case study.

2.7 Summaries

Based on the results obtained from the numerical case studies, the following conclusions are made regarding dynamic responses and damage distributions of a six-storey reinforced concrete frame structure under distant blast conditions:

1. The whole process of the frame structural dynamic responses can be approximately divided into two stages. The flexural responses are dominant in the plastic deformation of the structural members as compared to the shear responses. In the identical blast situation, the existence of reinforced concrete exterior cladding panels produces more severe dynamic responses than those of the bare frame structure.

2. Local damage is produced to the critical blast-loaded members at response stage I as indicated from the first case study. When considering the design, to keep this local damage under control at the objective performance level, the inelastic deformation of the blast-loaded members should be strictly limited. As a result, an effective performance-based blast resistant design for the reinforced concrete structural members is urgently needed and

implemented with the explicit consideration of their inelastic deformation, which will be discussed in Chapters 3 to 6.

3. Global damage due to the significantly MIDR responses is present at response stage II from the first and third case studies. Therefore, in order to ensure that the structural global damage is at the required performance level, it is necessary to control the MIDR responses during the design of the reinforced concrete frame structure in resisting such a blast loading as produced from the distant intense surface explosion. The procedures to fulfil this purpose will be addressed in Chapters 7 and 8.

CHAPTER THREE

PERFORMANCE–BASED BLAST RESISTANT DESIGN OF REINFORCED CONCRETE MEMBERS USING ENERGY SPECTRA — PART I. METHODOLOGY

Synopsis

The displacement and displacement ductility factor correlate with an expected performance level of a structural member in a blast event, thus both of these two parameters should be utilized as performance indicators in a blast resistant design. To meet an expected performance level defined by a combination of target displacement and target displacement ductility factor, a new blast resistant design approach is developed in this chapter for one-way reinforced concrete members on the basis of energy spectra, which are constructed from an elastic-perfectly-plastic single-degree-of-freedom (SDOF) system. By controlling the responses of maximum displacement and displacement ductility factor for the equivalent SDOF system of the reinforced concrete member to exactly reach the corresponding design targets, the effective depth and longitudinal reinforcement ratio of the member can be specifically determined against the given blast loading within the design. This chapter concentrates on the methodology of the developed blast resistant design using energy spectra while the evaluation of its effectiveness with the numerical analysis follows in Chapter 4. The analytical results indicate that this new approach has several advantages over the existing blast design guidance.

Keywords: Expected performance level, Target displacement, Target displacement ductility factor, Energy spectra, Equivalent SDOF system

3.1 Overview of Existing Design Guidance

Design and construction of reinforced concrete structural members against accidental or deliberate explosions is deemed necessary with the increasing importance laid upon explosion safety. For the explosions occurring at a relatively large standoff distance, the blast loadings exerting on the structural members can be properly simplified as uniformly distributed dynamic loadings characterized by their peak values and durations. In such cases, some level of inelastic deformation of structural members is allowed within the blast resistant design when subjected to severe blast loadings to dissipate energy. Therefore much blast design guidance [A2, A3, B1, M3, T1, T2] based on performance with the explicit consideration of inelastic deformation has been proposed in recent years. The purpose of these design guidance is to ensure the performance of designed member under the given blast force meet the requirement and objective of the owners, users, and society.

In a performance-based design framework, selection of the appropriate response parameter as the performance indicator to quantify the performance level of member in blast conditions is of particular importance. According to the selected parameter, the expected performance level can be established and applied to the design process in controlling member's responses or damages. Currently either the displacement (specified in TM5-1300 [T2] and Mays and Smith [M3]) or the displacement ductility factor (specified in TM5-855-1 [T1], Biggs [B1], and ASCE Manual 42 [A2]) has been suggested as the performance indicator. Given a target displacement y_t or a target displacement ductility factor μ_t for the significant point of the member to be designed (e.g. the mid-span of a member with two ends constrained or the free-end of a cantilever member), the blast design can be carried out. In these design guidance [T1, T2, M3, B1, A2], $y_t \approx l \tan\theta_t / 2$ is for one-way member of reinforced concrete with two ends constrained assuming plastic hinge formation at mid-span and fixed ends and a linear deflected shape between hinges, while $y_t \approx l \tan\theta_t$ is for the cantilever member (θ_t is the expected or target support rotation of the one-way member under the blast force). The other parameter of μ_t

can be defined as the target of y_m / y_e where y_m denotes the peak displacement response and y_e is the elastic response (recoverable displacement) for the designed member. The existing guidance [B1, T2, M3] involving y_t or μ_t alone in the blast design is reviewed as follows.

3.1.1 Work of Biggs

Biggs [B1] suggested the displacement ductility factor as the performance indictor. Thus after a certain level of μ_t is specified, the displacement ductility response of the member to be designed should be checked with this μ_t. Since the responses of structural member under the blast conditions depends upon its mass, stiffness and strength, which are all related to the cross-sectional size after specifying a constant longitudinal reinforcement ratio ρ, a trial and error method should be applied to the design. The related design flow chart is shown in Figure 3.1.

3.1.2 The TM5-1300 method

TM5-1300 [T2] is widely used in the design of protective structures against blast loadings. The selection of displacement rather than displacement ductility factor as the performance indicator is the main difference between TM5-1300 and Biggs's method. Therefore after a certain y_t is defined, the maximum displacement response of the member is to be checked with this y_t by specifying a constant ρ and assuming the member's cross-sectional size. Modifications of the cross section is performed until y_t is satisfied through a trial and error method.

3.1.3 Work of Mays and Smith

Based on TM5-1300 [T2], Mays and Smith [M3] suggested a design procedure where displacement alone is employed as performance indicator in the blast design. But in their method, by comparing t_d and T, the blast loading is divided into an

impulsive or a quasi-static/dynamic state based upon which the design is finished. The design flowchart is given in Figure 3.2.

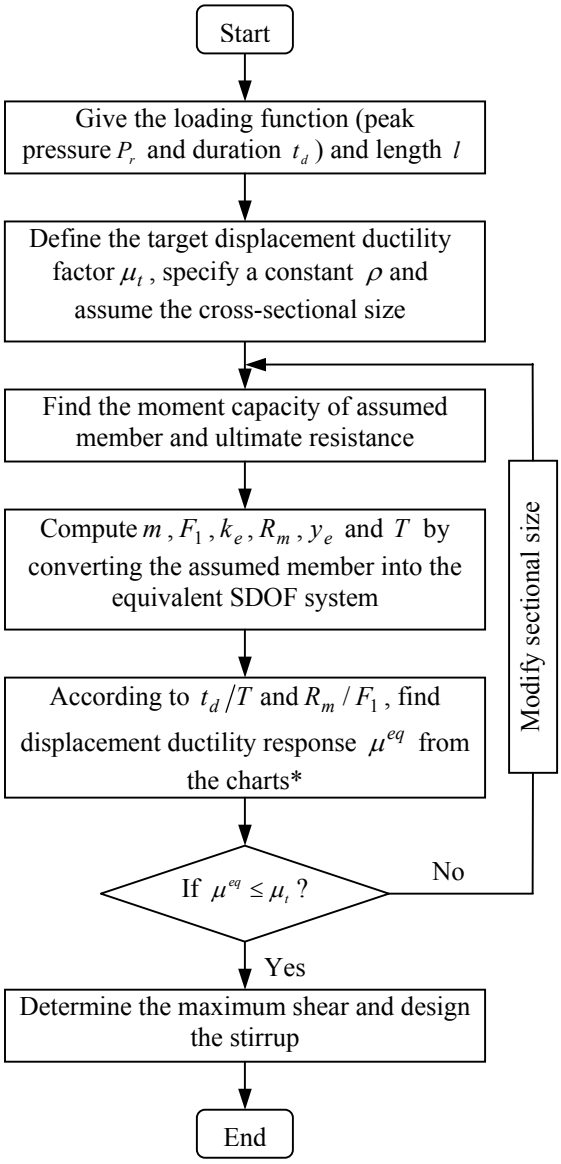

* Charts plotting the distribution of the displacement ductility factor (μ) against t_d/T with respect to R_m/F_1 for an elastic-perfectly-plastic SDOF system under triangular pulse loads

Figure 3.1 The design flowchart of Biggs's method [B1]

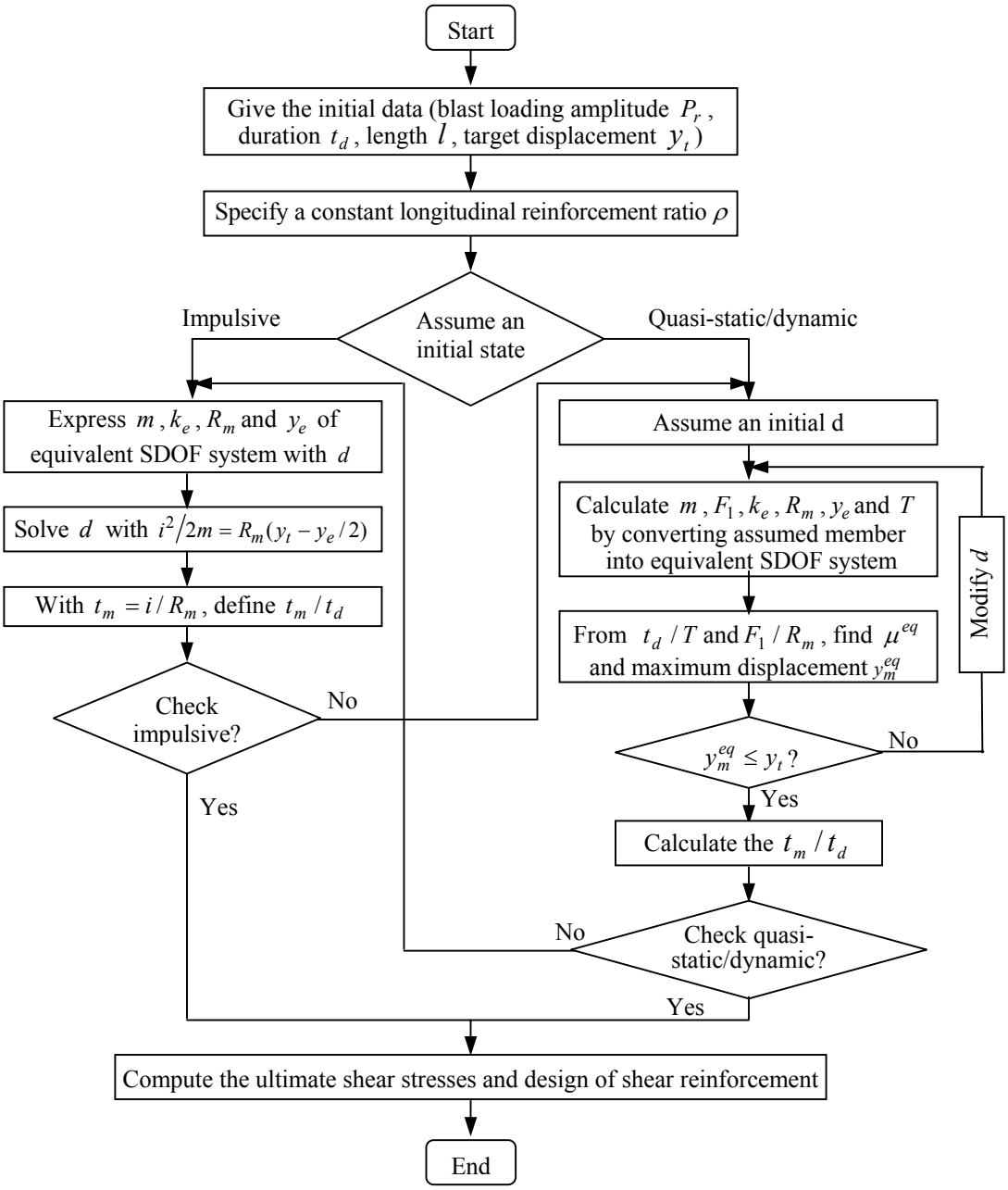

Figure 3.2 The design flowchart of Mays and Smith's method [M3]

The utilization of μ_t in Biggs's and TM5-855-1's design methods could obviously establish an effective control of the displacement ductility response of the member in blast conditions, however it may not be able to limit its maximum displacement response explicitly. In some cases if the maximum displacement response is too large, the subsequent secondary effect will be quite significant, which may cause further damage or even the destruction of the member. Besides the large displacement response may endanger the equipments and occupants within the building. On the other hand, in TM5-1300's as well as Mays and Smith's design procedures, using y_t alone could only control the maximum displacement response of the member, nevertheless in such cases its displacement ductility response is not restricted, which might lead to an ineffective design. For instance, in some severe blast conditions, a relatively large cross section of the member will be designed with the specified ρ to meet such a target of y_t. This design action will induce an unreasonably high displacement ductility demand. However the displacement ductility capacity of this designed member is bounded by the large cross section and thus could not guarantee satisfying such a high displacement ductility demand. Based on the above discussions, it seems that adopting either y_t or μ_t alone in the blast design may not be so adequate in the control of the responses of structural members fulfilling their expected performance level. In order to carry out an effective performance-based blast design, it is better to take simultaneous consideration of y_t and μ_t into the design process.

In addition, some subjectivity is involved in these existing design procedures [B1, T1, T2, M3]. Firstly ρ should be specified based on the engineering experience and judgment and keep unchanged during the design. Secondly with the Mays and Smith's method, it is assumed that the blast loadings are located in either an impulsive or a quasi-static/dynamic state thus establishing the watershed between these two states becomes critical. Many artificial division methods have been proposed in the past [M3, A3] to deal with this problem, however these methods seem to be quite empirical.

To date the appropriate response parameters as the performance indicators have not been unified in the performance-based blast design process; either the displacement or the displacement ductility factor has been adopted. However such an action could not promise an effective performance-based blast design. Both y_t and μ_t should be taken into account within the design. Therefore, in order to achieve the expected performance level defined by a combination of the dual targets y_t and μ_t, a new approach is developed herein based on the energy spectra, which are constructed for an elastic-perfectly-plastic SDOF system subjected to blast loadings. This design procedure could also overcome the shortcomings of the subjective specification of ρ at the initial design stage and could accommodate arbitrary blast loadings. The present research attempts to make contribution to the current worldwide efforts towards the development and elaboration of a basis for a genuine performance-based blast design practice.

3.2 Energy Spectra

Before the detailed description of this blast resistant design approach, the energy spectra need to be specified first because of the significant energy absorption during the inelastic behaviour of the structural member under blast conditions. Also they are important tools in incorporating the dual targets of y_t and μ_t into the blast resistant design thus to determine the cross-sectional size and reinforcement ratio of the member. The formation of energy spectra is discussed as follows.

3.2.1 Non-dimensional energy factor

When a structural member is subjected to a blast loading, the member deflects until such time as the strain energy of the member is developed sufficiently to balance the external work applied to it due to the blast loadings. Thus a rigorous approach to obtain this strain energy exactly becomes essential. To meet such an objective, a non-dimensional energy factor C is introduced, expressed as the ratio of maximum strain energy $E_{\max}$ to the ultimate elastic energy E_{el}. Thus

$$C = E_{\max} / E_{el} \tag{3.1}$$

In this study, the non-dimensional energy factor is computed from an elastic-perfectly-plastic SDOF system with the resistance function depicted in Figure 3.3. It is evident that the term of ultimate elastic energy E_{el} can be expressed as

$$E_{el} = k_e \, y_e^{\,2} / 2 \tag{3.2}$$

where y_e is the elastic (recoverable) displacement and k_e is the initial stiffness. The ultimate strength R_m for the SDOF system is

$$R_m = k_e \, y_e \tag{3.3}$$

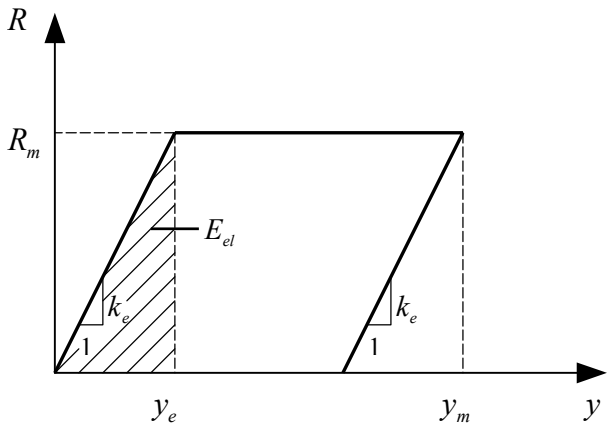

Figure 3.3 Resistance function for an elastic-perfectly-plastic SDOF system

3.2.2 Associated parameters

The basic equation of motion for the elastic-perfectly-plastic SDOF system in the elastic range by ignoring the damping effect [B1, K4] can be generally described as

$$m\ddot{y} + k_e\, y = F_1\, f(t, t_d) \tag{3.4}$$

where F_1 is the peak value of the force, $f(t, t_d)$ is a non-dimensional time function defined by a variable t and a given loading duration t_d, and y is the displacement response. It is convenient to normalize the parameters in Equation (3.4) through transforming the variables by letting $\eta = y/y_e$ and $\xi = t/T$, therefore the above expression in the elastic range becomes

$$\frac{1}{4\pi^2}\ddot{\eta} + \eta = \frac{F_1}{R_m} f(\xi, \frac{t_d}{T}) \tag{3.5}$$

Assuming $a = F_1/R_m$ and $b = t_d/T$ then

$$\frac{1}{4\pi^2}\ddot{\eta} + \eta = a\, f(\xi, b) \tag{3.6}$$

In the plastic range, the item $k_e y$ in Equation (3.4) becomes constant with a value of R_m thus Equation (3.7) may be refined from Equation (3.6) as

$$\frac{1}{4\pi^2}\ddot{\eta} + 1 = a\, f(\xi, b) \tag{3.7}$$

As such, the factor $\eta(\xi)$ is only related to the parameters a and b for a given loading function from Equations (3.6) and (3.7) and by solving them, $E_{\max}$ can be obtained by

$$E_{\max} = \int_0^{t_m} F_1 f(t, t_d)\, dy = \int_0^{t_m/T} a\, R_m f(\xi, b)\, d\eta(\xi)\, y_e = a\, k_e\, y_e^{\,2} \int_0^{t_m/T} f(\xi, b)\, \eta'(\xi)\, d\xi \tag{3.8}$$

where t_m is the time for the maximum displacement of the SDOF system. The non-dimensional energy factor C may be derived from substituting Equations (3.8) and (3.2) into Equation (3.1), hence

$$C = 2a\int_0^{t_m/T} f(\xi, b)\eta'(\xi)\,d\xi \tag{3.9}$$

The point that the ratio of t_m/t_d is a function of the factors a and b, has been proven by Biggs [B1], thus $t_m/t_d = g(a,b)$ (where $g(\bullet)$ is a function). Substituting this expression into t_m/T leads to

$$\frac{t_m}{T} = \frac{t_m}{t_d}\frac{t_d}{T} = g(a, b)\ b \tag{3.10}$$

By inserting Equation (3.10) into Equation (3.9), C is expressed as

$$C = 2a\int_0^{g(a,b)b} f(\xi, b)\eta'(\xi)\,d\xi \tag{3.11}$$

Equation (3.11) reveals that in order to obtain a response in terms of the non-dimensional energy factor C, one needs only know the values of F_1/R_m and t_d/T. Thus these two parameters are necessary and sufficient for computing the factor C. In this chapter, a group of curves, which represents the non-dimensional energy factor C against the ratio t_d/T with respect to various F_1/R_m, are defined as energy spectra; their formation is addressed as follows.

3.2.3 Formation procedures

Giving the discrete values for items a and b, Equations (3.6) and (3.7) are initially solved with the time history analysis for $\eta(\xi)$ to find the value of t_m/T. Further, the non-dimensional energy factor C is determined by the integration of Equation

(3.9). According to the distribution of C at various a and b, the energy spectra can be finally plotted.

3.2.4 Energy spectra for various loadings types

The energy spectra for an undamped elastic-perfectly-plastic SDOF system without initial motion for various patterns of dynamic loadings are illustrated in Figures 3.4 to 3.7. For the triangular pulse with a zero rise time, $f(\xi, b) = 1 - \xi / b$ up to $\xi = b$ and then zero as seen in Figure 3.4. While in the case of a rectangular pulse as shown in Figure 3.5, $f(\xi, b)$ is unity up to $\xi = b$ and zero thereafter. Figure 3.6 illustrates that when the force is constant with finite rise time, $f(\xi, b) = \xi / b$ up to $\xi = b$ and unity at a later time. As far as the triangular function as shown in Figure 3.7 is concerned, $f(\xi, b) = 2\xi / b$ up to $\xi = b/2$, followed by $f(\xi, b) = 2 - 2\xi / b$ up to $\xi = b$ and zero thereafter. The corresponding energy spectra are constructed by inserting these expressions for $f(\xi, b)$ into Equations (3.6) and (3.7) and obtaining the non-dimensional energy factor C through the integration of Equation (3.9) for various items a and b.

The non-dimensional energy factor C of an elastic-perfectly-plastic SDOF system when subjected to a triangular load pulse in Figure 3.4 tends to rise with the increase of t_d / T or F_1 / R_m. For the rectangular pulse in Figure 3.5, it is observed that C is equal to unity at $F_1 / R_m = 0.5$ for $t_d / T > 0.5$ and it tends to increase with t_d / T for a definite F_1 / R_m. Figure 3.6 illustrates the existence of a transition point occurring at the time $t_d / T = 1$ for the constant force with a finite rise time and before this time, C declines gradually with t_d / T for a definite F_1 / R_m. It should be also noticed that in this case, the peak force F_1 could not be greater than the strength R_m thus here only the ratios F_1 / R_m between 0 and 0.9 are listed.

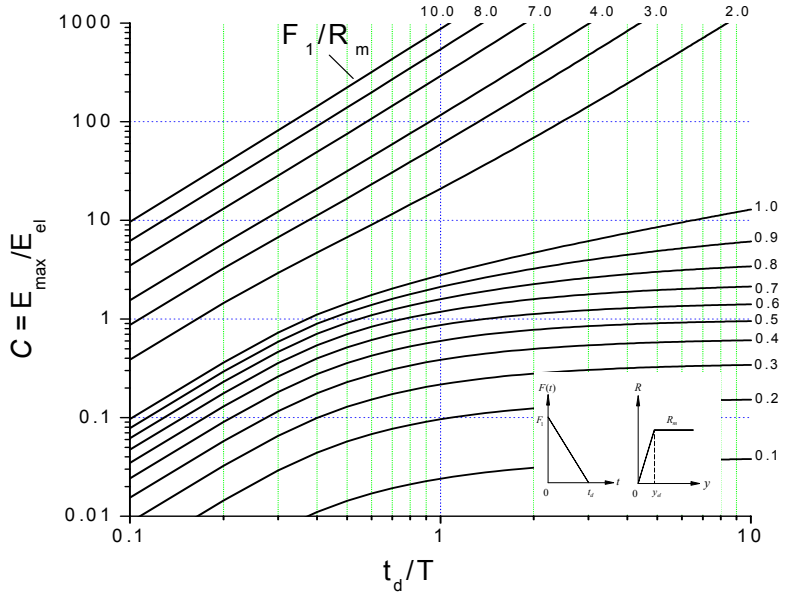

Figure 3.4 Energy spectra of an undamped elastic-perfectly-plastic SDOF system due to triangular load pulses with zero rise time

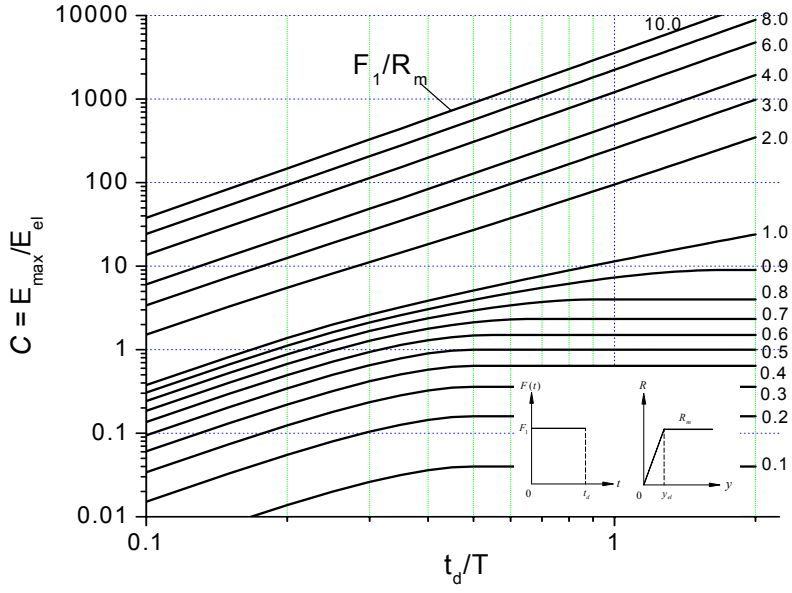

Figure 3.5 Energy spectra of an undamped elastic-perfectly-plastic SDOF system due to rectangular load pulses

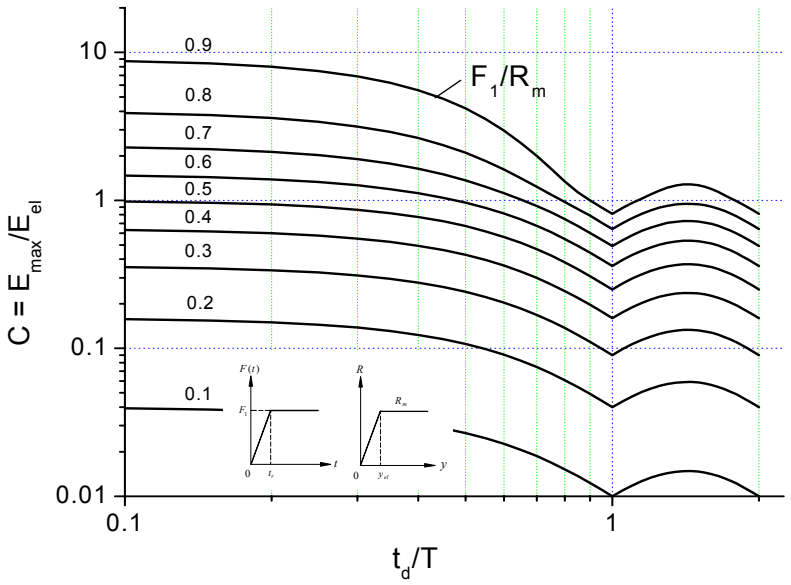

Figure 3.6 Energy spectra of an undamped elastic-perfectly-plastic SDOF system due to constant forces with finite rise time

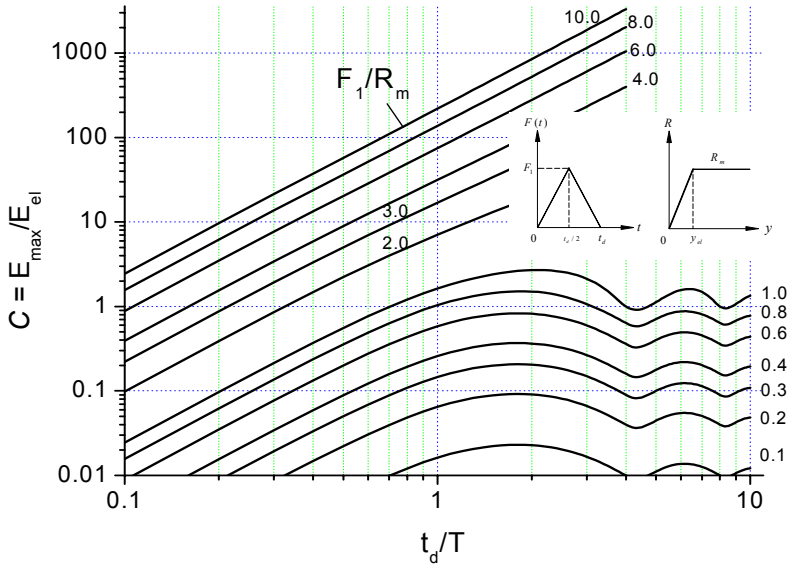

Figure 3.7 Energy spectra of an undamped elastic-perfectly-plastic SDOF system due to equilateral triangular load pulses

Generally the function of blast loading on structural member from the external explosion could be simplified into a triangular loading pulse if the reflected pressure and impulse are preserved [T1, H1]. Thus the inclusion of the energy spectra under triangular load pulses in Figure 3.4 into the design of one-way reinforced concrete members under blast loadings will be discussed in the following section. As for the design of members against other types of dynamic loadings, the respective energy spectra shown in Figures 3.5 to 3.7 could be utilized.

3.3 Design Criteria

A fundamental issue in the performance-based blast design is to determine the specific response parameters as performance indicators. The previous discussions in this chapter indicated that to carry out an effective blast design, both displacement and displacement ductility factor should be adopted as the performance indicators. To achieve the expected performance level defined by the dual targets of y_t and μ_t, a comparatively accurate design approach for the structural members against blast forces will be discussed based on the energy spectra.

The structural member with continuous mass and stiffness is simplified by converting it into an equivalent SDOF system involving lumped mass supported by an elastic-perfectly-plastic spring [B1]. The equivalent system is selected in such a way that the deflection response of the concentrated mass is the same as that for the significant point on the structural member. Thus the responses of equivalent system under the given blast force should also achieve the expected performance of y_t and μ_t. By using the energy spectra, a recurrent procedure is addressed herein to determine the initial stiffness k_e and ultimate strength R_m of the equivalent SDOF system for the given blast loading function and dual targets of y_t and μ_t. The derivation of cross-sectional size and reinforcement ratio of the member from the values of k_e and R_m of the equivalent system will be further identified.

3.4 Design of Equivalent Elastic-Perfectly-Plastic SDOF System Using Energy Spectra

An important point that needs to be addressed at this stage is that to achieve the performance level defined by y_t and μ_t simultaneously, k_e and R_m of the equivalent elastic-perfectly-plastic SDOF system against the blast loading could be determined specifically, which will be proven herein.

Given y_t and μ_t, the elastic displacement y_e of equivalent SDOF system is required as

$$y_e = \frac{y_t}{\mu_t} \tag{3.12}$$

Assume that there are three possible designs of the equivalent systems, which have satisfied the requirement of y_e but with various initial stiffness as shown in cases (a), (b) and (c) plotted in Figure 3.8 and

$$R_{ma} = k_{ea} y_e,\ R_{mb} = k_{eb} y_e, \text{ and } R_{mc} = k_{ec} y_e \tag{3.13}$$

(k_{ea}, R_{ma}), (k_{eb} R_{mb}) and (k_{ec}, R_{mc}) are the sets of initial stiffness and ultimate strength of the equivalent systems in various cases. Under the identical blast loading, the responses of these systems are compared as follows:

Case (a): Suppose that in this case the response of maximum displacement of the equivalent system having k_{ea} under the blast loading could reach y_t exactly.

Case (b): k_{eb} in this case is smaller than k_{ea} thus $R_{mb} < R_{ma}$ with Equation (3.13). Under the same blast loading, the maximum external work on the SDOF system in case (b) will inevitably be greater than that in case (a). A

larger maximum displacement response will be produced for the equivalent system in case (b) to dissipate the enlarged external work, thus $y_{tb} > y_t$.

Case (c): k_{ec} is larger than k_{ea} and $R_{mc} > R_{ma}$. In the same blast condition the maximum displacement response of the equivalent system in case (c) would be less than that in case (a), which is understandable since in such a case the maximum external work on the SDOF system in case (c) tends to be less than that in case (a), thus $y_{tc} < y_t$.

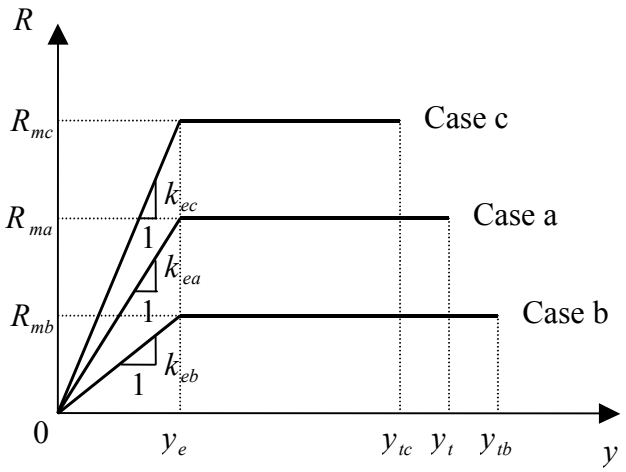

Figure 3.8 Various resistance functions

The above comparative analysis of various cases indicates that in the situation of the required y_e fulfilled, if supposing that maximum displacement response of the equivalent system having k_{ea} under the given blast loading reach y_t exactly, the maximum displacements of equivalent systems with initial stiffness larger or smaller than k_{ea} are not equal to y_t. Hence it can be concluded that in order to achieve the dual design targets of y_t and μ_t under the given blast loading simultaneously, there exists only one solution of the initial stiffness for the equivalent elastic-perfectly-plastic SDOF system as assumed in case (a) (see Figure 3.8). The ultimate strength of the equivalent system can be further specifically

determined from Equation (3.13). In such a case, $E_{\max}$ for the equivalent system necessary to balance the external work delivered by the blast loadings is equal to

$$E_{\max} = \frac{1}{2} k_{ea} y_e^{\,2} + k_{ea} y_e (y_t - y_e) \qquad (3.14)$$

To find this specific solution for k_e and R_m of the equivalent SDOF system in the blast design, the process is addressed as follows. Given the blast loading function (peak value F_1 and duration t_d), dual design targets (y_t and μ_t) and the mass (m) of the equivalent system, a recurrent procedure is needed to complete the design process. Firstly, y_e is computed with Equation (3.12). By assuming an initial stiffness k_e, the corresponding E_{el} and R_m are then obtained with Equations (3.2) and (3.3) respectively while $T = 2\pi\sqrt{m/k_e}$. Next determine the parameters F_1 / R_m and t_d / T, with which the non-dimensional energy factor C can be found from the energy spectra in Figure 3.4. $E_{\max}$ is further obtained with Equation (3.1) however, determination of the quantity of $E_{\max}$ will result in a new stiffness k_{e1}. By replacing k_{ea} in Equation (3.14) with k_{e1} and transforming Equation (3.14), k_{e1} is gained as

$$k_{e1} = \frac{E_{\max}}{y_e\, y_t - y_e^{\,2}/2} \qquad (3.15)$$

Thus make $k_e = k_{e1}$ and repeat the above procedures until the convergent condition $|k_{e1} - k_e| < \varepsilon$ is fulfilled after a few iterations (where ε is an arbitrary small value). The required strength R_m is finally obtained from the expression $R_m = k_e\, y_e$.

3.5 Design of Reinforced Concrete Member Using Energy Spectra

The structural member with continuous mass and stiffness is usually reduced to an equivalent elastic-perfectly-plastic SDOF system with the equivalent mass and stiffness [B1]. According to the above recurrent procedure, k_e and R_m for the equivalent system could be determined specifically with the energy spectra to achieve y_t and μ_t under the given blast condition. After considering some of the particular characteristics of concrete and the embedded reinforcement, ways to compute the cross-sectional size and reinforcement ratio for the reinforced concrete member from k_e and R_m of the corresponding equivalent SDOF system are discussed herein.

3.5.1 Determination of cross-sectional size

After computing k_e of the equivalent system with the energy spectra, the equivalent elastic stiffness k_a for the reinforced concrete member could be described as [T2, M3, N4]

$$k_a = \frac{k_e}{K_{LE}} \tag{3.16}$$

where K_{LE} is the load factor and listed in Table 3.1. For the members with various boundary conditions, k_a is given by

$$k_a = \alpha \frac{E_c I}{l^3} \tag{3.17}$$

where α is the coefficient at different boundary conditions, which can be also obtained from Table 3.1, E_c is the Young's modulus of concrete, l is the length, and I is the cross-sectional moment of inertia of the reinforced concrete member.

Table 3.1 Factors of one-way reinforced concrete members [B1, T2, M3, N4]

Boundary conditions and loading diagrams	Mass Factor K_M		K_{ME}	Load Factor K_L		K_{LE}	Factor α	Factor β	Ultimate Shear force V_u	Support reactions V_s
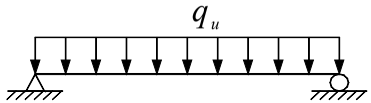	Elastic Plastic	0.50 0.33	0.42	Elastic Plastic	0.64 0.50	0.57	384/5	1/8	$q_u(\frac{1}{2}l-d)$	$\frac{q_u}{2}l$
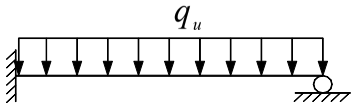	Elastic Elastic plastic Plastic	0.45 0.50 0.33	0.40	Elastic Elastic plastic Plastic	0.58 0.64 0.50	0.56	160	1/12	Left $q_u(\frac{5}{8}l-d)$ Right $q_u(\frac{3}{8}l-d)$	Left $\frac{5q_u}{8}l$ Right $\frac{3q_u}{8}l$
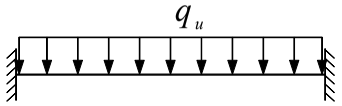	Elastic Elastic plastic Plastic	0.41 0.50 0.33	0.39	Elastic Elastic plastic Plastic	0.53 0.64 0.50	0.54	307	1/16	$q_u(\frac{1}{2}l-d)$	$\frac{q_u}{2}l$
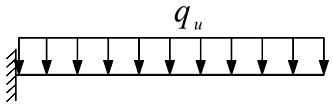	Elastic Plastic	0.26 0.33	0.30	Elastic Plastic	0.40 0.50	0.45	8	1/2	$q_u(l-d)$	$q_u l$

Equivalent elastic stiffness for one-way members $k_a = \alpha\frac{EI}{l^3}$;

Ultimate moment $M_u = \beta q_u l^2$ (for $M_N = M_P$, where M_N, M_P are moment capacity at the support and mid-span of one-way members); $K_{ME} = \left((K_{M-elastic} + K_{M-elasto-plastic})\times 0.5 + K_{M-plastic}\right)/2$ and $K_{LE} = \left((K_{L-elastic} + K_{L-elasto-plastic})\times 0.5 + K_{L-plastic}\right)/2$.

Generally, the moment of inertia of the cross section along reinforced concrete member is significantly influenced by the embedded reinforcement and the cracking propagation of the concrete. To deal with this problem, the moment of inertia could be modified by a reduction coefficient γ. For a rectangular cross section, as shown in Figure 3.9, it can be written as [T2, M3, N4]

$$I = \frac{I_g + I_c}{2} = \frac{1}{2}\left(\frac{b_w T_c^{\,3}}{12} + \frac{\gamma b_w d^3}{12}\right) \approx \frac{(\gamma+1) b_w d^3}{24} \tag{3.18}$$

Where I is the average moment of inertia of reinforced concrete cross section, I_g is the moment of inertia of the gross concrete cross section (neglecting all reinforcing steel), I_c is the moment of inertia of the cracked concrete cross section, T_c, d and b_w are the total depth, the effective depth and the width of the cross section respectively. The parameter of γ can be obtained from Figure 3.10 and it is observed that this coefficient varies with the reinforcement ratio ρ as well as the modulus ratio (E_s/E_c).

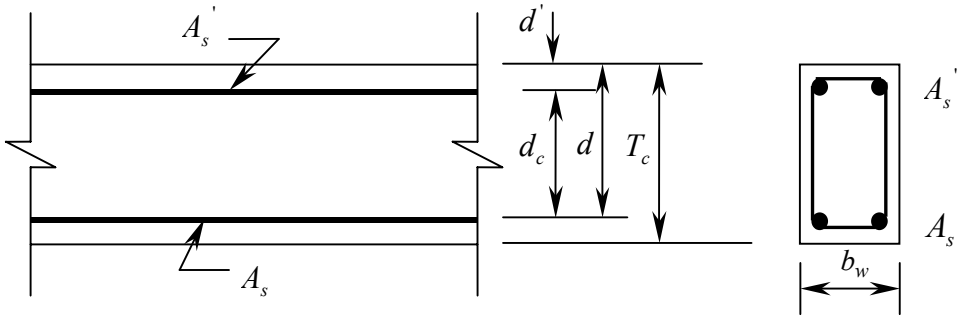

Figure 3.9 Reinforced concrete cross section with tension and compression reinforcement [T2, M3, N4]

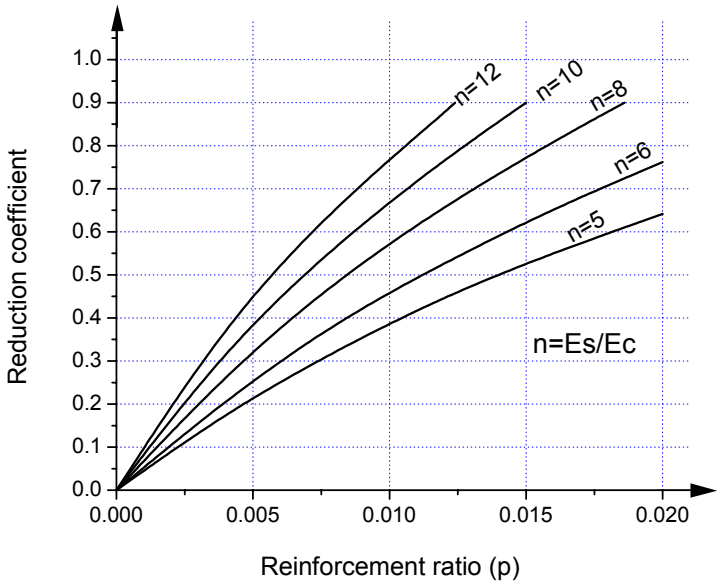

(a). with tension reinforcement only

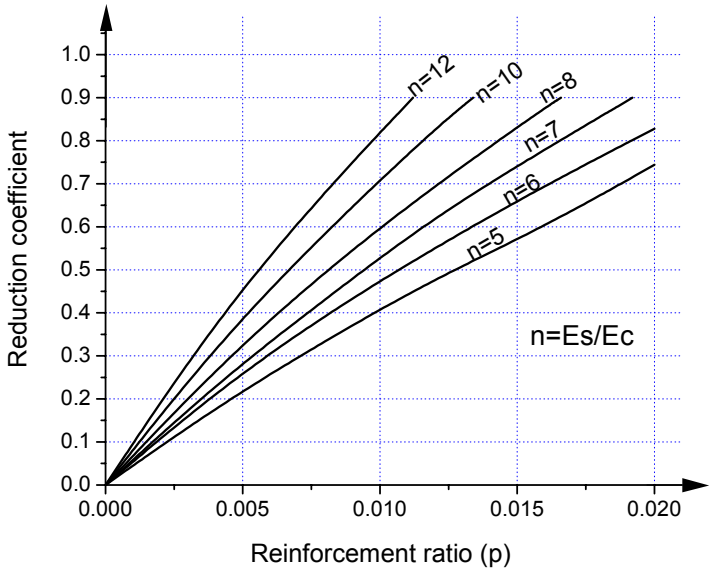

(b). with equal reinforcement on opposite faces

Figure 3.10 Reduction coefficient for moment of inertia of cracked section with different reinforcement layouts [T2, M3, N4]

Substituting Equation (3.18) into Equation (3.17) and then equating Equation (3.17) with Equation (3.16), the effective depth for the reinforced concrete member can be finally determined as

$$d = \left(\frac{24 l^3 k_a}{(\gamma+1) E_c b_w \alpha} \right)^{1/3} = \left(\frac{24 l^3 k_e}{(\gamma+1) \alpha K_{LE} E_c b_w} \right)^{1/3} \tag{3.19}$$

It should be pointed out that the parameter of b_w is not an independent variable within the design, which is generally taken as a unit for the design of a reinforced concrete wall and a constant ratio of d for the design of a beam [T2, M3, N4].

3.5.2 Determination of longitudinal reinforcement ratio

After establishing R_m of the equivalent SDOF system, the ultimate uniformly distributed force q_u applied to the reinforced concrete member is given as

$$q_u = \frac{R_m / K_{LE}}{l} \tag{3.20}$$

At various boundary conditions, the ultimate bending moment M_u of the reinforced concrete members when subjected to the uniformly distributed loadings can be described as

$$M_u = \beta q_u l^2 \tag{3.21}$$

where β is the factor varying with boundary situations and listed in Table 3.1.

Determining the reinforcement ratio with the ultimate bending moment M_u in Equation (3.21) depends on the reinforcement layout in the cross section of the member. If only tension reinforcement is adopted, M_u of a rectangular cross section is given by [P1]

$$M_u = A_s f_{ds} (d - c/2) \tag{3.22}$$

in which

$$c = A_s f_{ds} / 0.85 b_w f_{dc} \tag{3.23}$$

Where A_s is the cross-sectional area of the tensile reinforcement, c is the depth of the equivalent rectangular stress block. f_{ds} and f_{dc} are the dynamic yield strength for reinforcement and the dynamic ultimate compressive strength for concrete, written as

$$f_{ds} = DIF \times f_s \text{ and } f_{dc} = DIF \times f_c \tag{3.24}$$

Where f_s and f_c are the static yield strength for reinforcement and the static compressive ultimate strength for concrete respectively, DIF is the dynamic increase factor, which depends upon the rate of strain of the member increasing as the strain rate increases [D4, F5, G4, G5, G6, G7, M1, M2]. For the design purpose, a constant average DIF has been established in TM5-1300 [T2], where DIF equal to 1.17 is used for reinforcement in bending and a DIF equal to 1.19 is used for concrete in compression. Since the derivation of A_s from Equation (3.24) is carried out without considering the concrete tensile effects, the concrete tensile DIF is not considered within the design although the actual bending of member due to the tensile DIF effect may be higher than the predicted value.

With Equations (3.20) ~(3.24), the area of the tension reinforcement A_s could be determined from the ultimate strength R_m thus the tension reinforcement ratio ρ is

$$\rho = A_s / b_w d \tag{3.25}$$

Consideration is made of another major type of reinforcement layout in the cross section of member in the blast design as shown in Figure 3.9, where compression reinforcement and tension reinforcement are utilized simultaneously considering the rebound effect on the member subsequent to its maximum displacement response. If the concrete is assumed to be crushed and lose effectiveness in resisting moment, then the compression reinforcement area should be equal to the tension reinforcement area [T2]. In this case, the ultimate moment M_u of a rectangular section is given by

$$M_u = A_s f_{ds}\, d_c = A_s f_{ds} (d - d') \tag{3.26}$$

where A_s is the cross sectional area of tension or compression reinforcement and d_c is the distance between the centroid of the compression and the tension reinforcement, d' is the distance from the extreme compression fiber to the centroid of compression reinforcement. Hence, with Equation (3.26) the tension or compression reinforcement ratio (ρ or ρ') of the section can be determined as

$$\rho = \rho' = \frac{M_u}{f_{ds}\, b_w\, d\, (d - d')} \tag{3.27}$$

Substituting Equations (3.20) and (3.21) into Equation (3.27), the tension or compression reinforcement ratio utilized in the section is

$$\rho = \rho' = \frac{\beta R_m l}{K_{LE} f_{ds}\, b_w\, d\, (d - d')} \tag{3.28}$$

To ensure proper structural behaviour under blast loadings, a minimum amount of longitudinal tension reinforcement ratio should be required given by [N4]

$$\rho_{\min} = 1.38 / f_s \tag{3.29}$$

where f_s is the reinforcement yield strength in MPa. For the reinforcement with a yield strength of 460 MPa, the minimum reinforcement ratio is 0.30 %.

3.5.3 Determination of shear reinforcement ratio

The brittle effect of shear failure should be strictly avoided in the blast design. Thus sufficient amounts of shear reinforcement should be provided. Generally the ultimate shear is developed when the resistance reaches the ultimate values q_u and hence the shear reinforcement is a function of the resistance of member.

There are two critical locations where shear force should be considered in the design of reinforced concrete members, as discussed in the reference [T2, M3]. It is pointed out that the ultimate shear force should be calculated at a distance d from the face of the support to check the diagonal tension stress and to provide shear reinforcement in the form of stirrups. Whenever the ultimate shear force exceeds the shear capacity of the concrete, shear reinforcement must be provided to carry the excess. The required shear reinforcement ratio is calculated from

$$\rho_v = \frac{(V_u - V_c)}{\varphi f_{dv} b_w d} \tag{3.30}$$

Where V_u is the ultimate shear force, which can be obtained from Table 3.1, V_c is the shear capacity of the unreinforced concrete, ρ_v is the shear reinforcement ratio, φ is the capacity reduction factor, taken as 0.85, and f_{dv} is the dynamic yield strength of the stirrup. In order to ensure the full development of flexural reinforcement, the shear reinforcement ratio should not be less than 0.15% [N4].

On the other hand, the direct shear force or ultimate support shear force V_s should be checked at the supports, which is listed in Table 3.1. To avoid the direct shear failure at the supports, it was suggested by TM5-1300 [T2] that the magnitude of

the direct shear force V_s at the support that can be resisted by the member, be limited to

$$V_d = 0.18 f_{dc} b_w d \tag{3.31}$$

The total support shear force V_s produced by the applied loadings may not exceed V_d. If V_s exceeds V_d, the cross-sectional size of the member should be increased.

3.6 Design Flowchart

As discussed previously, Equation (3.19) demonstrates that d is a function of γ. Since γ varies with ρ as shown in Figure 3.10, d should be calculated with ρ known. On the other hand, Equation (3.28) indicates that ρ is determined by d. Therefore, a recurrent computational procedure needs to be employed to determine d and ρ of reinforced concrete structural member against the given blast loading. Combining it with the previous recurrent procedure of determining k_e and R_m of the equivalent SDOF system for the given blast loading and the dual targets of y_t and μ_t, the design flow chart depending on energy spectra to find d and ρ of the structural member is shown in Figure 3.11. In this developed design procedure, an initial data of d_0 and γ_0 are assumed so that the value of $E_{\max}$ for the equivalent SDOF system can be obtained from energy spectra. However this $E_{\max}$ will result in a new solution of d_1 and γ_1 and hence the process must be repeated until d and γ are consistent.

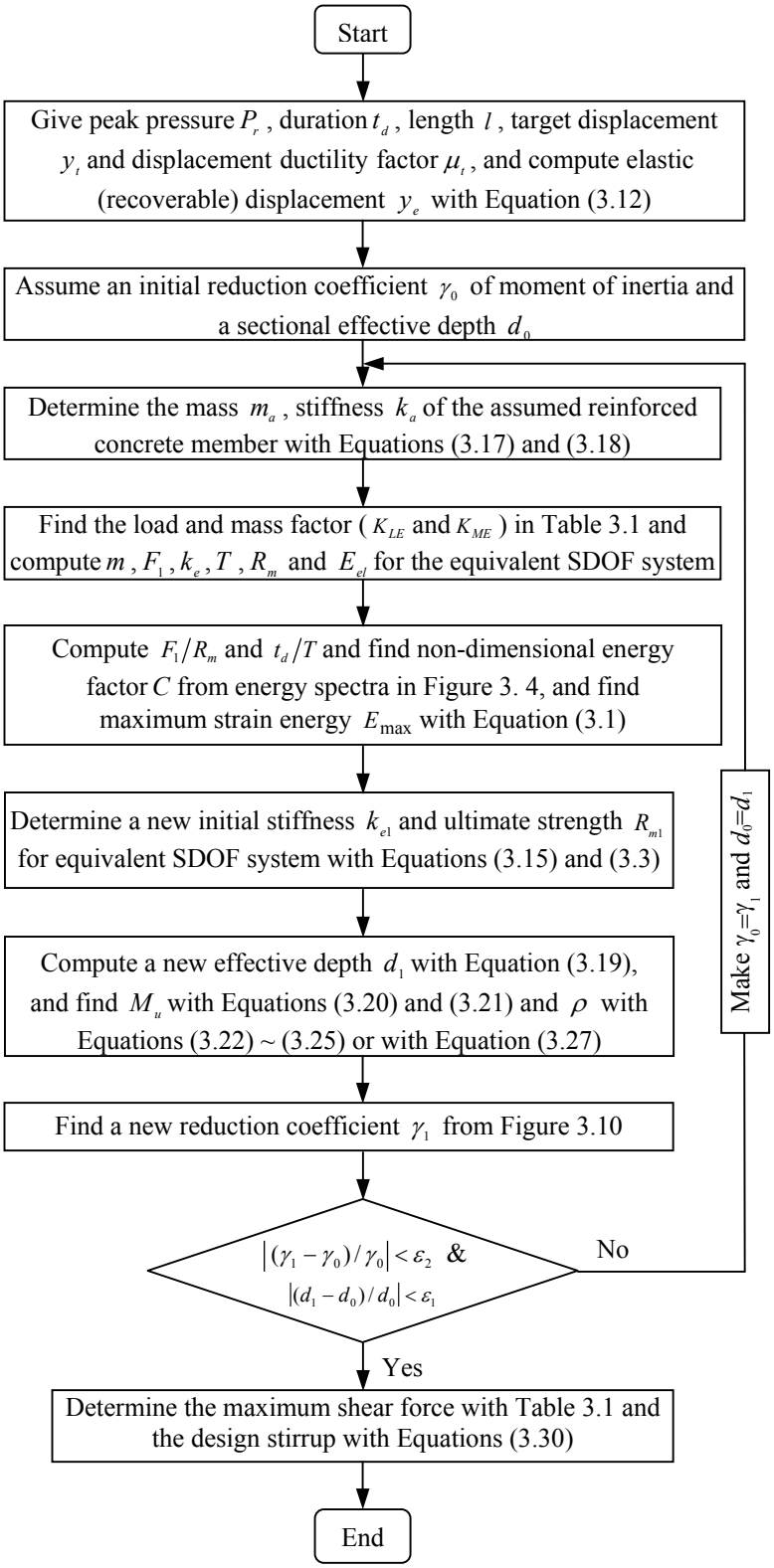

Figure 3.11 Flowchart of performance-based blast resistant design of reinforced concrete members using energy spectra (where $\varepsilon_1, \varepsilon_2$ are arbitrarily small values)

3.7 Advantages of the Design Approach Using Energy Spectra

Several advantages of the developed design approach using the energy spectra are stated as follows:

1. The values of y_t and μ_t, which always correlate with the expected performance levels of a reinforced concrete member in blast incidents, can be effectively incorporated into the design approach. Thus with this approach a comprehensive control of the responses of designed member under blast conditions in achieving the expected performance level can be efficiently and rationally accomplished.

2. Energy spectra are important tools in building up the recurrent procedures depending on which the blast resistant reinforced concrete member can be specifically designed in a simple way to reach the expected performance level defined by y_t and μ_t.

3. This design procedure could lead to the solution of d, ρ, ρ' and ρ_v of reinforced concrete member against blast loadings by controlling the responses of the corresponding equivalent SDOF system to meet the design targets of y_t and μ_t.

4. Current design recommendations are empirical and quite simplified. Although they usually help to produce safe structures, the safety margins are not well controlled. As for the developed design approach based on energy spectra, the member can be specifically designed using the recurrent procedure under the given blast loading to achieve the dual targets of y_t and μ_t, thus the safety margin of the member could be more effectively controlled in the design by giving conservative targets y_t and μ_t. Moreover since the solution of the design with this approach is unique, the difference of the responses of the designed member under the blast conditions that are

obtained from the explosive testing or numerical analysis with the corresponding design targets becomes analytical, which will be beneficial for the engineers in the reliability assessment of the design.

5. This design approach can also be utilized for the design of reinforced concrete members under other types of dynamic loadings, such as the rectangular load pulses, the constant force with finite rise time and the equilateral triangular load pulses. However their accomplishment depends on the corresponding energy spectra selected from Figures 3.5 to 3.7.

6. Application of the design approach is limited to the elastic-perfectly-plastic resistance functions of the equivalent SDOF system of RC member and simplified linear blast loading.

3.8 Summaries

A new approach for blast resistant design of reinforced concrete structural members is presented. It has been demonstrated that by controlling the responses of maximum displacement and displacement ductility factor for the equivalent SDOF system of reinforced concrete member to exactly achieve the expected performance level defined by both y_t and μ_t, the effective depth and longitudinal reinforcement ratio of the reinforced concrete member could be specifically determined for certain blast loading with this design approach. This solution is achieved through the recurrent computation on the basis of the energy spectra, which are constructed for an elastic-perfectly-plastic SDOF system.

The design approach developed in this chapter is more rational and straight-forward in incorporating y_t and μ_t simultaneously in the design of reinforced concrete members against blast loadings, providing the equivalent SDOF system of the member can be adequately characterised by an elasto-plastic rule. It provides the design engineers an attractive alternative to genuine performance-based blast resistant design of reinforced concrete structural members when the current design

guidance is inadequate. This design procedure has been implemented in a computer program and used to investigate several practical design examples, as presented in Chapter 4.

CHAPTER FOUR

PERFORMANCE–BASED BLAST RESISTANT DESIGN OF REINFORCED CONCRETE MEMBERS USING ENERGY SPECTRA — PART II. EVALUATION

Synopsis

This chapter concentrates upon the evaluation of the effectiveness of the performance-based blast resistant design approach using energy spectra developed in Chapter 3. The demonstration of the approach into the practical design of a reinforced concrete member illustrates its effectives in implementation. By comparisons of different design examples designed with the existing guidance as well as the presented approach, the effectiveness in keeping the responses of the equivalent SDOF system of the designed member under control to achieve the expected performance level is evaluated. Due to the complicated behaviours of reinforced concrete members under blast conditions, some differences exist for the actual responses of the designed member with those of the corresponding equivalent SDOF system. Thus the effectiveness of the presented design approach in controlling the actual responses of the designed member under the given blast loading to meet the expected performance level is further evaluated by performing numerical analysis. The analytical results demonstrate the existence of some errors between the responses of the designed member and their respective design targets. The errors are produced due to some simplifications in converting the continuous reinforced concrete members into equivalent SDOF systems and computing the cross-sectional moment of inertia and ultimate strength of the members.

Keywords: Expected performance level, Target displacement, Target displacement ductility factor, Equivalent SDOF system, Energy spectra, Error, Displacement ductility responses, Maximum displacement responses

4.1 Introduction

With the disastrous effects of blast loadings on structural member, an effective control of the responses of the member to reach an expected performance level within the blast resistant design is of vital importance. For this reason, a new performance-based blast resistant design approach using energy spectra is presented in Chapter 3. This chapter will focus on the evaluations of the effectiveness of the design approach from three aspects. The implementation effectiveness is illustrated from a demonstration of this approach into the practical design of a reinforced concrete member. A more critical concern about the effectiveness of this approach lies in its fundamental notion that the expected performance of structural members under blast loadings should be achieved by incorporating the dual design targets of displacement y_t and displacement ductility factor μ_t into the design and controlling the maximum displacement and displacement ductility responses of the equivalent SDOF system of the designed member to reach these dual targets exactly. This will be discussed in detail in this chapter through the comparisons of different practical design examples designed using the existing guidance and the presented approach.

The design approach using energy spectra is accomplished by converting a continuous reinforced concrete member into an equivalent SDOF system. To reach the performance level defined by the dual targets of y_t and μ_t for the given blast loading, the initial stiffness (k_e) and ultimate strength (R_m) of the equivalent SDOF system are computed, based on which the effective depth (d) and longitudinal reinforcement ratio (ρ) of the reinforced concrete member are further derived. Theoretically, the maximum displacement and displacement ductility responses for the equivalent SDOF system (y_m^{eq} and μ^{eq}) can be perfectly controlled to be equal

to the respective targets of y_t and μ_t with this design approach. However due to the complexities of the behaviours of the reinforced concrete member under blast conditions, the actual dynamic responses including maximum displacement (y_m^{rc}) and displacement ductility factor (μ^{rc}) at the significant point for the designed member under the given blast loading should be examined and compared with y_t and μ_t. Thus the latter part of this chapter will be concentrated on the evaluation of the effectiveness of the approach in controlling the actual responses of the designed member. Basically, y_m^{rc} and μ^{rc} should be measured through the explosion tests of the designed members under blast conditions. However, due to considerable costs involved in explosion tests and the difficulties in obtaining reliable data, performing numerical studies to derive y_m^{rc} and μ^{rc} becomes an attractive option. In this chapter, nonlinear finite element analysis is performed with the program ABAQUS [A1] on the designed reinforced concrete members under the given blast loadings. Comparisons indicate some errors of y_m^{rc} and μ^{rc} with the respective design targets of y_t and μ_t. The possible reasons for producing such errors are identified.

4.2 Implementation of the Design Approach

To evaluate the effectiveness of the presented design approach in implementation, a demonstration of this approach is given by involving a practical design of a reinforced concrete wall against blast loading, which was originally presented by Mays and Smith [M3]. This reinforced concrete wall to be designed resists the blast loading perpendicular to its plane that is simplified into a triangular pulse with the peak pressure and duration shown in Figure 4.1. The design gives a target support rotation (θ_t) of 4^o, thus y_t of the wall at the free end under the given blast condition can be obtained with an approximate expression: $y_t \approx l \tan(\theta_t)$. The compression reinforcement area is taken to be equal to the tension reinforcement area considering the rebound effect of the designed member subsequent to its maximum displacement response and the possibility of the explosion occurring in the opposite side of the wall to be designed.

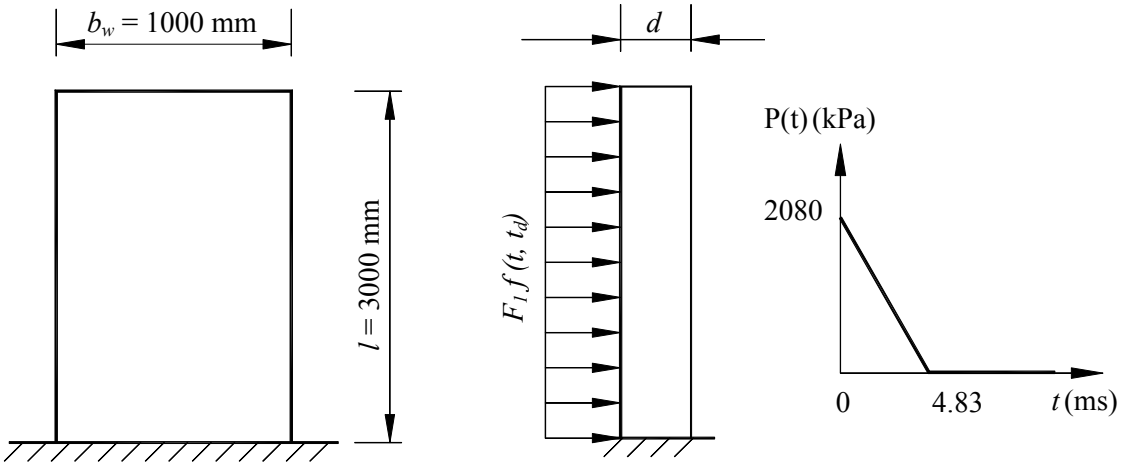

Figure 4.1 Sketch of a reinforced concrete wall

To perform the design with the developed approach, a reasonable μ_t should be given. For a cantilever member, the displacement ductility factor (μ) is closely related to the curvature ductility factor of the fixed-end section (φ_u / φ_y). Their relationship can be derived based on three assumptions [P1]. Firstly, the fixed-end sectional moment-curvature behaviour for the reinforced concrete member can be idealized to be elastic perfectly plastic. Secondly, the full length of the member has a contribution to the elastic displacement y_e thus $y_e = \int_0^l x\varphi\, dx$. Thirdly, the plastic hinge rotation $(\varphi_u - \varphi_y) l_p$ occurring in the vicinity of the fixed-end section performs the whole contribution to the plastic displacement of the free end of the cantilever member. φ_u and φ_y are the ultimate and yield curvatures of the fixed-end section and l_p is the equivalent plastic hinge length, which is approximately equal to d. Based on these above assumptions, μ for a cantilever member under the uniformly distributed force is given as [P1]

$$\mu = 1 + 4\left(\frac{\varphi_u}{\varphi_y} - 1\right)\left(\frac{d}{l} - \frac{d^2}{2l^2}\right) \tag{4.1}$$

Generally, the ratio of d/l for the wall is located in the range of 1/10 to 1/20. In this design, the upper value of 1/10 for d/l is chosen for the cantilever wall considering the severe blast loadings on it. Given a target φ_u/φ_y for the fixed-end section, μ_t can be calculated with Equation (4.1). Since the given θ_t = 4° corresponds to a state in which the member is close to collapse, a large target φ_u/φ_y = 20 is selected. Thus μ_t in this design case is approximately taken as 9.

The design procedures at each iterative step for the given y_t and μ_t are illustrated in Table 4.1. During the design, the value of the initial effective depth d_0 is taken as 3.0 m and the initial reduction coefficient γ_0 (1.0) is assigned as ρ_0=3.0%. The convergence condition, the difference between two iterative design results less than 0.001, is employed. In addition, to check whether y_t and μ_t is effectively achieved during the design, y_m^{eq} and μ^{eq} are computed and compared with y_t and μ_t.

It can be seen from Table 4.1 that this approach is insensitive to the initial data of d_0 and γ_0 and there is no difficulty in reaching convergence for the design. In this design case, even if an unreasonable d_0 and γ_0 are selected, it needs only seven iterative steps to satisfy $|(d_1-d_0)/d_0|<0.001$ and $|(\gamma_1-\gamma_0)/\gamma_0|<0.001$. Little time is consumed during the computation and for this design case it costs only 0.12 s using a computer program written with Matlab language [M13]. Furthermore, $y_m^{eq}=y_t$ and $\mu^{eq}=\mu_t$ can be observed, which indicates that the design could perfectly meet its dual targets of y_t and μ_t for the equivalent SDOF system of the designed member (see Figure 4.8). Thus it can be concluded that the presented blast design approach is not only efficient in implementation, but also accurate in controlling $y_m^{eq}=y_t$ and $\mu^{eq}=\mu_t$.

Table 4.1 Iterative procedures of the design approach using energy spectra for a cantilever wall at each step

y_t (m)	μ_t	γ_0	ρ_0 (%)	d_0 (m)	m (kg)	I (m^4)	k_e (N/m)	T (s)	R_m (N)	T/t_d	F_1/R_m	E_{el} (Nm)	C	$E_{\max}$ (Nm)	k_{e1} (N/m)	q_u (N/m)	M_u (Nm)	d_1 (m)	ρ_1 (%)	γ_1	y_m^{eq} (m)	μ^{eq}
		1.0000	3.000	2.0000	3979	0.667	2.21e9	8.43e-3	5.16e7	0.5731	0.048	6.02e5	3.82e-3	2.30e3	4.97e5	4.30e7	1.936e8	0.1216	9.858	1.0000		
		1.0000	9.858	0.1216	242	1.498e-4	4.97e5	1.39e-1	1.16e4	0.0348	215.1	135.38	2889.5	3.91e5	8.45e7	9.67e3	4.351e4	0.6736	1.025	0.7494		
		0.7494	1.025	0.6736	1340	1.909e-2	6.33e7	2.89e-2	1.48e6	0.1671	1.689	17244	0.742	1.28e4	2.76e6	1.23e6	5.542e6	0.2371	2.644	1.0000		
0.21	9	1.0000	2.644	0.2371	472	1.111e-3	3.69e6	7.11e-2	8.60e4	0.0679	29.01	1003.7	38.04	3.82e4	8.25e6	7.17e4	3.226e5	0.3102	1.486	0.8617	0.21	9
		0.8617	1.486	0.3102	617	2.142e-3	7.11e6	5.85e-2	1.66e5	0.0825	15.05	1935.3	14.98	2.90e4	6.27e6	1.38e5	6.221e5	0.2974	1.566	0.8811		
		0.8811	1.566	0.2974	591	1.931e-3	6.41e6	6.04e-2	1.49e5	0.0800	16.69	1744.4	17.36	3.02e4	6.54e6	1.24e5	5.607e5	0.2995	1.550	0.8772		
		0.8772	1.550	0.2995	595	1.963e-3	6.51e6	6.01e-2	1.52e5	0.0804	16.42	1773.4	16.95	3.01e4	6.50e6	1.26e5	5.700e5	0.2992	1.551	0.8775		

Design results: d = 0.2992 m; ρ or ρ' = 1.551%; ρ_V = 0.15%;

Parameters: $P_r = 2080$ kPa, $t_d = 4.83$ ms, Density of concrete $\rho_{den} = 2500$ kg/m^3,

$E_S = 200GPa$, $E_c = 28GPa$, $f_s = 460MPa$, $f_{ds} = 506MPa$, $f_c = 33MPa$, $f_{dc} = 40MPa$, $f_v = 250MPa$, $f_{dv} = 275MPa$

$\alpha = 8$, $\beta = 1/2$, $K_{LE} = 0.45$, $K_{ME} = 0.3$, (for elements with one end fixed and the other free in Table 3.1)

Equations: $y_e = y_t/\mu_t$ $m_a = \rho_{den}\, l\, b_w d_0$, $m = K_{ME} m_a$, $I \approx \dfrac{(\gamma_0+1) b_w d_0^{\,3}}{24}$, $k_a = \alpha E_c I/l^3$, $k_e = K_{LE} k_a$, $T = 2\pi\sqrt{m/k_e}$, $F_1 = P_r\, b\, l$, $R_m = k_e y_e$, $E_{el} = k_e y_e^{\,2}/2$, $E_{\max} = C\, E_{el}$

(C obtained from energy spectra), $k_{e1} = E_{\max}/(y_e y_t - y_e^{\,2}/2)$, $R_{m1} = k_{e1} y_e$, $q_u = \dfrac{R_{m1}/K_{LE}}{l}$, $M_u = \beta q_u l^2$ (for $\rho = \rho'$), $d_1 = \left(\dfrac{24 l^3 k_{e1}}{(\gamma+1)\alpha K_{LE} E_c b_w}\right)^{1/3}$, $\rho = \rho' = \dfrac{M_u}{f_{ds}\, b_w\, d\,(d-d')}$;

Convergence conditions: $|(d_1 - d_0)/d_0| < 0.001$ and $|(\gamma_1 - \gamma_0)/\gamma_0| < 0.001$

4.3 Effectiveness of the Design Approach in Achieving Expected Performance Level

Whether the responses of structural member can be effectively controlled to reach an expected performance in the blast design greatly depends on the selection of the proper response parameter as the performance indicator. Currently the displacement is chosen for the blast resistant design of reinforced concrete members in TM5-1300 [T2] and Mays and Smith [M3] while the displacement ductility factor is employed in TM5-855-1 [T1], Biggs [B1], and ASCE Manual 42 [A2]. However, in Chapter 3, it is pointed out that the utilization of either y_t or μ_t alone is not adequate in controlling the responses of the member reaching its expected performance level, and thus when carrying out an effective performance-based blast design it is better to incorporate both of them. This conclusion is mainly drawn from a brief conceptual analysis in Chapter 3; here to prove it in detail, three practical design examples with different boundary conditions documented in the current design guidance [T2, M3, B1] are critically examined and evaluated. These three design examples are further implemented with the design approach using energy spectra and thus to evaluate the effectiveness of the approach.

Design Example I (Mays and Smith)

This design example given in the book of Mays and Smith [M3], as shown in Figure 4.1, demonstrates the design of a cantilever wall loaded by a blast with their design procedure. In the design the expected performance of the designed wall under the blast condition was specified by $y_t = 210$ mm ($\theta_t = 4^o$). Since the blast loading only lasted for a relatively short period of time ($t_d = 4.83$ms), it was assumed by them that the blast force was located in the impulsive state. Thus

$$\frac{i^2}{2m} = R_m\left(y_t - \frac{1}{2}y_e\right) \tag{4.2}$$

According to Mays and Smith's design, for a unit width of the cantilever wall and by specifying $\rho = \rho' = 0.5\%$, the value of d was solved with Equation (4.2), where the parameters of R_m, y_e, and m for the equivalent SDOF system could be expressed with d. After that, the support reaction force was computed to find ρ_v. Mays and Smith's results are listed in case A1 in Table 4.2.

Design Example II (TM5-1300)

The analysis is further extended to the second typical design example given in TM5-1300 [T2]. This example intended to design an interior beam of a roof subjected to an overhead blast load. Structural configuration and the blast loading to be resisted are shown in Figure 4.2. The objective performance of this beam in the blast design was specified by y_t = 53 mm (θ_t=1°). The same interior beam except for the utilization of different material properties was also introduced in the design manual 2.08 (DM-2.08) by NFEC [N4].

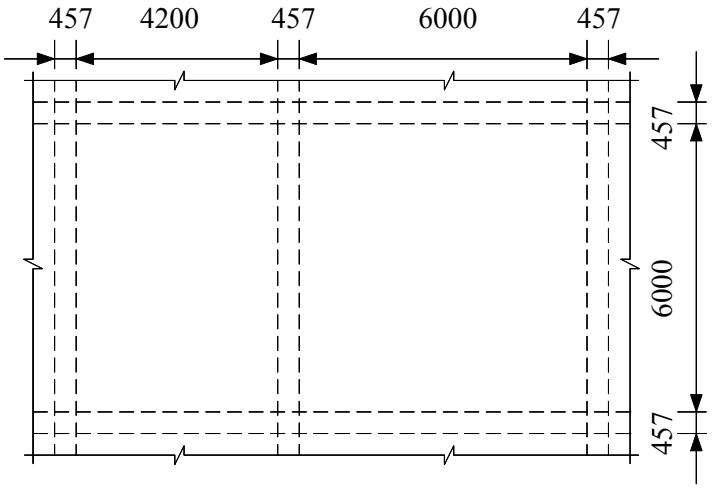

(a). Beam layout

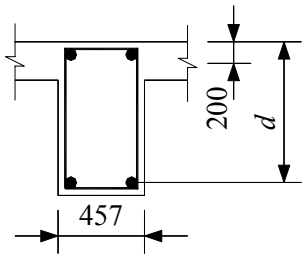

(b). Section dimension

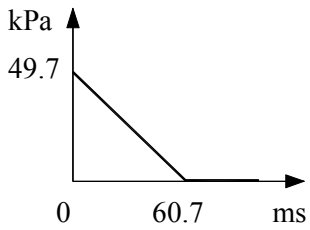

(c). Blast force

Figure 4.2 Layout of a fixed supported beam in design example II (unit: mm)

In TM5-1300 and DM-2.08 cases, three assumptions were made during the design process. Firstly, this particular beam was continuously connected to the adjacent floors thus the mass (m) necessary in computing T of the equivalent SDOF system of the designed beam, included the mass of the beam itself plus 20% of the slabs perpendicular to that beam. Secondly, the force applied to 50% of the adjacent floors would transfer to this interior beam. The third assumption was that the stiffness and strength contribution from adjacent floors was neglected. After a preliminary selection of a cross-sectional dimension and ρ by designer's experience, y_m^{eq} was examined with y_t. If it exceeded the target y_t, the cross section was modified and the above process was repeated. The results are listed in cases B1 and B2 in Table 4.2.

Design Example III (Biggs)

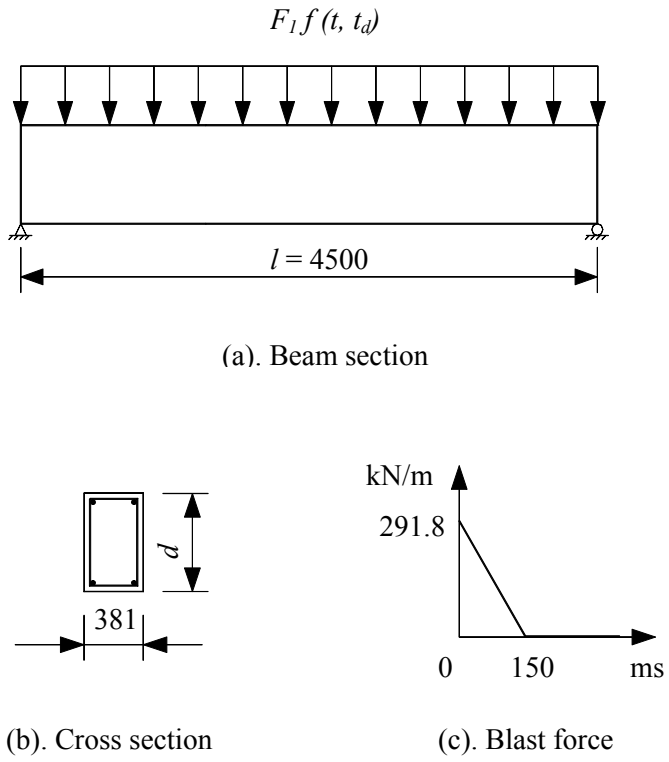

Figure 4.3 Sketch of a simply supported beam in design example III (unit: mm)

The third design example given in the book of Biggs [B1] is accomplished through limiting the displacement ductility response of the member to be less than the target. As shown in Figure 4.3, a simply supported reinforced concrete beam with a span of 4.5 m was considered which had been subjected to a uniformly distributed blast loading with the magnitude and time function shown. In addition to the weight of the beam itself, there was an attached dead weight of 1.75 kN/m. In this design the expected performance of the beam in the blast conditions was stated by $\mu_t = 3$. Since the blast loading lasted for a very long time (150 ms) in this example, then

$$R_m = F_1 \frac{1}{1 - 1/2\mu_t} \tag{4.3}$$

Equation (4.3) was used to obtain the first trial value of ultimate strength (R_m), based on which the primary selection of the cross section was finished by fixing ρ to be 1.5%. After converting this selected member into the equivalent SDOF system, μ^{eq} was examined with μ_t. Biggs's design results are listed in case C1 in Table 4.2. It can be seen that μ^{eq} was a little larger than μ_t thus it was recommended to increase the dimension of the beam cross section by about 10%.

Table 4.2 Design examples in current design guidance [B1, N4, M3, T2]

Case	l (mm)	P_r (kPa)	t_d (ms)	y_t (mm)	μ_t	f_{ds} (Mpa)	f_{dc} (Mpa)	Specified ρ (%)	d (mm)	ρ_v (%)	y_e^{eq} (mm)	μ^{eq}	y_m^{eq} (mm)	μ_{cd}	μ_{cc}
Design example I: Mays and Smith's cantilever wall															
A1	3000	2080	4.83	210		506	40	0.50	400	0.18	23	9	210	17.0	17.5
A2	3000	9961	3.12	210		506	40	0.50	835	0.15	11.1	18.9	210	19.7	15.8
A3	3000	2080	4.83	210		506	40	0.31	530	0.15	14	15	210	22.7	11.6
Design example II: TM5-1300's fixed supported beam*															
B1	6000	49.7	60.7	53		532	32.8	0.44	712	0.24	3.64	9	33		15.9
B2	6000	49.7	60.7	53		455	34.5	0.44	712	0.22	3.14	17	53		15.9
	(kN/m)					Design example III: Biggs's simply supported beam									
C1	4500	291.8	150		3	431	34.5	1.5	686		8.5	3.7	31.5		
C2	6000	291.8	150		3	575	34.5	2.2	550		33.3	3	100		

* B1: TM5-1300; B2: DM-2.08

In TM5-1300 [T2], DM-2.08 [N4] and Mays and Smith [M3] design procedures, the expected performance of reinforced concrete members is assumed to be fulfilled by a given y_t and with the response of $y_m^{eq} \le y_t$. However the control of μ^{eq} is not executed clearly in these design procedures. This may lead to such designs tending toward the unsafe side, which is illustrated by design case A2. This case was carried out with Mays and Smith's design procedure on the cantilever wall with the same pre-assumed ρ and design target θ_t but under a more severe blast loading. A

comparison of cases A2 with A1 indicates that d of the designed member has an obvious increase of 435 mm, which in turn diminishes the elastic displacement y_e^{eq} of the member from 23 mm to 11.1 mm and as a consequence μ^{eq} increases from 9 to 18.9. With Equation (4.1), the curvature ductility demand ($\mu_{cd} = \varphi_u / \varphi_y$) of the fixed-end section in design case A2 reaches 19.7. By comparing μ_{cd} with μ_{cc}, the curvature ductility capacity obtained from the section analysis, it is clear that design case A2 is not adequate in resisting the blast force since μ_{cc} for this designed member has only 15.8 to be less than μ_{cd}. This phenomenon also appears in design case B2. Obviously the unsafe design in these cases demonstrates that using y_t alone could not provide an effective design to fulfil the expected performance. Actually such a non-effective design of the members is due to the unreasonably pre-assumed ρ. As a relatively small ρ is specified in the early design stage, d has to be enlarged to meet y_t, which will cause an excessive μ^{eq}. This action is apparently reflected in design case A3, where the design of Mays and Smith's cantilever wall is repeated but with a relatively small ρ =0.31%. Certainly the increase in ρ will to some extent release the non-effectiveness of the design, however the problem is that a reasonable ρ is not evident at the start of the design process.

In TM5-855-1 [T1], Biggs [B1], and ASCE Manual 42 [A2] design guidance, the expected performance of reinforced concrete members in the blast design is assumed to be fulfilled by a given μ_t and with the response of $\mu^{eq} \le \mu_t$. However in these procedures, the corresponding maximum displacement y_m^{eq} is not restricted explicitly and in such situations the expected performance of designed members could not also be satisfied effectively. It can be illustrated from design case C2, where a comparatively small $\mu_t = 3$ is employed to control the member's responses at a relatively low damage level, however in this case y_m^{eq} has unexpectedly reached 100 mm (support rotation of the member about 2^o). Assuming that design case C2 is performed for a column, this unexpected large y_m^{eq} equivalent to a lateral drift of

1/30 at the mid-height could produce a significant secondary effect, which will cause more damage or even the collapse of the member.

The above detailed comparisons indicate that to control the member's responses in reaching their expected performance level, it is necessary to incorporate both y_t and μ_t into the blast design and satisfy $y_m^{eq} \le y_t$ and $\mu^{eq} \le \mu_t$. Although $y_m^{eq} < y_t$ and $\mu^{eq} < \mu_t$ will tend the design toward the safe side, the safety margin could still not be controlled effectively. And when considering technical efficiency and cost, they often lead to the over-design of members, which is not desirable for the clients. Thus it is better to control $y_m^{eq} = y_t$ and $\mu^{eq} = \mu_t$ with a relatively conservative y_t and μ_t to provide the necessary safety margin. The previous demonstration of the design approach involving the practical design case in Table 4.1 indicates that y_t and μ_t could be achieved exactly since in this case $y_m^{eq} = y_t$ and $\mu^{eq} = \mu_t$. Thus the responses of the structural members against blast forces can be effectively controlled to reach the target performance in the blast design with the approach based on energy spectra. To further explain this, the above three design examples are again executed with the developed approach as follows.

Combining the different targets of y_t and μ_t documented in the existing blast design guidance [T1, T2, B1, B4, N4, M3], four performance levels are defined according to the structural nature, function and importance as shown in Table 4.3 [S6]. It describes the damages associated with various levels of performance and suggests the corresponding μ_t and D_t for one-way reinforced concrete members, where $D_t = l/y_t$, the ratio of member length to target displacement. According to Table 4.3, the previous three design examples are implemented with the presented approach and the design results are listed in Table 4.4. The results indicate that $y_m^{eq} = y_t$ and $\mu^{eq} = \mu_t$ for all design cases thus the expected performance can be effectively fulfilled. Moreover the design approach overcomes the subjectivity involved in the existing design guidance where ρ is specified in somewhat arbitrary way. The implementation of this design approach into these examples also indicates

that this approach could account for arbitrary blast conditions.

Table 4.3 Performance levels for one-way reinforced concrete member defined by the combination of target displacement and displacement ductility factor [S6]

Performance level	Protection level	Description of damage	μ_t	D_t*
A	High	Superficial	1	240
B	Medium	Repairable	3	120
C	Low	Some elements unrepairable	6	60
D	Very low	Overall structure unrepairable	10	30

*Multiply D_t by 0.5 for fixed/free (cantilever) members

Table 4.4 Design results for the members at various performance levels with the design approach using energy spectra

Performance Level	μ_t	y_t (mm)	d (mm)	ρ or ρ'	ρ_v	μ_{eq}	y_m^{eq} (mm)
Design example I: May and Smith's cantilever wall (l=3000mm)							
A	1	25	563	3.21%	1.28%	1	25
B	3	50	482	1.59%	0.36%	3	50
C	6	100	411	1.21%	0.15%	6	100
D	10	200	328	1.19%	0.15%	10	200
Design example II: TM5-1300's fixed support beam (l=6000mm)							
A	1	25	431	2.93%	2.26%	1	25
B	3	50	414	1.75%	1.09%	3	50
C	6	100	382	1.61%	0.86%	6	100
D	10	200	324	1.79%	0.75%	10	200
Design example III: Biggs's simply support beam (l=4500mm)							
A	1	18.75	556	3.23%	1.34%	1	18.75
B	3	37.5	544	1.91%	0.63%	3	37.5
C	6	75	515	1.79%	0.53%	6	75
D	10	150	453	2.03%	0.52%	10	150

4.4 Numerical Verification of the Design Approach

Theoretically, the expected performance of reinforced concrete member in certain blast condition could be fulfilled with this approach since $y_m^{eq} = y_t$ and $\mu^{eq} = \mu_t$ are achieved simultaneously in the design. However, it should be noted that y_m^{eq} and μ^{eq} are obtained from the equivalent SDOF system of designed reinforced concrete member against the blast loading. Due to the complicated behaviours of continuous reinforced concrete members, some differences between the responses of equivalent SDOF system (y_m^{eq} and μ^{eq}) with those of the designed member (y_m^{rc} and μ^{rc}) under the given blast loading are conceivable and therefore will cause differences between y_m^{rc} and μ^{rc} and the corresponding targets of y_t and μ_t. To evaluate the effectiveness of the presented approach in controlling the responses of designed member to achieve the expected performance level, y_m^{rc} and μ^{rc} of the member under the given blast loading are computed with the program ABAQUS [A1] and compared with their respective targets (y_t and μ_t).

4.4.1 Finite element models

The detailed finite element models can be found in Chapter 2. The concrete model, which uses concepts of smeared cracking and isotropic compressive plasticity to represent the inelastic behaviour of concrete, is employed to represent the concrete properties. Reinforcement is simulated by the Von-Mises yield criterion with associated flow and isotropic strain hardening. Furthermore, Timoshenko beam elements are assigned to model the members while the rebar option is utilized to place each reinforcement at its exact location. To ensure the computational stability, the minimum and the maximum allowable time increment necessary in the automatic incrementation are taken as 1×10^{-7} s and 0.01 s, respectively. The finite element models have been effectively verified from a simply supported beam and a square slab subjected to blast loadings tested by Seabold [S3] and Keenan [K3] where numerically predicted responses have a good match with experimental ones.

It has been pointed out by Biggs [B1] and by Krauthammer [K4] that the damping effect could be properly neglected in the dynamic analysis of structural responses under blast conditions. In addition, the aim of dynamic analysis herein is to evaluate the effectiveness of the design approach using energy spectra. Since damping has been ignored in the design, it is more reasonable to neglect the damping effect in this dynamic analysis.

4.4.2 Results and discussion

With the finite element models above, the nonlinear dynamic analysis is performed on the designed cantilever wall shown in Table 4.1 under the given blast loading condition. Free-end responses of the wall in terms of displacement versus time are illustrated in Figure 4.4. It can be seen that y_m^{rc} is slightly less than y_t with a deviation of about 10% of y_t. Note that y_e^{rc} is computed from subtracting y_m^{rc} by the permanent set ($y_m^{rc} - y_e^{rc}$), which is equal to the neutral position for the axis of residue vibration. μ^{rc} for the designed walls under given blast conditions is determined by y_m^{rc} / y_e^{rc}, which is 5.18 to be less than $\mu_t = 9$. The deviation between μ^{rc} and μ_t is about 42.4% of μ_t. Thus it seems that the error between μ^{rc} and μ_t is larger than that between y_m^{rc} and y_t.

The dynamic response simulations of designed members in Table 4.4, when subjected to the respective blast loadings are also performed and the results are shown in Figures 4.5 to 4.7. It can be observed from these graphs that there are different levels of errors according to the boundary conditions. For the fixed/free members in design example I, their y_m^{rc} at the free end under the given blast loadings is better controlled since the error between y_m^{rc} and y_t is slight and unaffected by the various levels of performance. However, for the fixed/fixed members in design example II, with the increase of y_t and μ_t, it seems that the design produces more conservative error between y_m^{rc} and y_t.

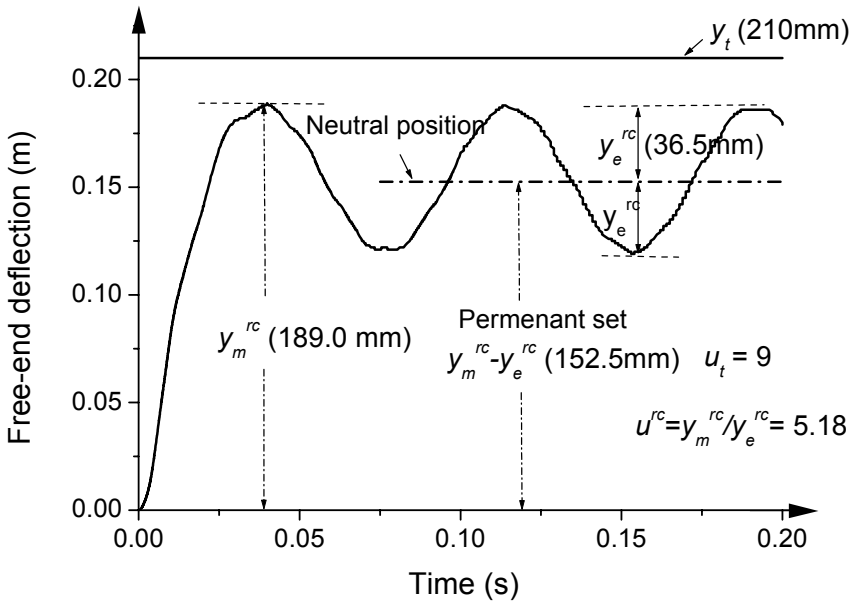

Figure 4.4 Deflection history of the cantilever wall designed in Table 4.1 under the given blast loading

Values of μ^{rc} for designed members at various levels of performance in design examples I, II and III for blast loadings are also displayed in Figures 4.5 to 4.7. A comparison of μ^{rc} with μ_t demonstrates that μ^{rc} is generally less than μ_t except for μ_t=1. Actually under blast conditions, concrete cracking will inevitably appear which leads to a slight plastic set of the designed member even if the design requires the member in the elastic limit state (μ_t=1). But such a slight non-conservative error, which does not exceed 4% of μ_t in all cases, is not significant since a very stringent responses target (μ_t=1) is required in the design. With an increase of μ_t, the design becomes more conservative.

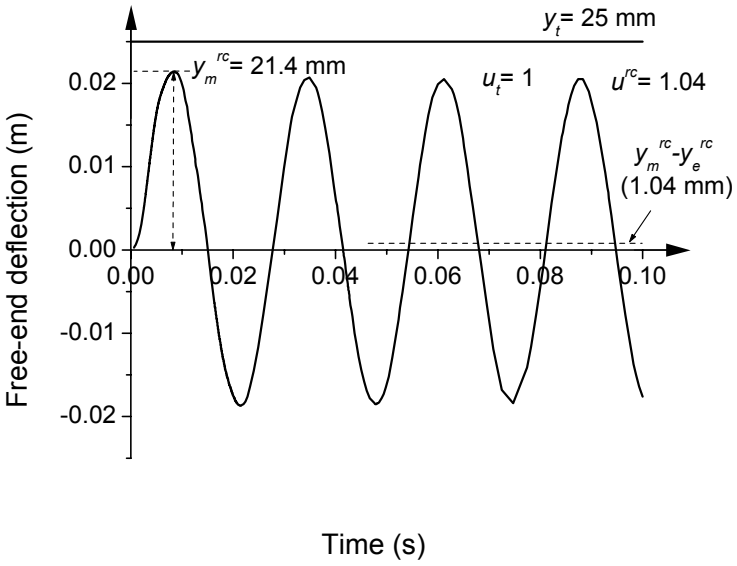

(a). At performance level A

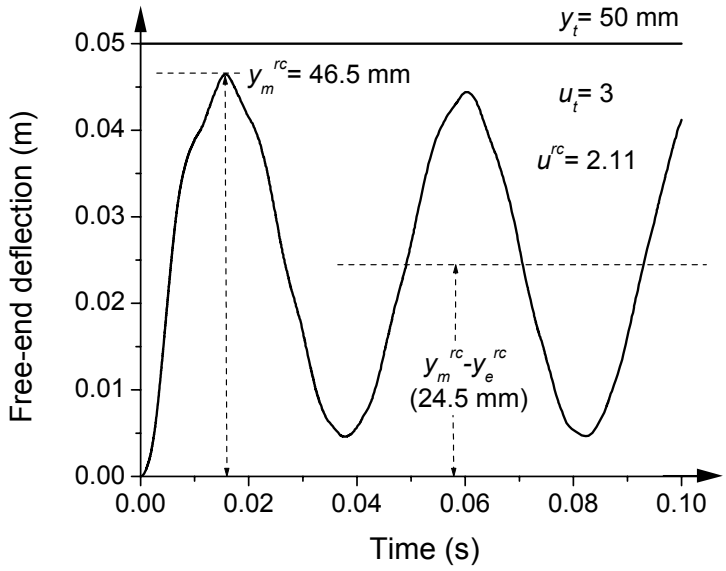

(b). At performance level B

Figure 4.5 Deflection history of the designed cantilever walls under the given blast loading (Example I)

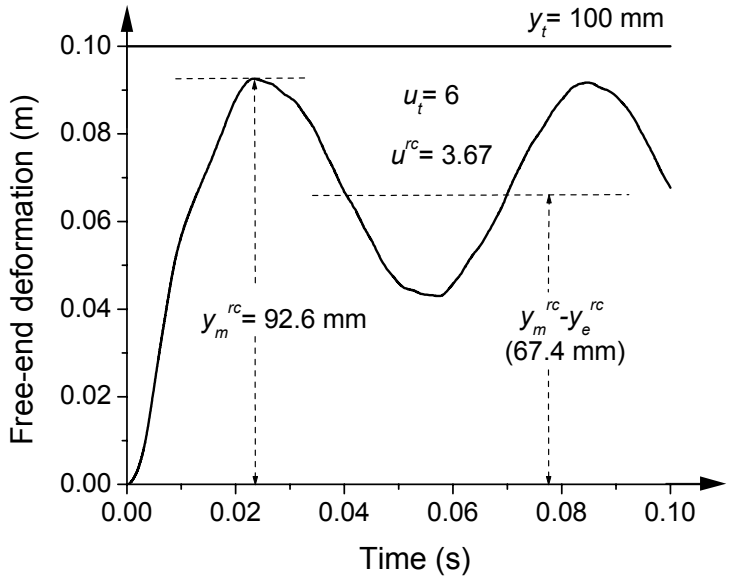

(c). At performance level C

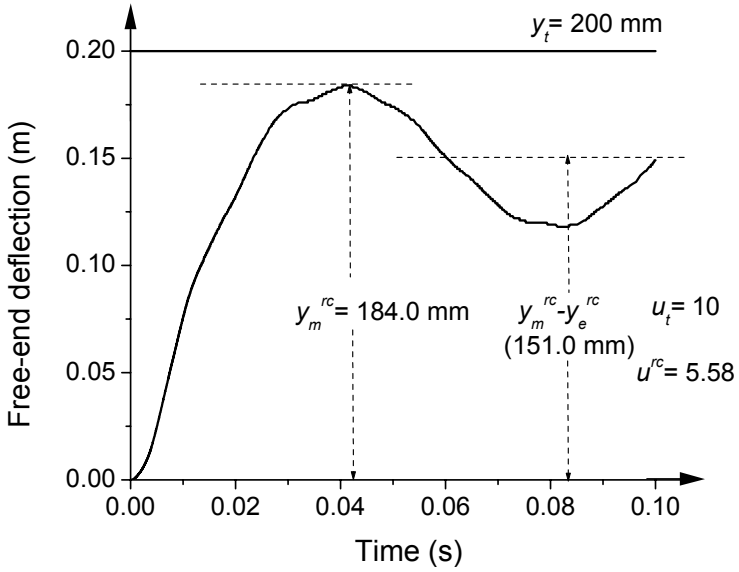

(d). At performance level D

Figure 4.5 (Continued)

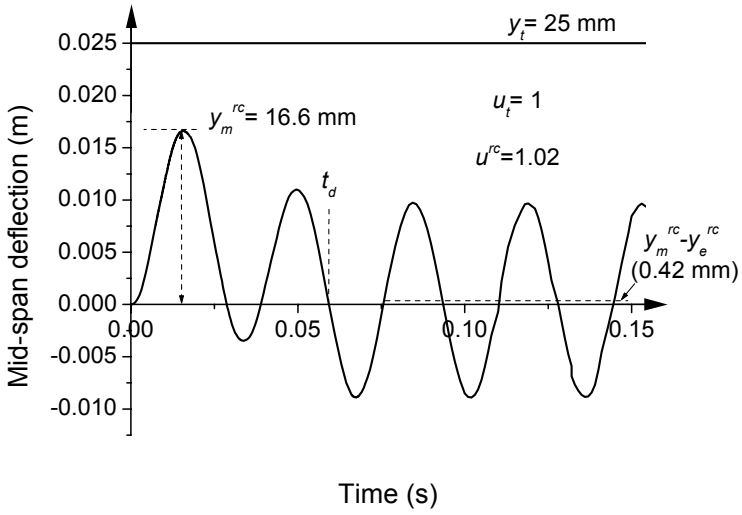

(a). At performance level A

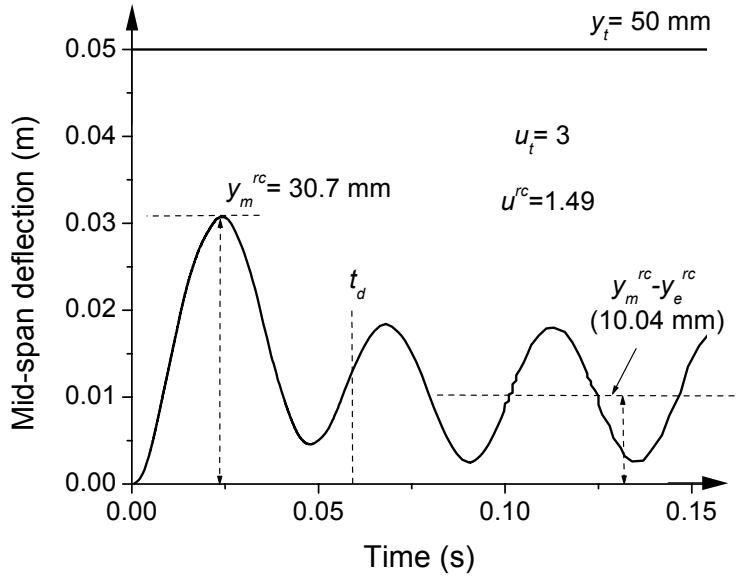

(b). At performance level B

Figure 4.6 Deflection history of the designed fixed-supported beams under the given blast loading (Example II)

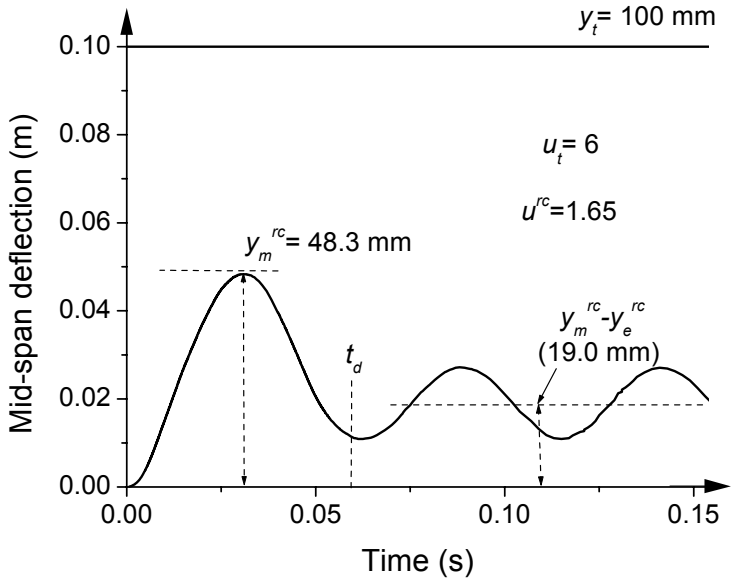

(c). At performance level C

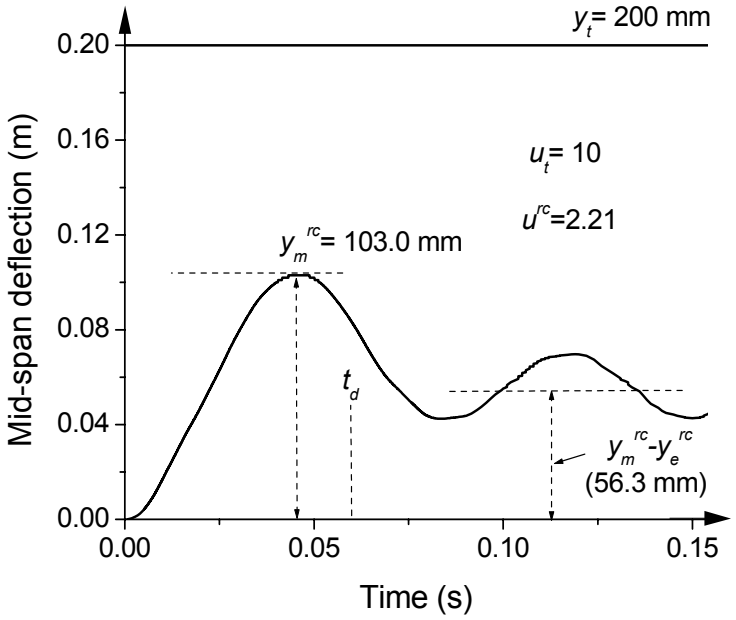

(d). At performance level D

Figure 4.6 (Continued)

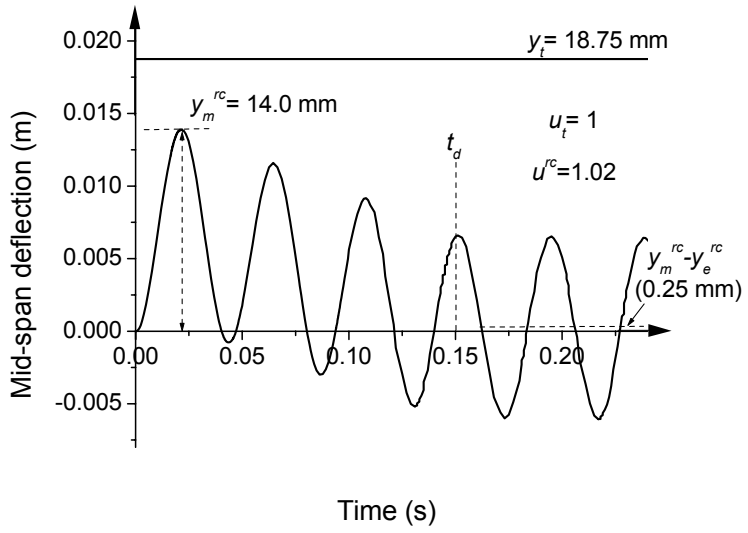

(a). At performance level A

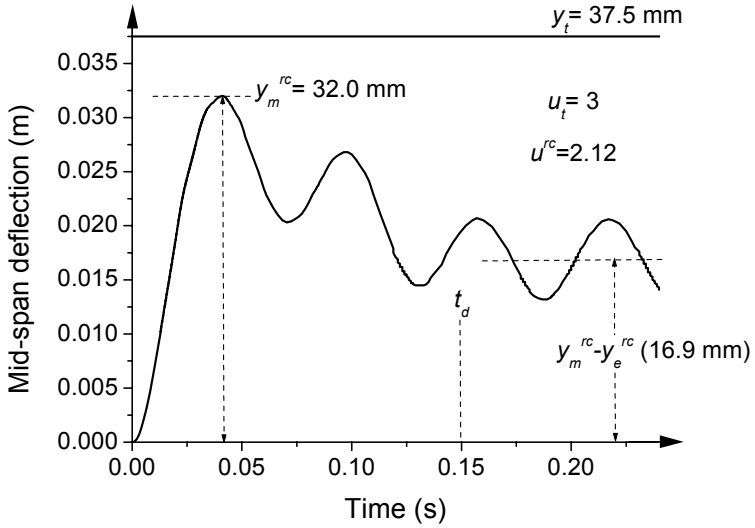

(b). At performance level B

Figure 4.7 Deflection history of the designed simply supported beams under the given blast loading (Example III)

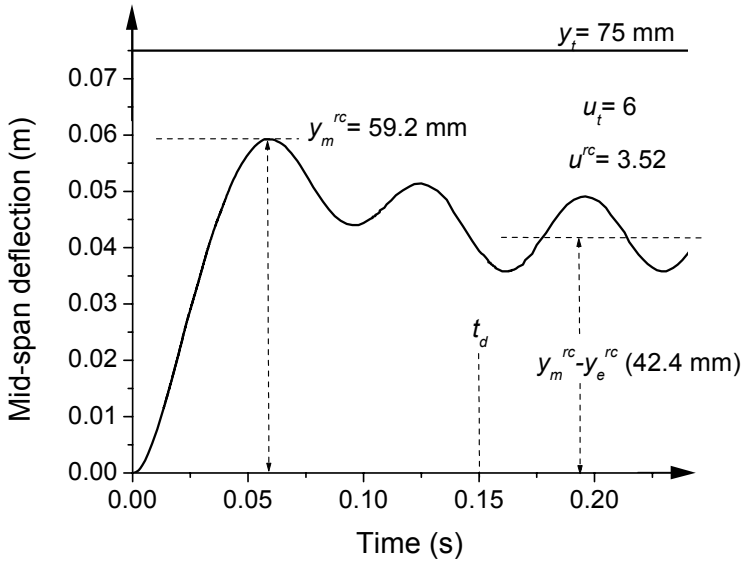

(c). At performance level C

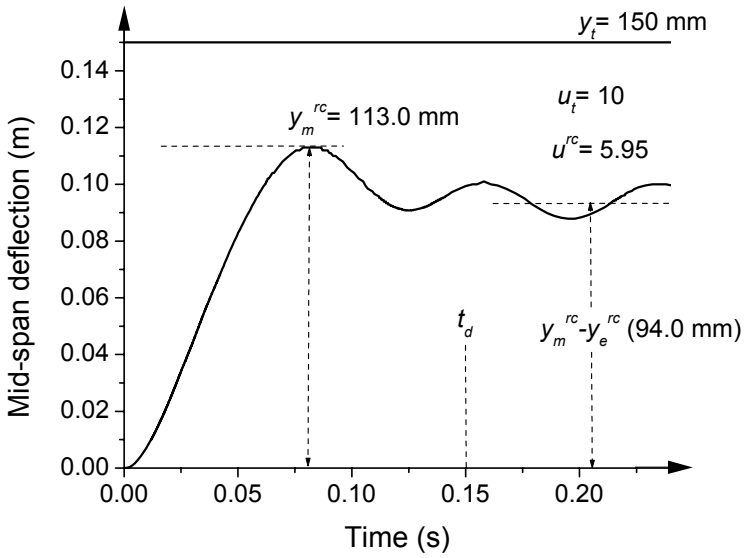

(d). At performance level D

Figure 4.7 (Continued)

From the above analysis, it can be summarized that some errors exist between the responses (y_e^{rc} and μ^{rc}) of the designed reinforced concrete member and their respective target values (y_t and μ_t). The reasons for producing such errors are mainly due to the simplifications adopted in the blast design. Basically, the design approach using energy spectra includes two stages. The first stage involves the computation of k_e and R_m of the equivalent SDOF system for y_t, μ_t and the given blast condition. After that, d and ρ of reinforced concrete member are derived from k_e and R_m according to the particular characteristics of concrete and reinforcement embedded. To find at which stage the errors are produced, a comparison of the dynamic responses of the equivalent SDOF system having k_e and R_m with those of designed reinforced concrete member having d and ρ under the given blast condition is performed on the cantilever wall in Table 4.1. The results are shown in Figure 4.8. It can be observed that y_m^{eq} and μ^{eq} of the equivalent SDOF system meet their targets exactly while for reinforced concrete member, their y_m^{rc} and μ^{rc} are less than the corresponding targets. This indicates that the errors are produced in the derivation of d and ρ from k_e and R_m in the design procedure.

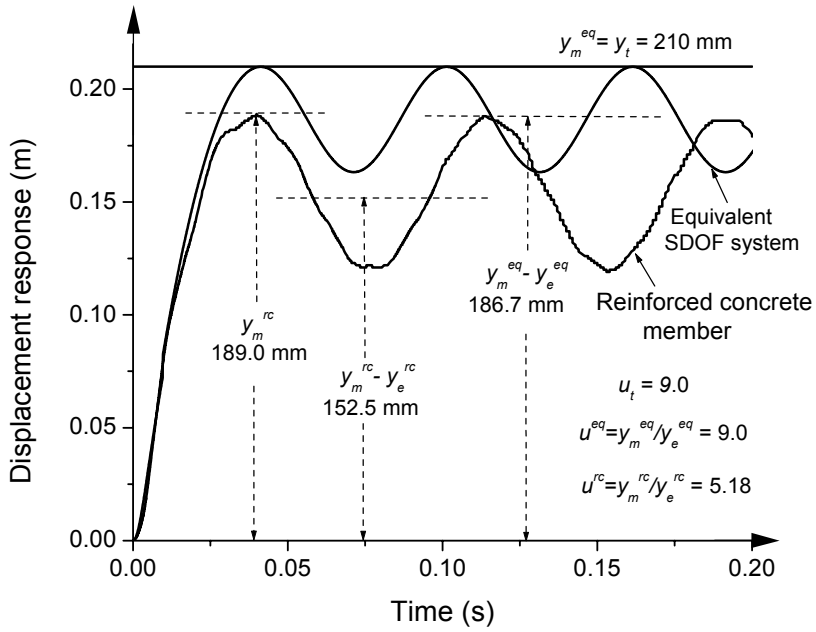

Figure 4.8 Comparison of the responses of the designed cantilever wall with those of the equivalent SDOF system under the given blast loading

Several points, which are involved in the derivation of d and ρ from k_e and R_m account for the errors between the responses (y_e^{rc} and μ^{rc}) and their respective target values (y_t and μ_t) as follows:

1. In converting the continuous reinforced concrete member into the equivalent elastic-perfectly-plastic SDOF system, the load and mass factors (K_{LE} and K_{ME}) are necessary, but their values are obtained in an approximate way. That is because the resistance of reinforced concrete member is a continuous process, however, in order to simplify the problem, it is represented as two or three independent linear stages. Thus the utilization of K_{LE} and K_{ME} in the design approach will produce some errors between the responses of the designed member and design targets.

2. The second reason for errors exists in the determination of average moment of inertia (I) of the cross section of reinforced concrete members. It is well known that the embedded reinforcement and the cracking propagation of the concrete have much effect on the value of I . To simplify this problem in the design, I obtained from the expression of $(\gamma+1)b_w d^3/24$ is used to calculate the member stiffness and the corresponding deformation. However the adoption of γ which is dependant upon the experimental data fitting will incur some errors in the design of reinforced concrete members.

3. Although R_m of the equivalent SDOF system for the reinforced concrete member is known, it is still difficult to determine ρ accurately, with which the ultimate strength of the designed member equates to the anticipated value (R_m) exactly. In these design examples, using $\rho = \rho' = \dfrac{M_u}{f_{ds}\, b_w\, d\,(d-d')}$ to calculate the equal tension and compression reinforcement ratio is conservative since it is assumed that concrete in the compression zone provides no contribution in the ultimate strength of the reinforced concrete member. Thus the reinforcement ratio tends to be enlarged in the design, which causes some errors in fulfilling the design targets.

4.5 Summaries

The effectiveness of the performance-based blast resistant design approach using energy spectra has been evaluated in this chapter. From the demonstration of the design approach, it is found that it is efficient and effective to apply this approach into the practical design of reinforced concrete members against blast loadings without the difficulty in convergence.

The design approach presented in Chapter 3 is effective in incorporating the performance level defined by both y_t and μ_t into the design and controlling the responses of y_m^{eq} and μ^{eq} to meet the respective target values exactly. Comparisons

of this design procedure with those existing design guidance indicate that this approach can overcome the disadvantages existing in the existing design guidance in terms of the effective control of the responses of the equivalent SDOF system of the designed member to achieve the expected performance level without any subjectivity involved.

Although the presented design approach tries to keep the responses of the equivalent SDOF system under control to reach the expected performance level with $\mu^{eq} = \mu_t$ and $y_m^{eq} = y_t$, the numerical verification shows that some errors do exist between the responses of designed reinforced concrete member (y_m^{rc} and μ^{rc}) under the given blast force and their respective targets (y_t and μ_t). The errors come from the derivation of d and ρ from k_e and R_m due to some simplifications in converting the continuous reinforced concrete members into equivalent SDOF systems and computing the cross-sectional moment of inertia and ultimate strength of the members. However since the reinforced concrete member can be specifically designed against the given blast condition with the presented approach, the errors can be further analysed. Numerical results indicate that the errors are influenced by the boundary conditions of the member as well as the performance targets of y_t and μ_t, and the error between μ^{rc} with μ_t seem to be greater than that between y_m^{rc} and y_t. Further research in Chapters 5 and 6 will derive the formulae to quantify the errors and involve the formulae into the modification of the design approach using energy spectra.

CHAPTER FIVE

PERFORMANCE–BASED BLAST RESISTANT DESIGN OF REINFORCED CONCRETE MEMBERS USING ENERGY SPECTRA — PART III. FORMULATION OF ERROR INDICES

Synopsis

One of the main advantages of the performance-based blast resistant design of reinforced concrete structural members using energy spectra addressed in Chapters 3 and 4 is that the two indices indicating the errors between the maximum displacement and displacement ductility responses of the designed member against the given blast loading and their corresponding design targets can be explicitly analysed, since with this design procedure the structural member can be uniquely designed. The knowledge about the errors will be significantly beneficial in keeping the actual responses of designed members under control rather than those of the corresponding equivalent SDOF system within the blast design. Therefore an analysis of these two error indices is carried out in an attempt to gain their simplified explicit expressions with a variety of basic variables including the peak pressure and duration of a blast loading, the target displacement and displacement ductility factor of the design, member dimensions, support conditions (*SC*), the strength and Young's modulus of concrete and reinforcement, and the longitudinal reinforcement ratio (ρ). It is discovered through the extensive numerical studies and statistical analyses that these two error indices could be properly formulated by two items: a nonlinear fitting function correlated with ρ and *SC*, and a random variable to consider the influence of the others. The formulae of error indices provide a valuable tool of modifying the performance-based blast resistant design of the members using energy spectra and assessing the performance of the designed

members probabilistically accounting for different uncertainties. These applications will be discussed in Chapter 6.

Keywords: Expected performance level, Target displacement, Target displacement ductility factor, Energy spectra, Equivalent SDOF system, Error indices Maximum displacement responses, Displacement ductility responses

5.1 Introduction and Background

To keep the responses or damages of designed members under control to satisfy an expected performance level, much blast resistant design guidance have been issued in TM5-1300 [T2], TM5-855-1 [T1], Biggs [B1], Mays and Smith [M3], and ASCE 7-42 [A2] *etc*. Within these available design guidance, only a single response: the displacement response or the displacement ductility response for the members at the significant point, is restricted by specifying a longitudinal reinforcement ratio in the initial stage of the design based on the designer's experience. To control both the displacement and displacement ductility response of a reinforced concrete member under blast loading simultaneously, a blast resistant design approach using energy spectra was developed and evaluated in Chapters 3 and 4. The effective depth (d) and longitudinal reinforcement ratio (ρ) of the reinforced concrete member can be specifically obtained in this approach by converting the continuous reinforced concrete member into an equivalent elastic-perfectly-plastic single-degree-of-freedom (SDOF) system [B1] and controlling its maximum displacement and displacement ductility responses (y_m^{eq} and μ^{eq}) to be exactly equal to the corresponding targets (y_t and μ_t).

Obviously, this design approach is accomplished based on an assumption that the responses (y_m^{rc} and μ^{rc}) of the designed reinforced concrete member at the significant point can be represented by the responses of its equivalent SDOF system (y_m^{eq} and μ^{eq}) under the given blast loading. However, a difference of y_m^{rc} and μ^{rc} with its respective y_m^{eq} and μ^{eq} is expectable due to the complexities of the

nonlinear dynamic behaviours of reinforced concrete members under blast conditions. This further causes the errors existing between y_m^{rc} and μ^{rc} and the design targets of y_t and μ_t, as indicated from the design and verification process for the blast resistant design of reinforced concrete members using energy spectra in Figure 5.1.

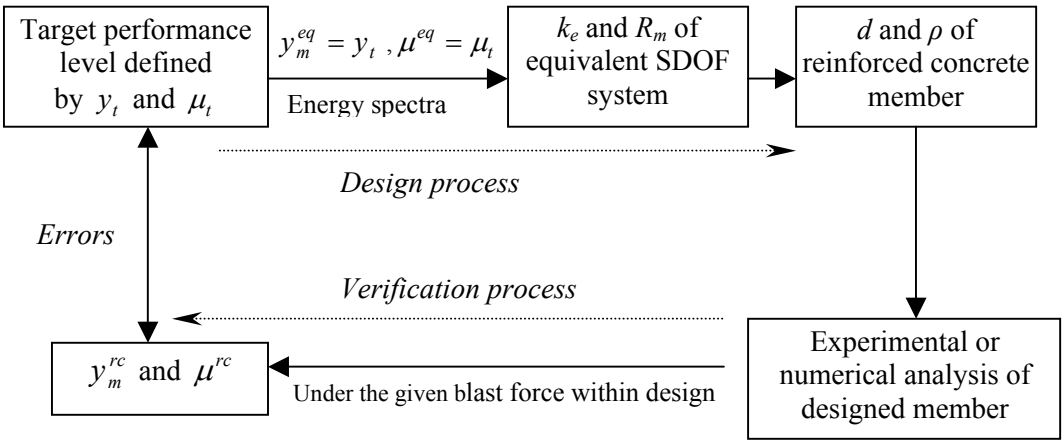

Figure 5.1 Design and verification process for performance-based blast resistant design of reinforced concrete members using energy spectra

In fact a good performance-based blast resistant design should be capable of controlling the responses of designed reinforced concrete member (y_m^{rc} and μ^{rc}) rather than those of the corresponding equivalent SDOF system (y_m^{eq} and μ^{eq}) with the given design targets (y_t and μ_t). To fulfil this objective, it is worthwhile to analyse the errors between y_m^{rc} and μ^{rc} of the member designed upon the blast resistant design approach using energy spectra and the corresponding targets of y_t and μ_t, since the knowledge of the errors can be applied in the modification of the design. Moreover, the errors also represent the differences of y_m^{rc} and μ^{rc} with the

respective y_m^{eq} and μ^{eq}, accordingly they provide a simpler way in the estimation of y_m^{rc} and μ^{rc} for a designed member under blast conditions from y_m^{eq} and μ^{eq}. Based on this point, the probabilistic performance of the member at various levels can be effortlessly assessed accounting for different types of uncertainties without performing nonlinear dynamic finite element analysis, which would otherwise consume a lot of computational effort.

In this chapter, after the definition of two non-dimensional error indices, the related variables affecting them are discussed. With a larger number of numerical studies of the error indices involving different variables effects and the subsequent statistical analyses, simple formulae to estimate the error indices are recommended with the applications of these formulae to be addressed in Chapter 6.

5.2 Definition of Error Indices

To obtain a consistent measurement of the degree of the errors between y_m^{rc} and μ^{rc} of the member designed with the developed approach and their respective y_t and μ_t, two non-dimensional error indices are defined as

$$\varsigma_y^{rc} = \frac{y_t - y_m^{rc}}{y_t} \tag{5.1}$$

$$\varsigma_\mu^{rc} = \frac{\mu_t - \mu^{rc}}{\mu_t} \tag{5.2}$$

where ς_y^{rc} is the displacement error index standing for the error between y_m^{rc} and y_t; and ς_μ^{rc} is the displacement ductility error index representing the error between μ^{rc} and μ_t.

Equations (5.1) and (5.2) describe the basic relationships between (y_m^{rc}, μ^{rc}), (y_t,

μ_t) and (ς_y^{rc}, ς_μ^{rc}). With ς_y^{rc} and ς_μ^{rc} initially known, they become beneficial in controlling y_m^{rc} and μ^{rc} within the blast resistant design or in assessing the performance probabilistically for designed members against potential blast loadings. The detailed implementation will be addressed in Chapter 6. However depending on these two equations to estimate ς_y^{rc} and ς_μ^{rc} seems to have few advantages since y_m^{rc} and μ^{rc} have to be firstly calculated. This entails explosion testing or numerical finite element analysis of the designed members under blast conditions, which are sure to consume much construction cost or intensive computational effort. Therefore, simple alternative formulae for the determination of ς_y^{rc} and ς_μ^{rc} rather than Equations (5.1) and (5.2) need to be developed.

5.3 Symbolical Expressions of Error Indices

One of main advantages of the blast resistant design using energy spectra is that by controlling $y_m^{eq} = y_t$ and $\mu^{eq} = \mu_t$, the design solution of d and ρ can be specifically gained with the given design variables including the blast loadings (P_r, t_d), design targets (y_t, μ_t), the support condition (SC), the length (l) and the strength and Young's modulus of elasticity of concrete and reinforcement in dynamic conditions (f_{dc}, E_c, f_{ds}, E_d, and f_{dv}). Therefore d and ρ could be symbolically expressed as functions of these variables

$$d = d(P_r, t_d, y_t, \mu_t, l, SC, f_{dc}, E_c, f_{ds}, E_s, f_{dv}) \qquad (5.3)$$

$$\rho = \rho(P_r, t_d, y_t, \mu_t, l, SC, f_{dc}, E_c, f_{ds}, E_s, f_{dv}) \qquad (5.4)$$

The responses (y_m^{rc} and μ^{rc}) of the designed member under the given blast force are also specifically determined, which can be symbolically written as

$$y_m^{rc} = y_m^{rc}(P_r, t_d, l, SC, f_{dc}, E_c, f_{ds}, E_s, f_{dv}, d, \rho) \qquad (5.5)$$

$$\mu^{rc} = \mu^{rc}(P_r, t_d, l, SC, f_{dc}, E_c, f_{ds}, E_s, f_{dv}, d, \rho) \qquad (5.6)$$

Substituting Equations (5.5) and (5.6) into Equations (5.1) and (5.2) respectively produces ς_y^{rc} and ς_μ^{rc} to be the functions of these variables, which is given by

$$\varsigma_y^{rc} = \zeta_y^{rc}(P_r, t_d, y_t, \mu_t, l, SC, f_{dc}, E_c, f_{ds}, E_s, f_{dv}, d, \rho) \qquad (5.7)$$

$$\varsigma_\mu^{rc} = \zeta_\mu^{rc}(P_r, t_d, y_t, \mu_t, l, SC, f_{dc}, E_c, f_{ds}, E_s, f_{dv}, d, \rho) \qquad (5.8)$$

5.4 Analytical Approach

To derive the explicit expressions of Equations (5.7) and (5.8) is almost impractical, since under most blast conditions the behaviours of reinforced concrete members will exhibit a significant geometric and material nonlinearity. A curve fitting technique with a large number of reliable data for ς_y^{rc} and ς_μ^{rc}, which are determined according to Equations (5.1) and (5.2) with y_m^{rc} and μ^{rc} obtained from nonlinear finite element analyses of the designed members, is executed in this chapter together with the statistical analyses so as to find simplified explicit expressions of Equations (5.7) and (5.8). The procedures are listed as follows:

1) Select the type of *SC*s of reinforced concrete members to be designed;
2) Sample the design variable vector $\{P_r, t_d, y_t, \mu_t, l, f_{dc}, E_c, f_{ds}, E_s, f_{dv}\}'$, where 2000 samples are taken to ensure the accuracy of the following statistical analysis;
3) Design the reinforced concrete member using energy spectra with each sample of the design variable vector to obtain d, ρ and further ρ', ρ_v and b_w of a ratio of d.
4) Repeat (3) until 2000 sampled design cases are accomplished;
5) Select 500 cases with ρ ranging from 0.31% to 2.2%;

6) Perform numerical finite element analysis on the selected 500 design cases to find y_m^{rc} and μ^{rc};
7) Compute ς_y^{rc} and ς_μ^{rc} of the 500 design cases with Equations (5.1) and (5.2);
8) Plot the distributions of ς_y^{rc} and ς_μ^{rc} with the basic design variables;
9) Carry out the curve fitting of the distributions of ς_y^{rc} and ς_μ^{rc} followed by statistical analyses;
10) Recommend the simplified formulae to estimate ς_y^{rc} and ς_μ^{rc}.
11) Change the type of *SC* s of the members and repeat above steps;

5.4.1 Selection of variables

In order to perform the curve fitting of the distributions of ς_y^{rc} and ς_μ^{rc} to find their simplified formulae, the design variables involved in the second step of the above procedure are randomly selected within their concerned ranges respectively which are discussed as follows.

For external explosions, the blast loadings which can be reasonably idealized into triangular pulses are basically dependent on P_r and i (where $t_d = 2i/P_r$) [H1, T1 T2]. Therefore the random selection of P_r and i is executed in their respective ranges from 150 kPa to 59 MPa and from 5.8×10^2 to 3.4×10^4 kPams for the blast resistant design and the following error indices analysis. This provides a significantly wide range of blast incidents. For the more severe blast cases, the design of the structural system with the alternate load path in redistributing loadings seems to be more reasonable and economic where the structural members immediately opposite the blast are allowed to fail. While in the situations of the slighter blasts, the blast loadings become less critical in the structural design.

The random selection of y_t and μ_t is executed in their different ranges according to the various scopes of the blast impulses as shown in Table 5.1 since within the

blast resistant design of a particular reinforced concrete member the determination of the reasonable design targets of y_t and μ_t should account for possible blast intensities. Some overlaps are allowed for the ranges of y_t and μ_t considering that there is no strict watershed for them at a particular impulse within the design. The maximum allowable y_t and μ_t are taken to be respectively larger than the limit of 4^o for non-laced reinforced concrete members recommended in TM 5-1300 [T2] and Mays and Smith [M3] and 10.0 specified in the ASCE special publication [B4] due to the possibility of the actual responses of the designed members in blast conditions located on the conservative side by comparing them with their respective targets of y_t and μ_t.

Table 5.1 Various design targets

Impulse (kPa ms)	$\le 10^3$	$10^3 \sim 10^4$	$10^4 \sim 2\times10^4$	$2\times10^4 \sim 3\times10^4$	$\ge 3\times10^4$
θ_t	$1^o \sim 1.8^o$	$1.4^o \sim 3.2^o$	$2.8^o \sim 3.6^o$	$3.2^o \sim 4.0^o$	$3.4^o \sim 4.8^o$
μ_t	3.0 ~ 8.5	4.5 ~ 10.5	5.5 ~ 12.5	6.0 ~ 14.5	7.0 ~ 16.5
$y_t = l\tan(\theta_t)/2$ for the member with two ends constrained; $y_t = l\tan(\theta_t)$ for member with one end free					

The parameter of l is selected in the range from 4.5 to 9.0 m for the members with two ends constrained while from 2.5 to 4.5 m for members with one end free, which cover the typical cases for most reinforced concrete structures. Due to strain rate effects, the parameters of material properties of concrete and reinforcement in dynamic conditions are implemented in this analysis whose possible ranges used in the design are listed in Table 5.2. Since the structural members exist in the context of structural systems, their real *SC*s are complex and generally depend on the connection with the adjacent members as well as the construction requirements. However in the blast resistant design they are generally idealized into one of the four types as listed in Table 5.3. Considering that reinforced concrete members should be designed to resist the negative deflection or rebound of the members

subsequent to its maximum positive deflection and that the possibility of the explosion occurs in the two opposite sides of the members to be designed, the type of reinforcement layout, where the compression reinforcement area is equal to the tensile reinforcement area, is employed in this study.

Table 5.2 Various material properties

Variable	Range
f_{dc}	35 ~ 45 MPa
E_c	25.5 ~ 30.5 GPa
f_{ds}	550 ~ 660 MPa
E_s	190 ~ 210 GPa
f_{dv}	280 ~ 360 MPa

Table 5.3 Various support conditions

Type	Support Condition
Simply-supported	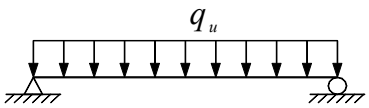
Fixed/free	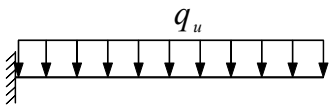
Fixed/roller-supported	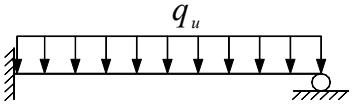
Fixed/fixed	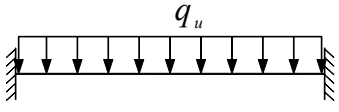

Based on the ranges of the variables discussed above, their random selections are executed by assuming them equally frequent or equally likely to occur. Doing so ensures the gain of a more general curve fitting of ς_y^{rc} and ς_μ^{rc} which could incorporate the effects of these variables as adequately as possible.

5.4.2 Numerical analysis

The step of numerical analysis on the selected design cases to find y_m^{rc} and μ^{rc} is executed with the program ABAQUS [A1]. The detailed finite element models can be found in Chapter 2. The concrete model based on smeared cracking and isotropic compressive plasticity is employed to represent the concrete properties while reinforcement is simulated by the Von-mises yield criterion. Timoshenko beam elements are employed for the modelling of the designed members. As damping is neglected within the design, its effect is still not taken into consideration in this error analysis process. This finite element models has been effectively verified from the numerical predicted responses with experimental ones [S3, K3].

5.5 Distributions of Error Indices

Based on the analytical procedure mentioned above, the distributions of ς_y^{rc} and ς_μ^{rc} for designed members under various *SC*s versus different variables (P_r, t_d, y_t, μ_t, d, l, E_c, E_s, f_{ds} and ρ) are obtained as plotted in Figures 5.2 to 5.5. Several observations can be drawn as follows:

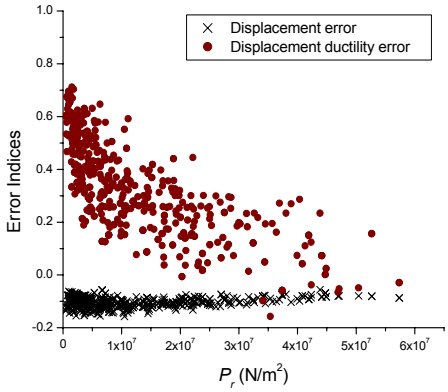

(a). Peak pressure versus error indices

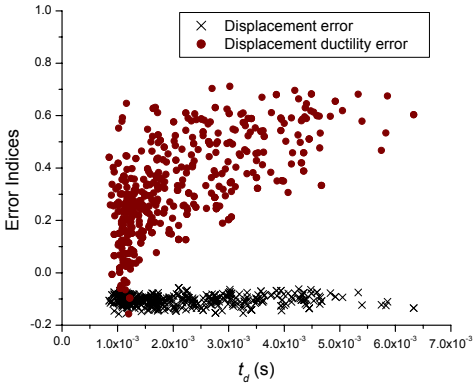

(b). Loading duration versus error indices

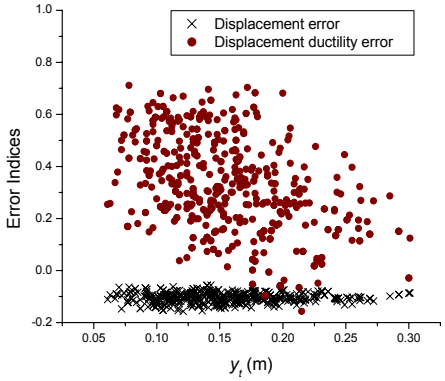

(c). Target displacement versus error indices

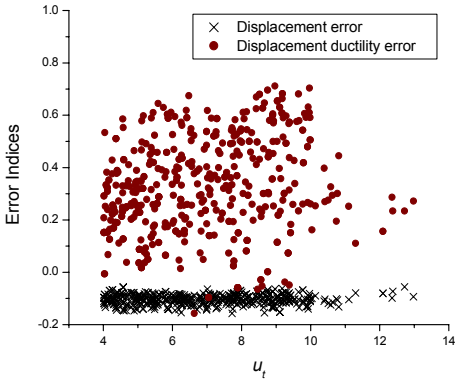

(d). Target displacement ductility factor versus error indices

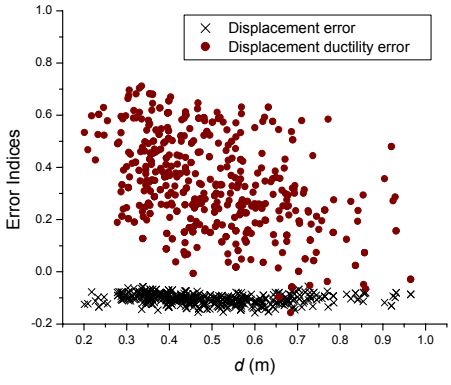

(e). Effective depth versus error indices

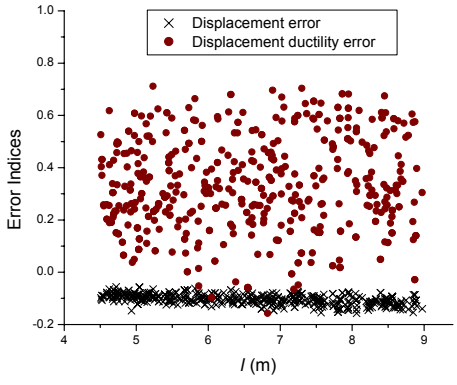

(f). Length of member versus error indices

Figure 5.2 Distributions of error indices with different basic variables for simply supported members

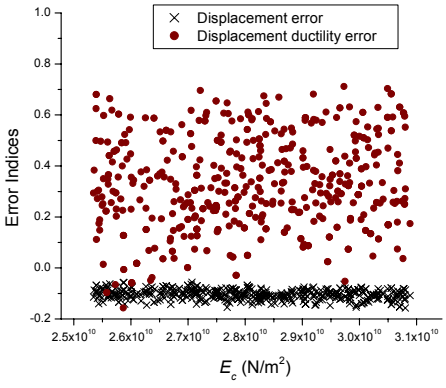

(g). Young's modulus of elasticity of concrete versus error indices

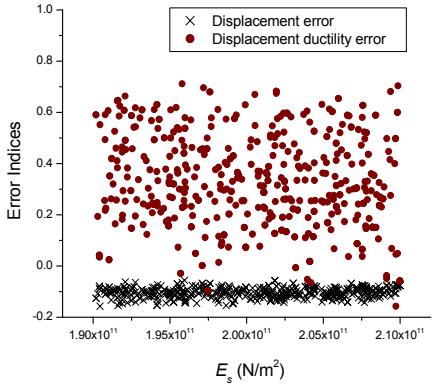

(h). Young's modulus of elasticity of reinforcement versus error indices

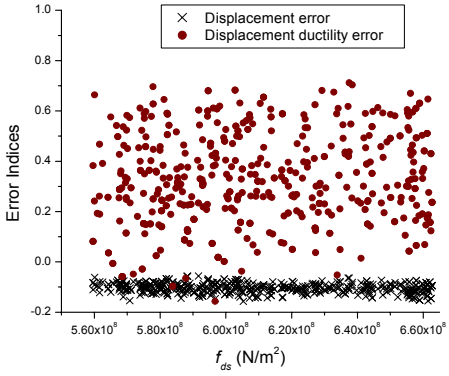

(i). Strength of reinforcement versus error indices

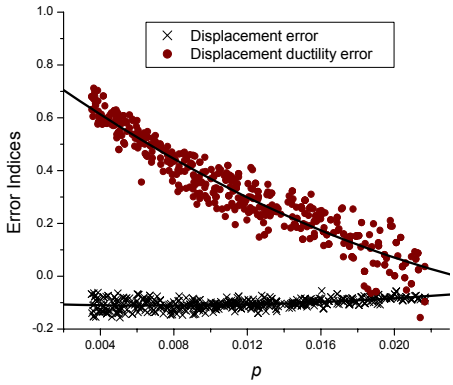

(j). Longitudinal reinforcement ratio versus error indices

Figure 5.2 (Continued)

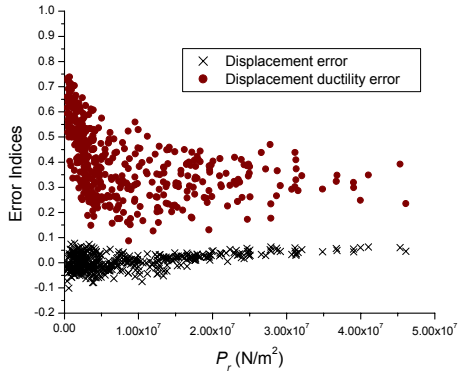

(a). Peak pressure versus error indices

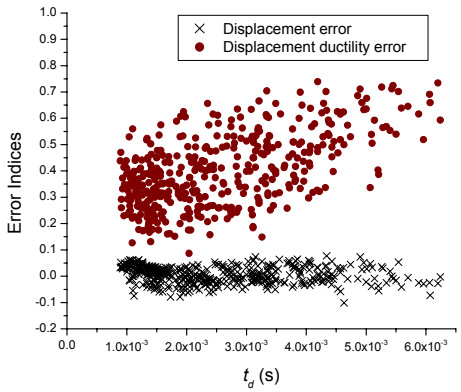

(b). Loading duration versus error indices

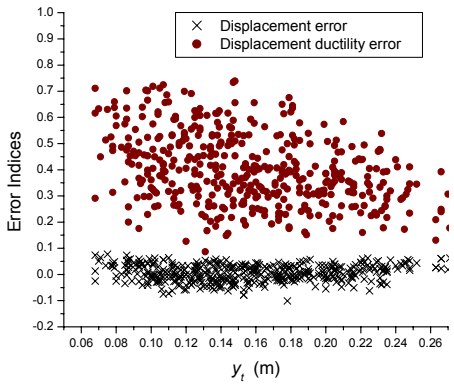

(c). Target displacement versus error indices

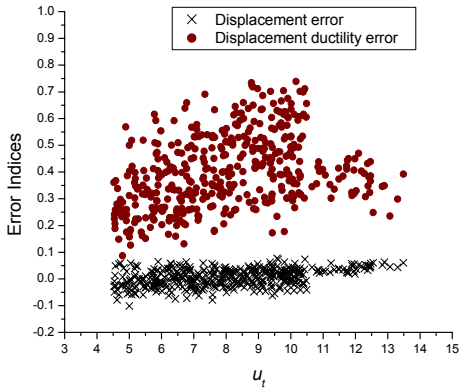

(d). Target displacement ductility factor versus error indices

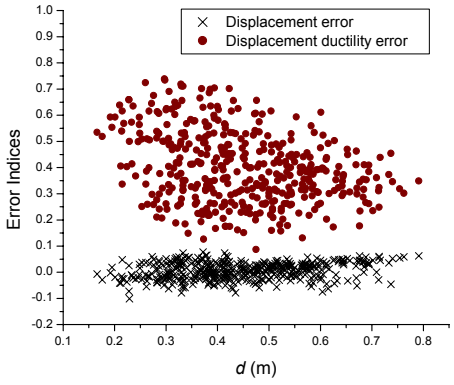

(e). Effective depth versus error indices

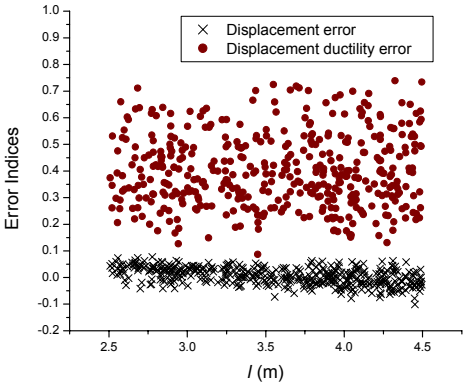

(f). Length of member versus error indices

Figure 5.3 Distributions of error indices with different basic variables for fixed/free members

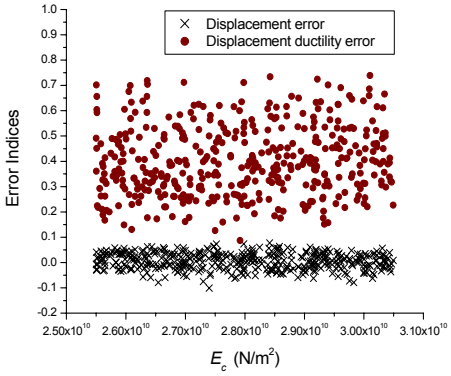

(g). Young's modulus of elasticity of concrete versus error indices

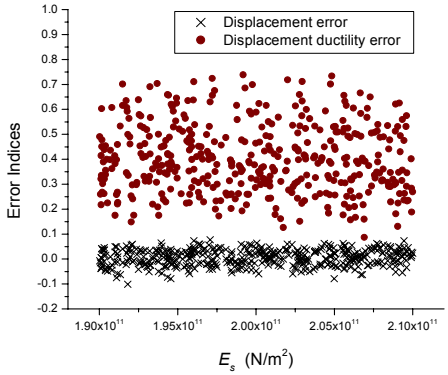

(h). Young's modulus of elasticity of reinforcement versus error indices

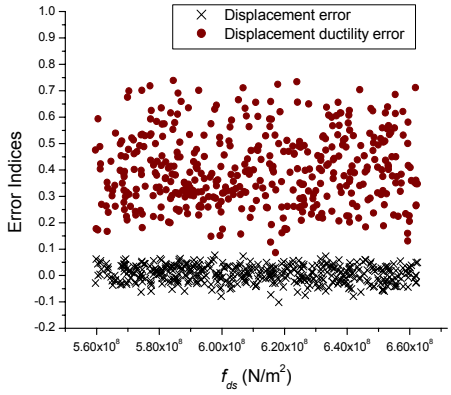

(i). Strength of reinforcement versus error indices

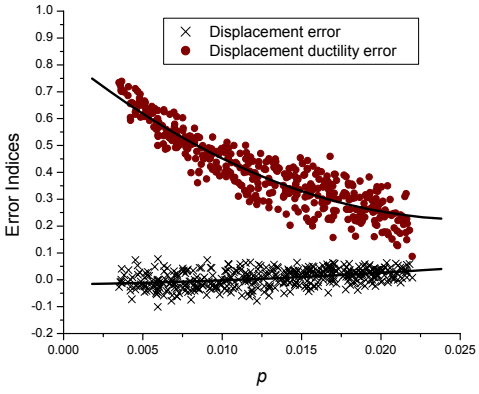

(j). Longitudinal reinforcement ratio versus error indices

Figure 5.3 (continued)

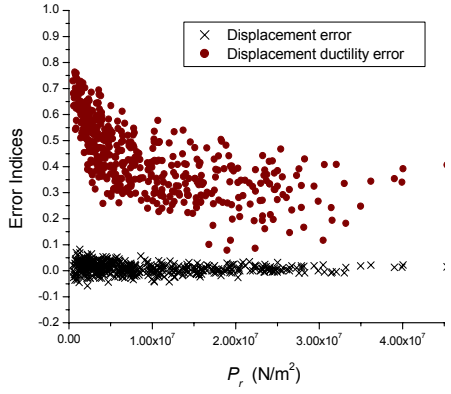

(a). Peak pressure versus error indices

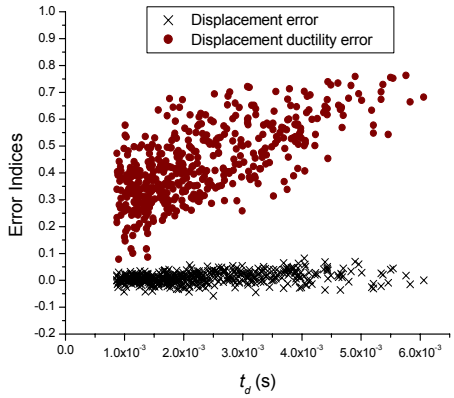

(b). Loading duration versus error indices

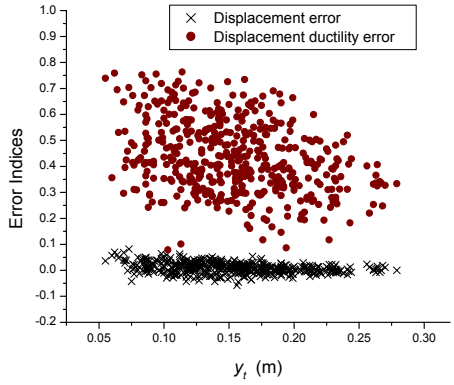

(c). Target displacement versus error indices

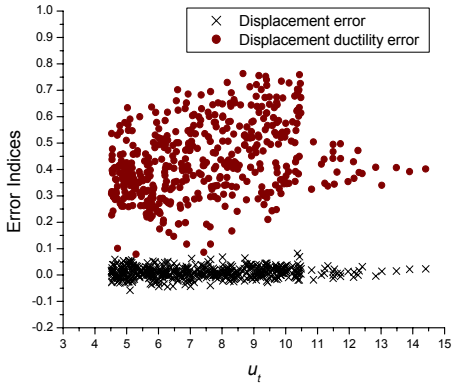

(d). Target displacement ductility factor versus error indices

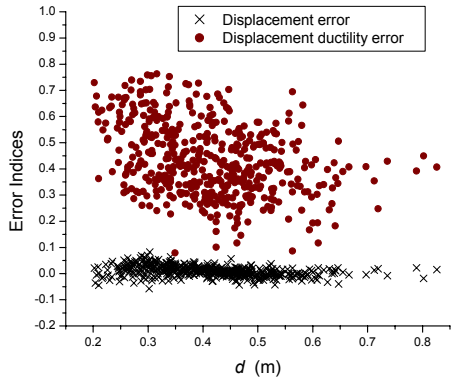

(e). Effective depth versus error indices

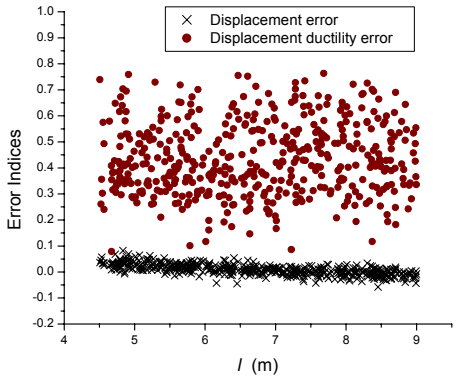

(f). Length of member versus error indices

Figure 5.4 Distributions of error indices with different basic variables for fixed/roller-supported members

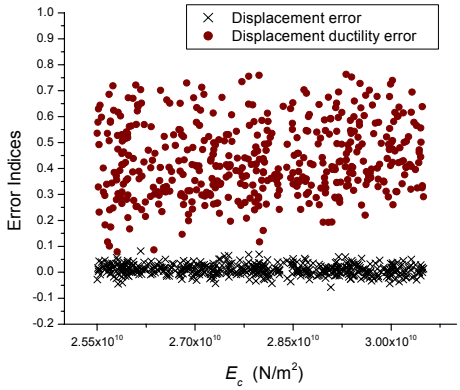

(g). Young's modulus of elasticity of concrete versus error indices

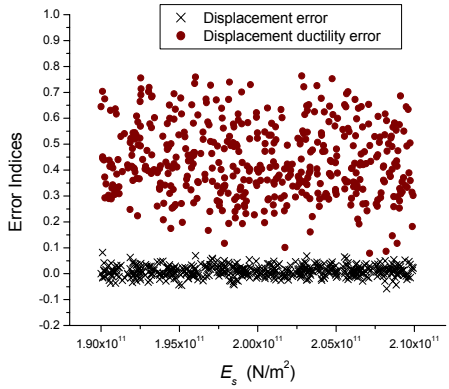

(h). Young's modulus of elasticity of reinforcement versus error indices

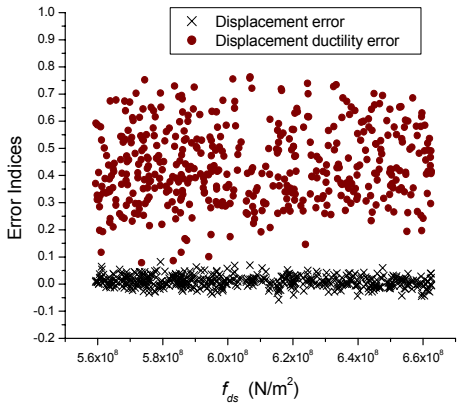

(i). Strength of reinforcement versus error indices

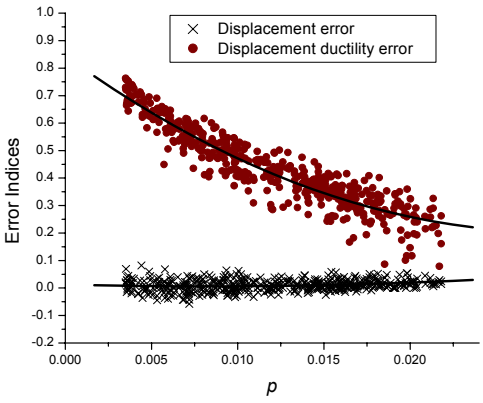

(j). Longitudinal reinforcement ratio versus error indices

Figure 5.4 (Continued)

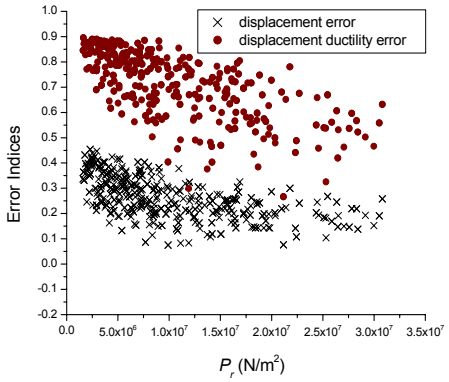

(a). Peak pressure versus error indices

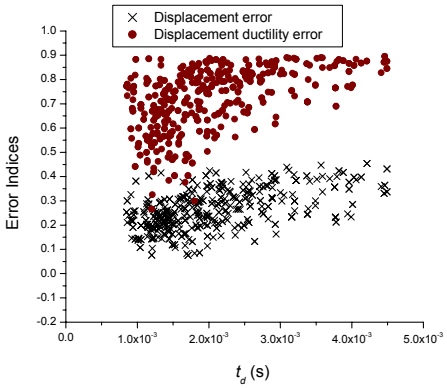

(b). Loading duration versus error indices

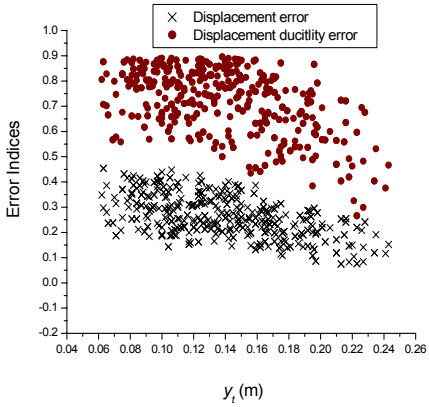

(c). Target displacement versus error indices

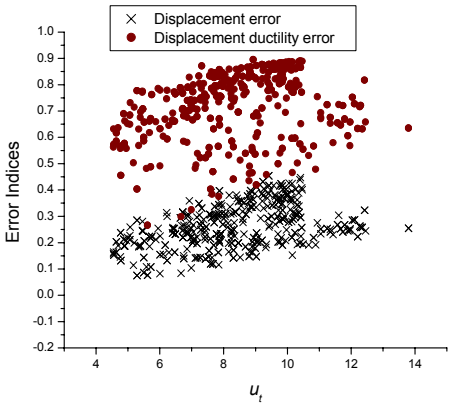

(d). Target displacement ductility factor versus error indices

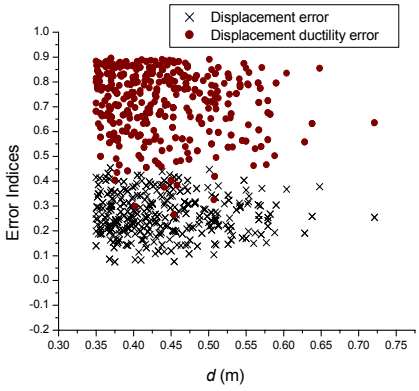

(e). Effective depth versus error indices

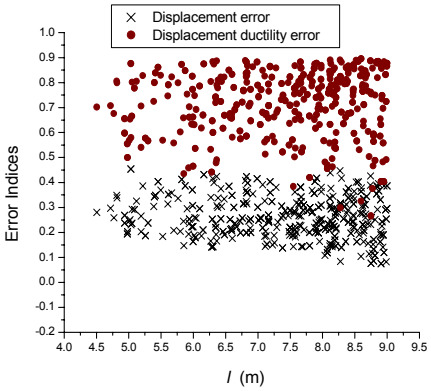

(f). Length of member versus error indices

Figure 5.5 Distributions of error indices with different basic variables for fixed/fixed members

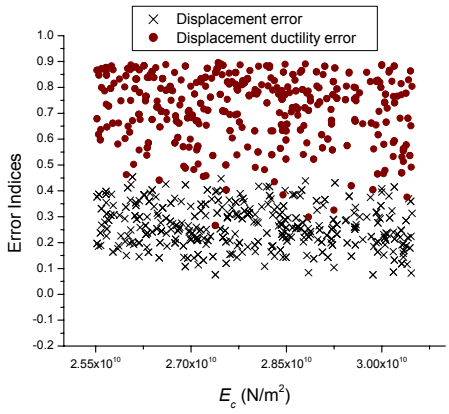

(g). Young's modulus of elasticity of concrete versus error indices

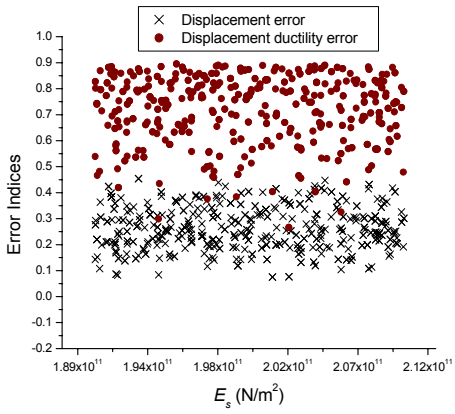

(h). Young's modulus of elasticity of reinforcement versus error indices

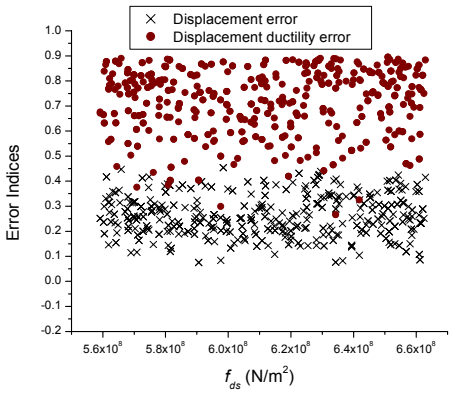

(i). Strength of reinforcement versus error indices

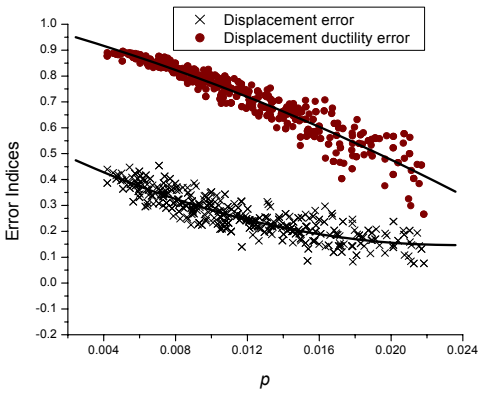

(j). Longitudinal reinforcement ratio versus error indices

Figure 5.5 (Continued)

1). The distributions of ς_y^{rc} are generally concentrated in the strips that are much narrower and closer to the X-Axis as compared to those of ς_μ^{rc} especially in the case of the first three types of *SC*s. This indicates a more effective control of y_m^{rc} of the members within the presented blast resistant design method. This result is reasonable since μ^{rc} is determined simultaneously by y_m^{rc} and the elastic (recoverable) displacement y_e^{rc} of the member at the significant point. As the continuous reinforced concrete member is converted into an equivalent SDOF system with its resistance function simplified by a bilinear curve, the elastic displacement of the designed member in blast incident is somwhat underestimated as shown in Figure 5.6. Therefore a conservative control of μ^{rc} is performed leading to the relatively large positive values of ς_μ^{rc}.

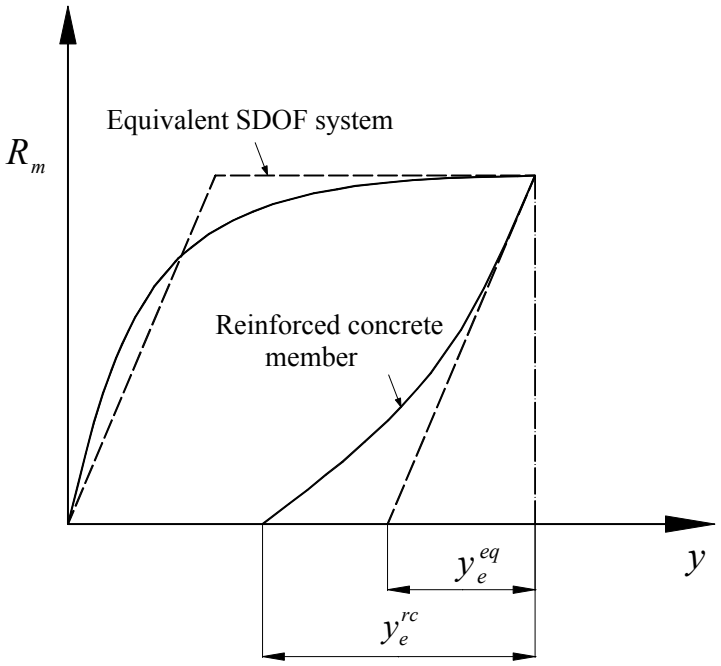

Figure 5.6 Comparison of resistance functions for the reinforced concrete member and the equivalent SDOF system

2). The convergent distributions of ς_y^{rc} and ς_μ^{rc} with respect to ρ under any *SC* as shown in Figures 5.2j to 5.5j indicate that ρ is an important parameter for them. It

should be pointed out that although the distributions of ς_y^{rc} versus other variables seem as concentrated as that versus ρ under the first three *SC*s conditions, it is mainly attributed to the effective control of y_m^{rc} within the presented design process. If other factors are present that influence the effective control of y_m^{rc} as occurring under the fourth *SC* condition, the convergent distributions of ς_y^{rc} will appear only with respect to ρ rather than the other variables as demonstrated in Figure 5.5.

The importance of ρ to ς_y^{rc} and ς_μ^{rc} can be conceptually accounted for from two of the three aspects which induce the errors between the responses (y_m^{rc}, μ^{rc}) and the corresponding design targets (y_t, μ_t) as discussed in Chapter 4. In the calculation of the equal compression and tension longitudinal reinforcement ratio (ρ) from the ultimate strength R_m, the contribution of concrete to R_m is ignored within the design. For the members with a small value of ρ where the concrete presents an important part in resisting external force, this ignorance will lead to a significantly conservative design and therefore a large value of the conservative error indices. With the increase of ρ, the contribution of concrete to R_m becomes smaller and so does the conservative degree of design. It also agrees quite well with the trend of ς_μ^{rc} with respect to ρ under all *SC*s and ς_y^{rc} to ρ under the fourth *SC*s. The second reason that makes ρ important to error indices is related to the calculation of the stiffness of reinforced concrete members where a reduction coefficient γ is applied to obtain the moment of inertia in the cross section along reinforced concrete members. Since γ is determined by ρ from the empirical data fitting curve, it is expected that there may be various values of ς_y^{rc} and ς_μ^{rc} for various ρ.

3). The support condition (*SC*) of a structural member also plays an important role in producing ς_y^{rc} and ς_μ^{rc}, which is demonstrated by the trends of ς_y^{rc} and ς_μ^{rc} with ρ tending to be different under various *SC*s. Comparing the Figures 5.2j to 5.4j with the Figure 5.5j indicates that both ς_y^{rc} and ς_μ^{rc} for fixed/fixed members are

generally larger than those of members under other *SC*s with the same ρ. This difference is induced by the application of unreasonable transformation factors K_{LE} and K_{ME} in the design of fixed/fixed members. As shown in Figure 5.7, the transformation of this type of continuous reinforced concrete member into the equivalent SDOF system can be divided into three stages with different values of transformation factors in each stage: the elastic stage with no plastic hinges, the elastic-plastic stage when two plastic hinges occurs at the two ends of the member and the purely plastic stage as a third plastic hinge appears in the mid-span. In the second stage, transformation factors are taken with the same values as those for a simply supported member. However the responses of a member with two ends pinned (plastic hinges formed at both ends) will be surely smaller than those of a simply supported member. This means the responses of fixed/fixed members are overestimated during the design thus leading to relatively larger error indices. In the cases of other *SC*s, such phenomenon is not present.

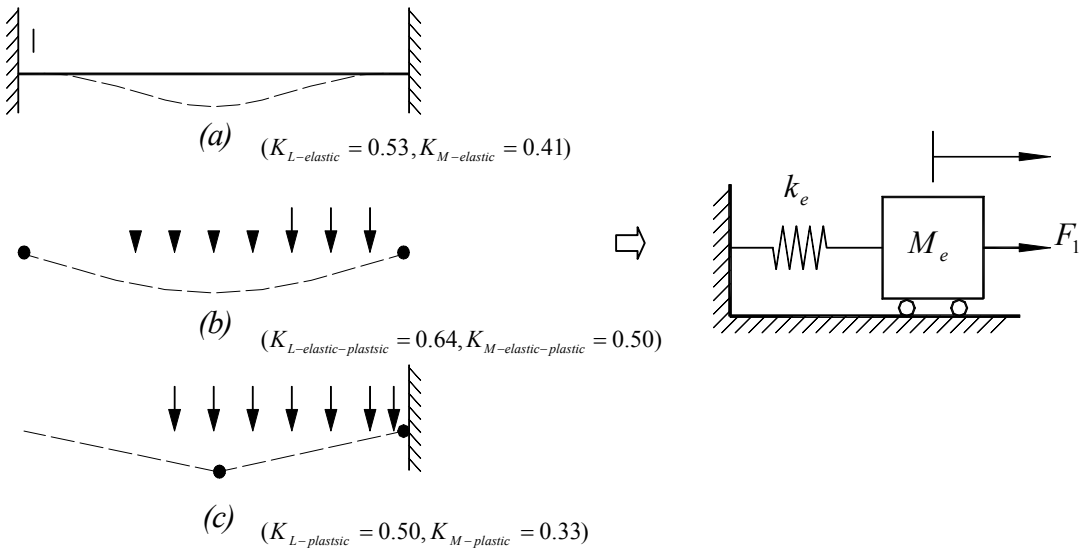

Figure 5.7 Stages of fixed/fixed members in the determination of transformation factors

The variables other than ρ and *SC* have some minor effects, which make the values of ς_y^{rc} and ς_μ^{rc} slightly scattered as ρ and *SC* are certain. Although these effects are not significant as compared to those of ρ and *SC*, they are also incorporated in the recommended formulae trying to consider all variable effects.

5.6 Recommended Formulae of Error Indices

Based on the distributions of ς_y^{rc} and ς_μ^{rc} with respect to different variables discussed above, in order to obtain the simplified expressions of Equations (5.7) and (5.8) the involved variables are divided into two groups: the important variables of ρ and *SC* and the secondary variables including the others such as P_r, t_d, y_t, μ_t, and d *etc*. To incorporate the influences of ρ and *SC* into the expressions, nonlinear curve fittings of ς_y^{rc} and ς_μ^{rc} versus ρ for various *SC*s as plotted in Figures 5.2j to 5.5j are carried out where the functions are expressed as $f(\rho, SC)$ and $g(\rho, SC)$ respectively. The effects of the secondary variables are dealt with by introducing two nominal random variables of e_y and e_μ that are assumed representing the deviation of ζ_y^{rc} and ζ_μ^{rc} around the fitting curves. As a consequence, Equations (5.7) and (5.8) can be simplified into

$$\varsigma_y^{rc} = f(\rho, SC) + e_y \tag{5.9}$$

$$\varsigma_\mu^{rc} = g(\rho, SC) + e_\mu \tag{5.10}$$

A quadratic function is selected for the curve fitting given by

$$f(\rho, SC) \text{ and } g(\rho, SC) = a_1 + a_2\rho + a_3\rho^2 \tag{5.11}$$

With the result functions of $f(\rho, SC)$ and $g(\rho, SC)$, the nominal random variables of e_y and e_μ can be obtained with

$$e_y = \zeta_y^{rc} - f(\rho, SC) \tag{5.12}$$

$$e_\mu = \zeta_\mu^{rc} - g(\rho, SC) \tag{5.13}$$

For members with various *SC*s, the results of the parameters a_1, a_2 and a_3 are listed in Table 5.4 while the histograms of e_y and e_μ are shown in Figures 5.8 to 5.11. It is indicated that the mean values of e_y and e_μ (E_{e_y} and E_{e_μ}) are approximate to zero and the standard deviations of e_y and e_μ (σ_{e_y} and σ_{e_μ}) are relatively minor indicating a slight effect of the variables other than ρ and *SC*. To graphically diagnose whether the data in e_y and e_μ come from a normal distribution, the corresponding normal probability plots are also listed in these figures. If those data are normal, the plot will be linear [K5]. The results display that it is generally more accurate for e_y and e_μ to be assumed as normal distribution although some deviation appears in some cases, i. e. when e_μ is out of the range from – 0.05 to 0.05 for the fixed/fixed members.

Table 5.4 Results of the nonlinear curve fitting

	SC	a_1	a_2	a_3
ε_y^{rc}	Simply-supported	-0.10369	-2.20114	160.30932
	Fixed/free	-0.01712	0.80877	66.84997
	Fixed/roller-supported	0.01276	-1.67032	100.93644
	Fixed/fixed	0.55459	-34.63653	735.20353
ε_μ^{rc}	Simply-supported	0.80257	-50.10919	675.55356
	Fixed/free	0.83085	-47.05548	911.90338
	Fixed/roller-supported	0.84443	-45.30174	800.57689
	Fixed/fixed	0.99826	-18.99113	-354.75711

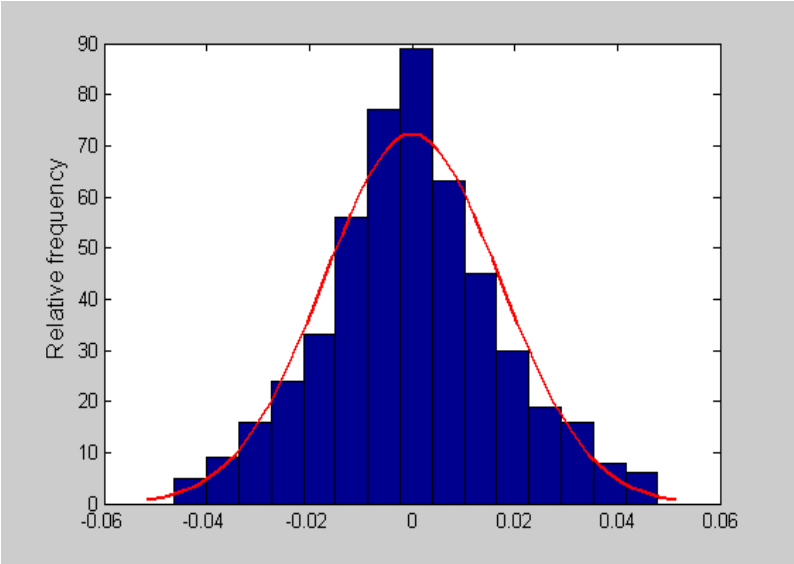

(a). Histogram of e_y ($\sigma_{e_y} = 0.0172$)

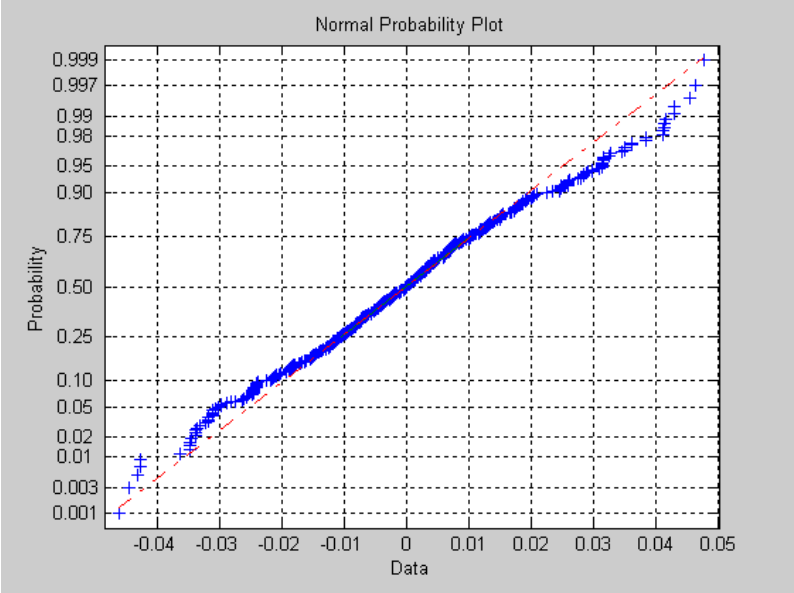

(b). Normal probability plot of e_y

Figure 5.8 The distributions of e_y and e_μ for simply supported members

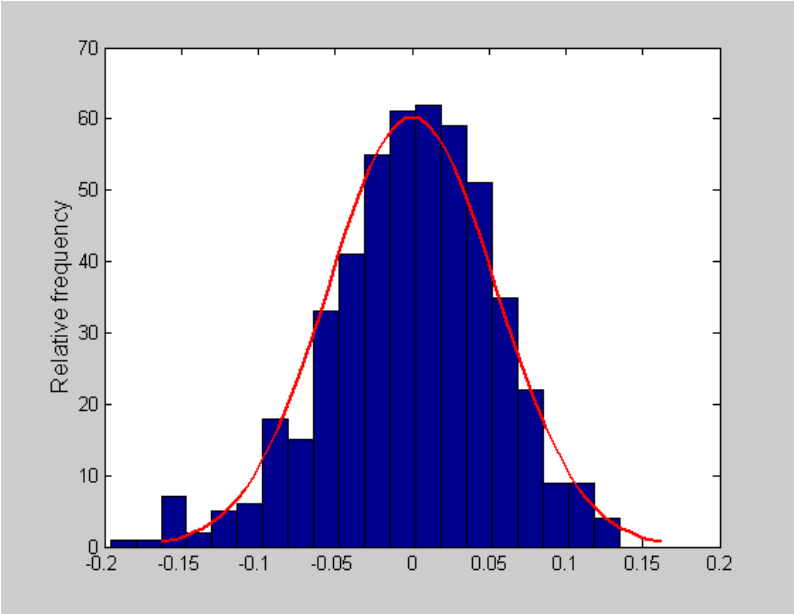

(c). Histogram of e_μ ($\sigma_{e_\mu} = 0.0543$)

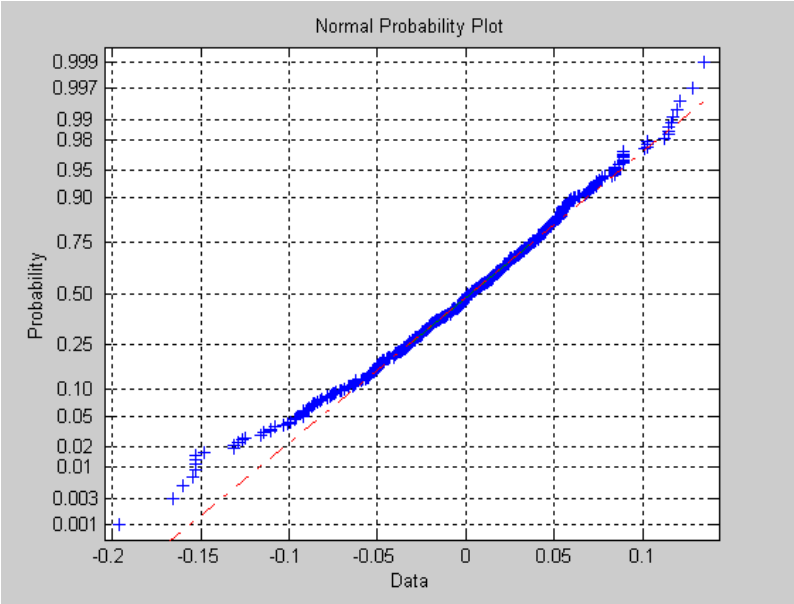

(d). Normal probability plot of e_μ

Figure 5.8 (Continued)

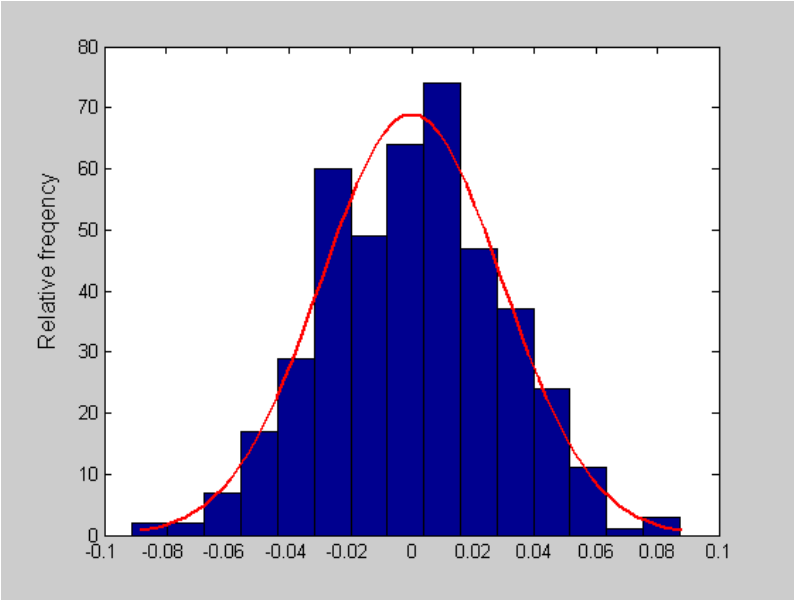

(a). Histogram of e_y ($\sigma_{e_y} = 0.0294$)

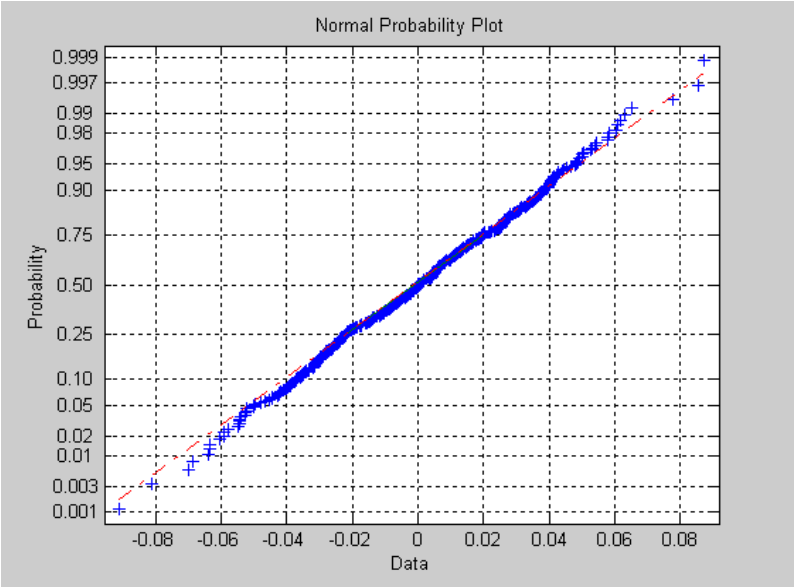

(b). Normal probability plot of e_y

Figure 5.9 The distributions of e_y and e_μ for fixed/free members

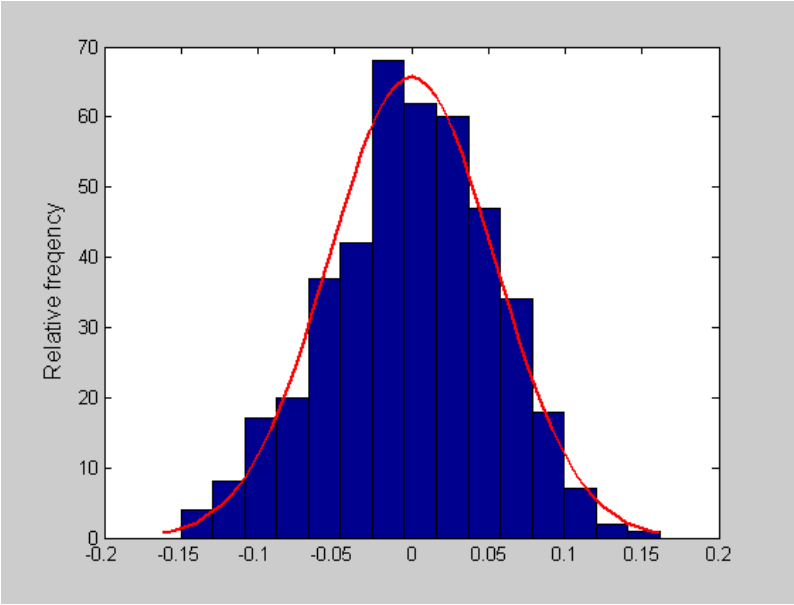

(c). Histogram of e_μ ($\sigma_{e_\mu} = 0.0539$)

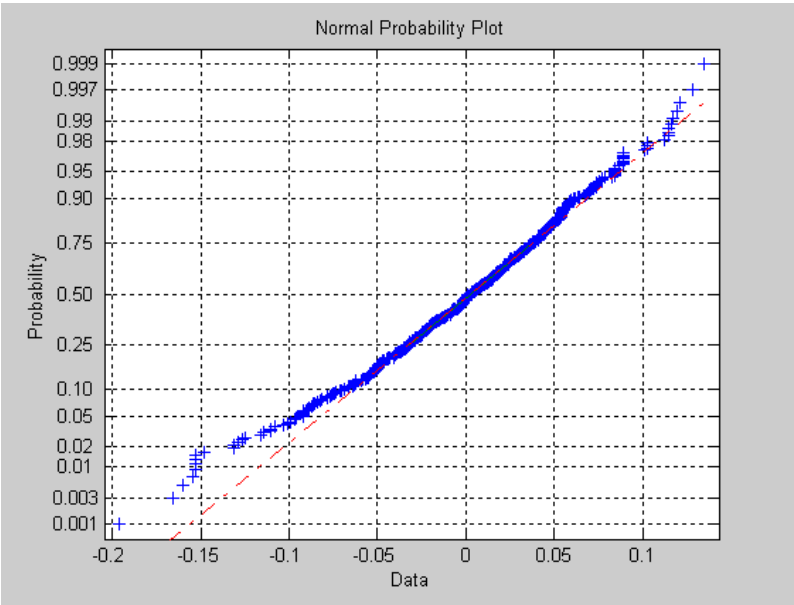

(d). Normal probability plot of e_μ

Figure 5.9 (Continued)

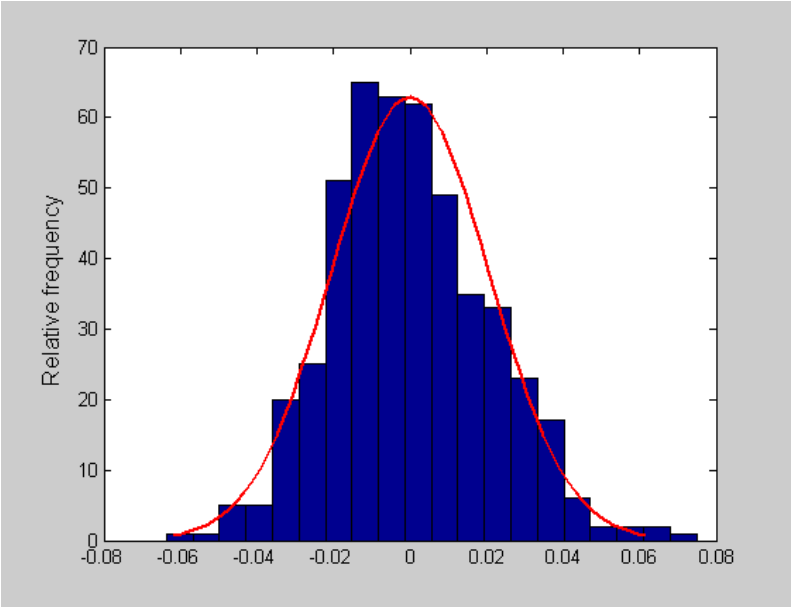

(a). Histogram of e_y ($\sigma_{e_y} = 0.0206$)

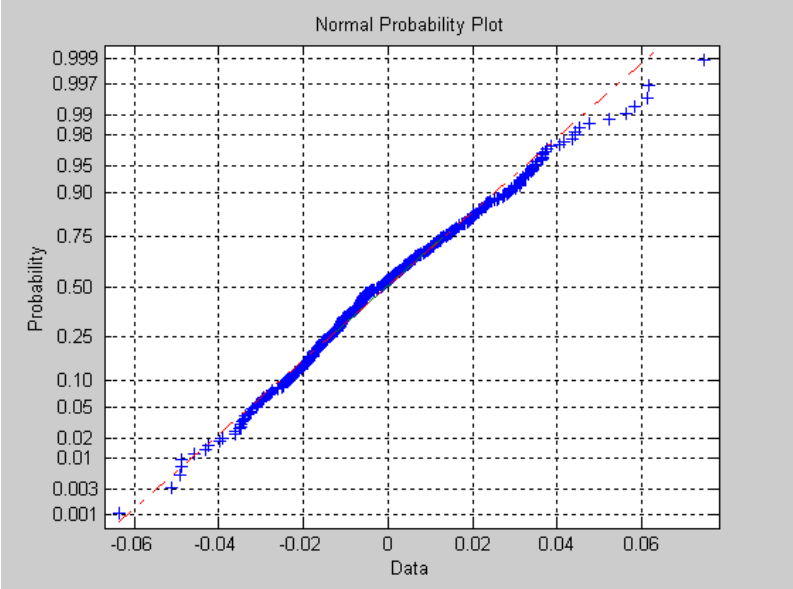

(b). Normal probability plot of e_y

Figure 5.10 The distributions of e_y and e_μ for fixed/roller-supported members

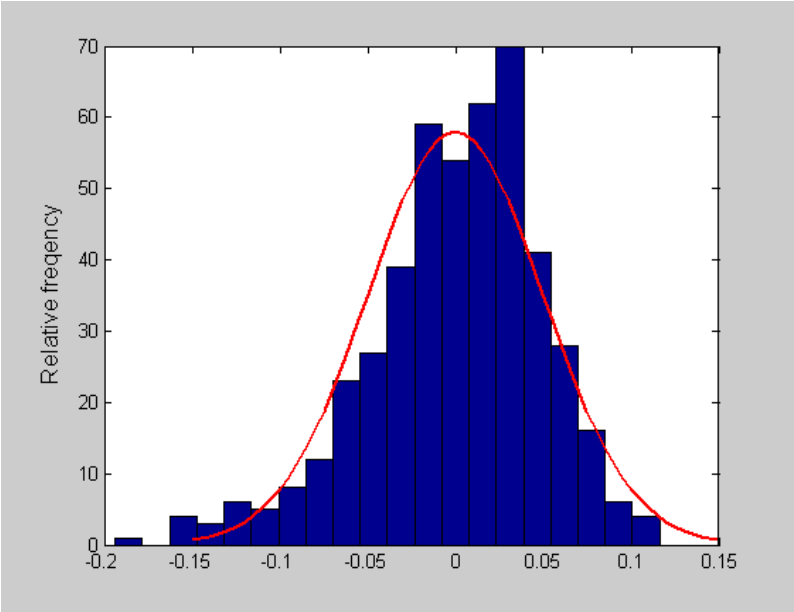

(c). Histogram of e_μ ($\sigma_{e_\mu} = 0.05$)

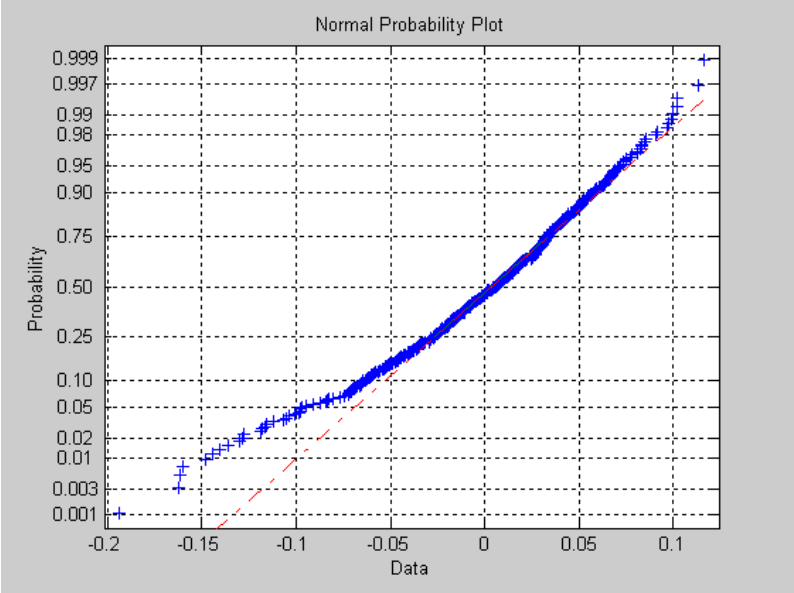

(d).Normal probability plot of e_μ

Figure 5.10 (Continued)

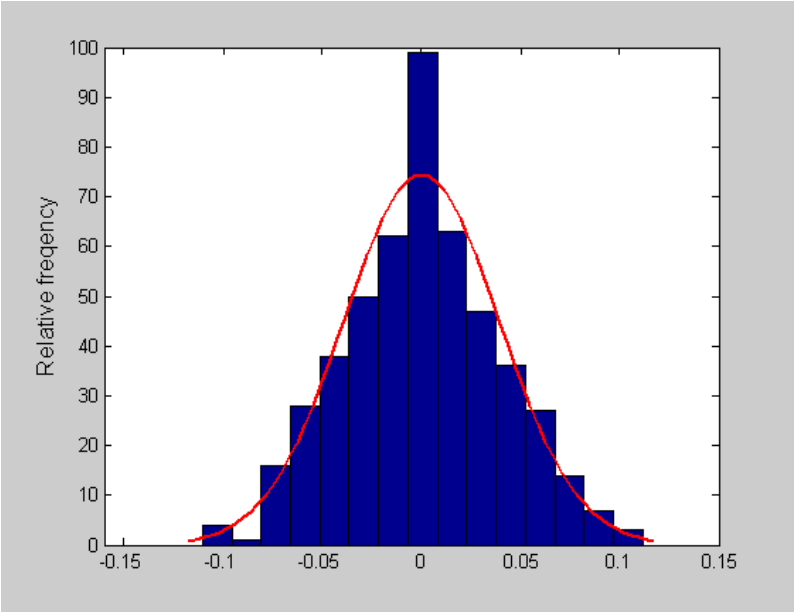

(a). Histogram of e_y ($\sigma_{e_y} = 0.0393$)

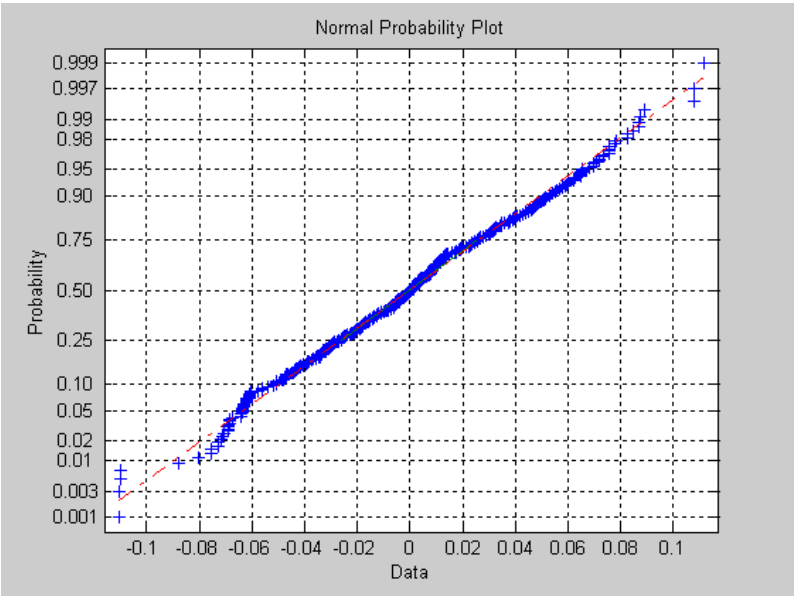

(b). Normal probability plot of e_y

Figure 5.11 The distributions of e_y and e_μ for fixed/fixed members

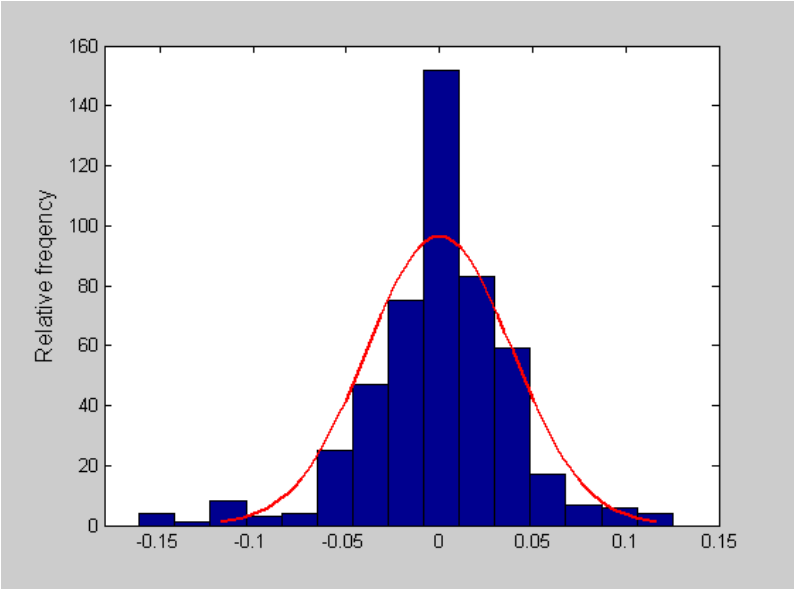

(c). Histogram of e_μ ($\sigma_{e_\mu} = 0.039$)

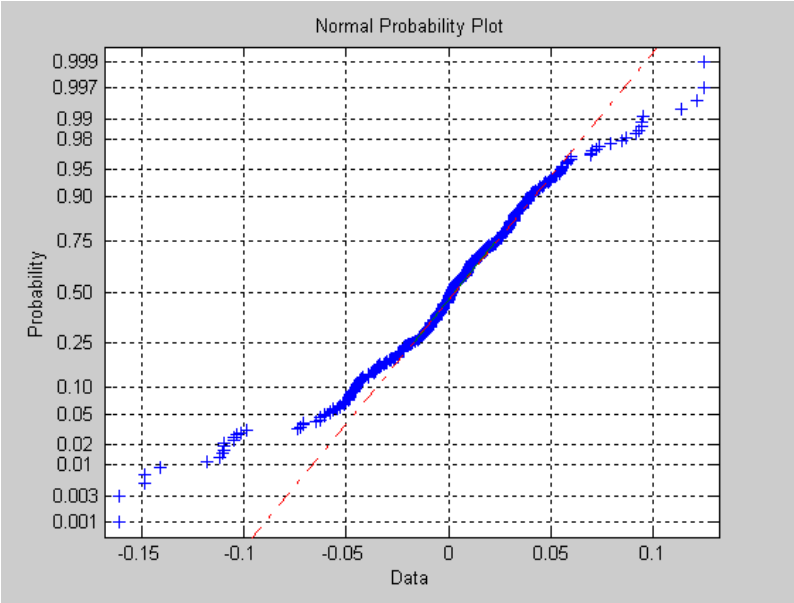

(d). Normal probability plot of e_μ

Figure 5.11 (Continued)

5.7 Summaries

Simple formulae have been developed for the estimation of ς_y^{rc} and ς_μ^{rc} produced within the blast resistant design of reinforced concrete members using energy spectra. The distributions of ς_y^{rc} and ς_μ^{rc} with different variables that have been selected randomly from their concerned ranges within the blast resistant design, are generated through a large amount of numerical analyses. By comparing these distributions, it is found that *SC* and ρ have profound effects on ς_y^{rc} and ς_μ^{rc} while the variables other than *SC* and ρ have some minor influences. As a result to incorporate all variables effects, the formulae of ς_y^{rc} and ς_μ^{rc} are recommended to include two items: a nonlinear fitting function correlated with ρ and *SC* and a random variable (e_y and e_μ respectively) to consider the influence of the others. These formulae provide a reasonable tool in modifying the performance-based blast resistant design of the members using energy spectra and assessing the performance of the designed members probabilistically accounting for different uncertainties. Their applications will be specifically identified in Chapter 6.

CHAPTER SIX

PERFORMANCE–BASED BLAST RESISTANT DESIGN OF REINFORCED CONCRETE MEMBERS USING ENERGY SPECTRA — PART IV. APPLICATIONS OF ERROR INDICES

Synopsis

The formulae of the two error indices for the performance-based blast resistant design approach of reinforced concrete members using energy spectra have been established in Chapter 5. This chapter aims to apply the two error indices into the modification of the design approach in order to keep the responses of the maximum displacement and displacement ductility factor of the designed member rather than those of the corresponding equivalent SDOF system under control. The process of the modified design approach with the error indices is discussed and demonstrated from several design examples. Nonlinear dynamic analysis of the design examples indicates that the modified design approach can more effectively control the response of the designed members than the original method. Moreover, this chapter introduces a simpler procedure of implementing the two error indices into the estimation of the distribution of the maximum displacement and displacement ductility responses for the designed members under blast loadings, where different types of uncertainties are accounted for without performing nonlinear dynamic finite element analysis. Based on this simper procedure, the probabilistic performance for the designed members under blast conditions is much more practically assessed.

Keywords: Expected performance level, Target displacement, Target displacement ductility factor, Maximum displacement responses, Displacement ductility responses, Error indices formulae

6.1 Introduction and Background

Two important topics exist concerning the blast resistance of reinforced concrete members, one of which is related to the blast resistant design approaches that are capable of controlling the responses of designed member to the expected performance level under a certain blast situation. The other is the probabilistic performance evaluation of the designed member against blast loadings accounting for different types of the uncertainties.

The blast resistant design approach using energy spectra has been developed and evaluated in Chapters 3 and 4. Both the maximum displacement and displacement ductility responses (y_m^{eq} and μ^{eq}) of the equivalent SDOF system of the designed member under the given blast force can be guarantied to reach their respective targets (y_t and μ_t) perfectly within the design, however it is found numerically that there still exist certain degree of errors between the responses (y_m^{rc} and μ^{rc}) of the designed member at their significant point and the corresponding targets (y_t and μ_t). Simple equations for the estimation of these errors represented by two error indices (ς_y^{rc} and ς_μ^{rc}) have been proposed in Chapter 5. From the distributions of ς_y^{rc} and ς_μ^{rc} obtained from a large number of numerical analyses, two types of undesirable design cases may occur with the design approach where a significantly conservative control of μ^{rc} in the case of a small value for ρ or a somewhat inadequate control of y_m^{rc} appears. Therefore modification of the design approach in keeping y_m^{rc} and μ^{rc} of the member under control instead of those (y_m^{eq} and μ^{eq}) of the equivalent SDOF system seems necessary through the utilization of ς_y^{rc} and ς_μ^{rc}. This particular area will be concentrated upon in the first part of this chapter where the flowchart of the modified design approach is presented depending on the error indices. Several design examples are demonstrated with the modified design approach as well as the original one. Numerical simulations of their displacement

and displacement ductility responses under the given blast force are performed while the results are compared.

In the probabilistic performance assessment of reinforced concrete flexural members under potential blast conditions, calculation of the distributions of the maximum displacement response and/or displacement ductility response provides a big practical problem for structural engineers since at present this task has to be fulfilled with nonlinear dynamic finite element analysis. The probabilistic performance assessment based on a combination of nonlinear dynamic finite element analysis and Monte-Carlo simulation [K5] is computationally considerably expensive. Hence a simpler way to find the distributions of maximum displacement and displacement ductility responses for members under blast loadings becomes much more valuable. The latter section of this chapter will introduce an efficient procedure of utilizing ς_y^{rc} and ς_μ^{rc} for the estimation of them followed by the combination of this procedure with the Monte-Carlo simulation into the probabilistic performance assessment. As an illustration, the performances of the members designed with the modified approach using energy spectra are probabilistically evaluated.

6.2 Modification of the Design Approach With Error Indices

6.2.1 Design modification with error indices

For the convenience of the following discussion, the design targets are distinguished from two different viewpoints. From a physical viewpoint, design targets are the final goals for designed members to be achieved under certain blast conditions therefore they should keep unchanged within a design. They are called the physical design targets (PHY-DTs). However from another point of view, design targets are only some of the important parameters involved in the design to control the responses of the designed members to reach their PHY-DTs just as those adopted in the blast resistant design approach using energy spectra presented in Chapter 3. In this sense, they are named the parametric design targets (PAR-DTs). In the

presented blast design approach the values of PAR-DTs are simply fixed to be equal to those of PHY-DTs, however this action induces some inevitable errors of the member's responses (y_m^{rc} and μ^{rc}) to the PHY-DTs. By properly adjusting the values of PAR-DTs within the design, the elimination of such errors can be simply achieved.

Denoting PHY-DTs for maximum displacement and displacement ductility responses as y_t and μ_t while PAR-DTs as y_{te} and μ_{te}, the two error indices introduced in Chapter 5 can be expressed through another form, written as

$$\zeta_y^{rc} = \frac{y_{te} - y_m^{rc}}{y_{te}} = f(\rho, SC) + e_y \tag{6.1}$$

$$\zeta_\mu^{rc} = \frac{\mu_{te} - \mu^{rc}}{\mu_{te}} = g(\rho, SC) + e_\mu \tag{6.2}$$

The detailed expressions of $f(\rho, SC)$, $g(\rho, SC)$ and the distribution properties of e_y, e_μ can be found in Chapter 5. Since in the design the responses of y_m^{rc} and μ^{rc} are required to be controlled in achieving the PHY-DTs of y_t and μ_t, that is $y_m^{rc} = y_t$ and $\mu^{rc} = \mu_t$, by subjecting them into Equations (6.1) and (6.2), the PAR-DTs of y_{te} and μ_{te} are obtained as

$$y_{te} = \frac{y_t}{1 - f(\rho, SC) - e_y} \tag{6.3}$$

$$\mu_{te} = \frac{\mu_t}{1 - g(\rho, SC) - e_\mu} \tag{6.4}$$

Equations (6.3) and (6.4) can be utilized to adjust the PAR-DTs so as to get a better control of the responses of y_m^{rc} and μ^{rc} within the design. However, two points

should be mentioned. Since e_y and e_μ are random variables which indicate the uncertain influences of the design variables other than ρ and SC on error indices, certain quantiles [K5] of $e_{y,n}$ and $e_{\mu,m}$ corresponding to n and m percentages of non-exceedance probabilities for e_y and e_μ have to be selected, and so Equations (6.3) and (6.4) are modified into

$$y_{te} = \frac{y_t}{1 - f(\rho, SC) - e_{y,n}} \tag{6.5}$$

$$\mu_{te} = \frac{\mu_t}{1 - g(\rho, SC) - e_{\mu,m}} \tag{6.6}$$

The physical meaning of such action can be explained as follows. Subtracting Equations (6.5) and (6.6) from Equations (6.1) and (6.2) respectively and rearranging them leads to

$$y_t - y_m^{rc} = y_{te}(e_y - e_{y,n}) \tag{6.7}$$

$$\mu_t - \mu^{rc} = \mu_{te}(e_\mu - e_{\mu,m}) \tag{6.8}$$

The item of $e_y - e_{y,n}$ in the bracket provides a random variable with a n percentage of probability whose value is less than zero as shown in Figure 6.1. Since y_{te} is always positive, it can be concluded from Equation (6.7) that the maximum displacement response y_m^{rc} of the members designed according to Equations (6.5) and (6.6) will have a $(1-n)$ percentage of probability of non-exceeding the PHY-DT of y_t (or a n percentage of exceeding probability). Equation (6.8) can be explained in the same way where the displacement ductility response μ^{rc} will have a $(1-m)$ percentage of probability of non-exceeding the PHY-DT of μ_t.

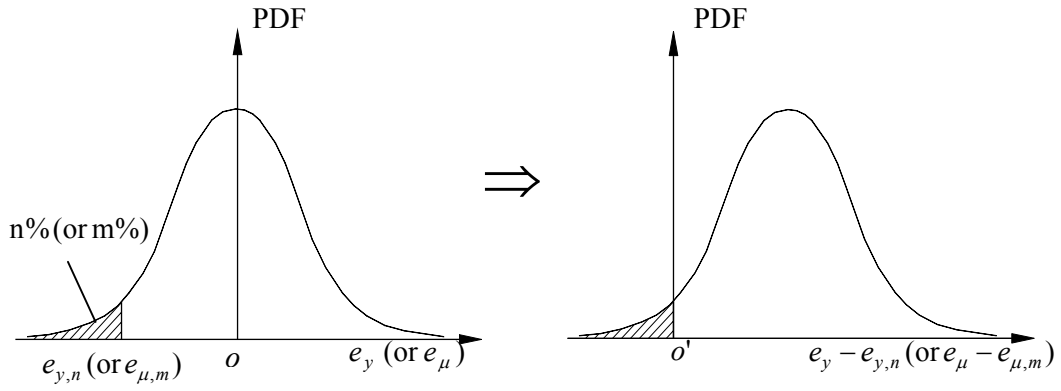

Figure 6.1 Distributions of $e_y - e_{y,n}$ or $e_\mu - e_{\mu,n}$

Another point that should be noted is that the determination of PAR-DTs of y_{te} and μ_{te} from Equations (6.5) and (6.6) is dependent on the longitudinal reinforcement ratio ρ. Therefore an iterative approach is needed in the design. After an assumed d and ρ, the PAR-DTs of y_{te} and μ_{te} are adjusted from the given α and PHY-DTs of y_t and μ_t. However to fulfil y_{te} and μ_{te}, a new d and ρ will be produced for the member with the design procedures using energy spectra that is developed in Chapter 3 and hence the process must be repeated until d and ρ are consistent. The flowchart of the modified performance-based blast resistant design using energy spectra is shown in Figure 6.2.

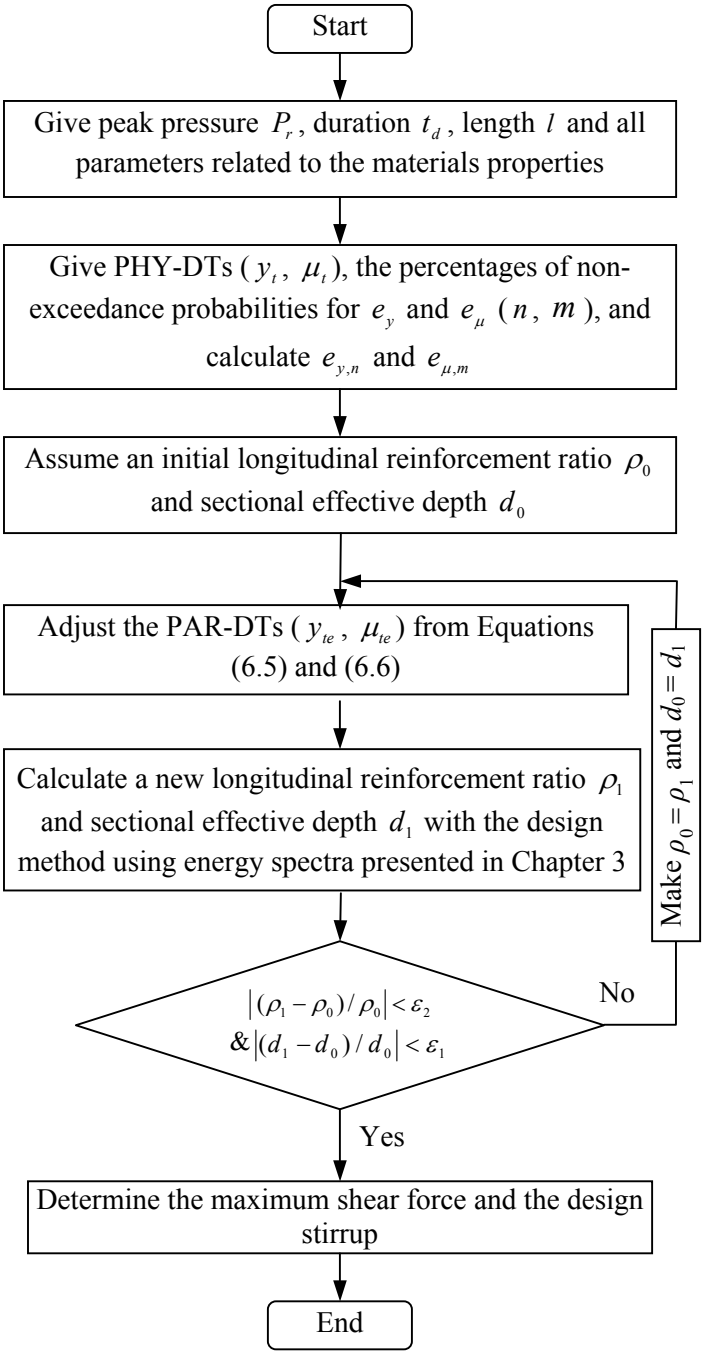

Figure 6.2 Flowchart of the modified performance-based blast resistant design using energy spectra with error indices (ε_1, ε_2 are arbitrarily small values)

6.2.2 Illustrative examples

In this section, the modified blast resistant design approach by incorporating error indices is applied to three illustrative examples that enable the reader to foresee its use in engineering practices. The examples plotted in Figures 6.3 to 6.5 are carried out for a simply-supported beam, a cantilever wall and a fixed/roller-supported beam in resisting the blast loadings produced by a variety of blast loadings. The example I and III tend to control the member's responses at a very low protection level thus a relatively higher target support rotation of $\theta_t = 4^o$ ($y_t \approx l \tan(\theta_t)/2$) and μ_t = 10 are given, while a low protective level is required for the example II where $\theta_t = 2^o$ ($y_t \approx l \tan(\theta_t)$) and μ_t = 6. The compression reinforcement area is taken to be equal to the tension reinforcement area considering the rebound effect of the member subsequent to its maximum displacement response. In these design examples, the values for n and m are taken to be 0.05 so as to ensure a 95 percent of probability for y_m^{rc} and μ^{rc} of the designed members non-exceeding the PHY-DTs of y_t and μ_t. The convergence conditions about ρ and d are defined with $\left|(\rho_1 - \rho_0)/\rho_0\right| \le 0.001$ and $\left|(d_1 - d_0)/d_0\right| \le 0.001$.

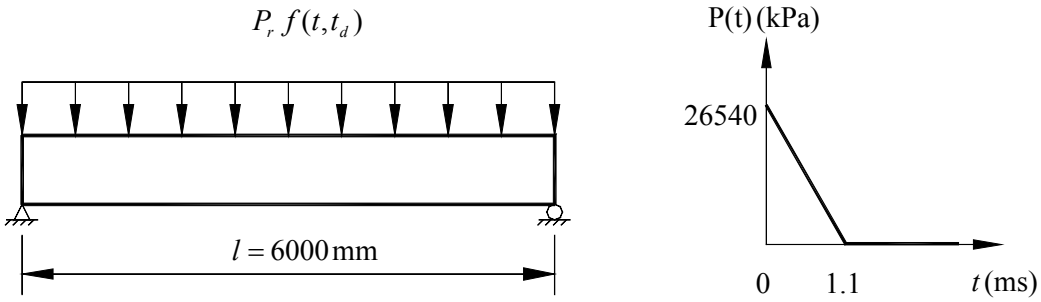

Figure 6.3 A simply supported beam under the blast loading (Design example I)

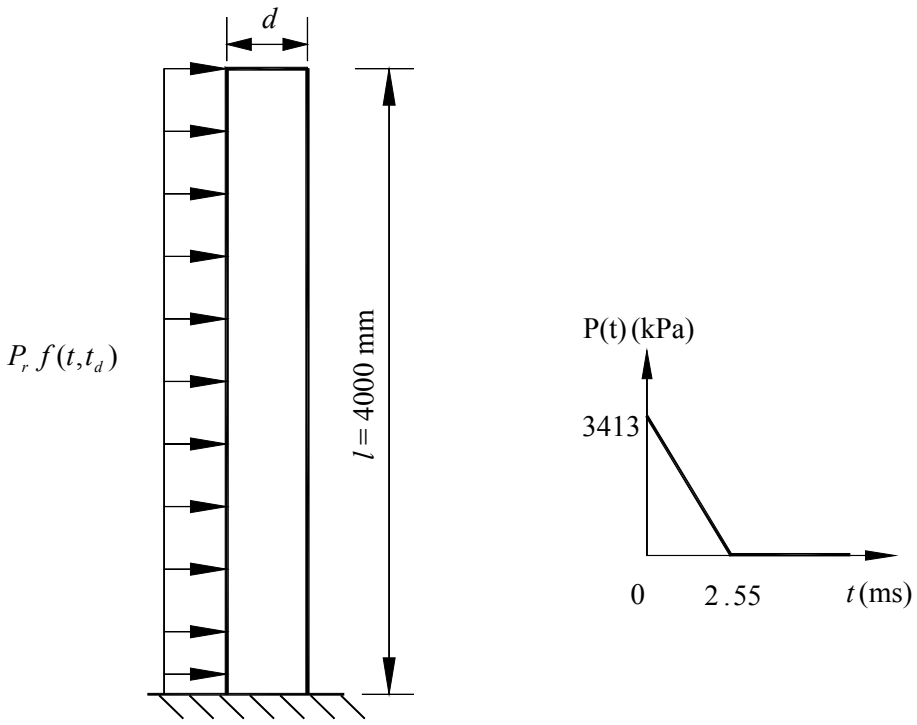

Figure 6.4 A cantilever wall under the blast loading (Design example II)

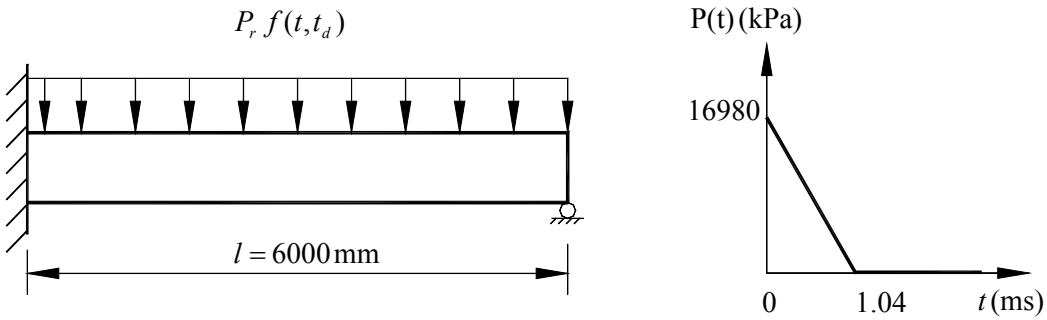

Figure 6.5 A fixed/roller-supported beam under the blast loading
(Design example III)

With the initial values of ρ_0 and d_0 taken as 1.00 % and 1000 mm, the whole design processes for these three design examples with the modified approach depending on the error indices are listed in Tables 6.1 to 6.3. For the purpose of comparison, the whole design procedures of the members with the original design method are also listed in these tables. It is indicated that there is no difficulty in reaching convergence for the modified design procedures however due to the adjustment of PAR-DTs from Equations (6.3) and (6.4) within the modified design, more iterative steps and computation time are needed to reach convergence than those with the original design method. Also there is an obvious decline in ρ while some increase in d for the member designed with the modified approach as compared to those with the original one.

Table 6.1 Iterative design procedures of the simply supported beam (Example I)

y_t (mm)	μ_t	$e_{y,0.05}$	$e_{\mu,0.05}$	d_0 (mm)	ρ_0 (%)	$f(\rho_0,SC)$	$g(\rho_0,SC)$	y_{te} (mm)	μ_{te}	d_1 (mm)	ρ_1 (%)	CPU time (s)
with the modified performance-based blast resistant design approach using energy spectra												
210.00	10.0	-0.028	-0.089	1000.00	1.000	-0.10966	0.36910	184.35	13.885	583.36	1.374	0.178
				583.36	1.374	-0.10364	0.24154	185.33	11.796	637.94	1.111	
				637.94	1.111	-0.10835	0.32950	184.56	13.161	658.28	1.005	
				658.28	1.005	-0.10961	0.36744	184.36	13.853	669.83	0.951	
				669.83	0.951	-0.11011	0.38709	184.28	14.241	675.79	0.925	
				675.79	0.925	-0.11032	0.39692	184.24	14.443	678.86	0.912	
				678.86	0.912	-0.11042	0.40190	184.23	14.547	680.45	0.905	
				680.45	0.905	-0.11046	0.40443	184.22	14.601	681.26	0.902	
				681.26	0.902	-0.11049	0.40573	184.22	14.629	681.67	0.900	
				681.67	0.900	-0.11050	0.40639	184.21	14.643	681.89	0.899	
with the original performance-based blast resistant design approach using energy spectra												
210.00	10.0			1000.00	1.000					478.57	2.172	0.102
				478.57	2.172					563.23	1.449	
				563.23	1.449			210.00	10.0	558.18	1.464	
				558.18	1.464					559.22	1.457	
				559.22	1.457					559.14	1.458	

$f_{ds} = 506\,\text{MPa}$, $f_{dc} = 40\,\text{MPa}$, $E_c = 40\,\text{GPa}$, $E_s = 200\,\text{GPa}$, $f_{dv} = 275\,\text{MPa}$

Convergence conditions: $\left|(\rho_1 - \rho_0)/\rho_0\right| \le 0.001$ and $\left|(d_1 - d_0)/d_0\right| \le 0.001$

Table 6.2 Iterative design procedures of the cantilever wall (Example II)

y_t (mm)	μ_t	$e_{y,0.05}$	$e_{\mu,0.05}$	d_0 (mm)	ρ_0 (%)	$f(\rho_0,SC)$	$g(\rho_0,SC)$	y_{te} (mm)	μ_{te}	d_1 (mm)	ρ_1 (%)	CPU time (s)
with the modified performance-based blast resistant design approach using energy spectra												
139.70	6.0	-0.048	-0.089	1000.00	1.000	-0.00235	0.45148	132.95	9.418	359.94	1.370	0.172
				359.94	1.370	0.00651	0.35733	134.08	8.205	467.57	0.731	
				467.57	0.731	-0.00764	0.53560	132.28	10.850	503.69	0.567	
				503.69	0.567	-0.01038	0.59327	131.94	12.113	520.56	0.509	
				520.56	0.509	-0.01127	0.61479	131.83	12.663	526.68	0.490	
				526.68	0.490	-0.01156	0.62222	131.79	12.865	528.77	0.483	
				528.77	0.483	-0.01165	0.62471	131.78	12.934	529.47	0.481	
				529.47	0.481	-0.01168	0.62553	131.78	12.957	529.70	0.481	
				529.70	0.481	-0.01169	0.62580	131.77	12.965	529.77	0.480	
with the original performance-based blast resistant design approach using energy spectra												
139.70	6.0			1000.00	1.000					299.68	2.259	0.109
				299.68	2.259					414.93	1.041	
				414.93	1.041			139.70	6.0	403.24	1.076	
				403.24	1.076					405.70	1.062	
				405.70	1.062					405.42	1.064	

$f_{ds} = 506\,\text{MPa}$, $f_{dc} = 40\,\text{MPa}$, $E_c = 40\,\text{GPa}$, $E_s = 200\,\text{GPa}$, $f_{dv} = 275\,\text{MPa}$

Convergence conditions: $\left|(\rho_1 - \rho_0)/\rho_0\right| \le 0.001$ and $\left|(d_1 - d_0)/d_0\right| \le 0.001$

Table 6.3 Iterative design procedures of the fixed/roller-supported beam (Example III)

y_t (mm)	μ_t	$e_{y,0.05}$	$e_{\mu,0.05}$	d_0 (mm)	ρ_0 (%)	$f(\rho_0,SC)$	$g(\rho_0,SC)$	y_{te} (mm)	μ_{te}	d_1(m)	ρ_1 (%)	CPU time (s)
with the modified performance-based blast resistant design approach using energy spectra												
210.00	10.0	-0.034	-0.082	1000.00	1.000	0.00615	0.47134	204.14	16.371	318.17	1.793	0.171
				318.17	1.793	0.01526	0.28944	205.96	12.614	400.33	1.071	
				400.33	1.071	0.00645	0.45110	204.19	15.846	425.99	0.865	
				425.99	0.865	0.00587	0.51233	204.08	17.548	441.04	0.774	
				441.04	0.774	0.00588	0.54162	204.08	18.499	447.94	0.735	
				447.94	0.735	0.00594	0.55445	204.09	18.949	451.09	0.719	
				451.09	0.719	0.00597	0.56010	204.10	19.154	452.52	0.711	
				452.52	0.711	0.00599	0.56262	204.10	19.247	453.16	0.708	
				453.16	0.708	0.00599	0.56375	204.11	19.289	453.44	0.706	
				453.44	0.706	0.00600	0.56425	204.11	19.307	453.57	0.706	
with the original performance-based blast resistant design approach using energy spectra												
210.00	10.0			1000.00	1.000					263.55	3.016	0.109
				263.55	3.016					356.72	1.201	
				356.72	1.201			210.00	10	367.90	1.330	
				367.90	1.330					360.55	1.401	
				360.55	1.401					360.90	1.402	

$f_{ds} = 506\,\text{MPa}$, $f_{dc} = 40\,\text{MPa}$, $E_c = 40\,\text{GPa}$, $E_s = 200\,\text{GPa}$, $f_{dv} = 275\,\text{MPa}$

Convergence conditions: $\left|(\rho_1 - \rho_0)/\rho_0\right| \le 0.001$ and $\left|(d_1 - d_0)/d_0\right| \le 0.001$

6.2.3 Numerical verification

In order to check whether y_m^{rc} and μ^{rc} for the designed members under the given blast loadings are controlled effectively with the modified design approach, nonlinear finite element analysis is performed on these members, in which the finite element models are taken as the same discussed in Chapter 2. The simulation results are demonstrated in Figures 6.6 to 6.8 where for comparison y_m^{rc} and μ^{rc} of the members designed with the original design procedure are also given.

Results indicate that the modified design approach has overcome the disadvantages existing in the control of y_m^{rc} and μ^{rc} for the simply supported beam and the cantilever wall designed with the original method, where y_m^{rc} slightly exceeds the target of y_t and μ^{rc} is too much conservative. Values of y_m^{rc} and μ^{rc} for these two members that are designed with the modified approach are both approximate to their respective targets and restricted to be a little on the conservative sides. Besides, y_m^{rc} seems to be controlled much closer to its target than μ^{rc} due to the smaller standard deviation of e_y. As for the fixed/roller-supported beam, due to the strict requirement of 95 percent of probability for y_m^{rc} non-exceeding y_t within the modified design procedures, the control of y_m^{rc} seems to be slightly more conservative than that from the original design procedures. However in this case μ^{rc} is still controlled much more approximate to μ_t with the modified approach. Therefore, comparison of these simulation results displays that the modified blast resistant design depending on ς_y^{rc} and ς_μ^{rc} is more effective in keeping y_m^{rc} and μ^{rc} under control with respect to the design targets.

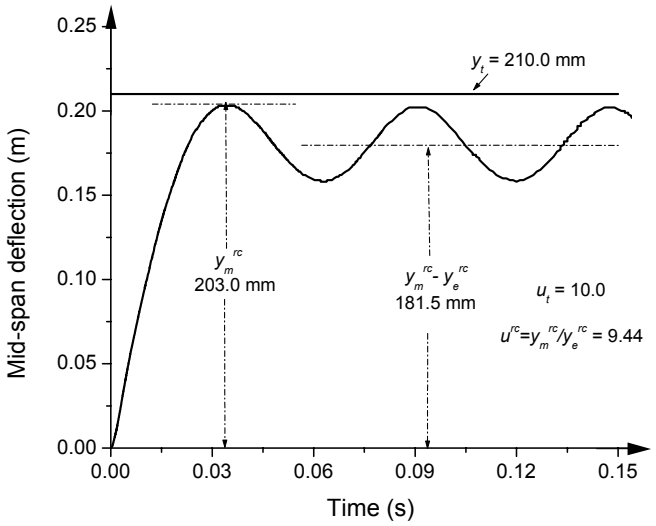

(a). Designed with the modified approach

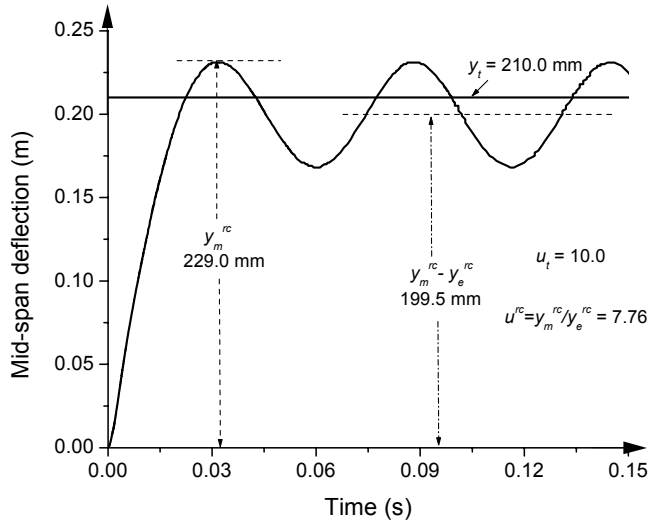

(b). Designed with the original approach

Figure 6.6 Deflection history of the designed simply supported beams under the given blast loading (Example I)

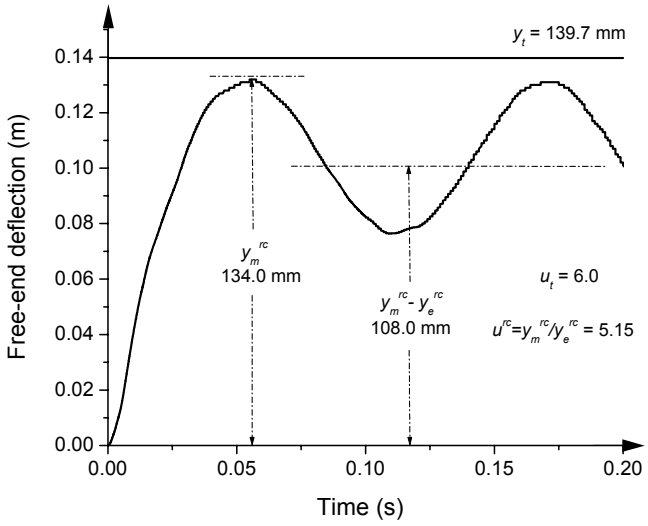

(a). Designed with the modified approach

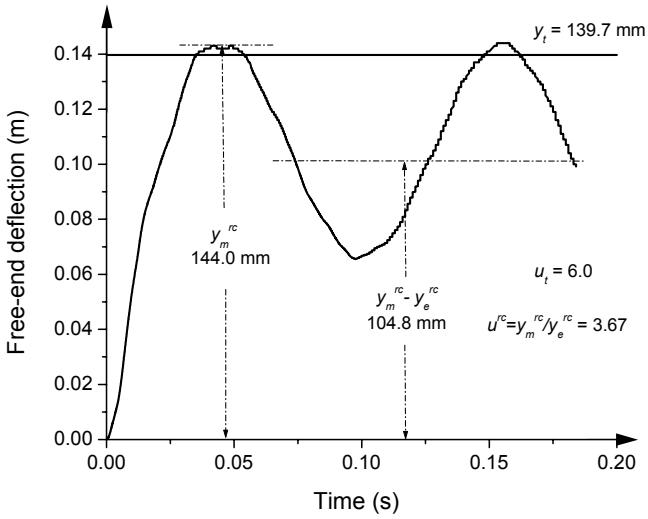

(b). Designed with the original approach

Figure 6.7 Deflection history of the designed cantilever walls under the given blast loading (Example II)

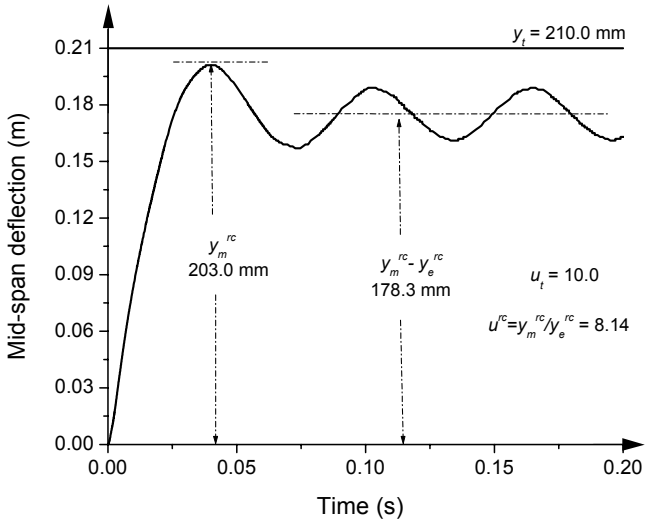

(a). Designed with the modified approach

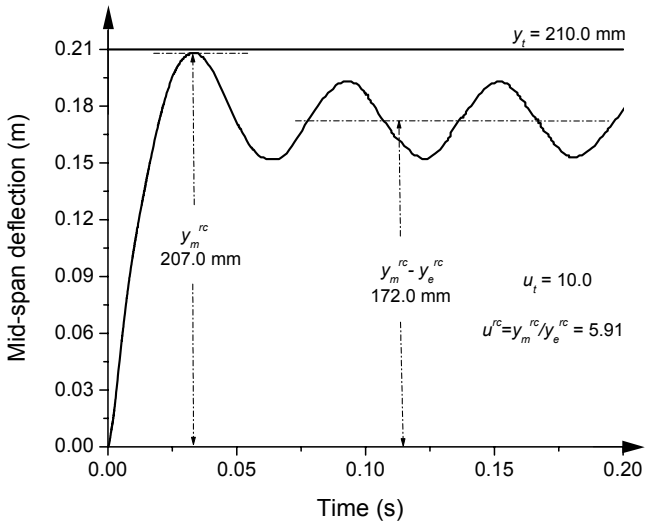

(b). Designed with the original approach

Figure 6.8 Deflection history of the designed fixed/roller-supported beams under the given blast loading (Example III)

6.3 Estimation of Response Distributions For Designed Members With Error Indices

6.3.1 Analytical procedures

Another important application of the error indices is that they provide a simpler way for the prediction of the responses (y_m^{rc} and μ^{rc}) for the designed member at its significant point under a possible blast loading without carrying out nonlinear dynamic analysis on it. By transforming Equations (6.1) and (6.2), y_m^{rc} and μ^{rc} are obtained as

$$y_m^{rc} = y_{te}(1 - f(\rho, SC) - e_y) \tag{6.9}$$

$$\mu^{rc} = \mu_{te}(1 - g(\rho, SC) - e_\mu) \tag{6.10}$$

Since within the original performance-based blast resistant design using energy spectra developed in Chapter 3, the members are so designed that the responses of their equivalent SDOF systems (y_m^{eq} and μ^{eq}) are controlled to be exactly equal to the PAR-DTs of y_{te} and μ_{te}, the error indices defined in Equations (6.1) and (6.2) also reflect the relationships of y_m^{rc} and μ^{rc} with y_m^{eq} and μ^{eq} . As a result, substituting y_{te} and μ_{te} with y_m^{eq} and μ^{eq} respectively into Equations (6.9) and (6.10) produces

$$y_m^{rc} = y_m^{eq}(1 - f(\rho, SC) - e_y) \tag{6.11}$$

$$\mu^{rc} = \mu^{eq}(1 - g(\rho, SC) - e_\mu) \tag{6.12}$$

According to Equations (6.11) and (6.12), the responses of y_m^{rc} and μ^{rc} of the designed member under a possible blast loading can be estimated from the corresponding y_m^{eq} and μ^{eq}, which are computationally simple and straightforward.

By converting the member into an equivalent SDOF system [B1], these parameters including equivalent mass (m), equivalent force (F_1), equivalent initial stiffness (k_e), equivalent ultimate strength (R_m), natural period (T), elastic displacement ($y_e^{eq} = R_m / k_e$), and elastic energy ($E_{el} = k\, y_e^{\,2} / 2$) can be obtained. Further, y_m^{eq} and μ^{eq} are effortlessly solved with these two expressions

$$y_m^{eq} = \frac{E_{\max}}{k_e y_e^{eq}} + \frac{y_e^{eq}}{2} \tag{6.13}$$

$$\mu^{eq} = \frac{y_m^{eq}}{y_e^{eq}} \tag{6.14}$$

where $E_{\max}$ is computed with the non-dimensional energy factor ($C = E_{\max} / E_{el}$) found from the energy spectra according to the ratios t_d / T and F_1 / R_m in Chapter 3.

However it should be pointed out that unlike the situation where the responses of y_m^{rc} and μ^{rc} could be exactly determined through nonlinear dynamic finite element analysis, Equations (6.11) and (6.12) only provide an approximate way to predict y_m^{rc} and μ^{rc} from the respective y_m^{eq} and μ^{eq} since e_y and e_μ are two uncertain nominal random variables following normal distribution as described in Chapter 5. Considering the random effects of e_y and e_μ, the coefficients of variation (COV) for y_m^{rc} and μ^{rc} are obtained as

$$COV(y_m^{rc}) = \frac{\sigma_{e_y}}{1 - f(\rho, SC)} \tag{6.15}$$

$$COV(\mu^{rc}) = \frac{\sigma_{e_\mu}}{1 - g(\rho, SC)} \tag{6.16}$$

where σ_{e_y} and σ_{e_μ} are standard deviations of e_y and e_μ listed in Chapter 5. The COVs for y_m^{rc} and μ^{rc} have no relationship with their respective y_m^{eq} and μ^{eq} and they tends to change with ρ and SC of the member. The trends are shown in Figure 6.9. It is evident that Equations (6.11) and (6.12) are more effective in the prediction of y_m^{rc} and μ^{rc} for the simply supported, fixed/roller-supported and cantilever members under blast conditions. The maximum COVs of y_m^{rc} for these members are generally less than 0.03, representing a significant concentration of y_m^{rc} around their mean values. The COVs of μ^{rc} for these types of members rang from 0.05 to 0.18 and rise gradually with the decline in ρ. As for fixed/fixed members, the predicted y_m^{rc} is also concentrated around its mean values with the maximum COV less than 0.08, however for μ^{rc} predicted from Equation (6.12), it has some deviation when ρ is less than 1.0 %.

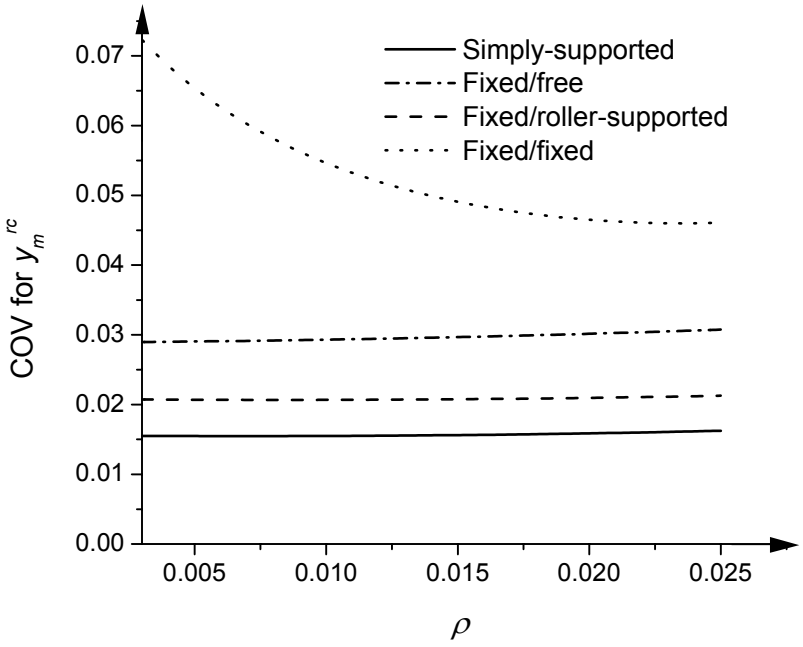

(a). COV for y_m^{rc} predicted from Equation (6.11)

Figure 6.9 COVs for y_m^{rc} and μ^{rc} due to the random effect of e_y and e_μ

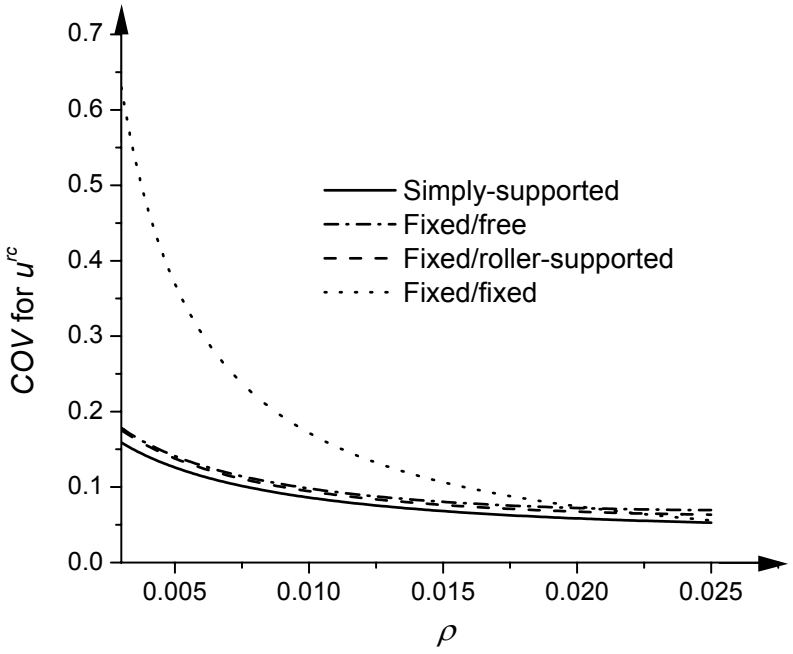

(b). COV for μ^{rc} predicted from Equation (6.12)

Figure 6.9 (Continued)

6.3.2 Implementation into probabilistic performance assessment

The combination of Equations (6.11) and (6.12) with the probabilistic methods such as the first-order second-moment (FOSM) method, or the Monte-Carlo simulation [B13, H8, K5, M18] provides a simpler solution for the probabilistic problem of reinforced concrete flexural members in blast conditions where the performance functions are defined in terms of maximum displacement and/or displacement ductility responses together with the corresponding performance criterion values. As an illustration, examples of the members designed above with modified approach are exhibited in which the probabilities of their responses in different performance levels are required. Referring to current literatures [T1, T2, M3, B4, S6], the performance levels in these examples are defined in three ways: displacement, displacement ductility factor, or both of them. Accordingly, the probability at the i th performance level can be calculated with any of the following expressions

$$P_i = P[(y - y_i) < 0] - P[(y - y_{i-1}) < 0] \tag{6.17a}$$

$$P_i = P[(\mu - \mu_i) < 0] - P[(\mu - \mu_{i-1}) < 0] \tag{6.17b}$$

$$P_i = P\{[(y - y_i) < 0] \cap [(\mu - \mu_i) < 0]\} - P\{[(y - y_{i-1}) < 0] \cap [(\mu - \mu_{i-1}) < 0]\} \tag{6.17c}$$

where y and μ are member's maximum displacement and displacement ductility responses accounting for different types of uncertainties, y_i and μ_i are upper limits of the i th performance level as listed in Table 4.3. P_i is the probability that the member's responses will locate within the i th performance level. The physical meanings of (6.17c) can be explained in Figure 6.10 where the shadow area displays the field of the i th performance level.

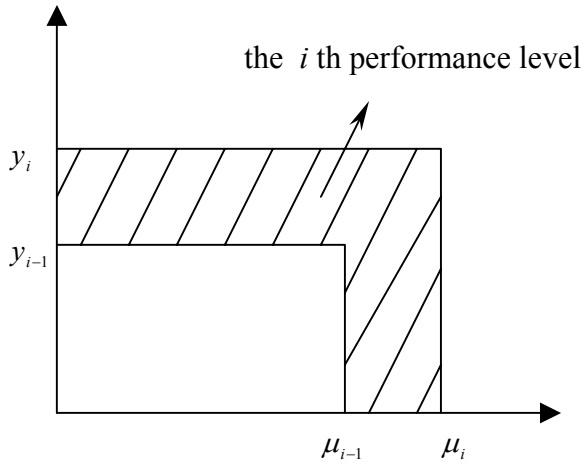

Figure 6.10 The field of the i th performance level

The uncertainties of different variables including f_s, f_c, E_s, E_c, A_s, d, and l are considered in the probabilistic performance assessment of these three design examples. Their means values are taken as those employed in the design process while their COVs [K20, M4, M5, V1] are listed in Table 6.4. The blast loadings bring out the most uncertainty to the structural responses, however to date not

enough information is available on the random properties of blast loadings applied to a structure in its lifetime. In this example it is assumed that P_r and t_d follow normal distributions with the mean values equal to those used in the design and the COVs shown in Table 6.4. e_y and e_μ are two additional independent random variable that link y_m^{rc} and μ^{rc} with the respective y_m^{eq} and μ^{eq}. Their distributions can be found in Chapter 5 with the zeros of mean values and the corresponding standard deviations at various *SC*s.

Table 6.4 Random variables for the designed members

Variables	f_s	E_s	f_c	E_c	A_s	d	l	P_r	t_d
Distribution	Normal								
COV	0.08	0.08	0.15	0.15	0.05	0.05	0.05	0.05	0.05

The probabilistic performance assessment of the designed members involving the uncertainty of the above variables is accomplished through Monte-Carlo simulation method. The choice of Monte-Carlo simulation for this case is justified because the procedure to predict y_m^{rc} and μ^{rc} with Equations (6.11) and (6.12) is very simple. As a consequence, the simulation sample size (20000 in these examples) can be selected relatively large so as to achieve an accurate estimation without consuming much computational time and work. The results of P_i for these designed members' responses (y_m^{rc} and μ^{rc}) are computed as listed in Table 6.5. For a comparison, by replacing y and μ respectively with y_m^{eq} and μ^{eq} into Equation (6.15), P_i for the equivalent SDOF systems of these members (y_m^{eq} and μ^{eq}) are also evaluated with the results shown in Table 6.5.

Table 6.5 Probabilities at various performance levels for the designed members under blast conditions

	Probabilities based on responses of designed member predicted from Equations (6.11) and (6.12)			Probabilities based on responses of equivalent SDOF system		
Design example I: the simply supported beam						
Performance level	y_m^{rc}	μ^{rc}	y_m^{rc} & μ^{rc}	y_m^{eq}	μ^{eq}	y_m^{eq} & μ^{eq}
A	0	0	0	0	0	0
B	0	0.0004	0	0	0	0
C	0.0020	0.0910	0.0016	0.0076	0.0004	0.0002
D	0.5346	0.5988	0.4798	0.7014	0.0662	0.0658
E	0.4634	0.3098	0.5186	0.2910	0.9334	0.9340
Design example II: the cantilever wall						
Performance level	y_m^{rc}	μ^{rc}	y_m^{rc} & μ^{rc}	y_m^{eq}	μ^{eq}	y_m^{eq} & μ^{eq}
A	0	0	0	0	0	0
B	0.0028	0.0522	0.0014	0.0032	0	0
C	0.5848	0.7232	0.5284	0.6020	0.0010	0.0010
D	0.4116	0.2176	0.4626	0.3942	0.1536	0.1536
E	0.0008	0.0070	0.0076	0.0006	0.8454	0.8454
Design example III: the fixed/roller-supported beam						
Performance level	y_m^{rc}	μ^{rc}	y_m^{rc} & μ^{rc}	y_m^{eq}	μ^{eq}	y_m^{eq} & μ^{eq}
A	0	0	0	0	0	0
B	0	0.0002	0	0	0	0
C	0.0022	0.1252	0.0022	0.0016	0	0
D	0.5400	0.5984	0.4858	0.5256	0.0052	0.0052
E	0.4578	0.2762	0.5120	0.4728	0.9948	0.9948

It is indicated from Table 6.5 that P_i assessed with y_m^{eq} alone for the simply supported and fixed/roller-supported beam is mainly concentrated on Level D while those with μ^{eq} alone is focused on Level E. As for the cantilever wall, P_i from y_m^{eq} alone is the most in Level C as compared to that in Level E from μ^{eq} alone. Such inconsistent results are mainly caused by the fact that these members' displacement ductility responses are significantly overestimated by μ^{eq} while the maximum displacement responses slightly underestimated by y_m^{eq}. Accordingly, the change trends of P_i assessed on the basis of both y_m^{eq} and μ^{eq} are generally estimated too highly at Level E. To overcome this, it is necessary to involve the error indices in Equations (6.11) and (6.12) to predict y_m^{rc} and μ^{rc} from y_m^{eq} and μ^{eq}, and so apply them into the assessment. The relatively reasonable P_i at different performance levels are obtained as indicated in Table 6.5 where, for instance, P_i evaluated from y_m^{rc}, μ^{rc} or both of them are all convergent in Level C for the cantilever wall. Therefore, the distributions of y_m^{rc} and μ^{rc} derived with Equations (6.11) and (6.12) depending on error indices are effective in the probabilistic performance assessment of designed members under the blast conditions accounting for different uncertainties.

6.4 Summaries

The applications of the formula of ς_y^{rc} and ς_μ^{rc} proposed in Chapter 5 are discussed in these two fields: modification of the performance-based blast resistant design approach using energy spectra in controlling y_m^{rc} and μ^{rc}, and estimation of the distributions of y_m^{rc} and μ^{rc} for the designed member under blast conditions accounting for uncertainties.

Through the adjustment of PAR-DTs with ς_y^{rc} and ς_μ^{rc}, the modification of the design approach is accomplished with iterative procedures. The implementation of the modified design approach into three design examples indicates that more iterative

steps are needed to reach convergence as compared to those of the original design procedure. However the responses of y_m^{rc} and μ^{rc} for the member designed with the modified design approach from the nonlinear numerical analysis are controlled more approximately to their targets and restricted to be a little on the conservative sides.

The estimation of y_m^{rc} and μ^{rc} for the designed members under possible blast forces is much simpler on the basis of ς_y^{rc} and ς_μ^{rc} from the corresponding y_m^{eq} and μ^{eq} that are computationally straightforward. By the combination of this procedure with Monte-Carlo simulation, the probabilistic performance of the members designed with the modified method under blast conditions can be conveniently and effectively evaluated accounting for different types of uncertainties.

CHAPTER SEVEN

PERFORMANCE-BASED BLAST RESISTANT DESIGN OF MULTI-STOREY REINFORCED CONCRETE FRAME STRUCTURES WITH EQUIVALENT STATIC FORCE (ESF) — PART I: THEORETICAL BASIS

Synopsis

Control of the maximum inter-storey drift ratio (MIDR) for a multi-storey reinforced concrete frame structure becomes critical when that structure is subjected to a blast loading from a distant intense surface explosion. For this purpose, a new design method is presented based on the transformation of the lateral blast force into an equivalent static force (ESF). The ESF is calculated in such a manner that the same MIDR effect will be produced as that under the blast condition. This chapter concentrates on the calculation model of ESF for a single-degree-of-freedom (SDOF) system as well as the design method based on ESF with the requirement of controlling its maximum displacement response. Implementations of the design method into several examples are demonstrated while the verifications of the displacement responses of the designed SDOF system are performed with nonlinear dynamic analyses. The analytical results indicate that the target displacement is well met for the designed SDOF system in resisting the given blast loading. The extension of the calculation model of ESF and the corresponding design method with ESF for a SDOF system to a multi-storey reinforced concrete frame structure will be discussed in Chapter 8.

Keywords: Maximum inter-storey drift ratio, Equivalent static force
Maximum displacement response, SDOF system

7.1 Introduction and Background

As discussed in Chapter 2, under a distant intense blast condition where the blast shock wave can be simplified into a planar wave, the dynamic responses for multi-storey reinforced concrete frame structures can be approximately divided into two response stages. At response stage II, a significant global response in terms of MIDR may be provoked inducing a certain degree of global damage and therefore, in the design of multi-storey reinforced concrete frame structures against the distant blast loadings, controlling their MIDR responses becomes an important consideration. Regarding this problem, in order to ensure the global response within the expected performance level, different levels of side-sway limits are given for the design of single-storey rigid frame structures in the current design guidance ([N4, B4]) according to the operational needs of the facility and the needs for reusability. Their values in terms of inter-storey drift ratio and the description of corresponding response levels and damage degrees are listed in Table 2.1.

Blast loadings act dynamically on structures with short durations, however the dynamic loadings are extremely difficult to handle within the structural design since they could not be directly implemented into the calculation of the interior forces of the structural members. In the seismic/wind resistant design procedures, the dynamic seismic/wind actions are generally transformed into the static loadings, which are deemed to be able to produce equivalent effects on structures [C10, C11, D1, J1, K14, P2, P6, R3, Z2]. Similarly if an equivalent static force (ESF) applied to the structure with the magnitude and direction that could closely represent the effects of the distant blast loadings can be found, it will greatly facilitate the blast resistant design.

The implementation of ESF into the blast resistant design for a single-storey rigid frame subjected to a relatively low blast overpressure has been suggested in the manual by NFEC [N4]. The dynamic load factors are provided for establishing equivalent static loads for the frame mechanism. Based upon the mechanism method, as employed in static plastic design, estimations are made for the required

plastic bending capacity. However these dynamic load factors were approximate and made no distinction for different end conditions. They were only expected to result in the estimation of the required resistance for a trial design. In order to confirm that a trial design meets the recommended deformation criteria, a rigorous frame analysis has to be performed.

This chapter together with Chapter 8 aims to present a new performance-based blast resistant design method for multi-storey reinforced concrete frame structural system based on the equivalent static force (ESF) of the distant blast action. For this purpose, this chapter concentrate on the description of the calculation model of the ESF and the corresponding design method based on the ESF for a SDOF system. Three illustrative examples are employed to demonstrate the implementation of the method while verifications of the displacement responses of the designed SDOF systems are carried out through nonlinear dynamic analysis. In Chapter 8, this presented design method is extended to a performance-based design for the multi-storey reinforced concrete frame structure by reasonably selecting the MIDR response as a global performance indicator, where the frame structure could not be simply idealized into a SDOF system in the blast condition.

Basically the developed design method with ESF is for the design of a multi-storey reinforced concrete frame structural system in controlling its MIDR response, which occurs at a time apparently later than the blast loading duration (t_d) as indicated by numerical simulations in Chapter 2. The description of the calculation model of ESF and the design method with ESF for a SDOF system herein is only to provide a theoretical basis. Therefore the assumption that the peak response (maximum displacement for a SDOF system or MIDR response for a frame structure) takes place after the duration t_d is generally adopted in Chapters 7 and 8. Only the SDOF systems that satisfy this assumption are of concern in this chapter.

7.2 ESF for a SDOF System

7.2.1 Process for the construction of ESF

Because of the short duration of the blast loading, the vibration of a SDOF system after reaching the peak response will be limited within its elastic range inducing no further cumulative damages [B1]. Therefore for a well-defined SDOF system, the maximum displacement response can adequately characterize its damage status in blast events. Under such conditions, if there exists a force, which makes it possible for the SDOF system to experience exactly the same maximum displacement response when statically applied, this force is called the equivalent static force (ESF) of the blast loading. To calculate the ESF of the blast loading on a SDOF system, a model is presented herein with its process plotted in Figure 7.1.

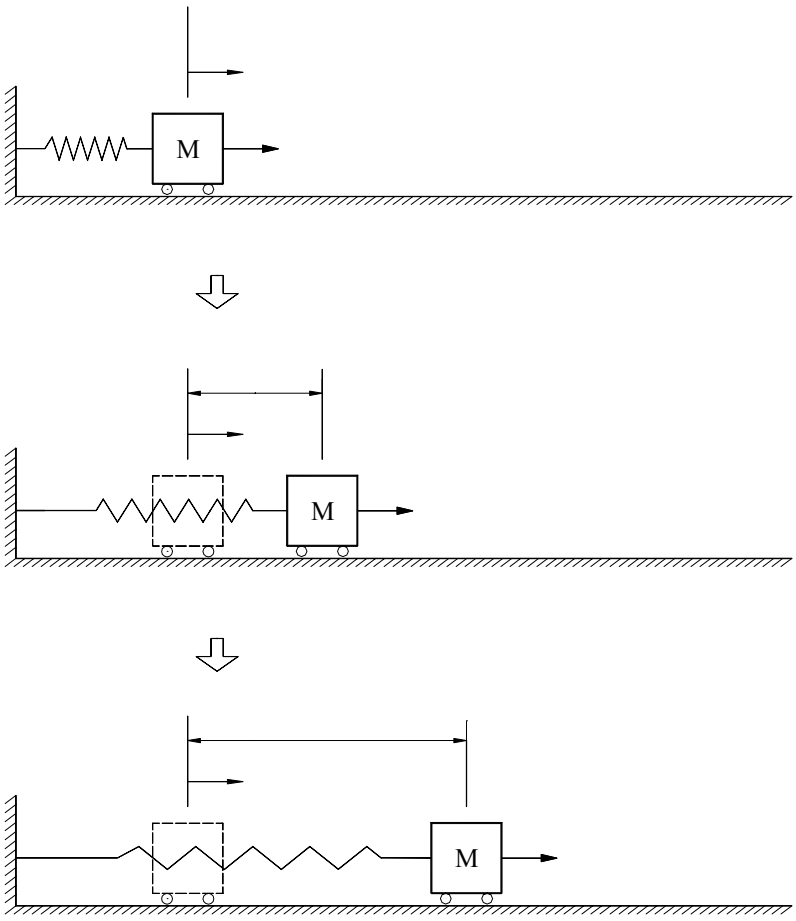

Figure 7.1 (a). Dynamic response process of the original SDOF system under the blast force

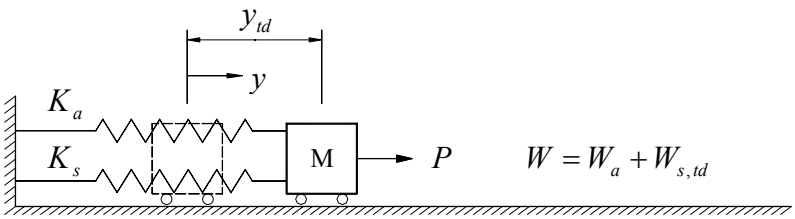

(b). Equivalent static system

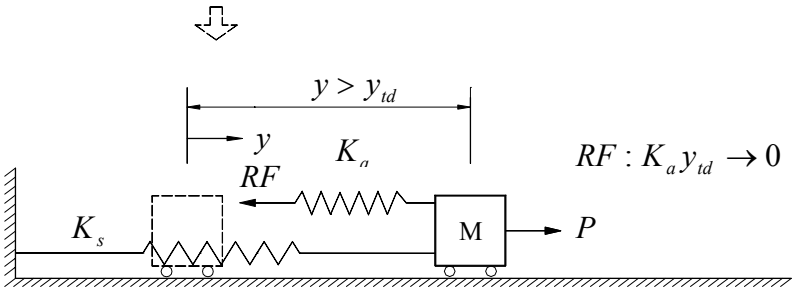

(c). Releasing the strain energy in spring K_a

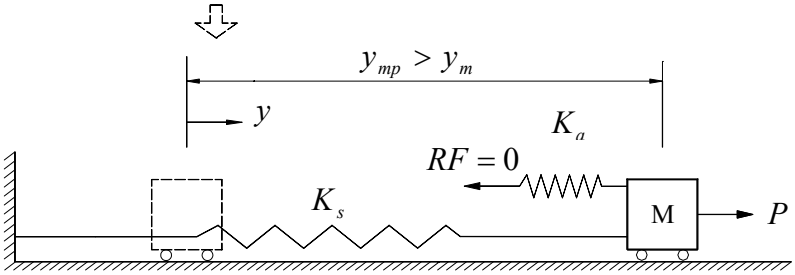

(d). Recovering to the original SDOF system plus the action of P

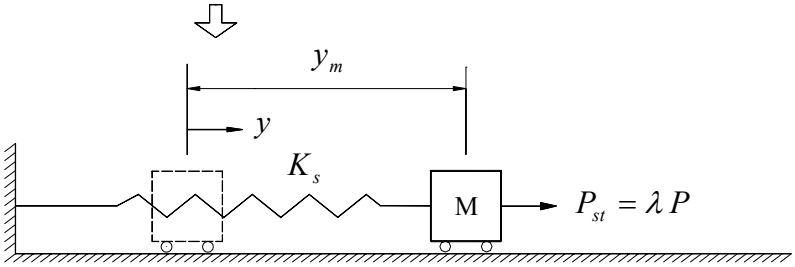

(e). Equivalent static force

Figure 7.1 Process for the construction of ESF for a SDOF system

The blast force can be reasonably simplified into a triangular pulse only if the peak pressure and impulse are preserved [H1], hence the function of the blast force is written as

$$F(t) = \begin{cases} F_1 (1 - t/t_d) & t \le t_d \\ 0 & t > t_d \end{cases} \tag{7.1}$$

where t_d is the duration and F_1 is the peak amplitude of the blast force. Since after t_d, the blast force will keep zero, no additional external energy is produced and the total energy within the SDOF system consisting of the kinetic energy and the strain energy will keep constant whose magnitude determines the maximum response by ignoring the damping effects [B1, K4]. The constant total energy can be obtained from the response state of the system at t_d plotted in Figure 7.1a, written as

$$W = W_{k,td} + W_{s,td} \tag{7.2}$$

where W is the constant total energy of the SDOF system; $W_{k,td}$ and $W_{s,td}$ are the kinetic and strain energy at the time t_d respectively. In order to simulate the energy components of the SDOF system equally at this time step, an equivalent static SDOF system is constructed as shown in Figure 7.1b, where an additional elastic spring is added to the original SDOF system. It is proposed that under a certain external static force P, the equivalent static system experience the same displacement response as y_{td} (the dynamic response of the original SDOF system at t_d) and therefore the strain energies within the spring K_s in both systems are identical. In order to model the kinetic energy, the strain energy W_a within the additional spring K_a should be equal to $W_{k,td}$, thus

$$M \dot{y}_{td}^{\ 2} / 2 = K_a \, y_{td}^{\ 2} / 2 \tag{7.3}$$

and

$$K_a = M\,\dot{y}_{td}^{\,2} / y_{td}^{\,2} \tag{7.4}$$

where $\dot{y}_{td}$ is the velocity of the original SDOF system at the time of t_d under $F(t)$, K_a is the elastic stiffness of the additional spring. From the equilibrium of the equivalent static system

$$P = F_s + F_a = F_s + K_a y_{td} = F_s + M\,\dot{y}_{td}^{\,2} / y_{td} \tag{7.5}$$

where F_s and F_a is the force produced respectively by the original and additional spring (K_s and K_a) in the equivalent static system in Figure 7.1b.

After t_d, the kinetic energy $W_{k,td}$ will be gradually transformed into the strain energy causing further displacement for the original SDOF system until the maximum response y_m is reached as shown in Figure 7.1a. For modelling this process with the equivalent static system, the strain energy W_a in the additional spring K_a needs to be released statically in such a way that this part of energy is transferred to the original spring K_s as shown in Figure 7.1c. With the support of the additional spring statically moving toward the spring until the support reaction force RF decreases to zero, the equivalent static system is recovered to the original SDOF system with the static force P exerting on it in Figure 7.1d. However it should be noted that during this process, an amount of extra positive external energy is produced by P together with the declining RF; and a relatively larger displacement response y_{mp} will be induced than y_m for the original SDOF system under the blast condition. Thus an ESF factor (λ) less than one is applied to P producing the ESF (P_{st}) that creates the same maximum response as y_m when statically applied to the original SDOF system as shown in Figure 7.1e

$$P_{st} = \lambda P \tag{7.6}$$

7.2.2 ESF factor

For a SDOF system with the elastic-perfectly-plastic resistance function, the close form solution of the ESF factor λ is derived with respect to three different cases according to the response states at the time t_d and t_m (the time for maximum displacement response) as plotted in Figure 7.2. They are

- Case I : in the elastic state at $t = t_d$ as well as $t = t_m$;
- Case II : in the elastic state at $t = t_d$ while in the plastic state at $t = t_m$;
- Case III: in the plastic state at $t = t_d$ and $t = t_m$.

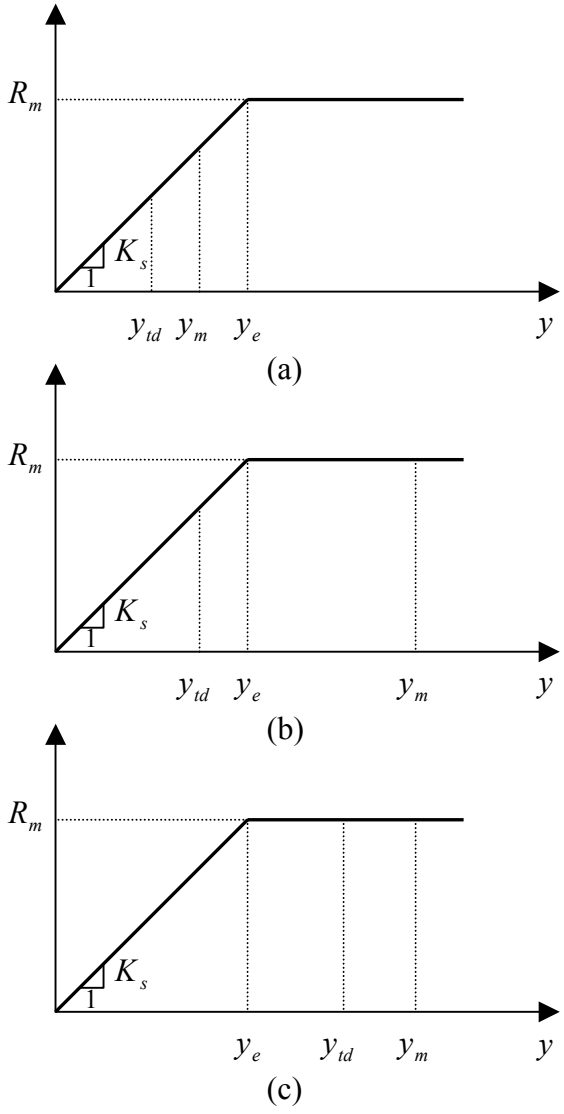

Figure 7.2 Three different response states for a SDOF system at the time t_d and t_m

Case I: In this case, since the SDOF system is still within its elastic limit during the whole response process as shown in Figure 7.2a, the constant total energy at t_d and t_m can be written as

$$W = K_s\, y_{td}^2 / 2 + M\, \dot{y}_{td}^2 / 2 \tag{7.7}$$

and

$$W = K_s\, y_m^2 / 2 \tag{7.8}$$

where K_s is the initial stiffness of the elastic-perfectly-plastic SDOF system. Equating Equations (7.7) with (7.8) leads to

$$M\, \dot{y}_{td}^2 = K_s (y_m^2 - y_{td}^2) \tag{7.9}$$

Subjecting Equation (7.9) into Equation (7.5) and considering that the spring K_s is in its elastic range at t_d

$$P = K_s\, y_m \frac{y_m}{y_{td}} \tag{7.10}$$

To meet the requirement that the same y_m appear for the SDOF system under the ESF, P_{st} should be equal to its resistance at the displacement y_m, which in the elastic range is given as

$$P_{st} = K_s\, y_m \tag{7.11}$$

Substituting Equations (7.10) and (7.11) into Equation (7.6), the ESF factor λ in this case is determined as

$$\lambda = \frac{y_{td}}{y_m} \tag{7.12}$$

Case II: For the second case, where the SDOF system has entered the plastic response stage, Equation (7.8) for the calculation of the constant total energy at t_m changes into

$$W = \frac{1}{2} K_s \, y_e \left(2\, y_m - y_e\right) \tag{7.13}$$

where y_e is the elastic limit displacement of the SDOF system. Equating the Equations (7.7) with (7.13) obtains

$$M\, \dot{y}_{td}^2 = K_s (2 y_e y_m - y_e^2 - y_{td}^2) \tag{7.14}$$

By subjecting Equation (7.14) into Equation (7.5) and considering that the spring K_s is in its elastic range at t_d, P is given as

$$P = K_s y_e \frac{(2y_m - y_e)}{y_{td}} \tag{7.15}$$

In order to statically produce the same maximum displacement as y_m in the blast condition, which is beyond the elastic limit of the SDOF system with elastic perfect plastic resistance function, the ESF (P_{st}) should be identical with the ultimate strength, thus

$$P_{st} = K_s \, y_e \tag{7.16}$$

The value of λ is finally obtained by subjecting Equations (7.15) and (7.16) into Equation (7.6) as

$$\lambda = \frac{y_{td}}{2\, y_m - y_e} \tag{7.17}$$

Case III: Since the SDOF system has entered its plastic response stage before t_d, W for the elastic-perfectly-plastic SDOF system at t_d is given by

$$W = \frac{1}{2} K_s y_e (2y_{td} - y_e) + \frac{1}{2} M \dot{y}_{td}^2 \tag{7.18}$$

In this case, Equation (7.13) is also valid for expressing W at t_m, therefore equating Equations (7.13) with (7.18) brings out

$$M y_{td}^2 = 2K_s y_e (y_m - y_{td}) \tag{7.19}$$

By taking $F_s = K_s y_e$ and subjecting Equations (7.19) into Equations (7.5), P is gained as

$$P = K_s y_e \frac{(2y_m - y_{td})}{y_{td}} \tag{7.20}$$

With Equation (7.16) for the evaluation of P_{st}, λ is derived from Equations (7.6) and (7.20) as

$$\lambda = \frac{y_{td}}{2y_m - y_{td}} \tag{7.21}$$

7.2.3 Calculation model for ESF

By summarizing the above analyses, a model to calculate the ESF for an elastic-perfectly-plastic SDOF system is presented in Equation (7.22). An extra variable X is introduced, which is for the convenience of extending this model to multi-storey reinforced concrete frame structures as discussed in Chapter 8. Obviously there is a 45^o linear relationship between λ and X as shown in Figure 7.3. The physical

meanings for the other variables have been well defined previously.

$$\begin{cases} P_{st} = \lambda P \\ P = F_s + F_a \\ \lambda = X \\ X = \begin{cases} y_{td} / y_m & y_m \le y_e \\ y_{td} /(2y_m - y_e) & y_{td} \le y_e \text{ and } y_m \ge y_e \\ y_{td} /(2y_m - y_{td}) & y_{td} \ge y_e \end{cases} \end{cases} \tag{7.22}$$

It should be pointed out that this model does not attempt to calculate the ESF with the purpose of assessing the maximum response of a particular SDOF system under the blast condition, but provides a powerful tool in designing the ultimate strength of the system to achieve the target of the displacement response. The design method based on this model is addressed in the following section.

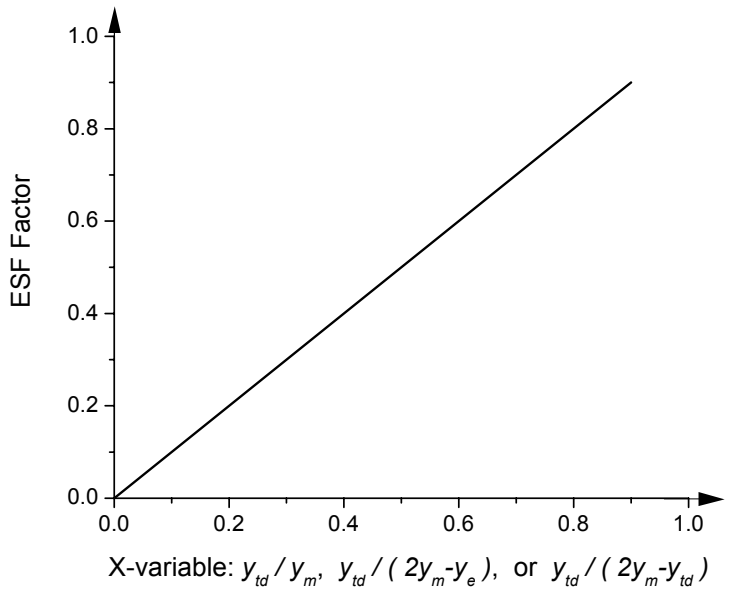

Figure 7.3 Distribution of the ESF factor for the SDOF system

7.3 Design of a SDOF System with the ESF

For the elastic-perfectly-plastic SDOF systems with the stiffness K_s, the mass M and the blast loading F_1 and t_d acting on them, the relationship between their ultimate strengths R_m and the corresponding maximum displacement responses y_m can be explained as follows. Supposing that there are two such SDOF systems but with different ultimate strengths $R_{m1} < R_{m2}$, two facts are considered that:

1) during any short period of time Δt within t_d, the displacement response for the first system with R_{m2} will not exceed that of the second system with R_{m1}, accordingly the total external work by the blast loading on the first system will be equal to or less than the correspondent on the second system;

2) with the same displacement response, the energy absorbing capacity by the deformation of the first system will not be less than that of the second one.

Accordingly, it can be derived that with the increase in the ultimate strength of the system, the maximum displacement response will decrease gradually as shown in Figure 7.4 where $R_{m1} < R_{m2} < R_{m3}$ and $y_{m1} > y_{m2} > y_{m3}$. However when R_m reaches the critical value of R_{mref} and y_m declines to y_{mref}, the whole response of the system is located in its elastic range. A further increase in R_m will have little effect on its maximum displacement response. That means that for this SDOF system with K_s, M, F_1 and t_d, its maximum response will never be smaller than y_{mref}, which can be obtained from dynamic analysis by assuming the SDOF system to be fully elastic.

Design of the ultimate strength for a SDOF system satisfying the given target maximum displacement response y_t is to find the value of R_m corresponding to $y_m = y_t$. If $y_t \geq y_{mref}$, then the maximum response of the designed SDOF system

will locate or be beyond its elastic limit state as shown in Figure 7.4. In such a case the ESF defined above is equal to the ultimate strength, that is, $R_m = P_{st}$. Therefore R_m and y_t should satisfy Equation (7.22) by replacing P_{st} and y_m with R_m and y_t respectively

$$\begin{cases} R_m = \lambda P \\ P = F_s + F_a \\ \lambda = X \\ X = \begin{cases} y_{td} / y_t & y_t \le y_e \\ y_{td} /(2y_t - y_e) & y_{td} \le y_e \text{ and } y_t \ge y_e \\ y_{td} /(2y_t - y_{td}) & y_{td} \ge y_e \end{cases} \end{cases} \tag{7.23}$$

On the other hand if $y_t < y_{mref}$, there exists no solution for R_m and in order to reach such a target y_t, it needs to increase K_s or M. According to the discussion, an iterative procedure is presented to gain this unique R_m based on the model of Equation (7.23). The flowchart is plotted in Figure 7.5.

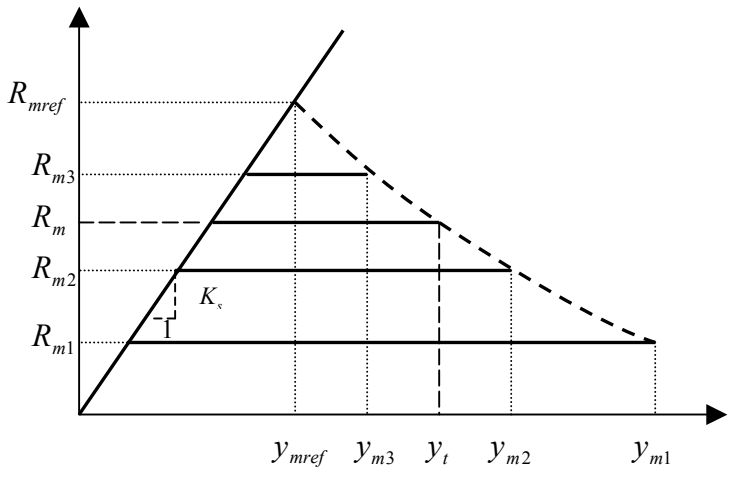

Figure 7.4 Relationship between the ultimate strength and the maximum displacement response

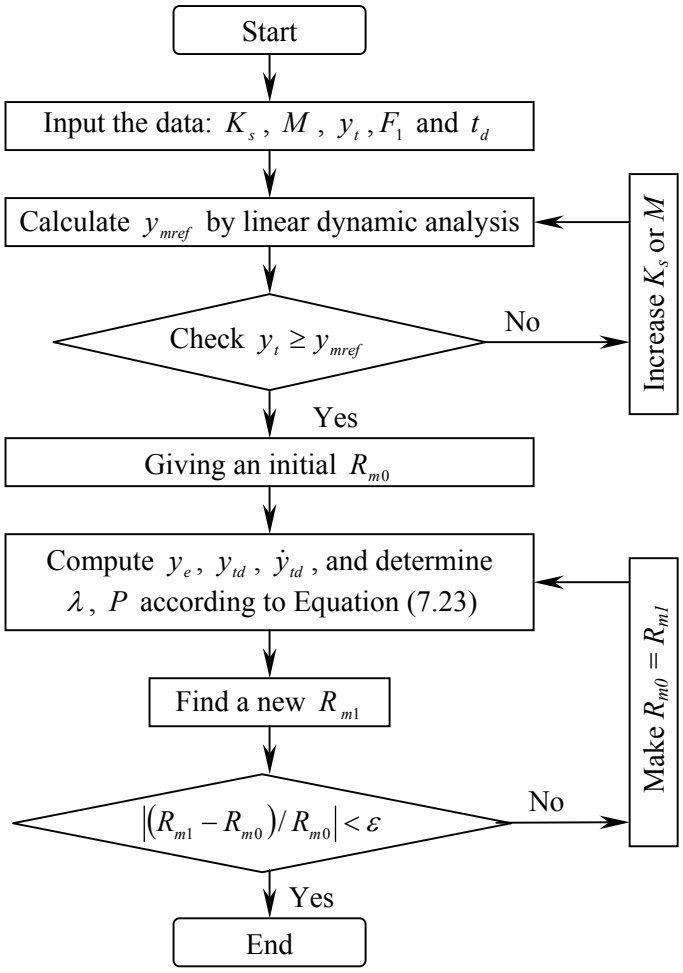

Figure 7.5 Flowchart of blast resistant design of an elastic-perfectly-plastic SDOF system with ESF (where ε is an arbitrarily small value).

7.4 Illustrative Examples

To illustrate the design procedures with ESF, three illustrative examples are presented as shown in Table 7.1 where a variety of target displacements are required for the SDOF systems in resisting different blast forces. The iterative procedures at each step of these design examples are demonstrated in Tables 7.2 to 7.4 where the initial ultimate strength R_{m0} is taken as the multiplication of K_s with y_{mref}. The convergence condition of $\left|(R_{m1} - R_{m0})/R_{m0} \leq 0.001\right|$ is employed.

Table 7.1 Parameters in three design examples

Design Example	F_1 (N)	t_d (s)	M (kg)	K_s (N/mm)	y_t (mm)
I	1000	0.04	100	10	100
II	2000	0.06	10	20	500
III	2000	0.06	100	10	50

Table 7.2 Design procedures for example I

Step	y_{mref} (mm)	R_{m0} (N)	y_e (mm)	y_{td} (mm)	$\dot{y}_{td}$ (mm/s)	P (N)	λ	$R_{m1}(P_{st})$ (N)
1	19.9	199.110	19.911	5.249	192.07	755.38	0.029	22.015
2		22.015	2.202	5.262	194.53	741.18	0.027	20.026
3		20.026	2.003	5.265	194.87	741.31	0.027	20.042

Table 7.3 Design procedures for example II

Step	y_{mref} (mm)	R_{m0} (N)	y_e (mm)	y_{td} (mm)	$\dot{y}_{td}$ (mm/s)	P (N)	λ	$R_{m1}(P_{st})$ (N)
1	109.4	2188.2	109.410	106.2	-1180	2254.9	0.119	268.81
2		268.81	13.441	203.5	4601	1309.2	0.256	334.50
3		334.50	16.725	196.2	4292	1273.4	0.244	310.92
4		310.92	15.546	198.8	4402	1285.8	0.248	319.06
5		319.06	15.953	197. 9	4364	1281.4	0.247	316.13
6		316.13	15.807	198.2	4377	1282.9	0.247	317.13
7		317.13	15.857	198.1	4373	1282.4	0.247	316.79
8		316.79	15.839	198.1	4374	1282.6	0.247	316.91

Table 7.4. Design procedures for example III

Step	y_{mref} (mm)	R_{m0} (N)	y_e (mm)	y_{td} (mm)	$\dot{y}_{td}$ (mm/s)	P (N)	λ	$R_{m1}(P_{st})$ (N)
1*	59.4							
			Design for K_{s1} = 20 *N/mm*					
1		831.69	41.58	22.32	496.24	1549.8	0.382	592.06
2		592.06	29.60	22.32	496.24	1549.8	0.317	491.29
3		491.29	24.56	22.32	496.24	1549.8	0.296	458.47
4	41.6	458.47	22.92	22.32	496.24	1549.8	0.290	448.72
5		448.72	22.44	22.32	496.24	1549.8	0.288	445.89
6		445.89	22.30	22.32	496.24	1549.4	0.287	445.08
7		445.08	22.25	22.32	496.24	1548.6	0.287	444.85

* $y_t < y_{mref}$

In design examples I and II, y_t is greater than y_{mref} thus R_m can be iteratively determined with respective to K_s listed in Table 7.1. However y_t is less than y_{mref} in design example III where to find the solution of R_m of the SDOF system, K_s given in Table 7.1 should be enlarged. By taking twice of the initial stiffness, the design is carried out and the results are shown in Table 7.4. It is indicated from the iterative procedures that there is no difficulty in reaching convergence for the design of the SDOF system with the ESF so as to find the unique R_m.

To evaluate the displacement responses for the SDOF systems designed based on ESF, nonlinear time history analyses are executed on them against the respective blast forces and the results are demonstrated in Figures 7.6 to 7.8. It is obvious that the maximum displacements of the designed SDOF systems exactly reach their respective objective values. Thus the design based on the ESF can effectively control the maximum displacement for the designed SDOF system in resisting the given blast force.

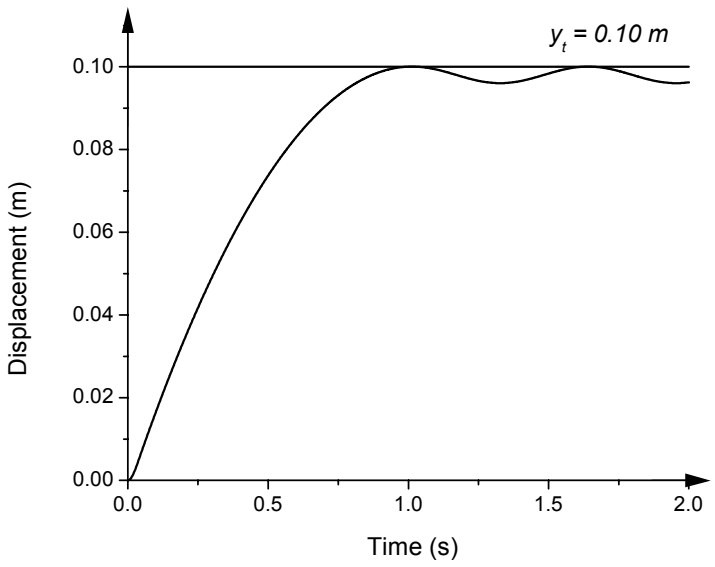

Figure 7.6 Displacement responses of the designed SDOF system under the given blast force (Example I)

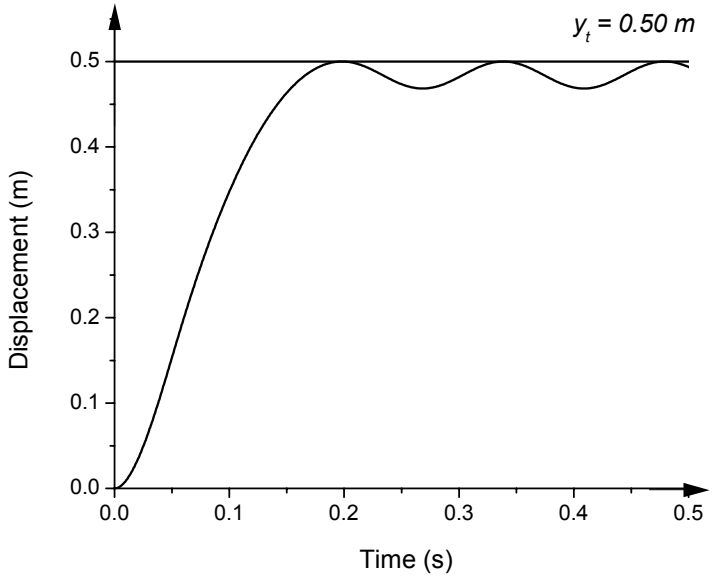

Figure 7.7 Displacement responses of the designed SDOF system under the given blast force (Example II)

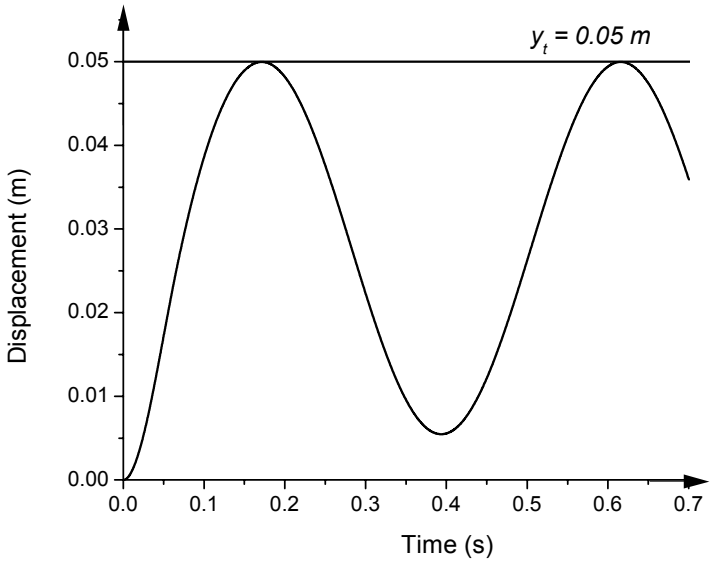

Figure 7.8 Displacement responses of the designed SDOF system under the given blast force (Example III)

7.5 Summaries

A calculation model for the ESF of the blast force and the design method using ESF for the elastic-perfectly-plastic SDOF systems are discussed in this chapter, which provide the theoretical basis for the performance-based blast resistant design of multi-storey reinforced concrete frame structures under distant explosion conditions in Chapter 8.

The model for the computation of ESF is derived based on the assumption that the peak response of the system is present after the blast loading duration t_d. An equivalent static SDOF system is derived which simulates the energy components of the original SDOF system at time t_d. Based on the equilibrium of equivalent static system, an external static force is computed. However this force tends to produce a larger maximum displacement demand than that of the original SDOF system under the blast force. As a result, an ESF factor is introduced to reduce the

external static force to obtain the final ESF. With respect to three different response states at time t_d and t_m, a closed-form solution of the ESF factor is obtained for the elastic-perfectly-plastic SDOF system. It is found that the ESF factor follows a 45^o linear relationship with an X-variable that is y_{td}/y_m, $y_{td}/(2y_m - y_e)$, or $y_{td}/(2y_m - y_{td})$.

By replacing the ESF with the ultimate strength as well as the maximum displacement with the required design target displacement, the computational model of the ESF is implemented for the design of an elastic-perfectly-plastic SDOF system. The ultimate strength of the SDOF system is solved iteratively during the design process so as to satisfy the specified target displacement. The presented design procedures have been illustrated via three numerical examples, which show no difficulty in convergence of the iterative procedures. The maximum displacement responses of the designed SDOF systems under the given blast conditions can be controlled to be exactly equal to their corresponding targets, as verified from nonlinear dynamic analysis.

CHAPTER EIGHT

PERFORMANCE-BASED BLAST RESISTANT DESIGN OF MULTI-STOREY REINFORCED CONCRETE FRAME STRUCTURES WITH EQUIVALENT STATIC FORCE (ESF) — PART II: IMPLEMENTATION AND EVALUATION

Synopsis

The model for the calculation of equivalent static force (ESF) and the design method with ESF for single-degree-of-freedom (SDOF) systems are extended into a performance-based design for multi-storey reinforced concrete frame structures in controlling their maximum inter-storey drift ratios (MIDR) under distant explosion conditions. An empirical formula for the ESF factor involved in the ESF model is presented based on a number of sample points of this factor, which are obtained by comparing the nonlinear dynamic responses of frame structures with corresponding nonlinear static pushover analytical results. For demonstration, two six-storey reinforced concrete frame structures are designed with the developed method against different blast intensities for various required performance levels. Numerical verification of the design method indicates the MIDR responses of these two designed structures in comparison to their respective targets are somewhat conservative. The reasons that may lead to the conservative designs are discussed.

Keywords: Maximum inter-storey drift ratio, Equivalent static force, Multi-storey reinforced concrete frame structure

8.1 Introduction

A performance-based design method by using ESF is developed for a multi-storey reinforced concrete frame structure system in this study. Four basic assumptions are made as follows:

1) The maximum inter-storey drift ratio (MIDR) can be treated as a reasonable and sufficient response parameter for the identification of the global performance level, and the critical side-sway limits in term of inter-storey drift ratio documented in the ASCE special publication [B4] as listed in Table 2.1 can properly reflect different global performance levels for a frame structure;
2) The MIDR response will occur at a time later than the blast loading duration (t_d), therefore the further inter-storey drift ratio response after t_d occurs as a result of the transformation of kinetic energy into strain energy of the structure. For most multi-storey frame structures, this assumption is acceptable considering the relatively short duration t_d of the blast force;
3) The nonlinear relationship of displacement and resistance of the frame structure under the action of the lateral forces can be reasonably idealized an elastic-perfectly-plastic function, consequently the calculated ESF will be the minimum required ultimate strength of the structure system based on which the reinforcements of the structure are designed;
4) The model for calculation of ESF has a similar form to that of Equation (7.22) for a multi-storey reinforced concrete frame structure.

Based on above assumptions, the process for the construction of the ESF for a SDOF system can be extended to a multi-storey reinforced concrete frame structure in term of vectors, however there is a main difference in the determination of the ESF factors through numerical studies rather than closed form solutions. A simple empirical equation for the ESF factor is derived for the convenience of the blast resistant design with ESF. For illustration and evaluation of the developed design method, two design examples are given for six-storey reinforced concrete frame

structures under different blast loadings followed by the numerical verifications.

8.2 ESF for a Multi-storey Reinforced Concrete Frame Structure

8.2.1 Process for the construction of ESF

For a frame structure with n storeys, the ESF (P_{st}) is defined as the column vector of the force applied to each floor level, which produce the same MIDR response as that under the blast action when it is statically exerted on the frame structure, thus

$$P_{st} = \left\{P_{st,1}, P_{st,2}, \cdots, P_{st,n}\right\}^T \tag{8.1}$$

where $P_{st,i}$ represents the component of ESF at the i th floor level. The process of the construction of P_{st} is plotted in Figure 8.1. At the end of the blast loading duration t_d, the frame structure responds with a distribution of displacement and velocity as shown in Figure 8.1a, where $y_{td} = \left\{y_{td,1}, y_{td,2}, \cdots, y_{td,n}\right\}^T$ and $y_{td,i}$ stands for the i th floor displacement at this time station. With the increase in time, the distributed kinetic energy as a function of the velocity will be gradually transformed into further deformation reaching the MIDR response Δ_m. Therefore, if the total kinetic energy within the part of the structure located halfway above and below the i th floor level at the time t_d, which is denoted by $W_{k,i}$ herein, is concentrated and represented by the strain energy $W_{a,i}$ of an additional spring $K_{a,i}$ at the corresponding floor level with the same deformation as $y_{td,i}$, an equivalent static system in Figure 8.1b can be established with

$$W_{a,i} = \frac{1}{2} K_{a,i}\, y_{td,i}^2 = W_{k,i} \tag{8.2}$$

or

$$K_{a,i} = \frac{2W_{k,i}}{y_{td,i}^2} \tag{8.3}$$

where $K_{a,i}$ is the stiffness of the additional elastic spring at the i th floor level. According to the equilibrium of the equivalent static system, the external static force ($P = \{P_1, P_2, \cdots, P_n\}^T$) will include two parts: the recovery force of the frame structure ($F_s = \{F_{s,1}, F_{s,2}, \cdots, F_{s,n}\}^T$) with the deformation of y_{td} and the force ($F_a = \{F_{a,1}, F_{a,2}, \cdots, F_{a,n}\}^T$) by additional springs, thus

$$P = F_s + F_a \tag{8.4}$$

where $F_{a,i}$ for the additional elastic spring at the deformation of $y_{td,i}$ is given as $F_{a,i} = K_{a,i} y_{td,i}$. Substituting Equation (8.3) into it produces

$$F_{a,i} = \frac{2W_{k,i}}{y_{td,i}} \tag{8.5}$$

In order to simulate the transformation of the kinetic energy into further deformation after t_d , the strain energy within the springs $K_{a,1}, K_{a,2}, \cdots K_{a,n}$ are statically released in such a manner that their supports move towards the springs until the equivalent static system is recovered to the original frame structure with P acting on it. However when considering the extra positive external work produced by P together with the declining reaction force of the springs at their supports during the energy transformation process, a larger MIDR will be induced in this way than that of the frame structure under the blast loading (Δ_m) as shown in Figure 8.1c. Thus an ESF factor λ is introduced to decrease P so as to produce the ESF (P_{st}), which creates the same MIDR as Δ_m when statically applied to the original frame structure as illustrated in Figure 8.1d

$$P_{st} = \lambda P \tag{8.6}$$

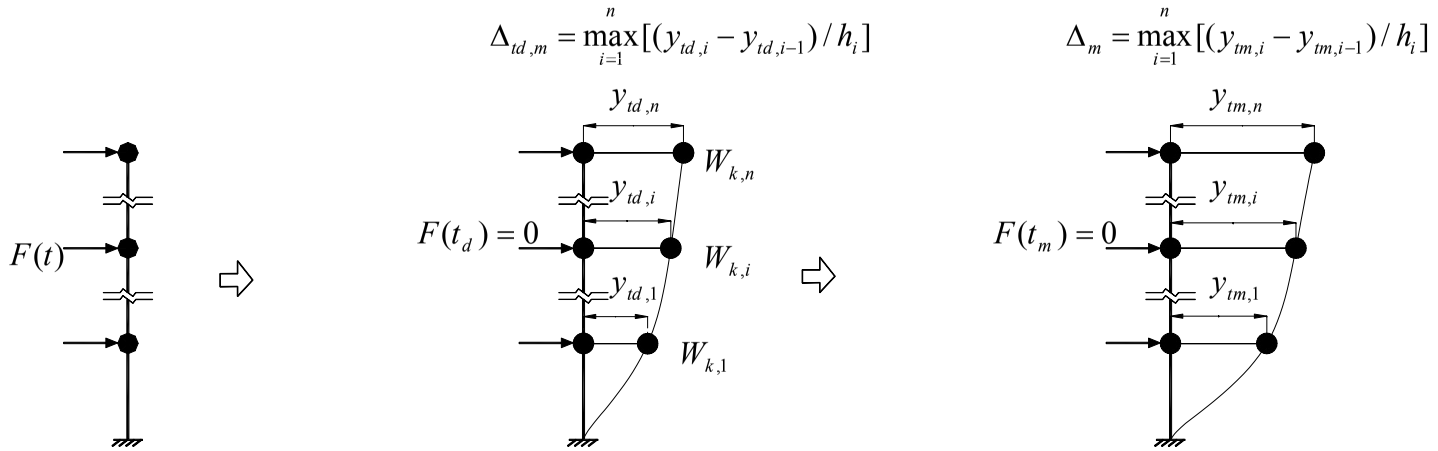

(a). Dynamic response under the blast force

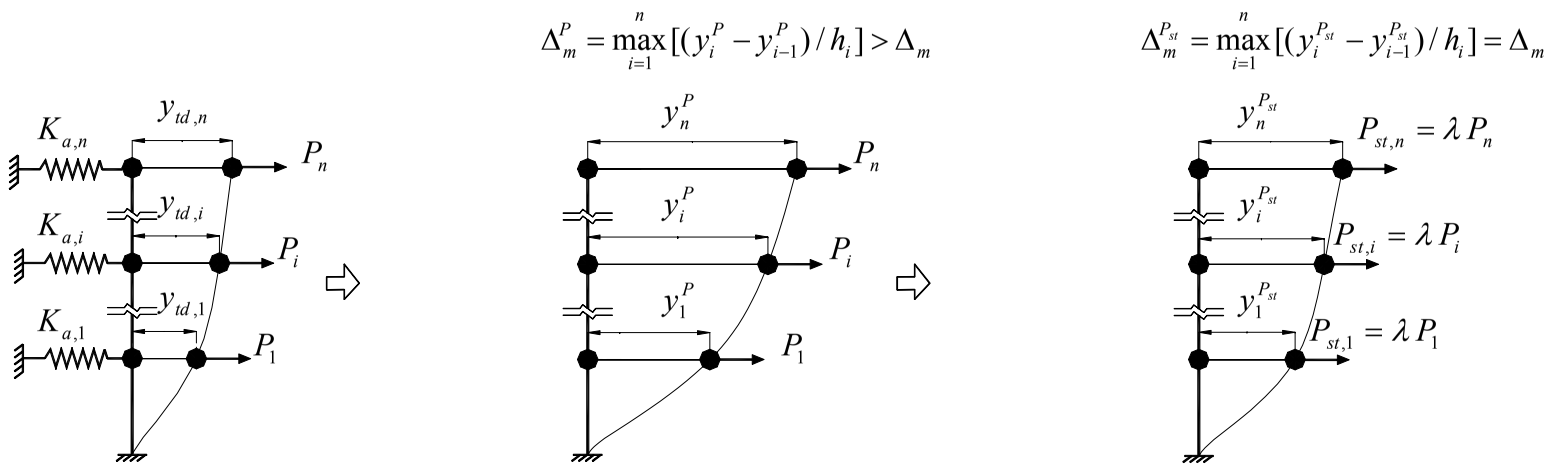

(b). Equivalent static system (c). Static responses under P (d). Static responses under P_{st}

Figure 8.1 Process for the construction of ESF for a multi-storey reinforced concrete frame structure

8.2.2 ESF factor

For a multi-storey reinforced concrete frame structure under the blast condition, it is difficult to derive a closed form expression for λ such as that in Equations (7.22) or (7.23), an empirical formula through numerical studies seems to be a practical solution. If a number of sample points (the accurate values of λ for different frame structures under various blast loadings) are available, the empirical formula can be found with the optimum technique, which makes the closest estimation for these points. Therefore two main works are performed in the determination of the ESF factor formula, which are to get reliable sample points of λ and to establish such a formula.

8.2.2.1 Sample points of the ESF factor

The sample point of λ is obtained by comparing the MIDR response of a multi-storey reinforced concrete frame structure under the blast condition with the corresponding nonlinear pushover analytical result of the structure under an external lateral force with the same distribution as P. The procedures are listed in the following:

1. Establish a frame structure and a lateral blast loading acting on it;
2. Evaluate $y_{td,i}$, $W_{k,i}$ and MIDR within the whole dynamic response Δ_m with numerical simulation;
3. Calculate the recovery force F_a by applying y_{td} to the structure through nonlinear static analysis;
4. Compute the external static force P with Equation (8.4);
5. Carry out the nonlinear pushover analysis of the frame structure under a gradually increasing load vector with the same distribution as P;
6. Plot the resulted curves of load versus the inter-storey responses, and find the value of λ corresponding to Δ_m as shown in Figure 8.2.

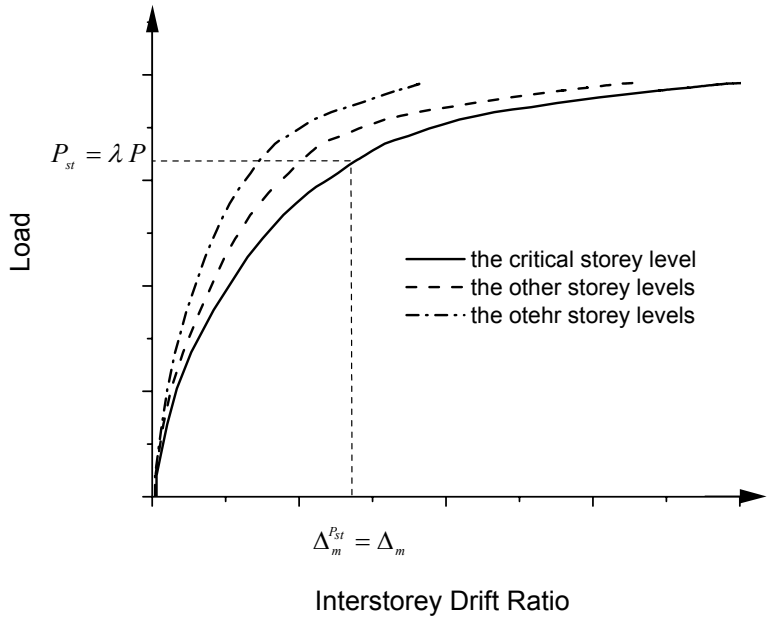

Figure 8.2 Nonlinear pushover analysis under an external lateral force vector with the same distribution as P

Sixty sample points of λ are evaluated by using above procedures, where four different planar frame structures are subjected to a variety of lateral blast forces applied to the exterior columns and the service loads uniformly distributed along the beams (F_{ser}) in a vertical direction. Additional masses along with the beams (M_{add}) are involved that are contributed by the adjacent floors. The details of the frame structures and the analytical results for λ are respectively shown in Tables 8.1 and 8.2, where $\Delta_{td,m}$ (MIDR response at the time t_d) and Δ_m (MIDR response during the whole dynamic responses) for the frame structures are obtained through the nonlinear finite element analyses with the program ABAQUS [A1, A5]. The details about the finite element models for the dynamic analyses and the static pushover analyses of the structures are described in Chapter 2.

Table 8.1 Different frame structures involved in the determination of sample points of λ

Structural Type	Storey level	Height (mm)	Width (mm)	Column section (mm × mm)	Beam section (mm × mm)	Column reinforcement Ratio* (%)	Beam reinforcement ratio** (%)		
							End section	Mid-span section	Interior Support
I-1	1-2 3-6	4500 3300	3×6000	600×600 500×500	300×600	1.5	1.1/0.5	0.5/0.8	1.1/0.5
I-2	1-2 3-6	4500 3300	3×6000	700×700 600×600	300×700	1.1	0.9/0.4	0.3/0.6	0.9/0.4
II	1-4	3600	3×5400	500×500	300×500	2.0	1.5/0.7	0.6/1.2	1.5/0.7
III	1-2 3-9	4500 3300	3×6000	800×800 700×700	300×700	1.0	0.8/0.5	0.3/0.6	0.8/0.5

Material properties: Concrete dynamic compressive strength of 40 MPa;

Longitudinal reinforcement dynamic yield strength of 520 MPa;

*: Total reinforcement ratio in the cross section of the columns where the tension and compression reinforcements are equal;

**: The upper / lower longitudinal reinforcement for the beam cross section;

Table 8.2 Sixty different cases in the determination of sample points of λ

Case	Structural type	P_r * (kPa)	t_d (ms)	F_{ser} (kN/m)	M_{add} (kg/m)	$\Delta_{td,m}$ (%)	Δ_m (%)	λ
1	I-1	434	42.8	60	No	0.488	2.301	0.160
2	I-1	434	42.8	No	No	0.594	2.811	0.129
3	I-1	217	42.8	60	No	0.258	0.878	0.230
4	I-1	217	42.8	No	No	0.252	0.964	0.169
5	I-1	200	30.0	60	No	0.125	0.517	0.226
6	I-1	200	30.0	No	No	0.141	0.564	0.255
7	I-1	300	30.0	60	No	0.191	0.844	0.201
8	I-1	300	30.0	No	No	0.222	0.978	0.232
9	I-1	400	30.0	60	No	0.257	1.216	0.170
10	I-1	400	30.0	No	No	0.311	1.516	0.193
11	I-1	500	30.0	60	No	0.335	1.743	0.160
12	I-1	500	30.0	No	No	0.408	2.101	0.162
13	I-1	100	30.0	60	No	0.061	0.203	0.272
14	I-1	700	30.0	60	No	0.499	2.855	0.124
15	I-1	100	35.0	60	No	0.077	0.303	0.247

Table 8.2. (Continued)

16	I-1	200	50.0	60	No	0.290	1.051	0.301
17	I-2	200	50.0	60	No	0.222	0.661	0.319
18	I-1	200	50.0	60	2700	0.164	0.517	0.400
19	I-1	300	50.0	60	No	0.453	1.970	0.256
20	I-2	300	50.0	60	No	0.338	1.233	0.260
21	I-1	300	50.0	60	2700	0.260	0.861	0.345
22	I-1	400	50.0	60	No	0.655	3.093	0.211
23	I-2	400	50.0	60	No	0.435	1.953	0.215
24	I-1	400	50.0	60	2700	0.366	1.240	0.236
25	I-1	500	50.0	60	No	0.888	4.478	0.169
26	I-2	500	50.0	60	No	0.576	2.845	0.168
27	I-1	500	50.0	60	2700	0.474	1.584	0.271
28	I-1	200	60.0	60	No	0.406	1.361	0.244
29	I-1	200	60.0	60	2700	0.180	0.641	0.199
30	I-1	300	60.0	60	No	0.608	2.532	0.192
31	I-1	300	60.0	60	2700	0.296	1.171	0.199
32	I-1	400	60.0	60	No	0.887	4.068	0.147

Table 8.2. (Continued)

33	I-1	400	60.0	60	2700	0.434	1.784	0.187
34	I-1	150	60.0	60	No	0.302	0.882	0.331
35	I-1	150	60.0	60	2700	0.126	0.451	0.196
36	II	434	42.8	54	2880	0.377	1.484	0.152
37	II	300	42.8	54	2880	0.258	0.944	0.185
38	II	200	42.8	54	2880	0.166	0.582	0.183
39	II	800	42.8	54	2880	0.719	3.156	0.144
40	II	600	42.8	54	2880	0.519	2.255	0.142
41	II	300	60.0	54	2880	0.371	1.329	0.255
42	II	200	60.0	54	2880	0.231	0.780	0.251
43	II	600	60.0	54	2880	0.875	3.307	0.237
44	II	800	60.0	54	2880	1.243	5.167	0.229
45	II	500	50.0	54	2070	0.657	2.349	0.341
46	II	600	50.0	54	2070	0.825	3.100	0.317
47	II	700	50.0	54	2070	1.003	3.992	0.294

Table 8.2. (Continued)

48	II	600	35.0	54	2070	0.467	2.081	0.137
49	II	800	35.0	54	2070	0.636	2.875	0.124
50	II	900	42.8	54	2475	0.656	2.630	0.130
51	III	434	42.8	60	3150	0.156	0.758	0.127
52	III	600	42.8	60	3150	0.229	1.206	0.084
53	III	500	42.8	60	3150	0.183	0.930	0.106
54	III	300	42.8	60	3150	0.105	0.475	0.196
55	III	500	60.0	60	3150	0.296	1.574	0.149
56	III	700	60.0	60	3150	0.486	2.962	0.129
57	III	500	60.0	60	2100	0.346	1.998	0.090
58	III	300	60.0	60	2100	0.168	0.861	0.112
59	III	500	50.0	60	3360	0.345	1.688	0.149
60	III	300	50.0	60	3360	0.187	0.792	0.153

* P_r : Lateral blast peak pressure.

8.2.2.2 Formulae of the ESF factor

It is assumed that the relationship of λ with $\Delta_{td,m}$ and Δ_m follows a similar form as that for a SDOF system in Equation (7.22), thus it can be written as

$$\begin{cases} \lambda = A\,X + B \\ X = \begin{cases} \Delta_{td,m}/\Delta_m & \Delta_m \le a \\ \Delta_{td,m}/(2\Delta_m - a) & \Delta_{td,m} \le a \text{ and } \Delta_m \ge a \\ \Delta_{td,m}/(2\Delta_m - \Delta_{td,m}) & \Delta_{td,m} \ge a \end{cases} \end{cases} \tag{8.7}$$

Two facts exist however in that the value of λ is determined by the relationship of load versus the inter-storey response of the frame structure, which is a continuously curved function, and that the process of releasing the kinetic energy into further deformation after t_d for a frame structure under the blast condition is more complicated than the process of releasing the strain energy of the additional springs in the equivalent static system. As a consequence, it is more appropriate to treat A, B and a in Equation (8.7) as three parameters whose values are determined in such a manner that Equation (8.7) could make the closest predictions for the available sample points of λ. In terms of mathematics, it can be expressed with the following optimum model

$$\begin{cases} \text{find}: & A, B \text{ and } a \\ \text{minimize}: & \Phi = \sum_{j=1}^{m} \left[\lambda_{samp,j} - \lambda_j\right]^2 \\ \text{subject to}: & \lambda_j = A\,X_j - B \end{cases} \tag{8.8}$$

$$X_j = \begin{cases} \Delta^j_{td,m}/\Delta^j_m & \Delta^j_m \le a \\ \Delta^j_{td,m}/(2\Delta^j_m - a) & \Delta^j_{td,m} \le a \text{ and } \Delta^j_m \ge a \\ \Delta^j_{td,m}/(2\Delta^j_m - \Delta^j_{td,m}) & \Delta^j_{td,m} \ge a \end{cases}$$

where $\lambda_{samp,j}$, $\Delta^j_{td,m}$ and Δ^j_m indicate the j th sample point of the ESF factor, the

corresponding MIDR at time t_d and that during the whole response process as listed in Table 8.2; λ_j is the predicted value of the ESF factor according to Equation (8.7).

A lot of algorithms are available currently, which can be applied for solving such an optimum problem. In this study, with the help of the function 'Fminsearch' provided in the software MATLAB [M13], a program is written for solving this particular Equation (8.8). The results are plotted in Figure 8.3, where $A \approx 1.996$, $B \approx -0.074$ and $a \approx 0$, and the line C-D indicates the optimized $\lambda - X$ function. It can be seen in Figure 8.3 that the sample points of λ_{samp} are scattered around this optimized function within a straight strip bounded by an upper-envelop (E-F) and a lower-envelop line (G-H). By submitting the optimum results of the parameters *A, B* and *a* into Equation (8.7), the line C-D can be written as

$$\begin{cases} \lambda = 1.996\,X - 0.074 \\ X = \Delta_{td,m}/(2\Delta_m - \Delta_{td,m}) \end{cases} \tag{8.9}$$

The lines E-F and G-H are expressed respectively with

$$\begin{cases} \lambda_{upp} = 1.996\,X + 0.023 \\ X = \Delta_{td,m}/(2\Delta_m - \Delta_{td,m}) \end{cases} \tag{8.10}$$

and

$$\begin{cases} \lambda_{low} = 1.996\,X - 0.160 \\ X = \Delta_{td,m}/(2\Delta_m - \Delta_{td,m}) \end{cases} \tag{8.11}$$

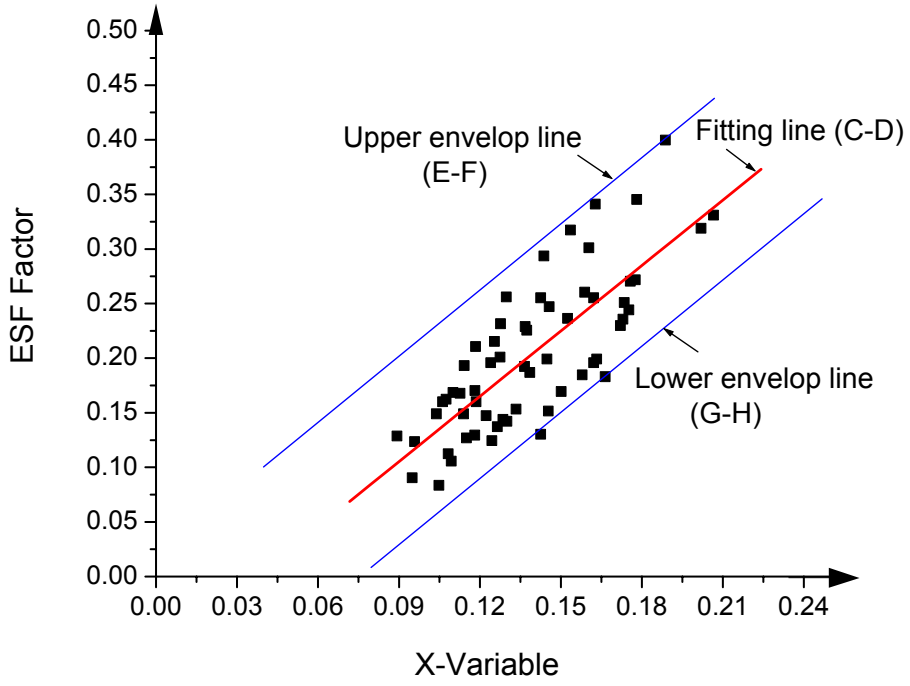

Figure 8.3 Distribution of sample points of the ESF factors and the optimum fitting curve

8.3 Design of a Multi-storey Reinforced Concrete Frame Structure with the ESF

Similar to the trend of ultimate strength with the maximum displacement response for a SDOF system, if the resistance of a frame structure between its inter-storey drift ratio response and an increasing later load vector distributed as P (illustrated in Figure 8.2) can be idealized into an elastic-perfectly-plastic function, the MIDR response of the structure under the blast condition is closely related to the ultimate strength R_m. With a predefined target MIDR Δ_t, the required R_m of the structure should be equal to the predicted ESF according to the previous process by taking its MIDR response Δ_m as Δ_t, which can be applied to determine the reinforcements after giving the dimension of the frame members.

The required R_m (ESF) is predicted from the product of P with the ESF factor λ. Although Equation (8.9) can provide an optimum value for λ, it may in some cases result in an inadequate estimation of R_m. For the purpose of design, considering the safety of the frame structure, the conservative upper-envelop line (E-F) is suggested and therefore by combining Equations (8.4), (8.6) and (8.10), and replacing P_{st} and Δ_m with R_m and Δ_t respectively, it is obtained as

$$\begin{cases} R_m = \lambda_{upp} P \\ P = F_s + F_a \\ \lambda_{upp} = 1.996 X + 0.023 \\ X = \Delta_{td,m} /(2\Delta_t - \Delta_{td,m}) \end{cases} \tag{8.12}$$

With Equation (8.12), the performance-based blast resistant design using the ESF is iteratively accomplished as follows. According to the expected global performance level for the frame structure, a target MIDR Δ_t is defined at the start of the design. Giving the dimensions of different structural members and the initial reinforcement ratios ρ_0, the required R_m is gained from Equation (8.12), which together with service loadings will induce new reinforcement ratios ρ_1. Hence make $\rho_0 = \rho_1$ and repeat the above steps until the convergence in reinforcement ratios is reached.

There exists the possibility that the cross-sectional sizes of structural members are specified to be unreasonably small during the design stage. With the above iterative design procedures the reinforcement ratios could be determined as well, however they might exceed the allowable maximum value. In such cases, modifications to the dimensions of the frame members are needed. The final design flowchart is shown in Figure 8.4.

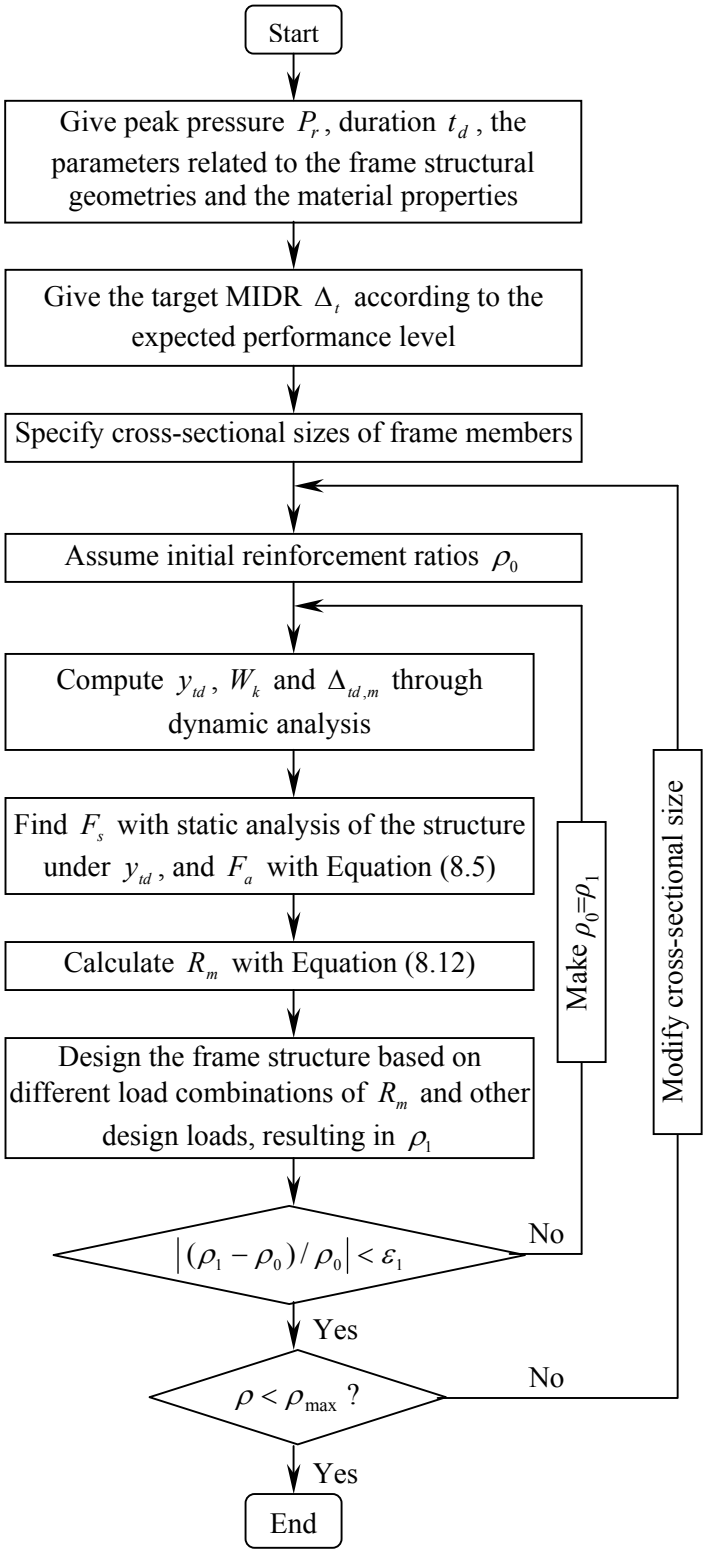

Figure 8.4 Flowchart of blast resistant design of a multi-storey reinforced concrete frame structure with ESF (ε_1 is an arbitrarily small value)

8.4 Illustrative Examples

For the illustration of the developed performance-based blast resistant design procedures with the ESF, two design examples are carried out for planar six-storey reinforced concrete frame structures in resisting blast loadings from distant explosions as shown in Figure 8.5. The basic objective of the design is to ensure that the global damage of the designed structural systems be within the expected performance levels defined by the target MIDR response. Three types of external actions are considered within the design, which include the blast loadings, the dead loads (DL) and live loads (LL). The blast loadings consist of the lateral pressures on the columns and vertical roof pressures. However, as discussed from the comparison study of a planar one-storey frame structure by Baker [B2], the vertical roof pressures have a slight effect on the frame sidesway response, the limitations of which are of main concern in these design examples, therefore they are ignored in these examples. The consideration of the vertical roof loadings can be involved in the blast resistant design of the roof beams with the approach addressed in Chapters 3 to 6. The detailed loading profiles are displayed in Figure 8.5, where DL=30 kN/m, LL=24 kN/m.

In the first design example, a low protection level is required for the frame structure, accordingly a relatively large target MIDR of $\Delta_t = 3.5\%$ is given which is slightly less than the side-sway limit corresponding to the state that the structure may lose its integrity or even collapse as listed in Table 2.1. In the second example, a higher protective level is expected for the frame structure to resist the blast loading and thus a lower target MIDR of $\Delta_t = 1.5\%$ is defined.

At the start of design, the cross-sectional sizes for frame members are specified to be 600 mm × 600 mm for the columns in the first and second storeys, 500 mm × 500 mm for the other columns and 300 mm × 600 mm for all frame beams. Giving the initial values for reinforcement ratios ρ_0, R_m is computed at each iterative step from Equation (8.12). The determination of ρ_1 is accomplished with the integrated

building design software ETABS [E4] according to four user-specified loading combinations (1.4DL+1.6LL+1.0 R_m, 1.4DL+1.6LL-1.0 R_m, 1.4DL+1.6LL, 1.4DL).

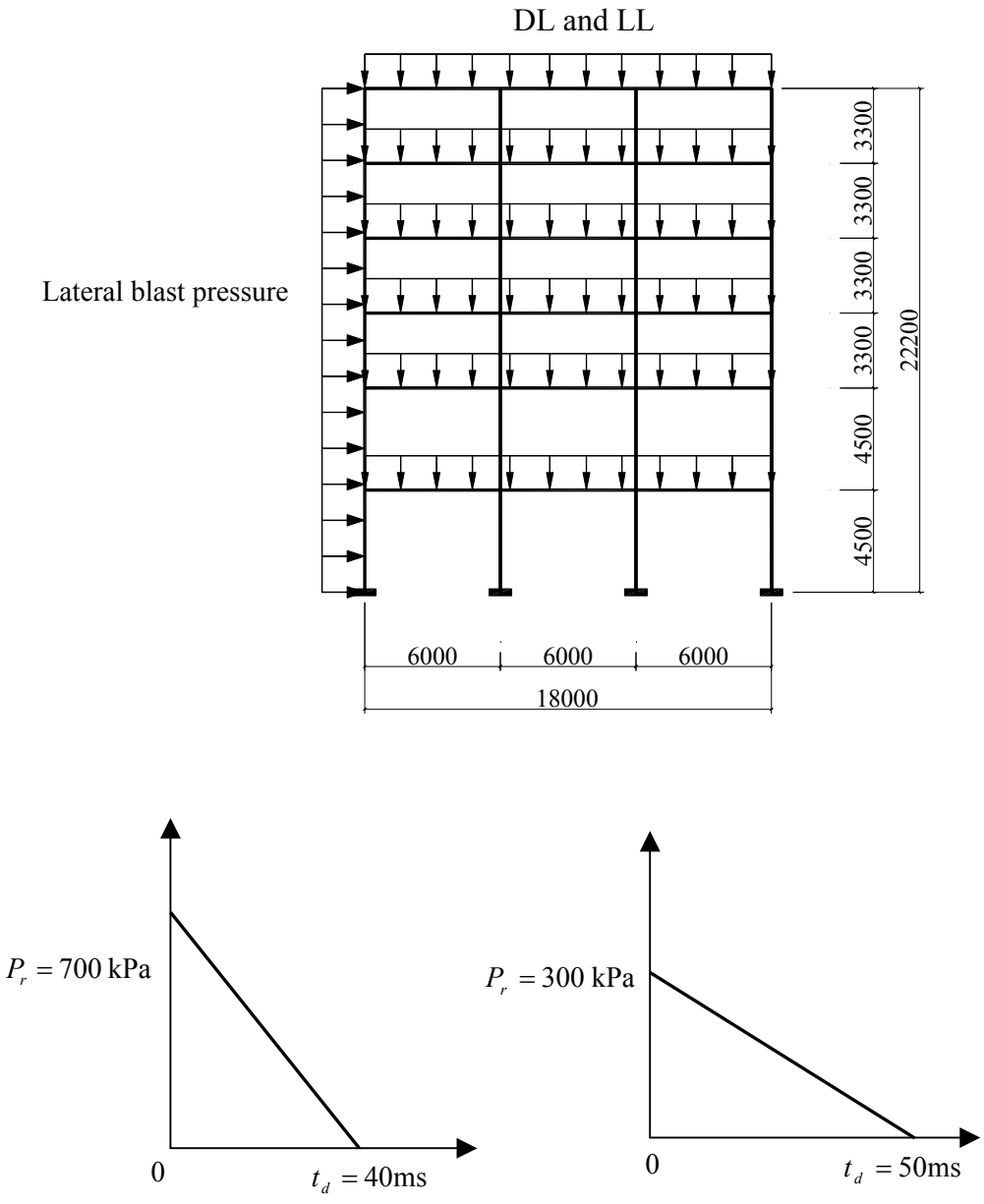

I: lateral blast pressure

II: lateral blast pressure

Figure 8.5 A six-storey reinforced concrete frame structure under blast forces (Examples I and II)

The whole design procedures for these two design examples with the presented method based on ESF are listed in Tables 8.3 and 8.4 where the convergence condition is defined as $\left|(\rho_1 - \rho_0)/\rho_0\right| \le 0.05$. It can be observed that there is no difficulty in reaching the convergence for the design with ESF, as only three iterative steps are needed for both design examples. Although the nonlinear dynamic analysis is needed to find y_{td} and W_k at each step, little computational time is consumed to accomplish this analysis since only slight nonlinear behaviours appear to the frame structure at the time t_d due to the short duration of blast loading. Moreover, the solved reinforcement ratios for the members are all located in their suitable ranges hence there is no need for a change to the initially specified cross-sectional sizes of the frame members.

Table 8.3 Design procedures for example I

The First Iterative Design Step									
i	$y_{td,i}$ (mm)	$W_{k,i}$ (Nm)	$F_{a,i}$ (N)	$F_{s,i}$ (N)	P_i (N)	$\Delta_{td,m}$ (%)	X	λ	$P_{st,i}$ (N)
6	10.80	0.93×10^4	1.72×10^6	-3.91×10^5	1.33×10^6	0.441	0.067	0.157	2.09×10^5
5	19.25	1.73×10^4	1.80×10^6	3.99×10^5	2.20×10^6				3.45×10^5
4	20.40	2.48×10^4	2.43×10^6	0.11×10^5	2.44×10^6				3.84×10^5
3	20.77	2.80×10^4	2.69×10^6	-2.08×10^5	2.49×10^6				3.91×10^5
2	22.85	2.61×10^4	2.28×10^6	0.75×10^5	2.36×10^6				3.70×10^5
1	19.83	1.10×10^4	1.11×10^6	1.19×10^6	2.30×10^6				3.61×10^5

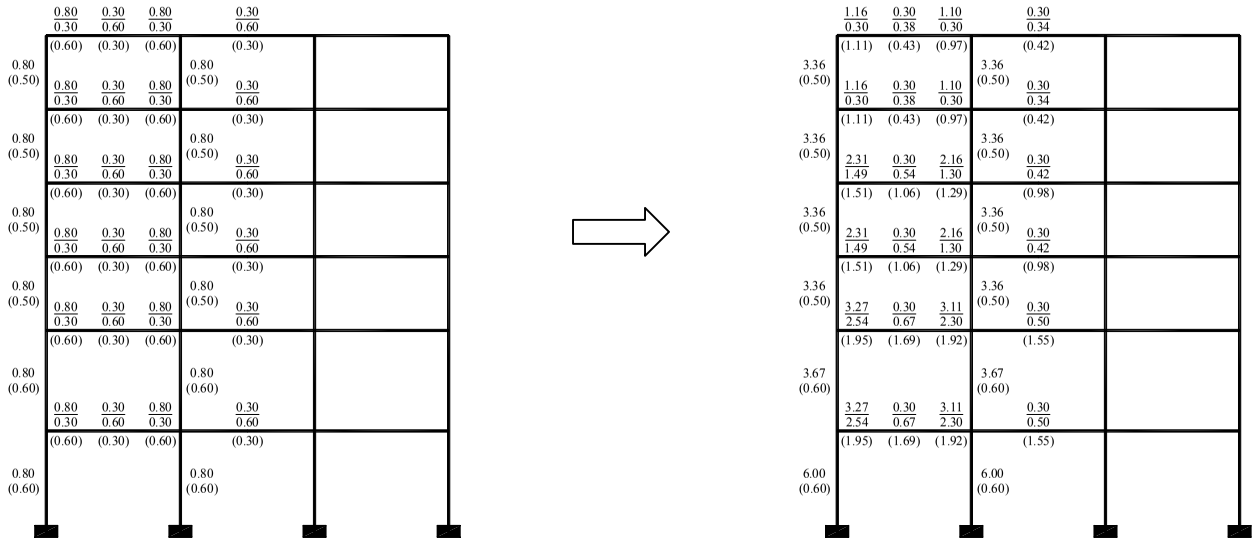

(a). Initial reinforcement ratios (%)

(b). New reinforcement ratios (%)

Note: The item inside the bracket is the total required area of shear reinforcement per unit length (mm).

Table 8.3 (Continued)

The Second Iterative Design Step									
i	$y_{td,i}$ (mm)	$W_{k,i}$ (Nm)	$F_{a,i}$ (N)	$F_{s,i}$ (N)	P_i (N)	$\Delta_{td,m}$ (%)	X	λ	$P_{st,i}$ (N)
6	11.13	0.91×10^4	1.64×10^6	-4.15×10^5	1.22×10^6	0.348	0.052	0.127	1.55×10^5
5	19.73	1.67×10^4	1.70×10^6	3.19×10^5	2.02×10^6				2.57×10^5
4	22.07	2.45×10^4	2.22×10^6	1.50×10^5	2.37×10^6				3.02×10^5
3	22.11	2.38×10^4	2.15×10^6	-4.01×10^5	1.75×10^6				2.23×10^5
2	24.03	3.43×10^4	2.86×10^6	7.07×10^5	3.56×10^6				4.54×10^5
1	15.65	0.36×10^4	0.46×10^6	1.48×10^6	1.94×10^6				2.47×10^5

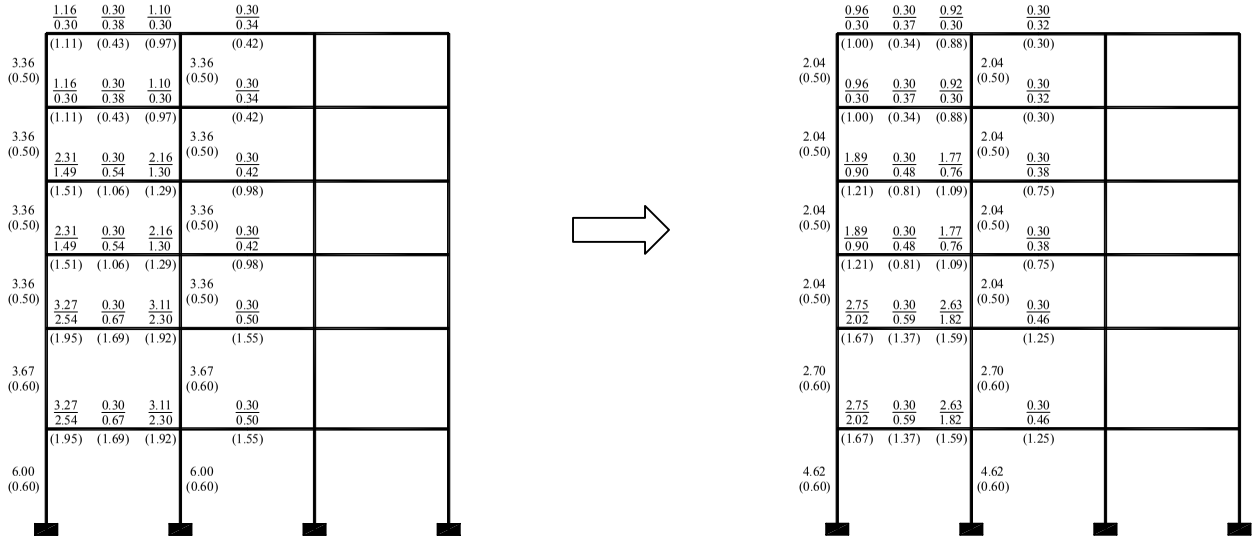

(a). Initial reinforcement ratios (%)

(b). New reinforcement ratios (%)

Table 8.3 (Continued)

The Third Iterative Design Step									
i	$y_{td,i}$ (mm)	$W_{k,i}$ (Nm)	$F_{a,i}$ (N)	$F_{s,i}$ (N)	P_i (N)	$\Delta_{td,m}$ (%)	X	λ	$P_{st,i}$ (N)
6	10.84	0.78×10^4	1.44×10^6	-4.05×10^5	1.03×10^6	0.364	0.055	0.132	1.37×10^5
5	19.65	1.84×10^4	1.87×10^6	3.35×10^5	2.21×10^6				2.92×10^5
4	21.77	2.19×10^4	2.01×10^6	1.42×10^5	2.15×10^6				2.85×10^5
3	21.58	2.43×10^4	2.25×10^6	-3.71×10^5	1.88×10^6				2.49×10^5
2	23.52	3.33×10^4	2.83×10^6	5.18×10^5	3.35×10^6				4.43×10^5
1	16.36	0.32×10^4	0.39×10^6	1.50×10^6	1.89×10^6				2.50×10^5

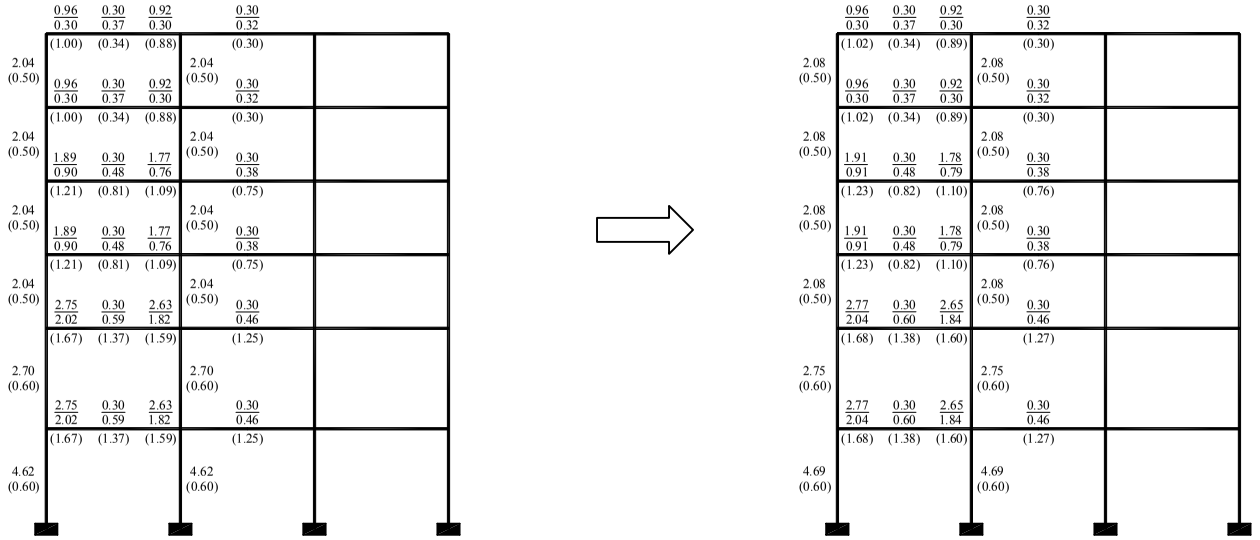

(a). Initial reinforcement ratios (%) (b). New reinforcement ratios (%) (final design)

Table 8.4 Design procedures for example II

The First Iterative Design Step									
i	$y_{td,i}$ (mm)	$W_{k,i}$ (Nm)	$F_{a,i}$ (N)	$F_{s,i}$ (N)	P_i (N)	$\Delta_{td,m}$ (%)	X	λ	$P_{st,i}$ (N)
6	9.07	2.94×10^3	6.49×10^5	-2.02×10^5	4.47×10^5	0.242	0.088	0.198	8.88×10^4
5	12.62	2.84×10^3	4.49×10^5	1.05×10^5	5.55×10^5				1.10×10^5
4	14.71	4.52×10^3	6.15×10^5	1.29×10^5	7.44×10^5				1.47×10^5
3	15.02	7.18×10^3	9.56×10^5	-2.64×10^5	6.92×10^5				1.37×10^5
2	17.01	5.80×10^3	6.82×10^5	3.68×10^5	1.05×10^6				2.08×10^5
1	10.90	0.32×10^3	5.96×10^4	6.31×10^5	6.91×10^5				1.37×10^5

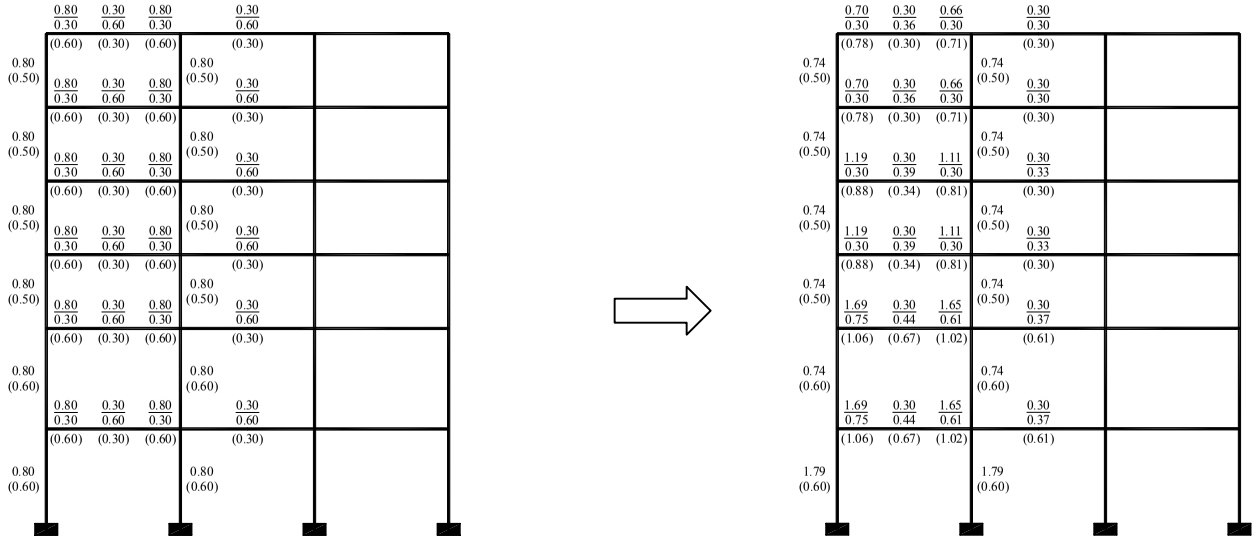

(a). Initial reinforcement ratios (%)

(b). New reinforcement ratios (%)

Note: The item inside the bracket is the total required area of shear reinforcement per unit length (mm).

Table 8.4 (Continued)

The Second Iterative Design Step									
i	$y_{td,i}$ (mm)	$W_{k,i}$ (Nm)	$F_{a,i}$ (N)	$F_{s,i}$ (N)	P_i (N)	$\Delta_{td,m}$ (%)	X	λ	$P_{st,i}$ (N)
6	8.94	2.45×10^3	5.48×10^5	-1.97×10^5	3.51×10^5	0.233	0.084	0.191	6.71×10^4
5	12.65	2.37×10^3	3.74×10^5	1.11×10^5	4.85×10^5				9.28×10^4
4	14.78	4.73×10^3	6.40×10^5	1.06×10^5	7.46×10^5				1.43×10^5
3	15.22	7.43×10^3	9.76×10^5	-2.52×10^5	7.24×10^5				1.38×10^5
2	17.10	5.09×10^3	5.96×10^5	4.56×10^5	1.05×10^6				2.01×10^5
1	10.50	0.14×10^3	2.60×10^4	6.48×10^5	6.74×10^5				1.29×10^5

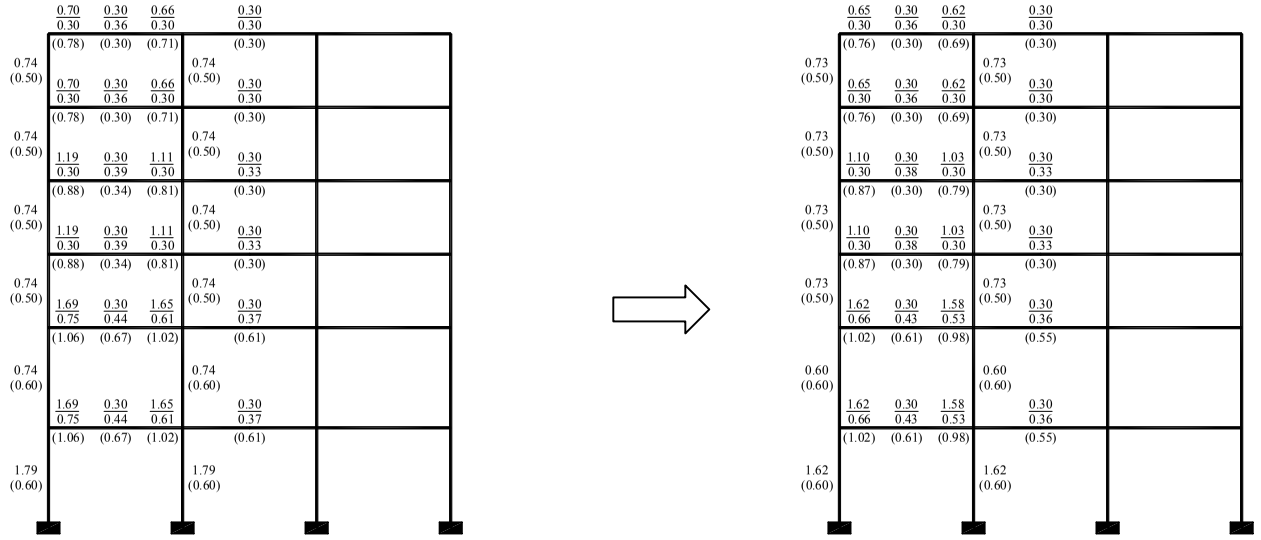

(a). Initial reinforcement ratios (%)

(b). New reinforcement ratios (%)

Table 8.4 (Continued)

The Third Iterative Design Step									
i	$y_{td,i}$ (mm)	$W_{k,i}$ (Nm)	$F_{a,i}$ (N)	$F_{s,i}$ (N)	P_i (N)	$\Delta_{td,m}$ (%)	X	λ	$P_{st,i}$ (N)
6	8.91	2.43×10^3	5.46×10^5	-1.95×10^5	3.51×10^5	0.235	0.085	0.193	6.79×10^4
5	12.64	2.27×10^3	3.60×10^5	1.12×10^5	4.71×10^5				9.10×10^4
4	14.77	4.71×10^3	6.38×10^5	1.07×10^5	7.45×10^5				1.44×10^5
3	15.16	7.35×10^3	9.70×10^5	-2.57×10^5	7.13×10^5				1.38×10^5
2	17.11	5.56×10^3	6.50×10^5	4.44×10^5	1.09×10^6				2.11×10^5
1	10.60	0.18×10^3	3.54×10^4	6.49×10^5	6.84×10^5				1.32×10^5

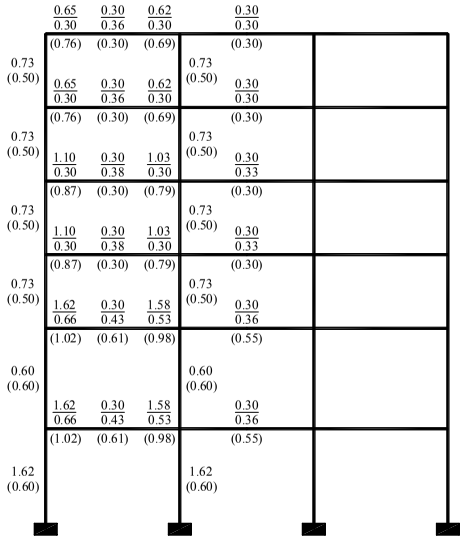

(a). Initial reinforcement ratios (%)

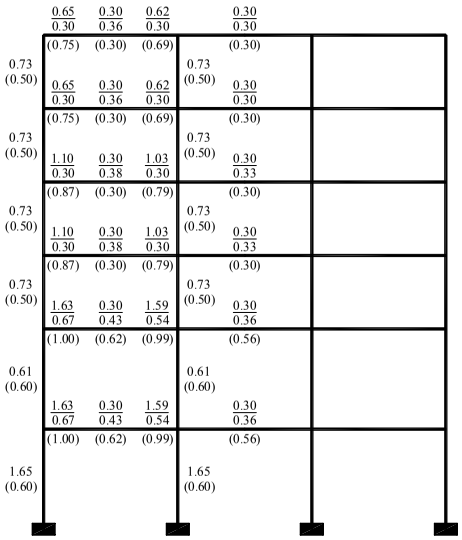

(b). New reinforcement ratios (%) (final design)

8.5 Numerical Verification of the Design Method

To check whether the MIDR responses are controlled effectively with the above design method, nonlinear finite element analyses are performed on the designed frame structures against the given blast forces. Two steps of analysis are involved in which the nonlinear static analysis under the DLs and LLs is carried out followed by the nonlinear dynamic analysis of the designed structures under the blast force. The simulation results are demonstrated in Figures 8.6 and 8.7, which show a conservative MIDR response at 1.31% and 0.72% respectively for these two frames as compared to their target values.

The reasons for the conservative design with ESF can be explained from two aspects. First, the prediction of the ESF factor λ based on its upper-envelop line induces an overestimation of R_m from Equation (8.12). The second relies on the assumption that the resistance of the designed structure be an elastic-perfectly-plastic function and therefore the calculated ESF will be equal to the required R_m. The strengthening of the structure after reaching this R_m is not considered in the design procedure. From the viewpoint of structural safety, such a conservative design result can be acceptable.

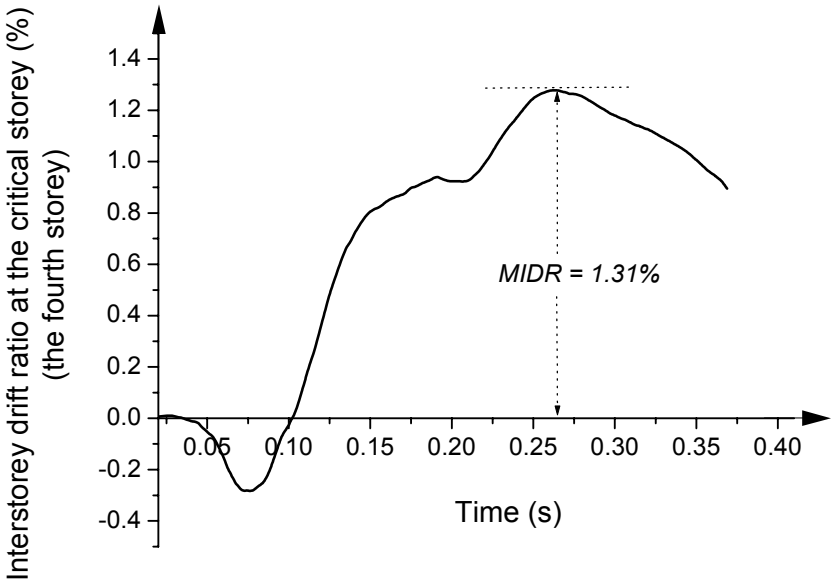

Figure 8.6 Responses of the designed frame structure under the given blast force (Example I)

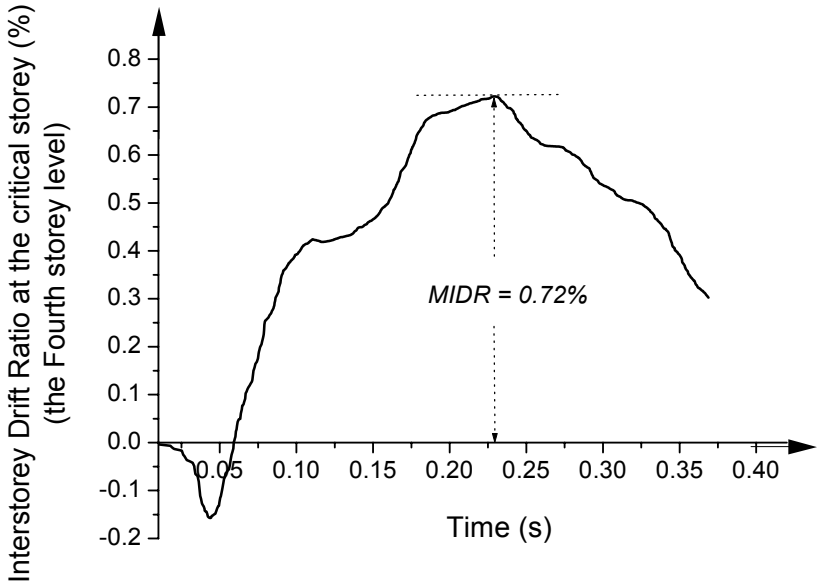

Figure 8.7 Responses of the designed frame structure under the given blast force (Example II)

8.6 Summaries

A new performance-based blast resistant design method has been developed in this study for a multi-storey reinforced concrete frame structure with the ESF in keeping the MIDR response under proper control to meet the expected global performance level under the distant explosion conditions.

An equivalent static system is constructed for the purpose of simulating the kinetic energy at t_d by the strain energy of the additional springs. According to the equilibrium of the equivalent static system, the external static force is obtained, however this force will produce a larger MIDR demand than that of the frame structure under the blast condition and thus the ESF factor λ is introduced to reduce the external static force to finally obtain the ESF.

By comparing the nonlinear dynamic responses of frame structures with corresponding nonlinear static pushover analytical results, a number of sample points of λ are obtained, from which a function of λ is determined with the optimum technique for the closest estimation for these points. It shows that the sample points of λ are scattered around this optimized function within a straight strip that is bounded by an upper-envelop and a lower-envelop line. The upper-envelop line is utilized into the design for structural safety.

By substituting the ESF with the ultimate strength and the MIDR responses with the required design target, the calculation model of the ESF is implemented into the design of a multi-storey reinforced concrete frame structure. For given cross-sectional sizes of the frame members, the reinforcement ratios are iteratively solved. Two numerical examples show that there is no difficulty in getting computational convergence for the design method based on ESF. However since the ESF factor is based on the upper-envelop line and the strengthening of the structure after reaching the ESF, some safety margin is provided as part of the design to control the MIDR responses of the frame structure as indicated from the numerical verifications.

CHAPTER NINE

CONCLUSIONS AND RECOMMENDATIONS

9.1 Conclusions

The conclusions drawn as a result of the theoretical work carried out in this thesis have been generally been given at the end of each chapter. A summary of those conclusions is as follows:

1. The whole dynamic response process of frame structures with/without exterior cladding panels under distant blast conditions can be approximately divided into two stages. Localized responses of the blast-loaded members are critical at response stage I while the global responses of the structural system dominate at response stage II.

2. According to the differences of the damage distributions in the two response stages, the blast resistant design for a multi-storey reinforced concrete frame structure under distant blast conditions should include two parts: the design of critical blast-loaded members capable of controlling the degree of the local damage at response stage I and the design of frame structural systems in limiting the excessive global damage at response stage II. To meet such requirements, the performance-based blast resistant design should be performed not only for the structural members but also for the frame structural systems.

3. The developed performance-based blast resistant design approach for structural members using energy spectra is accomplished in such a manner that both the displacement and the displacement ductility response

parameters are taken as the performance indicators. For the expected performance level defined by a combination of target displacement and target displacement ductility factor, the effective depth and longitudinal reinforcement ratio of structural members could be exactly solved so that the maximum displacement and displacement ductility responses of the equivalent SDOF system of the designed member can be precisely controlled to be equal to their targets.

4. Some errors do exist between the actual maximum displacement and displacement ductility responses for the designed member under the given blast loading and the respective design targets, as indicated from numerical verification analysis of the design approach using energy spectra. This error is induced by some simplifications, which are adopted in converting the continuous reinforced concrete members into the equivalent SDOF systems and computing the cross-sectional moment of inertia and ultimate strength of the members.

5. Formulae for the two error indices, which quantify the errors between the actual responses of designed member under the given blast loading and the design targets, are derived through extensive numerical studies and statistical analyses. Two items are included in the formulae: a nonlinear fitting function that is correlated with the longitudinal reinforcement ratio and the support conditions, plus a nominal random variable to consider the uncertain influence of the other parameters.

6. Modification of the performance-based blast resistant design approach using energy spectra is accomplished depending on the formulae of the two error indices, where the actual maximum displacement and displacement ductility responses of designed member rather than those of the equivalent SDOF system are controlled. Although more iterative steps are needed to reach convergence as compared to those of the original design procedure, a better agreement is achieved between the actual responses of the member designed

with the modified approach and their targets.

7. The formulae for the two error indices provide a simple way to predict the maximum displacement and displacement ductility responses of the members from those of the corresponding equivalent SDOF systems without performing the numerical finite element analysis. Consequently, by using the Monte-Carlo simulation and introducing two independent nominal random variables in the error indices, the assessment of the distributions of these two responses under blast conditions accounting for different types of uncertainties becomes more efficient.

8. Taking the MIDR response parameter as the global performance indicator, a performance-based blast resistant design approach is presented for the multi-storey reinforced concrete frame structural system by using the equivalent static force (ESF). This approach is firstly addressed for the design of a SDOF system controlling its maximum displacement response and then extended into the design of a frame structure controlling its MIDR response. An equivalent static system is built up to simulate the energy components of the SDOF/frame structural system at the time t_d (blast loading duration). Based on the equilibrium of the equivalent static system, an external static force P is computed, however this force tends to produce a larger maximum displacement/MIDR response when statically applied to the SDOF/frame structural system than that under the blast actions. Therefore, an ESF factor is introduced to reduce P to finally obtain the ESF.

9. The closed form expression of the ESF factor for an elastic-perfectly-plastic SDOF system is evaluated. However for multi-storey reinforced concrete frame structures, an empirical formula of the ESF factor is numerically derived from a number of sample points of the ESF factor obtained by comparing the nonlinear dynamic responses of frame structures with corresponding nonlinear static pushover analytical results. It is shown that these sample points are scattered within a straight strip bounded by upper

and lower envelop lines. For structural safety reasons, the upper line is suggested for the calculation of the ESF and applied into the design.

10. By replacing the ESF with the ultimate strength and the maximum displacement/MIDR response with the required design target, the calculation model of the ESF is implemented into the design of an elastic-perfectly-plastic SDOF system/multi-storey reinforced concrete frame structural system. The ultimate strength for the SDOF system/the reinforcement ratios of the frame members for the given cross-sectional sizes can be iteratively solved during the design in order to satisfy the target displacement/MIDR.

11. The presented performance-based design procedures using ESF have been illustrated via several design examples for the SDOF systems and multi-storey frame structures, which display that there is no difficulty in convergence of the iterative procedures. The maximum displacement responses of the designed SDOF systems under the given blast forces are controlled to be exactly equal to the design targets. However the MIDR responses of the frame structural systems are limited on the conservative sides as compared to their targets. That is because the ESF factor is predicted from the upper-envelop line and the strengthening of the structure after reaching the ESF that is assumed to be the ultimate strength is not considered within the design.

Based on the study in the thesis, the methodology of the performance-based design for a multi-storey reinforced concrete frame structure against the distant blast loadings is summarized in Figure 9.1. After defining the expected performance level according to the requirements and objectives of the owners, users, and society for the frame structure under the given distant explosion conditions, the design is carried out for the reinforced concrete structural members using energy spectra as well as for frame structural system with ESF. The more critical design results are selected as the final design

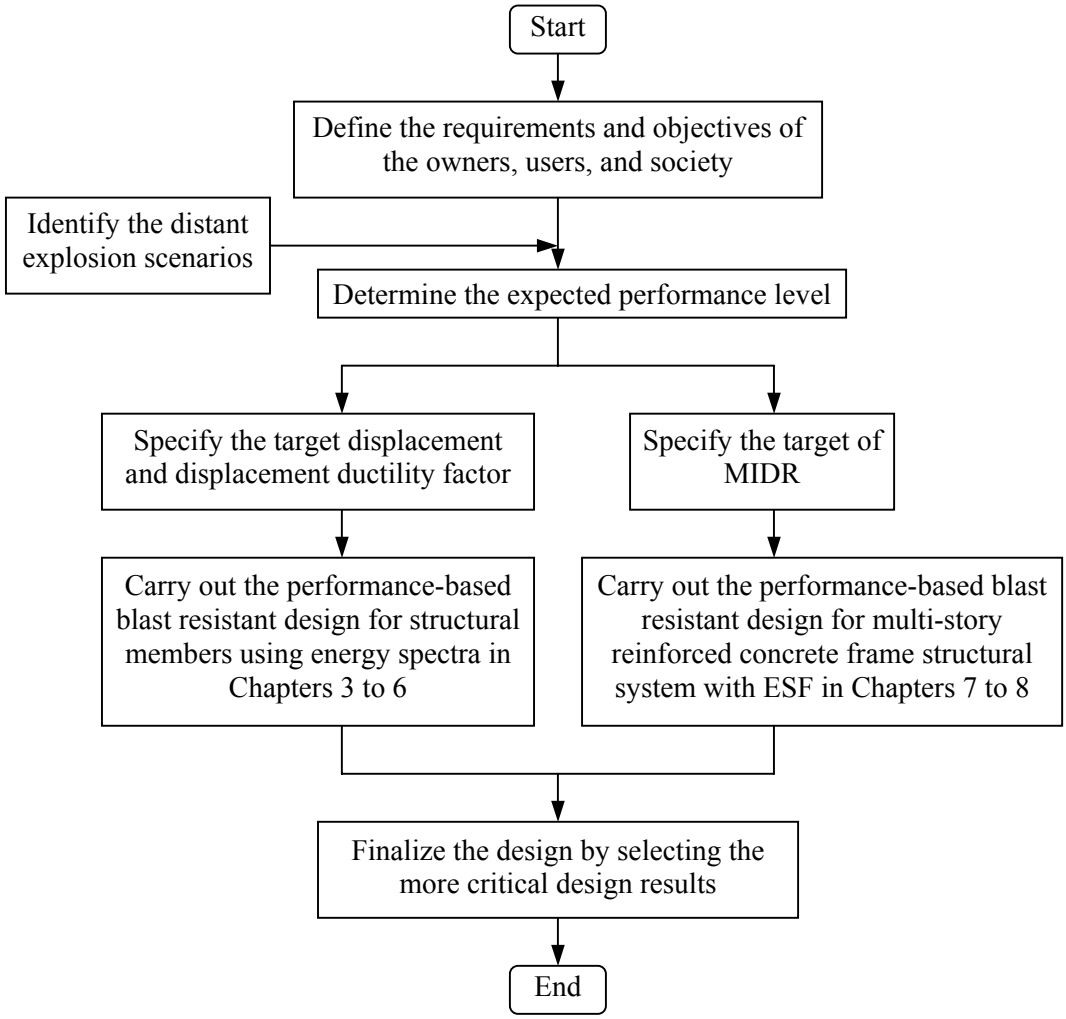

Figure 9.1 Performance-based blast resistant design methodology of multi-storey reinforced concrete frame structures against distant explosions

9.2 Recommendations for Future Works

Several issues related to this study deserve further investigation. These include:

1. The effects of the interior infill walls on the dynamic responses and damage distributions for the frame structure in resisting the blast loadings from distant intense surface explosions should be investigated.

2. The explosion tests should be conducted for a frame structure with different

types of exterior cladding panels in order to verify the numerical analytical results of the damage distributions.

3. Performance-based blast resistant design using energy spectra has been proposed for the reinforced concrete members without the effects of the initial conditions such as the axial force; future studies are necessary for the blast resistant design of the members taking into consideration of these initial conditions.

4. The performance-based design procedures using energy spectra can be also utilized for the design of reinforced concrete members under other types of dynamic loadings such as the rectangular load pulses, the constant force with finite rise time, and the equilateral triangular load pulses with zero rise time, etc. Their accomplishment depends on the corresponding energy spectra through controlling the responses of equivalent SDOF system of reinforced concrete member to reach the design targets. The accuracy of the design in controlling the responses of the designed member under such loading conditions can be also assessed through numerical analysis.

5. The experimental verifications of the blast resistant design method with the ESF for the multi-storey reinforced concrete frame structures in controlling its MIDR responses should be conducted.

REFERENCES

[A1] ABAQUS (2004), *ABAQUS/Standard User's Manual*, Version 6.4, HKS, Inc.

[A2] ASCE Manual 42 (1985), *Design of Structures to Resist Nuclear Weapons Effects*, American Society of Civil Engineers.

[A3] Allgood J.R. and Swihart G. R. (1970), *Design of Flexural Members for Static and Blast Loadings*, ACI Monograph Series, No. 5.

[A4] ASCE 7-98 (1998), *Minimum Design Loads for Buildings and other Structures*, American Society of Civil Engineers Publication.

[A5] ABAQUS (2004), *ABAQUS Theory Manual, Version 6.4*, HKS, Inc.

[B1] Biggs J. M. (1964), *Introduction to Structural Dynamic*, McGraw-Hill, New York.

[B2] Baker W. E., Cox. P. A., Westine P. S., Kulesz J. J. and Strehlow R. A. (1983), *An Explosion Hazard and Evaluation: Fundamental Studies in Engineering*, Elsevier Scientific Publishing Company, NY.

[B3] BS 8110 (1997), *Structural Use of Concrete. Part 1*, Code of Practice for Design and Construction, British Standard.

[B4] Bounds, W. L., et al. (1997), *Design of Blast Resistant Building in Petrochemical Facilities*, ASCE Task Committee Report on Blast Resistant Design.

[B5] Brode H. L. (1955), "Numerical Solution of Spherical Blast Waves", *Journal of Applied Physics*, No. 6

[B6] Beshara, B. A. (1991), "Nonlinear Finite Element Analysis of RC Structures Subjected to Blast Loading", *Ph. D. thesis*, City University, London.

[B7] Bangash M.Y.H. (1997), *Impact and Explosion: Analysis and Design*, Blackwell Scientific Publication, Oxford.

[B8] Breen J. E. and Siess C. P. (1979), "Progressive Collapse-symposium Summary", *ACI Journal*, Vol. 76 (9), 997-1005.

[B9] Baker, W. E. (1973), *Explosions in Air*, Univ. of Texas Press, Austin, Texas.

[B10] Bingham B. L., Collins J. A., and Keller, J. A., et al. (1993), "Sophisticated Material Modeling and Finite Element Method for Explosive Breaching Analysis, Advances in Numerical Simulation Techniques for Penetration and Perforation", *Journal of Applied Mechanics*, American Society of Mechanical Engineers, 167-179

[B11] Beshara F. B. A. (1994), "Modeling of Blast Loading on Aboveground Structures—I. General Phenomenology and External Blast", *Computers & Structures*, Vol. 51 (5), 585-596

[B12] Beterno V. V. (1997), "Performance-based Seismic Engineering: a Critical Review of Proposed Guideline", *Proceedings of the International Workshop on Seismic Design Methodology for the Next Generation of Codes*, Bled/Slovenia, 1-31.

[B13] Bratley P., Fox B. L., and Schrage E. L. (1987), *A Guide to Simulation, the 2nd version*, Springer-Verlag, New York.

[C1] Corley W. G., Mlakar P.F., Sozen M.A. and Thornton C.H. (1998), "The Oklahoma City Bombing: Summary and Recommendation for Multi-hazard Mitigation", *Journal of Performance of Constructed Facilities*, ASCE, Vol. 12 (3), 100-112.

[C2] Chowdhury, M. R. (1987), "Responses of Beam Structures due to Blast Loadings", *PH. D thesis*, University of Cincinnati.

[C3] CEB-FIP Model Code 1990, *Design Code*. (1993), Thomas Telford, Lausanne, Switzerland.

[C4] Clough R. W. Penzien J. (1993), *Dynamic of Structures*, Second Edition, McGraw-Hill, Inc.

[C5] Corley W. G. (2004), "Lessons Learned on Improving Resistance of Buildings to Terrorist Attacks", *Journal of Performance of Constructed Facilities*, ASCE, Vol. 18 (2), 68-78

[C6] Crawford, R. E., Higgins, C.J., and Bultman, E.H. (1974), *The Air Force Manual for Design and Analysis of Hardened Structures*, AFWL-TR-74-102, Air Force Weapons Laboratory, Albuquerque, N.M.

[C7] Crawford, J. E. and Malvar L.J. (1997), *User's and Theoretical Manual for K&C Concrete Model*, Rep. TR-97-53.1, Karagozian & Case Structural Engineers, Burbank, California.

[C8] Crouch R. S., Chrisp T. M. (1989) "The Response of Reinforced Concrete Slabs to Non-nuclear Blast Loading", *Proceedings of the First International Conference on Structures under Shock and Impact*,

Massachusetts, USA, 69–76.

[C9] Committee for the Compilation of Materials on Damage Caused by the Atomic Bombs in Hiroshima and Nagasaki, (1981), *Hiroshima and Nagasaki*, Basic Book Publication, New York, NY.

[C10] Choi W.S. and Park G. J. (1999), "Transformation of Dynamic Loads into Equivalent Static Loads based on Modal Analysis", *International Journal for Numerical Methods in Engineering*, Vol. 46, 29-43.

[C11] Chen Xinzhong and Kareem Ahsan, (2004), "Equivalent Static Wind Loads on Buildings: New Model", *Journal of Structural Engineering*, ASCE, Vol. 130 (10), 1425-1435.

[D1] Davenport, A. G. (1985). "The Representation of the Dynamic Effects of Turbulent Wind by Equivalent Static Wind Loads." *Journal of Structural Engineering*, ASCE, Vol. 126 (8), 936–943.

[D2] Douglas Sunshine, Ali Amini, and Mark Swanson, (2004), "Overview of Simplified Methods and Research for Blast Analysis", *Structural Congress: Building on the Past: Securing the Future*, ASCE Conf. Proc. 137-155.

[D3] Department of Defense (DoD) (2002), *Unified Facilities Criteria (UFC), DoD Minimum Antiterrorism Standards for Buildings*, UFC 4-010-01, U.S. Army Corps of Engineering, Washington, D.C.

[D4] Dharan, C.K.H, and Hauser, F.E. (1970), "Determination of Stress-strain Characteristics at Very High Strain Rates", *Experimental Mechanics*, Vol.10, 370-376.

[D5] Donze, F.V., Magnier, S.A., Daudeville, L., Mariotti, C. and Davenne, L. (1999), "Numerical Study of Compressive Behaviour of Concrete at High Strain Rates", *Journal of Engineering Mechanics*, ASCE, Vol. 125, 1154-1163.

[E1] Ellingwood B. and Leyendecker E.V. (1978), "Approaches for Design Against Progressive Collapse", *Journal of Structural Engineering*, ASCE Vol. 104, No.ST3, 413-423.

[E2] Ettouney M., Smilowitz R. and Rittenhours T. (1996), "Blast Resistant Design of Commercial Building", *Practice Periodical on Structural Design and Construction*, ASCE, Vol. 1 (1), 31-39.

[E3] Eamon C. D., Baylot J. T. and O'Daniel L. (2004), "Modelling Concrete Masonry Walls Subjected to Explosive Loads", *Journal of Engineering Mechanics*, ASCE, Vol. 130 (9), 098-1106

[E4] ETABS. (2002), "Integrated Building Design Software: Concrete Frame Design Manual", *Computers and Structures*, Inc. Berkeley, California, USA.

[F1] Forbes D. F. (1999), "Blast Loading on Petrochemical Buildings", *Journal of Energy Engineering,* ASCE, Vol. 125 (3), 94-102.

[F2] FEMA-283 (1996), *Performance Based Seismic Design of Building: an Action Plan for Future Studies*, Federal Emergence Management Agency, Washington D.C.

[F3] FEMA-273, (1997), *NEHRP Guidelines for the Seismic Rehabilitation of Buildings*, Federal Emergency Management Agency, Washington, D.C.

[F4] FEMA-274, (1997), *NEHRP Commentary on the Guidelines for the Seismic Rehabilitation of Buildings*, Federal Emergency Management Agency, Washington, D.C.

[F5] Fu, H.C., Erki, M.A. and Seckin, M. (1991a), "Review of Effects of Loading Rate on Concrete in Compression", *Journal of Structural Engineering*, ASCE, Vol. 117 (12), 3645-3659.

[F6] Fu, H.C., Erki, M.A. and Seckin, M. (1991b), "Review of Effects of Loading Rate on Reinforced Concrete", *Journal of Structural Engineering*, ASCE, Vol. 117 (12), 3660-3679.

[G1] Ginsburg S. and Kirsch U. (1983), "Design of Protective Structures against Blast", *Journal of Structural Engineering*, ASCE, Vol. 109 (6), 1490-1505.

[G2] Glasstone, S., and Dolan, P.J. (1977), *The effects of Nuclear Weapons*, U.S. Dept. of Defense and U. S. Dept. of Energy, Third edition, Washington, D.C.

[G3] General Services Administration (GSA), (2000), *Progressive collapse Analysis and Design Guidelines for New Federal Office Buildings and Major Modernization Projects*, Office of Chief Architect, Washington, D.C.

[G4] Georgin, J.F., Reynouard, J.M. and Merabet, O. (1998), "Modelling of Concrete at High Strain Rate", *Computational Modelling of Concrete Structures*, Vol. 2, 593-601.

[G5] Goldsmith, W., Polivka, M. and Yang, T. (1966), "Dynamic Behaviour of Concrete", *Experimental Mechanics*, Vol. 6, 65-79.

[G6] Gorham, D.A. (1980), "Measurement of Stress-strain Properties of Strong Metals at Very High Strain Rates", *Institute of Physics Conference Series No: 47*, 16-24.

[G7] Grote, D.L., Park, S.W. and Zhou, M. (2001), "Dynamic Behavior of Concrete at High Strain-rates and Pressures: I. Experimental Characterization", *International Journal of Impact Engineering*, Vol. 25, 869-886.

[G8] Ghobarah Ahmed (2001), " Performance-based Design in Earthquake Engineering: State of Development", *Engineering Structures*, Vol.23, 878-884.

[H1] Hyde D. W. (1991), *ConWep: Weapons Effects Calculation Program Based on Technique Manual, TM5-855-1*, United States Army Engineer Waterways Experiment Station.

[H2] Hinman E.E. and Hammond D.J. (1997), *Lessons from the Oklahoma City Bombing: Defensive Design Techniques*, Published by ASCE press. New York.

[H3] Haluk S., Ergin C. and Sinan A. (1994), "Resistance Mechanisms in RC Building Frames Subjected to Column Failure", *Journal of Structural Engineerin*g, ASCE, Vol. 120 (3), 765-783.

[H4] Hsin Yu Low and Hong Hao (2002) "Reliability Analysis of Direct Shear and Flexural Failure Modes of RC Slabs under Explosive Loading", *Engineering Structures*, Vol. 24 (2), 189-198.

[H5] Henrych J., (1979), *The Dynamics of Explosion and Its Use*, Elsevier, Amsterdam.

[H6] Hilleborg, A., M. Modeer, and P. E. Petersson (1976) "Analysis of Crack Formation and Crack Growth in Concrete by Means of Fracture Mechanics and Finite Elements," *Cement and Concrete Research*, Vol. 6, 773–782.

[H7] Hamburger R. O., Foutch D. A, Cornel C. A., (2000), " Performance Basis for Guidelines For Evaluation, Upgrade and Design of Moment-Resisting Steel Frames", *Proceedings of 12th World Conference on Earthquake Engineering*, Paper No. 2543.

[H8] Hammersley J. M., and Handscomb D. C. (1964), *Monte Carlo Methods*, Methuen, London.

[I1] ISC, (2001), *ISC Security Design Criteria for New Federal Office Building and Major Modernization Projects*, The Interagency Security Committee. GSA.

[J1] James G. MacGregor and F. Michael Bartlett, (2000), *Reinforced Concrete: Mechanics and Design*, Prentice Hall Canada Inc., Scarborough, Ontario.

[K1] Kletz T. A. (1975), "The Flixborough Cyclohexane Disaster", *Loss Prevention*, American Institute of Chemical Engineers, New York, Vol. 8, 106-118,

[K2] Krauhammer T. Shanaa H. M., Assadi A. (1994), "Responses of Structural Concrete Elements to Severe Impulsive Loads", *Computers & Structures*, Vol. 53 (1), 119-130.

[K3] Keenan, W. A. (1969), *Strength and Behavior of Restrained Reinforced Concrete Slabs under Static and Dynamic Loadings*, Technical Report R-621, Y-F008-08-02-123, DASA-RSS3318, Naval Civil Engineering

Laboratory, California.

[K4] Krauthammer, T (1993) "Structural Concrete Slabs under Impulsive Loads", *FORTIFIKATORISK NOTAT NR 211/93*, 43-45.

[K5] Kottegoda N. T. and Rosso R. (1996), *Statistical, Probability and Reliability for Civil and Environmental Engineers*, The McGraw-Hill Companies, Inc.

[K6] Karl Vincent HØiseth, (1992) "Nonlinear Analysis of Reinforced Concrete Structures Exposed to Transient Loadings", *PH. D thesis*, NIT, the University of Trondheim, Norway.

[K7] Kinney, G. F., and Graham, K. J. (1985), *Explosive Shocks in Air*, Springer-Verlag, N. Y. Inc.

[K8] Kingery, C.N. (1966), *Airblast Parameters versus Distance for Hemi-spherical TNT Surface Bursts,* BRL Report No. 1344, Aberdeen, Proving Ground, Maryland.

[K9] Khalid M. Mosalam and Ayman S. Mosallam, (2001), "Nonlinear Transient Analysis of Reinforced Concrete Slabs Subjected to Blast Loading and Retrofitted with CFRP Composites" *Composites Part B: Engineering*, Vol. 32 (8), 623-636

[K10] Kaewkulchai Griengsak and Williamson Eric B., (2004), "Beam Element Formulation and Solution Procedure for Dynamic Progressive Collapse Analysis", *Computers & Structures*, Vol. 82 (7-8), 639-651

[K11] Krauthammer, T., Hall, R. L., and Woodson, S. C. et al. (2002), *Development of Progressive Collapse Analysis Procedure and Condition Assessment for Structures*, National Workshop on Prevention of

Progressive Collapse in Rosemont, Ill. Multihazard Mitigation Council of the National Institute of Building Sciences.

[K12] Kennedy, W. D. (1946), *Explosions and Explosives in Air, Effects of Impact and Explosion*, M.T. White, Summary Technical Report of Division 2, NDRC, Vol. I, Washington, D. C.

[K13] Krauthammer T., Bazeos N., Holmquist T. J., (1986), "Modified SDOF Analysis of RC Box-type Structures", *Journal of Structural Engineering*, ASCE, Vol. 112 (4), 726–44.

[K14] Kang B. S., Choi W. S., Park G. F., (2001), " Structural Optimization under Equivalent Static Loads Transformed From Dynamic Loads Based on Displacement", *Computers & Structures*, Vol. 79, 145-154.

[K15] Kausel Eduardo (1998), "Blast Loads versus Point Loads: The Missing Factor", *Journal of Engineering Mechanics*, ASCE, Vol. 124 (2), 243-244.

[K16] Kowalsky M. J. (2002), " A Displacement-based Approach for the Seismic Design of Continuous Concrete Bridges", *Earthquake Engineering and Structural Dynamics*, Vol. 31, 719-747

[K17] Krawinkler H. (1996), "A Few Basis Concept for Performance Based Seismic Design" *Proceedings of 11th World Conference on Earthquake Engineering*, Mexico. Paper No. 1133.

[K18] Krauthammer T., Assadi-Lamouki A. and Shanaa H. M., (1993), " Analysis of Impulsively Loaded Reinforced Concrete Structural Elements—I. Theory", *Computers & Structures*, Vol. 48 (5), 851-860.

[K19] Krauthammer T., Assadi-Lamouki A. and Shanaa H. M., (1993), " Analysis of Impulsively Loaded Reinforced Concrete Structural Elements—II. Implementation", *Computers & Structures*, Vol. 48 (5), 861-871.

[K20] Kappos A. J., M. K. Chryssanthopoulos and C. Dymiotis, (1999), " Uncertainty Analysis of Strength and Ductility of Confined Reinforced Concrete Members", *Engineering Structures*, Vol. 21 (3), 195-208.

[L1] Longinow A. and Mniszewski K.R. (1996), "Protective Building Against Vehicle Bomb Attacks", *Practice Periodical on Structural Design and Construction*, ASCE, Vol. 1 (1), 51-54.

[L2] Li B., Z. W. Huang, and T. C. Pan (2003), " The Local and Global Structural Responses of a Tall Building Subjected to Close-in Detonations", *Conference on Design and Analysis of Protective Structures against Impact/Impulsive/Shock Loads (DAPSIL)*, Japan, 388-401.

[L3] Luccioni B.M., Ambrosini R.D. and Danesi R.F. (2003), "Analysis of Building Collapse under Blast Loads", *Engineering Structures*, Vol. 26 (1), 63-71.

[L4] Li B., H.C. Rong, and T. C. Pan (2003), "Probabilistic Performance Assessment of Reinforced Concrete Moment-Resisting Frames in a Large Standoff Blast Environment", *Conference on Design and Analysis of Protective Structures against Impact/Impulsive/Shock Loads (DAPSIL)*, Japan, 256-269.

[L5] Lee C. K. B., Giltrud M. (1997), "Scaling of Explosion-Generated Blast Loadings on Walls of Room", *Journal of Engineering Mechanics*, ASCE, Vol. 123 (10), 1096-1102.

[M1] Malvar L.J. and Crawford J.E. (1998), "Dynamic Increase Factors for Concrete", *Twenty-Eighth DDESB Seminar*, Orlando, FL.

[M2] Malvar L.J. and Crawford J.E. (1998), "Dynamic Increase Factors for Steel Reinforcing bar", *Twenty-Eighth DDESB Seminar*, Orlando, FL.

[M3] May G. C. and Smith P. D. (1995), *Blast Effect on Building: Design of Buildings to Optimize Resistance to Blast Loading*, Thomas Telford.

[M4] Mirza, S. A., Hatzinikolas, M., and MacGregor, J.G. (1979), " Statistical Descriptions of Strength of Concrete," *Journal of Structural Engineering*, ASCE, Vol. 105 (6), 1021-1036.

[M5] Mirza, S. A., and MacGregor, J. G. (1979a), " Variations in Dimensions of Reinforced Concrete Members", *Journal of Structural Engineering*, ASCE, Vol. 105 (4), 751-765.

[M6] Mlakar P. F., Corley W.G., and Sozen, M. A. et al. (1998), "the Oklahoma City Bombing: Analysis of Blast Damage to the Murrah Building", *Journal of Performance of Constructed Facilities*, ASCE, Vol. 12 (3), 113-119.

[M7] Mo Y. L. (2004), "Performance Simulation of Nuclear Containments for Security", *Journal of Performance of Constructed Facilities*, ASCE, Vol. 18 (2), 107-115

[M8] Mazars, J. (1986) "A Description of Micro and Macroscale Damage of Concrete Structures", *Engineering Fracture Mechanics*, Vol. 25 (5/6), 729-737.

[M9] Malvar L. J., Crawford J. E., Wesevich J. W. and Simons D. (1997), " A Plasticity Concrete Material Model for DYNA3D", *International Journal*

of Impact Engineering, Vol. 19 (9-10), 847-873

[M10] Marjanishvili S. M., (2004), "Progressive Analysis Procedure for Progressive Collapse", *Journal of Performance of Constructed Facilities*, ASCE, Vol. 18 (2), 79-85

[M11] Majid, K.I. (1972), *Nonlinear Structure*, Wildy-Interscience, A Division of John Wiley and Sons, Inc. New York.

[M12] Mayrhofer C., (2002), "Reinforced Masonry Walls under Blast Loading", *International Journal of Mechanical Sciences*, ASCE, Vol. 44 (6), 1067-1080

[M13] MATLAB, (2001), *MATLAB: The Language of Technical Computing*, Version 6.1, The MathWorks, Inc.

[M14] Bischoff, P.H. and Perry, S.H. (1991), "Compression Behavior of Concrete at High Strain-rates", *Materials and Structures*, Vol. 24, 425-450.

[M15] Mays G. C., Hetherington J. G., Rose T. A., (1999) "Response to Blast Loading of Concrete Wall Panels with Openings", *Journal of Structural Engineering*, ASCE, Vol. 125 (12), 1448-1450.

[M16] Munshi J. A., (2004), "Seismic versus Blast Loading: Comparing the Similarities and Differences when Designing Reinforced Concrete Buildings", *Concrete International*, May, 58-64.

[M17] Malvar, L. J., Crawford, J. E., and Morrill, K. B. (1999a), *K&C Concrete Material Model, Release III: Automated Generation of Material Model Input*, Rep. TR-99-24, Karagozian & Case Structural Engineers, Burbank, California.

[M18] Melchers Robert E., (1998), *Structural Reliability Analysis and Prediction*, John Wiley & Sons.

[N1] Newmark, N. M. (1972), "External Blast", *Proceeding of International Conference On the Planning and Design of Tall Building*, Lehigh University, Vol. Ib, 661-676.

[N2] Newmark, N. M. and Hansen, R. J. (1961), *Design of Blast-resistant Structures*, in Shock and Vibration Handbook, Vol. 3, edited by Harris and Crede, McGraw-Hill.

[N3] Norris C. H., Hansen R. J., Holley M. J., Biggs J. M., Namyet S. and Minami J. V. (1959), *Structural Design for Dynamic Loads*, McGraw-Hill Book Company, N. Y.

[N4] NFEC (1986), *Blast Resistant Structures*, Naval Facilities Engineering Command, Design Manual 2.08, Alexandria, VA.

[O1] Olatidoye O., Sarathy S., and Jones G. et al. (1999), *A Representative Survey of Blast Loading Models and Damage Assessment Methods for Buildings Subjected to Explosive Blasts*, CEWES MSRC/PET TR/98-36, Nichols Research Corporation.

[P1] Park R. and Paulay T. (1975), *Reinforced Concrete Structures*, John Willey & Sons, N.Y.

[P2] Paulay T. and M.J.N. Priestley, (1992), *Seismic Design of Reinforced Concrete and Masonry Buildings*, John Wiley & Sons, Inc.

[P3] Pan Youguang, Watson Alan, (1998), "Effect of Panel Stiffness on Resistance of Cladding Panels to Blast Loading", *Journal of Engineering Mechanics*, ASCE, Vol. 124 (4), 414-421.

[P4] Priestley M. J. N. (2000), "Performance Based Seismic Design", *Proceedings of 12th World Conference on Earthquake Engineering*, Paper No. 2831.

[P5] Priestley M. J. N., Kowalsky M. J. (2000), " Direct Displacement-based Seismic Design of Concrete Buildings", *Bulletin of the New Zealand Society for Earthquake Engineering*, Vol. 33 (4), 421-443.

[P6] G. Piccardo and G. Solari (1996) " A refined Model for Calculating 3-D Equivalent Static Wind Forces on Structures", *Journal of Wind Engineering and Industrial Aerodynamics*, Vol. 65 (1-3), 21-30.

[R1] Ross, T. J. (1983), "Direct Shear Failure in Reinforced Concrete Beams under Impulsive Loadings", *PH. D. thesis*, Standford University.

[R2] Rossi, P., Van Mier, J.G.M., Toutlemonde, F., Le Maou, F., and Boulay, C. (1994), "Effect of Loading Rate on the Strength of Concrete Subjected to Uniaxial Tension", *Materials and Structures*, Vol. 27, 260-264.

[R3] Repetto, M. P., and Solari, G. (2004). "Equivalent Static Wind Actions on Vertical Structures." *Journal of Wind Engineering and Industrial Aerodynamics*, Vol. 100 (7), 1032–1040.

[S1] Smith P. D. and Hetherington J. G. (1994), *Blast and Ballistic Loading of Structures*, Butterworth-Herinmann Ltd, Linacre House, Jordan Hill, Oxford Ox2 8DP.

[S2] Sozen M.A., Thornton C.H., Corley W. G. and Mlakar P. F. (1998), "The Oklahoma City Bombing: Atructural and Mechanisms of the Murrah Building", *Journal of Performance of Constructed Facilities*, ASCE, Vol. 12 (3), 120-136.

[S3] Seabold, R. H. (1967), *Dynamic Shear Strength of Reinforced Concrete Beams, Part II*, Naval Civil Engineering Laboratory, Port Hueneme, California.

[S4] SEAOC. (1995), *Version 2000 Performance Based on Seismic Engineering of Buildings*, The Structural Engineers Association of California, San Francisco, USA

[S5] Schmidt, J. A. (2003), "Structural Design: Structural Design for External Terrorist Bomb Attacks", *Structure Magazine*, March, 1-5.

[S6] Stephen P. Ward (2004), "Retrofitting Existing Masonry Buildings to Resist Explosions", *Journal of Performance of Constructed Facilities*, ASCE, Vol.18 (2), 95-99

[T1] TM 5-855-1, (1986), *Fundamental of Protective Design for Conventional Weapons,* United States Department of the Army, Washington D. C.

[T2] TM5-1300, (1990), *Structures to Resist the Effects of Accidental Explosions, Volume IV, Reinforced Concrete Design*, United States Department of the Army, Washington D. C.

[T3] TR-62 (1976), *Increasing Blast and Fire Resistance in Buildings: Design Techniques for Combined Nuclear Weapon Effects*, Department of Defense, Defense Civil Preparedness Agency

[T4] Tang, T.X., Lawrence, E.M. and David, A.J. (1992), "Rate Effects in Uniaxial Dynamic Compression of Concrete" *Journal of Engineering Mechanics*, ASCE, Vol. 118, 108-124.

[U1] UFC 4-010-01, (2002), *DoD Minimum Antiterrorism Standards for Buildings*, United States Department of Defense.

[V1] Val V. D., Bljuger F. and Yankelevsky D. Z. (1997), "Reliability Assessment of Damaged RC Framed Structures", *Journal of Structural Engineering*, ASCE, Vol. 123 (7), 889-895.

[X1] Xue Qiang, Chen Cheng-Chung (2003), "Performance-Based Seismic Design of Structures: a Direct Displacement-Based Approach", *Engineering Structures*, Vol. 25, 1803-1813.

[Y1] Yamada Y., Kawai T. and Yoshimura N. (1968), *Proceedings of the Second Conference on Matrix Methods in Structural Mechanics*, AFFDL-TR-68-150.

[Z1] Zehrt W. H., Jr., LaHoud P. M., and Bogosian D.D. (1998), " Blast Responses in Concrete Walls", *Concrete International*, 27-31.

[Z2] Zhou, Y., Kareem, A., and Gu, M., (2000). "Equivalent Static Buffeting Loads on Structures", *Journal of Structural Engineering*, ASCE, Vol. 126 (8), 989–992.

APPENDIX 1

BLAST LOADINGS ON A CLOSED TARGET

Front Load

At low pressure ranges, the variation of pressure with the front faces for a closed rectangular aboveground target is shown in Figure 2.2 whose parameters can be obtained with

- $P_{tc} = P_{so} + C_D\, q \;\; (C_D = 1)$
- $t_c = 3S/U$
- S = clearing distance = W_s /2 or H_s, the building half-width or height respectively, whichever is less
- $t_{of} = 2i_s / P_{so}$

where P_r and P_{so} is peak reflected and incident pressure of the shock wave reaching the front face; q is peak dynamic pressure, U is shock front velocity, i_s is incident blast impulse.

However, at higher pressure ranges the above equations may yield a ficticious pressure-time curve due to the extremely short pressure pulse durations involved. To overcome it, a comparison is made by constructing a second curve (dashed triangular line as indicated in Figure 2.2) where the fictitious duration t_r is

- $t_r = 2i_r / P_r$

The parameter i_r is the reflected impulse of the blast wave. The curve, which gives the smaller value of the impulse (area under curve), is used in calculating the front face loading. The reflected pressure impulse includes the effects of both the incident and dynamic pressure.

Top and side load

Top and side faces will experience less blast loading than the front wall face due to little or no reflection of the blast wave, assuming a generally flat roof and a horizontally traveling blast wave. The form of this load is shown in Figure 2.2, where

- $P_{or} = C_E P_{sob} + C_D\ q_{ob}$
- C_E = overpressure averaging factor depending on L_{wb} / L (<1.0)
- C_D = drag coefficient depending on q_{ob}
- $t_1 = D / U_D$
- $t_2 = t_b - t_f + t_{of}$

P_{sob} , q_{sob} and L_{wb} are peak incident pressure, dynamic pressure, and blast wave length occurring at point b, t_f and t_b is the arrival time of the blast wave reaching the point f and b , U_D is the wave front velocity at point d while D can be calculated from D / L that is a function of L_{wb} / L.

Rear load

The rear or back face of a building is loaded, similar to the side faces and roof, by the averaged attenuated overpressure pulse with peak value P_{ob} and rise time as shown Figure 2.2, where

- $P_{ob} = C_E P_{soe} + C_D \ q_{oe}$
- $t_3 = t_b - t_f$
- $t_4 = D' / U_{D'}$
- $t_5 = t_3 + t_e - t_f + t_{of}$

P_{soe}, q_{soe} and t_e are blast wave parameters at point e, D' can be calculated from D'/S that is a function of L_{we}/L, and $U_{D'}$ is the wave front velocity at point d'.

In the above expressions these blast wave parameters including the blast incident impulse, the reflected impulse, the incident and reflected pressure, the dynamic pressure, the arrival time, and the velocity can be determined with the conventional blast loadings program of CONWEP [H1] that is developed based on TNT-equivalence models using information provided in TM5-855-1 [T1].